INSIGHT INTO XYLAN O-ACETYLATION DURING PLANT CELL WALL BIOSYNTHESIS

by

HSIN-TZU WANG

(Under the Direction of William S. York and Breeanna R. Urbanowicz)

ABSTRACT

Xylans are the most abundant hemicellulosic polysaccharides in dicots and are often heavily *O*-acetylated. The degree of *O*-acetylation of xylan not only plays a role in maintaining cell wall architecture and plant growth, but it also affects the physicochemical properties and thus our utilization of lignocellulosic biomass. Despite the importance of polysaccharide *O*-acetylation, the detailed mechanism behind it remained enigmatic until recently. The enzymes involved in *O*-acetylation of cell wall polysaccharides belong to the TRICHOME BIREFRINGENCE-LIKE (TBL) family, which is composed of 46 members in *Arabidopsis thaliana*. In this study, my work focused on the biochemical and structural characterization of the most highly expressed TBL protein during secondary wall formation: XYLAN *O*-ACETYLTRANSFERASE1 (XOAT1). Detailed characterization of XOAT1-catalyzed reactions by real-time NMR showed it regiospecifically 2-*O*-acetylates xylosyl backbone residues. Structural analysis of XOAT1 revealed a conformation that bears similarities to the $\alpha/\beta/\alpha$ topology of the GDSL-like esterase/lipase family and possesses a deep cleft formed by two unequal lobes that accommodate the substrate. Biochemical analyses and molecular dynamics (MD) simulations were used to show that XOAT1 catalyzes acetylation through formation of an acyl-enzyme intermediate by a double

displacement bi-bi mechanism involving a Ser-His-Asp catalytic triad and forms an oxyanion hole using an Arg residue. Unfortunately, a ligand-bound structure was unavailable for XOAT1. To gain more insight into the optimal orientation of xylan in the binding cleft of XOAT1 and key residues involved in enzyme-substrate interactions, docking and MD simulations coupled with site-directed mutagenesis and biochemical analyses were used, which revealed the major lobe of XOAT1 is important for xylan binding. The resulting XOAT1 variants with various enzymatic efficiencies were applied to one-pot synthesis of xylan polymers with different degrees of *O*-acetylation, confirming the utility of this approach. Finally, I also characterized a second *Arabidopsis* TBL protein, TBL3, and present its novel biochemical activity as a bifunctional xylan 2-*O*-transacetylase that is able to use acetylated xylan as an acetyl donor, suggesting its role in regulating *O*-acetylation levels and/or patterning along the xylan backbone. Taken together, these studies provide new molecular level insights into the process of xylan *O*-acetylation during plant cell wall biosynthesis.

INDEX WORDS: plant cell wall, xylan *O*-acetyltransferase, enzyme mechanism, crystal structure, computational modeling, enzyme engineering, biomass modification

INSIGHT INTO XYLAN O-ACETYLATION DURING PLANT CELL WALL BIOSYNTHESIS

by

HSIN-TZU WANG

B.S., National Taiwan University, Taiwan, 2009

M.S., National Taiwan University, Taiwan, 2012

A Dissertation Submitted to the Graduate Faculty of The University of Georgia in Partial Fulfillment of the Requirements for the Degree

DOCTOR OF PHILOSOPHY

ATHENS, GEORGIA

2021

INSIGHT INTO XYLAN O-ACETYLATION DURING PLANT CELL WALL BIOSYNTHESIS

by

HSIN-TZU WANG

Major Professor:	William S. York
	Breeanna R. Urbanowicz
Committee:	Alan G. Darvill
	Michael G. Hahn
	Kelley W. Moremen

Electronic Version Approved:

Ron Walcott
Vice Provost for Graduate Education and Dean of the Graduate School
The University of Georgia
August 2021

DEDICATION

This dissertation is dedicated to my parents in Taiwan, George Wang and Frances Lee, who have always loved me unconditionally and been tremendously supportive throughout my years at UGA. I would also like to thank my boyfriend, Hao-Tun Kao, for being a constant source of loving support and encouragement all through my graduate studies.

ACKNOWLEDGEMENTS

I would like to thank Dr. William S. York and Dr. Breeanna R. Urbanowicz for their enlightened guidance, generous support, optimism and kindness, which helped me overcome all the difficulties and obtain fruitful results from the challenging research projects. I would also like to thank my committee members, Dr. Alan G. Darvill, Dr. Michael G. Hahn and Dr. Kelley W. Moremen, for their knowledgeable insights and valuable advices on my research projects and dissertation. In addition, I would like to express my gratitude to members of York lab and Urbanowicz lab for their help and encouragement throughout my graduate career. In particular, I thank Dr. Maria J. Peña for her training and suggestions that largely contributed to my accomplishments.

TABLE OF CONTENTS

Page

LIST OF TABLES

Page

LIST OF FIGURES

Page

CHAPTER 1

INTRODUCTION AND LITERATURE REVIEW

Plant cell wall structure

All plant cells are surrounded by cell walls, which provide mechanical support against physical forces in the environment as well as flexibility to allow cell expansion and resist internal turgor pressure. In addition, plant cell walls are also involved in carbohydrate storage, pathogen resistance, cell signaling and cell-cell interactions depending on the cell type and developmental stage [1]. Plant cell walls are composed of polysaccharides including cellulose, hemicelluloses and pectins, and other non-polysaccharide components such as phenolic esters and proteins. There are two types of cell walls formed by plants, primary and secondary walls, with distinct compositions and functions. Primary cell walls surround growing cells to allow expansion and division but at the same time provide structural support to maintain the cell shape. In primary walls of dicots, the main pectic polysaccharides include homogalacturonans, rhamnogalacturonans, substituted galacturonans, and arabinogalactans, while the major hemicellulosic polysaccharide is xyloglucan [2-4]. Besides dicots, primary walls in grasses contain a significant amount of glucuronoarabinoxylans and mixed-linkage glucans [5].

On the other hand, secondary walls are deposited after cells cease growing, and are predominantly composed of cellulose embedded in a matrix formed by hemicelluloses and lignins. The major types of secondary wall hemicelluloses in woody tissues, grasses, and gymnosperms are glucuronoxylan, arabinoxylan, and glucomannan, respectively, and the type and amount vary

depending on plant species and tissue [6]. Secondary cell walls are much thicker and stronger than primary walls, and provide the rigidity required to facilitate vertical water and nutrient transport in plants that grow upright. The thickened secondary walls account for a major part of terrestrial biomass, and also contribute to human society since biomass-based materials are widely used in various industries, such as food, pulp, cosmetics, agriculture and fuel production [7]. Understanding the structure of plant cell walls and how the major component polysaccharides are biosynthesized can provide us opportunities to modify lignocellulosic feedstocks and thus enhance our utilization of plant biomass.

Structure of dicot xylan

In dicots, glucuronoxylan is the dominant hemicellulose comprising 20-30% of secondary cell walls [6]. Glucuronoxylan consists of a backbone that is formed by 1,4-linked β-D-xylopyranosyl (Xyl) residues, which are further substituted by 1,2-linked α-D-glucuronic acid (GlcA) and/or its 4-*O*-methyl derivative (MeGlcA) [8]. The xylosyl backbone of glucuronoxylan can be di-acetylated at both *O*-2 and *O*-3, mono-acetylated at the *O*-2 or *O*-3 of non-glycosylated xylosyl residues, or at the *O*-3 of xylose residues substituted with a 2-*O*-(Me)GlcA (Figure 1.1a) [9-13]. In grasses, the xylan backbone is further decorated with α-L-arabinofuronose at *O*-3, and the attached arabinosyl residues are frequently substituted with α-L-arabinofuronose or a β-D-xylopyranose at *O*-2 to form glucuronoarabinoxylan (Figure 1.1b) [14]. In gymnosperms, arabinoglucuronoxylan composed of glucuronoxylan with 3-*O*-α-L-arabinofuronose substituents on the backbone, which is not *O*-acetylated, is the second most dominant hemicellulose after galactoglucomannan (Figure 1.1c) [15].

The degree of acetylation (DA) of a xylan is defined as the number of acetyl substituents per backbone residue, and varies between species. In general, most dicot species such as *Arabidopsis*, Aspen, Eucalyptus, etc., have been reported to synthesize glucuronoxylan with a DA of approximately 0.6 [9-12], which means more than half of the xylosyl backbone are acetylated. In addition to acetylation levels, 3-*O*-acetylated xylosyl residues in dicot xylans have been observed in different studies and are more abundant compared to 2-*O*-acetylated residues [9, 10, 12, 13]. However, the processes used for extraction of xylan from plant tissue could result in spontaneous migration of acetyl groups (described in the following section); thus, the ratio of *O*-3 to *O*-2 acetylated residues in native xylans *in planta* is difficult to experimentally determine.

The distribution of acetyl moieties on glucuronoxylan has been described in previous studies. In *Arabidopsis*, a pattern of acetylation has been proposed, based on mass fragmentation analysis, wherein every other Xyl residue of the glucuronoxylan backbone bears an acetyl substituent [9]. This positioning of the acetyl groups was suggested to contribute to the interactions between xylan and cellulose microfibrils in cell walls [16, 17]. In contrast, the distribution of acetyl moieties observed along the backbone of glucuronoxylan in *Paulownia* species was not uniform, unlike the regular distribution of *O*-Ac observed in *Arabidopsis* [11].

Non-enzymatic migration of acetyl groups

Acetyl group migration was first described by Emil Fischer in 1920 [18], and it has been widely observed in different monosaccharides and oligosaccharide molecules including galactopyranosides, glucopyranosides, mannopyranosides and xylopyranoside derivatives [19-22]. Due to migration, it has been challenging to distinguish the exact position of acetyl groups on

a sugar moiety as well as to characterize the regiospecificities of enzymes involved in deacetylation/acetylation processes. Thus, it is important to understand the spontaneous migration behavior of acetyl substituents to unambiguously evaluate the structure of the direct products of enzyme-catalyzed reactions.

It has been reported that an acetyl moiety initially on *O*-2 of a mannosyl residue could travel around the monosaccharide in a 'clockwise' direction, i.e., from *O*-2 to *O*-3, and then to *O*-4 if it is on a non-reducing end residue, and finally to *O*-6 (Figure 1.2) [19, 20, 23, 24]. Such migration is favored in polar solvents at high pH and/or high temperature [25-28]. 'Anticlockwise' migration and migration to other saccharide units in an oligosaccharide also have been observed [19, 29, 30]. High pH (pH > 6) and high temperature usually facilitates acetyl migration and increases the migration rate [20]. At extremely low pH (e.g., pH 1.0), relatively slow hydrolysis of the acetyl groups occurs without any migration [20]. Thus, it is important that conditions that do not favor acetyl migration are used in esterase/acetyltransferase assays to minimize bias when characterizing an enzyme's regiospecificity.

Since the biological environment could also lead to acetyl migration, the distribution of *O*-acetyl groups on natural polysaccharides accumulated in plant cell walls might not necessarily reflect the direct products of the biosynthetic process. *O*-acetylation of hemicellulosic polysaccharides takes place in Golgi apparatus where TBL proteins are localized [31-34], and a pH gradient higher than pH 6 has been observed from the *trans*-compartment of Golgi cisternae (pH 6.9) to *trans*-Golgi network (TGN; pH 6.1) in tobacco epidermal cells [35] that can facilitate acetyl group migration. It has been shown that the ratio of synthetic 2-*O* and 3-*O*-acetylated mono- and oligosaccharides in equilibrated mixtures corresponds well to naturally acetylated mannans

and xylans [19, 36], which suggests that the natural distribution of acetyl moieties in cell wall polysaccharides is the result of the progression of acetyl migration toward equilibrium.

Biosynthesis of xylan

The biosynthesis of all non-cellulosic polysaccharides, including xylan, occurs in the Golgi apparatus [6], with an exception of callose [37]. After completion of xylan biosynthesis in the *trans*-Golgi network, the newly synthesized xylan is transported to cell walls through vesicles. The deposited xylan then forms interactions with the hydrophilic surface of cellulose microfibrils likely through Van der Waals contacts and hydrogen bonding [16, 17, 38-40]. In contrary to the synthetic procedure of xylan that occurs in the intracellular compartment, further xylan modifications involving hydrolysis and transglycosylation can take place in the extracellular matrix after xylan is incorporated into the cell wall [41, 42]. These modifications are catalyzed by apoplast-localized xylosidases and transglycosylases in response to stresses from the environment and/or during active plant growth.

Xylan backbone and reducing end synthesis

The enzymes involved in the elongation of the xylan backbone include IRREGULAR XYLEM 9 (IRX9), IRX10 and IRX14, which are proposed to function non-redundantly and interact with one another physically to form a Golgi-localized xylan synthase complex (XSC) [43-48]. The XSC is composed of at least three core components, IRX9, IRX10 and IRX14, which are preferentially expressed during secondary cell wall formation, together with other potential interaction partner(s) [46]. In addition, a similar XSC composed of their homologs (IRX9L,

IRX10L and IRX14L) is specifically expressed in primary wall forming tissues [49], indicating that synthesis of xylans in the primary and secondary walls are performed by two different sets of XSC complexes. According to previous studies, the expression of XSC proteins involved in the primary wall xylan synthesis can partially rescue secondary wall XSC mutants, demonstrating that functionally exchangeable features are shared by the two sets of XSC proteins [44, 49]. The XSC proteins are crucial for plant growth, as deletion of XSC genes in Arabidopsis results in dwarf plants with an irregular xylan (*irx)* phenotype and significant decreases in xylan content in *Arabidopsis* [50, 51]. Notably, down regulation of XSC expression results in less recalcitrant secondary cell walls and increased plant volume [52], suggesting new approaches for improving biomass feedstocks.

The XSC also interacts with other proteins, such as UDP-ARABINOPYRANOSE MUTASE (UAM), which provides the substrate for XYLAN ARABINOTRANSFERASES (XAT) that catalyzes the addition of arabinose substituents to the xylan backbone [47, 53, 54]. This suggests that the XSC can indirectly affect xylan modification as well. Besides UAM, XSC also interacts with two hormone-associated proteins, VERNALIZATION-RELATED GENE 2 (VER2) and GERMIN-LIKE PROTEIN (GLP) [47], suggesting that hormones such as jasmonic acid (JA) and auxin might play roles in the biosynthesis of secondary cell wall xylan.

A tetrasaccharide β-Xyl-(1,3)-α-Rha-(1,2)-α-GalA-(1,4)-Xyl (i.e., Sequence 1) is present at the reducing end of xylans in dicots and gymnosperms (Figure 1a and 1c). The function of this reducing end structure remains poorly understood, but is hypothesized to be a primer for the elongation of the xylan backbone from the reducing end to the non-reducing end [8, 55]. According to previous studies, mutations of the genes associated with synthesis of Sequence 1, *IRREGULAR XYLEM8* (*IRX8*) and *FRAGILE FIBER8* (*FRA8*), result in severe changes in xylan content and

structure as well as secondary cell wall formation [50, 56, 57]. Sequence 1 was also proposed to play a role in xylan trafficking via a transporting mechanism analogous to the biosynthetic processing of heparan sulfate (HS) proteoglycan. Similar to xylan, HS also contains a distinct reducing end sequence, which is attached to a protein, facilitating transport of HS to the cell surface [58].

Glycosyl sidechain substitution of glucuronoxylan

The enzymes involved in transferring (Me)GlcA moieties onto the glucuronoxylan backbone have been identified, which include GLUCURONIC ACID SUBSTITUTION OF XYLAN (GUX) 1, GUX2, and GUX3 [49, 59-61]. GUX1 and GUX2 were first shown to be involved in glucuronidation of xylans by observation that, in *Arabidopsis,* the double mutant *gux1gux2* lacks both detectable (Me)GlcA substituents on xylans, and microsomes isolated from these plants have reduced glucuronyltransferase activity [61]. Using microsomes from tobacco BY2 cells in which GUX enzymes were overexpressed, GUX1, GUX2 and GUX3 were also shown to function as glucuronyltransferases, catalyzing the transfer of GlcA from UDP-GlcA to xylohexaose *in vitro* [60].

GUX1 and GUX2 have been demonstrated to generate distinct GlcA distribution patterns along the xylan backbone. GUX1 is suggested to have a preference of transferring one GlcA onto xylans every 8 or 10 residues, which forms major domains of xylan chains with loosely spaced substituents. In contrast, GUX2 is proposed to generate randomly distributed GlcA substituents on minor domains of xylans, defined as regions of the polymer decorated with substituents every 5-7 residues [59]. On the other hand, GUX3 is proposed to be the glucuronyltransferase that is solely

involved in adding a GlcA to a unique xylan bearing pentosylated side chain in *Arabidopsis* primary cell walls [49].

O-acetyl substituents

In addition to glycosyl substituents, glucuronoxylan bears *O*-acetyl groups on more than half of its Xyl residues[12, 13]. The level of acetylation could affect physical properties, such as hydrophobicity of xylan polysaccharides [62], and could also influence the interaction between xylan and other cell wall polymers [17]. In previous studies, a decrease of DA on xylans led to an increase of xylan-cellulose affinity [39]. Also, the acetyl groups on xylans have been observed to correlate with another cell wall polymer, lignin, through physical contacts with feruloyl and syringyl units [63]. Besides affecting physicochemical properties of cell wall polymers, cell wall acetylation has been shown to influence physiological functions including freezing tolerance and pathogen resistance in *Arabidopsis* [64-68]. In industry, the level of acetylation in biomass affects its processing and conversion into products [62, 69], so understanding the mechanisms of cell wall acetylation is essential not only to evaluate the physiological effects of this crucial modification, but also to develop improved technologies for the utilization of biomass-based materials.

So far, there are three protein families that are reported to be involved in cell wall acetylation, including REDUCED WALL ACETYLATION (RWA) proteins, the ALTERED XYLOGLUCAN 9 (AXY9) protein, and the TRICHOME BIREFRINGENCE-LIKE (TBL) protein family (Figure 1.3). The RWA proteins have been proposed to be involved in plant cell wall acetylation based on studies of *Arabidopsis rwa* mutants. The *rwa2* single mutants revealed around 20% lower overall cell wall acetylation in leaf tissues [66], while cell walls of the triple

and quadruple mutants of all four RWA members in *Arabidopsis* also showed reductions in the degree of acetylation of different wall components [70]. The nonspecific impact of the *rwa* mutants on the acetylation levels of various cell wall polysaccharides, along with a distinct RWA structure composed of ten predicted transmembrane domains lacking GDSL or DxxH catalytic domains, which are conserved among many esterases and lipases and are required for catalysis, suggest that RWAs play a role in translocating acetyl groups from the cytosol into the Golgi lumen. However, further evidence is required to validate this hypothesis [66, 71]. AXY9 is another protein that has been found to affect the acetylation level in cell wall polysaccharides [72]. A forward genetic screen in *Arabidopsis* has shown that *axy9* mutants exhibit reduced acetylation levels for both xyloglucan and xylan in cell walls. This non-specific impact on acetylation of cell wall polysaccharides led to a hypothesis that AXY9 generates an acetylated intermediate utilized as an acetyl donor by TBL proteins (Figure 1.4) [72].

TBL proteins comprise the third category of protein families involved in the plant cell wall acetylation pathway. Nine members of the TBL family in *Arabidopsis* have been shown to possess xylan *O*-acetyltransferase activities with different regiospecificities, adding acetyl groups to *O*-2 and/or *O*-3 of xylosyl residues [31-34, 73]. Among all xylan-specific TBL proteins, XYLAN *O*-ACETYLTRANSFERASE 1 (XOAT1) has been biochemically characterized as a xylan 2-*O*-acetyltransferase. This result was based on a nuclear magnetic resonance (NMR) spectroscopy technique that allows the reaction progress to be monitored in real-time[65, 74], thus minimizing the ambiguity introduced by the widely-observed non-enzymatic acetyl migration [19-22, 75]. In mutant studies in *Arabidopsis*, *esk1* plants (null mutants in the *XOAT1* gene) showed collapsed xylem vessels and a ~60% reduction of xylan *O*-acetylation [76, 77], and more tolerance to freezing, drought and salt [78, 79]. In addition to the reduction of xylan acetylation shown in the

esk1 mutant, the even-pattern of acetyl and Me(GlcA) substituents on alternate xylosyl residues was disrupted, suggesting a role for XOAT1 in patterning xylan decorations [16]. However, the mechanisms by which the enzyme interacts with its substrate to control acetyl distribution require further study.

TBL3, another TBL protein that is highly expressed during secondary wall synthesis, is phylogenetically close to XOAT1 (Figure 1.3), suggesting that it is also involved in the complex mechanism of xylan *O*-acetylation. Previous studies reveal that *tbl3* mutants have lower levels of crystalline cellulose and esterified pectins in trichomes and stems, demonstrating that TBL3 affects the deposition of secondary wall cellulose, possibly by altering esterification of pectic polysaccharides [80]. The *tbl3 tbl31* double mutant revealed a reduced level of xylan 3-*O*-acetylation [81]. Biochemical analysis of TBL3 using *in vitro* assays further established its enzymatic role in 2-*O* and 3-*O*-acetylating xylan [82]. Furthermore, the TBL3 homologs PtrXOAT7 and OsXOAT8 from *Populus trichocarpa* and *Oryza sativa* have also been shown to function as xylan *O*-acetyltransferases [83, 84].

Orthologs of TBL proteins

O-acetylation of various polysaccharides in non-plant species has also been studied, and intriguingly, the machinery used by different species share some similarities [71]. Cas1P has been identified as a transmembrane protein that *O*-acetylates the capsular polysaccharide, glucuronoxylomannan (GXM), in *Cryptococcus neoformans* [85]. Cas1P is predicted to have multiple C-terminal transmembrane domains, reminiscent of the structure of RWA in plants, but it differs in that it contains catalytic GDS and DxxH motifs in its N-terminal domain (Figure 1.5),

suggesting that Cas1P might play roles in both the translocation of acetyl donors from the cytoplasm and the catalysis of *O*-acetylation of GXM. A similar topology for catalytic domains and multi-transmembrane domains has been found in CasD1, the ortholog of Cas1P in humans, which is essential for 9-*O*-acetylation of sialic acids commonly found as terminal residues in glycoproteins and glycolipids [86, 87]. The purified catalytic domain of CasD1, which is localized in the Golgi lumen, has been shown to catalyze *O*-acetylation *in vitro*, transferring acetyl groups from acetyl-CoA to Cytidine-5'-monophospho (CMP)-sialic acid. The formation of an acetyl-enzyme intermediate involving the catalytic serine residue (Ser94) in the GDS motif of CasD1 has also been demonstrated [87].

In Gram-positive bacteria, the bimodular protein *O*-ACETYLTRANSFERASE A (OatA) has been implicated in *O*-acetylation of the bacterial cell wall polymer, peptidoglycan. Based on studies of human pathogens, including *Staphylococcus aureus* and *Streptococcus pneumoniae*, OatA has been shown *in vitro* to 6-*O*-acetylate the *N*-acetylmuramoyl (MurNAc) residue that forms the repeating unit with *N*-acetylglucosaminyl (GlcNAc) in peptidoglycan [88, 89]. The structural orientation of OatA differs from that of acetyltransferases in fungi and mammals, having multiple transmembrane domains at the N-terminus and a catalytic GDS domain at the C-terminus (Figure 1.5). The crystal structure of the catalytic domain reveals a SGNH-like hydrolase fold containing a Ser-His-Asp catalytic triad [88, 90, 91]. OatA homologs are also found in other Gram-positive bacterial species such as *L. monocytogenes* [92], *E. faecalis* [93], *Lactobacillus plantarum* [94], and *Lactococcus lactis* [95].

In contrast, Gram-negative bacteria have exopolysaccharide *O*-acetylation machinery that requires multiple proteins with two enzymatic functionalities. The first one catalyzes the translocation of the acetyl moiety across the plasma membrane from the cytoplasm to the

periplasm. The other catalyzes the transfer of acetyl groups to polysaccharide acceptors in the periplasm [96]. In the pathogen *Pseudomonas aeruginosa*, four enzymes are involved in *O*-acetylating alginate (Figure 1.5), a biofilm exopolysaccharide that is thought to protect the microbe from the host immune response and antibiotics [97, 98]. It is hypothesized that AlgF, AlgI, AlgJ and AlgX form a protein complex in which AlgI plays a role similar to RWA, translocating acetyl-donors into periplasm, while AlgJ functions like AXY9, passing the acetyl moieties to AlgX, which catalyzes the *O*-acetylation of mannuronic acid residues in alginate. The function of AlgF was previously unknown [99-103] until a current report showing its role in the alginate *O*-acetylation machinery as an adaptor in the AlgI-AlgJ-AlgF multiprotein complex, which is linked to AlgX and the alginate polymerase, Alg8, to mediate *O*-acetylation of nascent alginate based on mutual stability analysis and pull-down experiments [104]. In other Gram-negative bacterial species, a two-protein system has been found for *O*-acetylation of extracellular polysaccharides [105]. It is proposed that in *Neisseria gonorrhoeae,* an ortholog of AlgI called PatA (initially named PacA), transports the acetyl donors from the cytoplasm into the periplasm [106, 107]. PatB (initially named Ape2) then catalyzes *O*-acetylation of the MurNAc residues in peptidoglycan (Figure 1.5) [96, 105].

So far, two distinct systems composed of either a single protein or multi-protein complex have been identified in Gram-positive and Gram-negative bacteria, respectively, to *O*-acetylate extracellular polysaccharides. *Bacillus anthracis* is notably distinct from other Gram-positive bacteria, as it requires both Oat and Pat systems to fully *O*-acetylate MurNAc residues in peptidoglycan (Figure 1.5) [108]. Secondary cell wall polysaccharides (SCWPs) of *Bacillus* consist of trisaccharide repeating unit, β-ManNAc-(1,4)-β-GlcNAc-(1,6)-α-HexNAc-(1,4)-, where HexNAc can be GalNAc or GlcNAc [109, 110]. It has been shown that some *Bacillus*

species utilize Pat machinery composed of multiple proteins, including PatA1, PatA2, PatB1 and PatB2 to *O*-acetylate SCWPs [111, 112]. Moreover, a recent report on the PatB1 protein in *B. anthracis* established its *O*-acetyltransferase activity, acting on the β-GlcNAc in the SCWP trisaccharide repeating unit. Structural data further revealed a Ser-His-Asp catalytic triad within the enclosed active site of PatB1, suggesting that PatB1 directly *O*-acetylates the terminal end of SCWP. This activity is similar to that of PatB in *N. gonorrhoeae,* although the two proteins have low sequence identity [112]. In *B. anthracis,* PatB2 exhibits acetylesterase rather than acetyltransferase activity, but the exact role that PatB2 plays in the *O*-acetylation machinery has not been established [112]. In contrast, PatA1 and PatA2 are predicted to be integral membrane proteins and belong to the family of membrane-bound *O*-acetyltransferases (MBOAT; pfam 03062). They share high similarity with AlgI in *P. aeruginosa* and PatA in *N. gonorrhoeae*, and have been proposed to play a role in translocating acetyl moieties across the plasma membrane [108, 111]. Analysis of *B. anthracis* mutant strains *patA1 patA2* revealed a significant reduction of the *O*-acetylation levels in both peptidoglycan and SCWP [108, 111].

In algal species, orthologs of the proteins involved in *O*-acetylation of cell wall polysaccharides have not yet been extensively studied. So far, phylogenetic analysis has identified TBL genes in charophycean green algal species, although biochemical analysis of their recombinant gene products showed no acetyltransferase activity. This suggests that TBL proteins emerged in algae, but didn't recruit acetyltransferase activities until bryophytes appeared during the evolution of land plants [113]. Orthologs of RWA2 in *Arabidopsis* have been found, via sequence alignment, in two green algal species, *Chlorophyta* and *Charophyta*, [71]. AXY9 orthologs have not be identified in any green algae [72], indicating that the ancestral gene for RWA emerged before that of AXY9.

Mechanism of acetylation – from small molecules to natural polymers and proteins

Acetylation is a universal phenomenon that modifies the structures of diverse molecules, from proteins to metabolites and other small molecules in various species. In general, acetylation is the process of transferring an acetyl group from a donor to an acceptor molecule, forming a covalent bond involving atoms such as oxygen, nitrogen or sulfur depending on the chemical identity of the nucleophile (hydroxyl, amino or thiol group, respectively) in the acceptor molecule. This ubiquitous modification plays diverse and important biological roles in virtually every taxonomic species.

Acetylation of polysaccharides, polyphenolics and small molecules

Acetylation of certain organic chemicals in animals is crucial for maintaining a functional physiological system. For example, aralkylamine *N*-acetyltransferase (AANAT) plays an important process involved in conversion of serotonin to melatonin, which affects the day/night rhythm of human behavior and mood disorder [114, 115]. Choline *O*-acetyltransferase (ChAT) is responsible for generating the neurotransmitter, acetylcholine, which transfers signals between neurons and cells in glands and muscles [116]. In microbial organisms, chloramphenicol *O*-acetyltransferase catalyzes the attachment of an acetyl group to the antibiotic chloramphenicol, preventing it from binding to bacterial ribosomes. This detoxifies the drug, preventing it from inhibiting protein translation [117-119]. As a defense against attack by host organisms, *O*-acetylation of *N*-acetylmuramic acid (NAM) and *N*-deacetylation of *N*-acetylglucosamine (NAG) prevent the effective binding of lysozyme to bacterial cell wall peptidoglycan as a defense mechanism [120].

As discussed above, acetylation is also a widely observed substitution on many natural polymers, such as chitins, polyphenol lignin, and plant cell wall polysaccharides including pectic polysaccharides, xyloglucan, xylan and mannan [71, 121]. Enzymes involved in *O*-acetylation of plant cell wall polysaccharides share two consensus motifs, GDS and DxxH, which reside in the TBL domain and the Domain of Unknown Function 231 (DUF231), respectively. So far, 46 members of the plant-specific TBL/DUF231 protein family have been identified in *A. thaliana* (Figure 1.3) and 64 members have been identified in *P. trichocarpa*. TBL/DUF231 proteins have been reported to possess *O*-acetyltransferase activities specific for distinct polysaccharides in plant cell walls [31-33, 55, 83, 122-126]. The GDS and DxxH motifs are also conserved in the SGNH-hydrolase family, which is named for the strictly invariant sequence Ser-Gly-Asn-His present in the four conserved blocks (I, II, III and V, Figure 1.6) contained in these proteins [127, 128]. The SGNH-hydrolase family belongs to the GDSL superfamily of esterases and lipases [129], which share several common features such as a flexible active site and broad substrate specificities. The four consensus residues in SGNH hydrolases are all involved in catalysis. The catalytic Ser in block I (i.e., GD**S**) acts as a nucleophile that attacks the donor substrate. This process is facilitated by the His in block V (i.e., Dxx**H**), which acts as a general base that deprotonates the hydroxyl group on the Ser side chain. The Gly and Asn residues in block II and III serve as proton donors that contribute to the positive charge of the oxyanion hole, stabilizing the tetrahedral intermediate formed during the reaction. The Asp in the **D**xxH motif also contributes to catalysis by polarizing the catalytic His by forming a H-bond. Together with the catalytic Ser residue, this Asp residue forms a Ser-His-Asp catalytic triad that is present and utilized by all SGNH-hydrolase family members [127]. TBL/DUF231 proteins completely lack conserved blocks II and III found in SGNH proteins, but retain the Ser-His-Asp catalytic triad, and have been suggested to use a ping-

pong bi-bi/double displacement mechanism to catalyze *O*-acetylation on hemicellulosic polysaccharides [74].

Peptidoglycan *O*-acetylation in bacteria prevents their cell walls from being hydrolyzed by lysozymes produced by the host's innate immune system. A mechanism for peptidoglycan *O*-acetylation has been proposed based on a biochemical and structural study of OatA in *S. pneumoniae* [88]. OatA utilizes a ping-pong bi-bi mechanism to transfer the acetyl group from the donor to the C-6 position of the MurNAc in peptidoglycan according to the following process. First, the acetyl donor binds to OatA, which causes a conformational change such that the Asn491 is properly positioned in the oxyanion hole. H-bonds between the residues in the Ser-His-Asp catalytic triad then facilitate the nucleophilic attack of the carbonyl center of the acetyl donor by the Ser side-chain oxygen (Figure 1.7, i). The tetrahedral intermediate thus formed is stabilized by the backbone amide of the catalytic Ser438 and side-chain amide of Asn491 (Figure 1.7, ii). Formation of an acetyl-enzyme intermediate is facilitated by protonation of His571. After the deacetylated donor departs, a MurNAc residue of the peptidoglycan substrate binds to the OatA active site (Figure 1.7, iii and iv). The hydroxyl group at the 6-position of MurNAc is deprotonated by His571 (acting as a general base) generating a nucleophile that attacks the carbonyl center of the acetyl-enzyme intermediate to form a second tetrahedral intermediate (Figure 1.7, v and vi). Ser438 is then protonated by His571 (acting as a general acid) facilitating the formation and release of the 6-*O*-acetyl peptidoglycan product (Figure 1.7, vii).

Another ubiquitous polysaccharide in nature is chitin, which is composed of chains of β-1,4-linked GlcNAc. Chitin is widely present in fugal cell walls, exoskeletons of arthropods and certain structures in fish and invertebrates. The synthesis of chitin requires the formation of GlcNAc units, which involves *N*-acetylation of D-glucosamine-6-phosphate (GlcN-6-P). GlcN-6-

P *N*-acetyltransferase (EC 2.3.1.4) catalyzes this reaction using acetyl-CoA as the acetyl donor substrate [130]. This enzyme belongs to the Gcn5-related *N*-acetyltransferase (GNAT) superfamily along with certain lysine acetyltransferases that share a structurally conserved GNAT core involved in acetyl-CoA binding. Members of the GNAT family use a bi-bi catalytic mechanism wherein the enzyme forms a ternary complex with its substrates [131]. Although chitin comprises a minor portion of cell walls in *Saccharomyces cerevisiae*, the homologous enzyme involved in *N*-acetylating GlcN-6-P in this species was identified and designated GNA1 (GlcN-6-P *N*-acetyltransferase 1) [132]. The structure of GNA1 in *S. cerevisiae* has been described along with its proposed mechanism. Briefly, the electronegative carbonyl oxygen of the backbone of Asp134 enhances the nucleophilicity of the amino group of GlcN-6-P, facilitating attack of the carbonyl carbon of acetyl-CoA, resulting in the formation of a tetrahedral intermediate. The acidic hydroxyl group of Tyr143 then stabilizes the thiolate anion of the CoA as it leaves the catalytic pocket (Figure 1.8) [133]. Three residues, Glu98, Asp99 and Ile100, polarize the carbonyl bond in acetyl-CoA and contribute to formation of the oxyanion hole that stabilizes the tetrahedral intermediate. The crystal structure of a GNA1-CoA-GlcNAc6P ternary complex has been described, providing additional insight into the catalytic feature of this enzyme [133].

Lignin is another a distinctive class of cell wall polymers in plants and some red algae. This phenolic polymer is sometimes covalently cross-linked with other cell wall polysaccharides, providing hydrophobicity and rigidity required for water transport and upright growth. *O*-acetylation of lignin has been observed in both hardwoods and non-woody species [134-136], with acetyl groups frequently attached to the γ-position (or 9-position) on the sidechain of syringyl (3,5-dimethoxy-4-hydroxyphenyl) and guaiacyl (4-hydroxy-3-methoxyphenyl) units [137]. One study demonstrated that *O*-acetylation of monolignol precursors occurs before free-radical

polymerization to form lignin polymers [138]. Although lignin has been shown to be naturally acylated by acids other than acetic acid [139], the catalytic mechanisms of such acylation and the identities of the enzymes involved (if any) remain unclear. The physiological functions of lignin acetylation are also poorly understood.

Acetylation is also an important modification of many small biomolecules. As introduced above, aralkylamine *N*-acetyltransferase (AANAT) is an important enzyme involved in transferring an acetyl group from acetyl-CoA to the primary amine of serotonin. Methylation of the 5-hydroxy group of the product, *N*-acetylserotonin, is catalyzed by hydroxyindole-*O*-methyltransferase (HIOMT), to generate the circadian neurohormone melatonin [140]. AANAT also belongs to the GNAT superfamily, which contains a conserved acetyl-CoA binding region. The structure of AANAT in complex with a bisubstrate analog, coenzyme A-S-acetyltryptamine, has been reported along with a proposed mechanism [141], similar to that elucidated for other GNAT members, wherein the primary amino group of serotonin acts as a nucleophile that directly attacks the carbonyl carbon of acetyl-CoA. The neurotransmitter acetylcholine is generated when choline is *O*-acetylated by ChAT, an enzyme that uses a sequential 'hit-and-run' (Theorell-Chance) catalytic mechanism that does not result in accumulation of a ternary complex. The acetyl group is transferred directly to choline from acetyl-CoA, facilitated by an essential His that functions as a general acid/base in the catalytic cycle [142-144].

O-acetylation of the 3-hydroxyl group of chloramphenicol (CAM) prevents this drug from binding to bacterial ribosomes [145], functioning as an antibiotic-resistance mechanism used by microbes. The enzyme involved in *O*-acetylating CAM is chloramphenicol acetyltransferase (CAT; EC 2.3.1.28) [146], which transfers the acetyl group directly from acetyl-CoA to CAM. A key catalytic residue required for *O*-acetylation by CAT is a conserved His that deprotonates the

3-hydroxyl group of CAM. The resulting oxyanion attacks the carbonyl carbon of the thioester in acetyl-CoA [147-149] to initiate the acetyltransfer reaction.

Protein N-acetylation

Two major types of protein N-acetylation have been described. These are named N-terminal (Nt) acetylation (α-amino group) and lysine acetylation (ε-amino group), based on the amino acid that is acetylated. Such co- or post-translational protein modifications are crucial aspects of metabolism and gene expression in cell biology [150-153]. Nt acetylation is an irreversible modification catalyzed by Nt acetyltransferases (NATs). Nt is most often observed in eukaryotes, but a few cases have also been found in bacteria [154-156]. In contrast to Nt acetylation, lysine acetylation is reversible. Acetylation is catalyzed by lysine (K) acetyltransferases (KATs) These enzymes were previously called histone acetyltransferases (HATs) due to their initial discovery in the modification of histones [157, 158]. In recent years, it has been established that internal protein residues other than lysine can be acetylated. These include serine, threonine and histidine in some bacterial species [159-162].

KATs can be divided into different families according to their sequence homology, protein structures and functions. The KAT families include two major groups, GNAT and MYST (named for the founding members MOZ, Ybf2 (Sas3), Sas2 and Tip60) [150, 163], and other smaller groups such as p300/CBP, nuclear receptor coactivators, $TAF_{II}250$, TFIIIC, Rtt109, and CLOCK [164-167]. Different KAT families employ distinct strategies to catalyze acetylation of the ε-amino group of the target lysine. GNATs transfer an acetyl group directly from acetyl-CoA to the acceptor substrate through a bi-bi ternary complex mechanism [168]. The reaction can occur only after both

the donor and acceptor substrates are bound to GNAT. Usually, a catalytic glutamate residue (but sometimes Asp or Ser) is used as a general base to deprotonate the ε-amino group of the target lysine, to form a nucleophile that attacks the carbonyl carbon of the acetyl group of the enzyme-bound acetyl-CoA. The acetylated substrate is released, and the CoA thiolate is then protonated (often by a conserved Tyr or Ser at the active site) to facilitate release of the CoA product (Figure 1.9) [167-169].

ESA1 is a member of MYST protein family in yeast. This family also uses a ping-pong bi-bi mechanism to acetylate lysine residues in histones via a mechanism involving the formation of an acetyl-cysteine enzyme intermediate [170]. The catalytic cysteine (Cys304) that is acetylated is strictly conserved in the MYST family. The other conserved residue in the active site is Glu338, which is proposed to serve as a general base that sequentially deprotonates Cys304 and the ε-amino group of lysine to facilitate the first and second nucleophilic attacks of the mechanism, respectively [170]. Interestingly, it has been suggested that ESA1 can utilize a different bi-bi ternary complex mechanism when incorporated into a Piccolo NuA4 complex. In this case, the reaction is not as strongly dependent on catalytic Cys304, indicating that the same MYST protein can use distinct strategies to acetylate histones depending on the biochemical environment (i.e., free or incorporated into a physiologically relevant protein complex) [171].

Distinct from GNAT and MYST family members, p300/CBP transcriptional coactivator family has not been shown to employ a conserved glutamate residue as a general base for catalysis. Rather, structural analysis, combined with mutagenesis and kinetic studies of the homogeneous p300 domain, suggests that the conserved Tyr1467 acts as a general acid to catalyze acetylation [172]. Another strictly conserved residue in the p300/CBP KAT family is Trp1436, which is proposed to act as a guide, accurately positioning the target lysine in the active site [172]. The

structural and biochemical data also suggests a sequential Theorell-Chance catalytic mechanism for members of the p300/CBP family [172, 173]. The mechanisms of the rest of the KAT families are not well-established.

Nt acetylation is catalyzed by NATs. So far, six NATs, including NatA, NatB, NatC, NatD, NatE and NatF have been found to be conserved across eukaryotes. The first five of these NATs (A-E) are involved in co-translational protein modification and associate with ribosomes, whereas NatF is Golgi-associated and acetylates transmembrane proteins [174-176]. NatG is less conserved and localized in chloroplasts [177], while NatH has been recently identified and shown to specifically recognize and acetylate actins [178]. Each NAT has distinct substrate specificity and subunit composition, but all NATs contain catalytic subunits that belong to the GNAT family, sharing structural features common to the GNAT-domain[176].

Potential applications of xylan acetylation/deacetylation for biomass improvement

Xylan is the dominant hemicellulosic polysaccharide in secondary cell walls of dicot plants. It is covalently linked to lignin, forming a matrix that embeds cellulose fibrils. Due to its abundance and intimate contact with cellulose in the cell wall, xylan is a potential target for bioenergy crop modification to improve the saccharification efficiency and product yield for biofuel and bioproducts production. The acetyl moieties attached to xylans hinder xylanolytic enzymes from accessing their polysaccharide substrates during biomass processing, and thus reduce the overall rate of biomass hydrolysis [62]. Furthermore, acetates released from the biomass during the biomass pretreatment lower pH and thereby inhibit the growth of microbes, decreasing

the yield of fermentation products [69, 179, 180]. Therefore, modifying acetylation levels in xylans could be an important strategy to reduce biomass recalcitrance in biofuel industry.

Previous studies of post-synthetic modification of plant cell walls have been carried out by *in muro* expression of an acetyl xylan esterase (AXE) from *Aspergillus nidulans* in *Arabidopsis*. Increased esterase activity, along with a decrease in cell wall acetylation, were observed in transgenic lines, but these effects were not associated with significant changes in the yield of reducing sugars in biomass hydrolysates [181, 182]. More recently, an AXE protein from *Aspergillus niger* was expressed in *Arabidopsis*. When compared to the wild-type, the transgenic lines exhibited elevated esterase activity *in muro*, reduced xylan acetylation in plant tissues, and a 20% increase in sugar yield during enzymatic saccharification. This indicated that xylans in the transgenic lines are more susceptible to β-1,4-endoxylanase during saccharification, which resulted in a 70% increase in ethanol yield [183]. When the same approach was applied to hybrid aspen, similar results were obtained: transgenic lines exhibited lower xylan acetylation without decreasing plant growth and a 25% increase in glucose yield [184]. Another recent study produced a 27% increase in glucose yield during enzymatic saccharification of biomass from transgenic hybrid aspen expressing a Carbohydrate Esterase (CE) family 5 AXE from the fungus *Hypocrea jecorina* under the control of a wood-specific promoter [185]. The aforementioned studies suggest that heterologous expression of appropriate esterases in plants under the control of tissue-specific promoters and targeting of these enzymes to cell walls is a promising strategy to engineer lignocellulosic biomass to improve the saccharification for biofuel and bioproduct generation.

In addition to post-synthetic modification of xylan acetylation within the plant cell wall, direct regulation of the biosynthetic genes involved in xylan acetylation may provide another way to fine-tune acetyl content in biomass and reduce its recalcitrance. A previous study showed that

downregulation of four paralogous *RWA* genes through RNA interference (RNAi) in *Populus* decreased wood acetylation by 25% without affecting plant growth, resulting in increased glucose and xylose yields during enzymatic hydrolysis [186]. Interestingly, while reducing acetyl content in woody tissues can decrease recalcitrance, upregulation of the genes involved in *O*-acetylation of wall polysaccharides can also affect cell wall composition and promote saccharification. Overexpression of a *Populus deltoids* DUF231 protein, PdDUF231A, involved in xylan *O*-acetylation in this species showed not only an increase in acetylated xylan, but also higher transcript levels for cellulose-biosynthesis genes. These, in turn, led to higher glucose and cellulose content in the transgenic plants and improved the rate of glucose release during enzymatic saccharification [187].

Goals of this work

Although enzymatic acetylation is a universal modification observed in diverse molecules across a broad range of species, little is known about the structural features and catalytic mechanisms of the enzymes involved in cell wall polysaccharide *O*-acetylation *in planta*. The primary goal of this work is to gain more detailed understanding of the structures, functions and catalytic mechanisms of the acetyltransferases involved in xylan *O*-acetylation. Chapter 2 describes the structure, substrate specificity and regiospecificity of XYLAN *O*-ACETYLTRANSFERASE 1 (XOAT1), which is highly expressed during secondary cell wall formation in *Arabidopsis*. Through X-ray crystallography, the three-dimensional structure of XOAT1 is reported, representing the first protein structure that has been determined for a member of the plant TBL family of polysaccharide *O*-acetyltransferases. These data, together with the results of site-directed mutagenesis (SDM) of the catalytic residues in XOAT1, resulted in a

proposed mechanism for the acetyl transfer reaction catalyzed by the TBL enzymes. Chapter 3 describes a continuing study of XOAT1 in which we carried out molecular docking and molecular dynamics (MD) simulations to evaluate enzyme-substrate binding modes to identify key residues involved in acceptor substrate binding and catalysis. Chapter 4 focuses on another xylan acetyltransferase, TRICHOME BIREFRINGENCE-LIKE 3 (TBL3), that is phylogenetically close to XOAT1. We present the results of *in vitro* assays showing that TBL3 is distinct from XOAT1 in its donor substrate specificity. Specifically, we show that TBL3 is able to transfer acetyl groups from one xylan substrate to another, acting as a transacetylase. I hope that my research will shed light on the mechanisms and other essential features of *O*-acetylation of cell wall polysaccharides *in planta*, and promote new routes to generate modified lignocellulosic feedstocks for applications in biomass-based industries.

Figure 1.1

Structures of glucuronoxylan from poplar (a), glucuronoarabinoxylan from switchgrass (b) and arabinoglucuronoxylan from spruce (c). (Adapted from ref. [8])

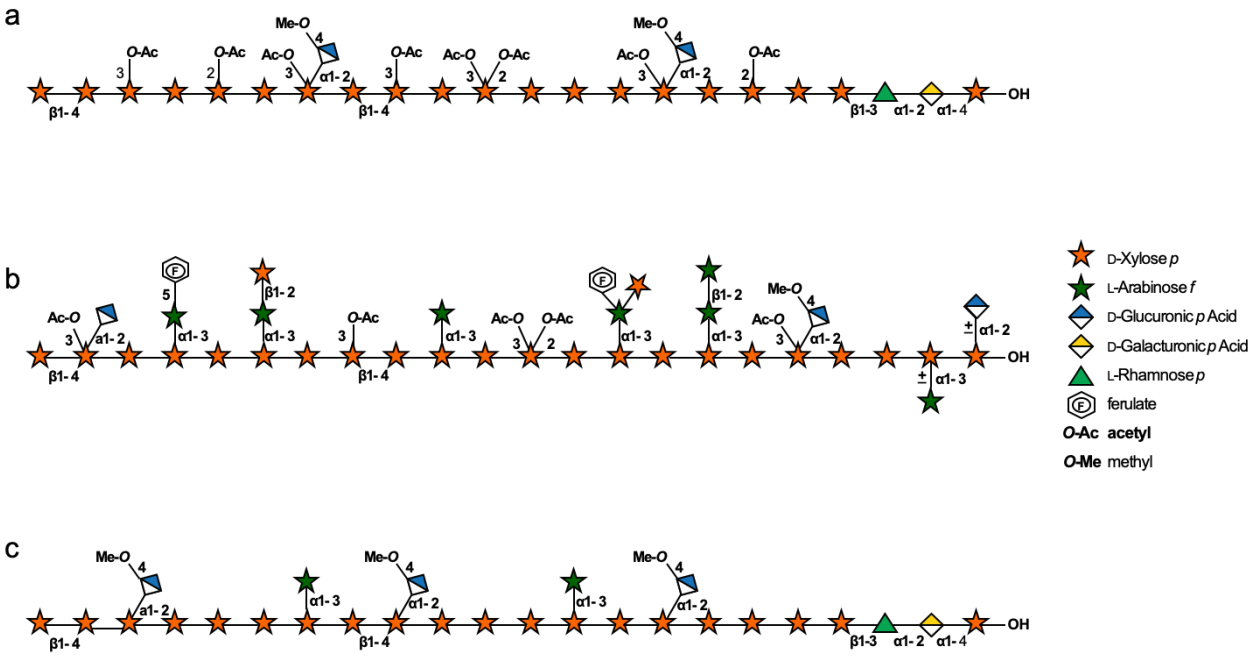
a
b
c
Me-O
O-Ac
Ac-O
β1-4
α1-2
α1-3
β1-2
β1-3
α1-4
OH
D-Xylose p
L-Arabinose f
D-Glucuronic p Acid
D-Galacturonic p Acid
L-Rhamnose p
ferulate
O-Ac acetyl
O-Me methyl

Figure 1.2

Scheme of acetyl group migration and hydrolysis in the acetylated 1-*O*-methyl-α-D-mannopyranoside. (Sourced from ref. [19])

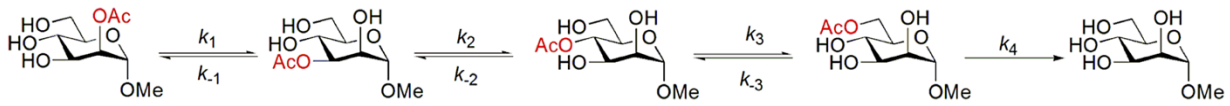
HO
OAc
HO
HO
O
OMe
k_1
k_{-1}
HO
OH
HO
AcO
O
OMe
k_2
k_{-2}
HO
OH
AcO
HO
O
OMe
k_3
k_{-3}
AcO
OH
HO
HO
O
OMe
k_4
HO
OH
HO
HO
O
OMe

Figure 1.3

Phylogenetic analysis of Arabidopsis TBL protein family. Biochemically characterized substrate specificities of the TBLs are colored and labeled. XOAT1 and TBL3 in the xylan-specific subclade studied in this research are marked with red asterisks. The phylogenetic tree was built with UPGMA (Unweighted Pair Group Method using Arithmetic averages) algorithm, and the 0.2 scale represents 20% differences between two sequences.

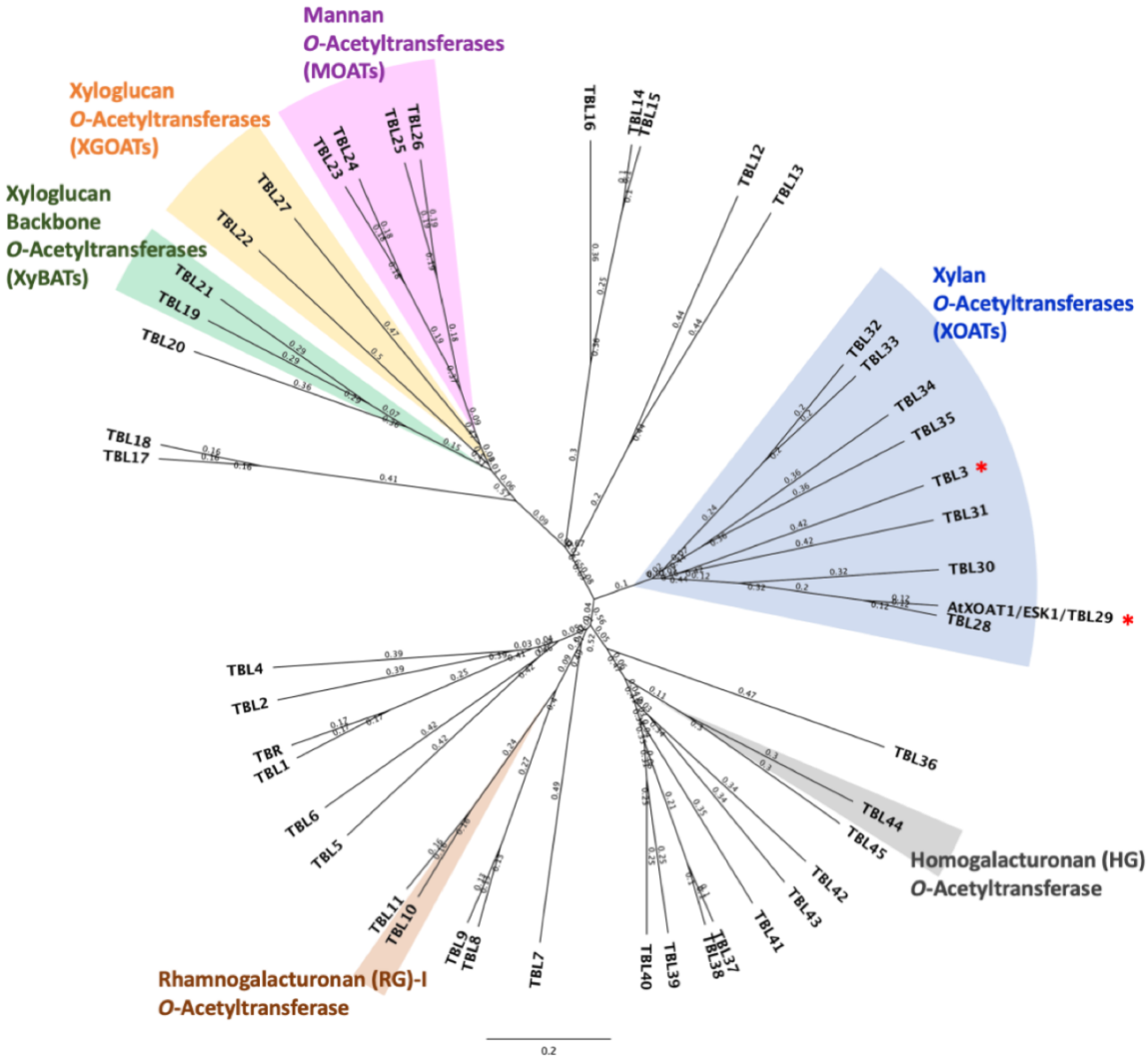
Mannan
O-Acetyltransferases
(MOATs)
Xyloglucan
O-Acetyltransferases
(XGOATs)
Xyloglucan
Backbone
O-Acetyltransferases
(XyBATs)
Xylan
O-Acetyltransferases
(XOATs)
Homogalacturonan (HG)
O-Acetyltransferase
Rhamnogalacturonan (RG)-I
O-Acetyltransferase
TBL16
TBL14
TBL15
TBL12
TBL13
TBL26
TBL25
TBL24
TBL23
TBL27
TBL22
TBL21
TBL19
TBL20
TBL18
TBL17
TBL32
TBL33
TBL34
TBL35
TBL3 *
TBL31
TBL30
AtXOAT1/ESK1/TBL29 *
TBL28
TBL4
TBL2
TBR
TBL1
TBL6
TBL5
TBL36
TBL44
TBL45
TBL42
TBL43
TBL41
TBL37
TBL38
TBL39
TBL40
TBL7
TBL9
TBL8
TBL11
TBL10
0.2

Figure 1.4

Hypothetical model for the machinery of plant cell wall polysaccharide *O*-acetylation. RWA is proposed as a translocator to transport an acetyl donor from cytoplasm into the Golgi lumen; AXY9 is suggested to be an intermediate that provides the acetyl source to TBLs to catalyze *O*-acetylation on specific cell wall polysaccharides.

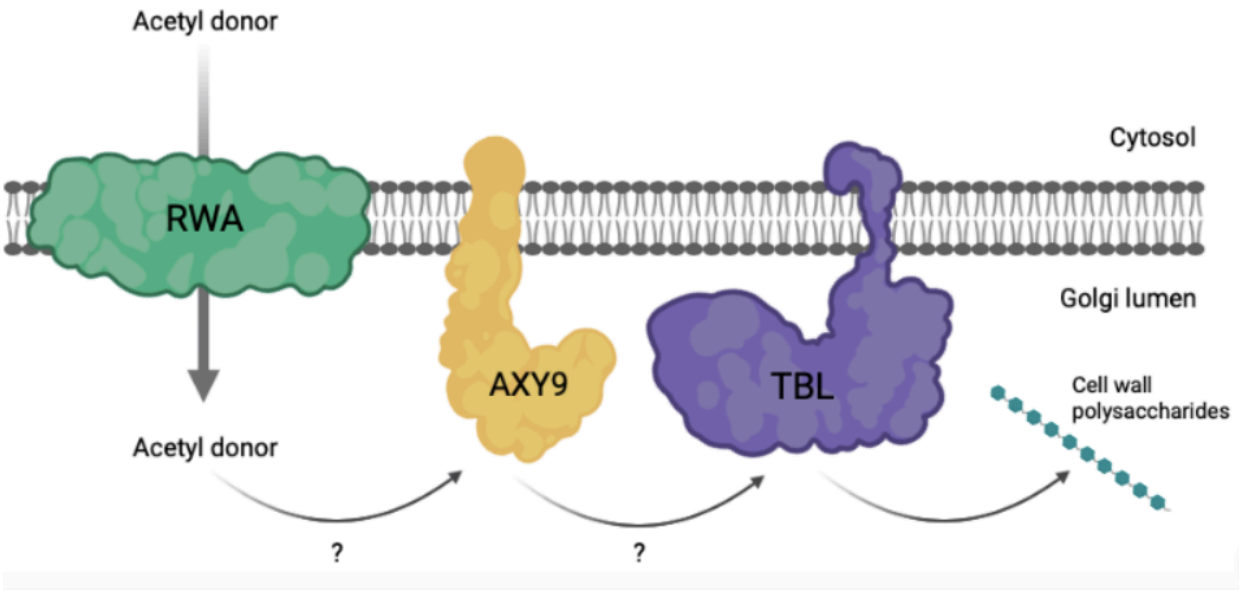
Acetyl donor
Cytosol
RWA
Golgi lumen
AXY9
TBL
Cell wall
polysaccharides
Acetyl donor
?
?

Figure 1.5

Orthologs of TBL proteins and the proposed models for the mechanism of wall polysaccharide *O*-acetylation in various organisms. Multi-transmembrane proteins that are possibly involved in translocating acetyl donors across membranes are shown as yellow ovals; Membrane-localized proteins containing a single transmembrane domain are shown as blue ovals; GDS and DxxH motifs in the TBL and DUF231 catalytic domains, respectively, are shown in red squares. (Sourced from ref. [71])

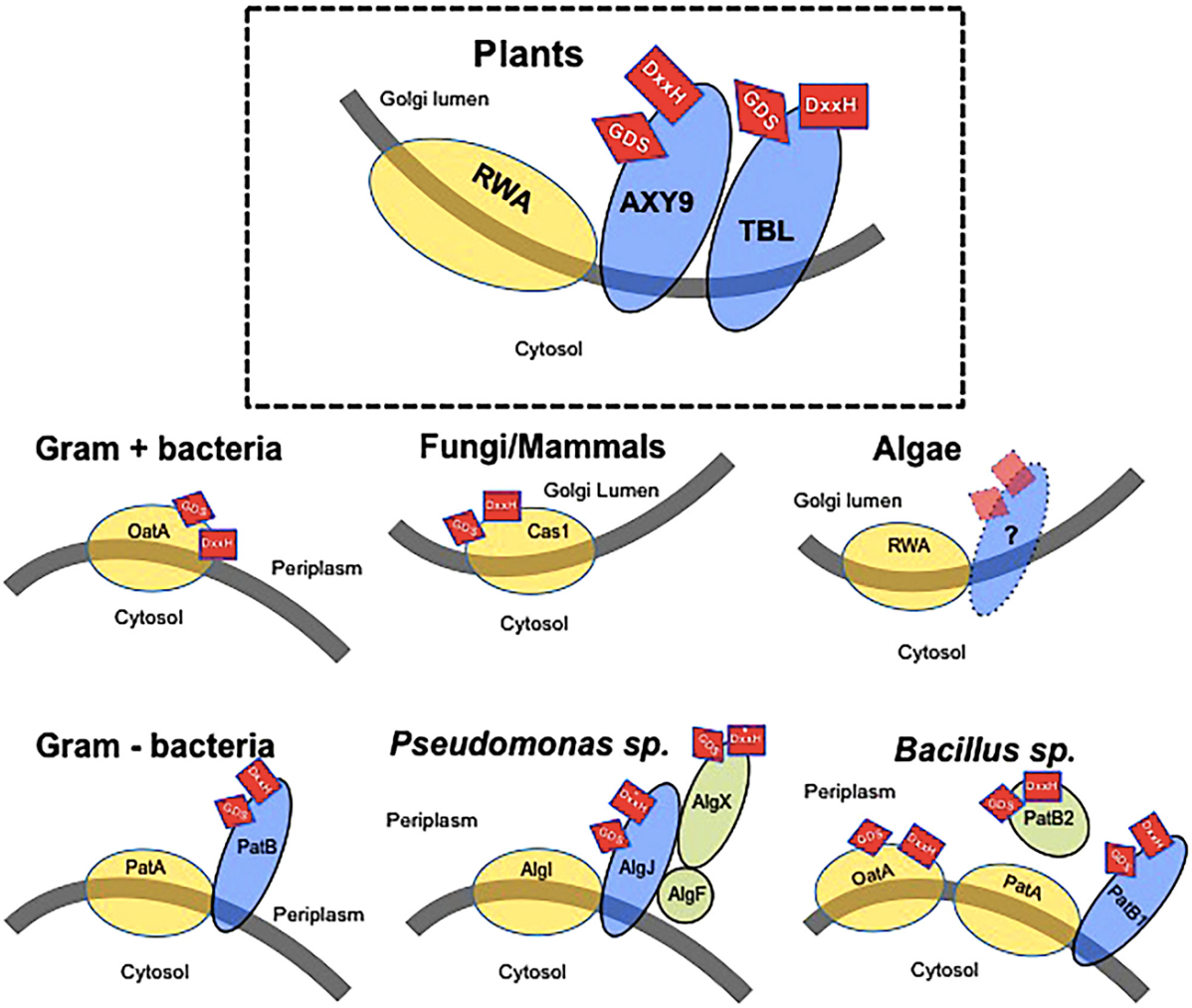
Plants
Golgi lumen
DxxH
GDS
GDS
DxxH
RWA
AXY9
TBL
Cytosol
Gram + bacteria
OatA
Periplasm
Cytosol
Fungi/Mammals
Golgi Lumen
Cas1
Cytosol
Algae
Golgi lumen
RWA
?
Cytosol
Gram - bacteria
PatA
PatB
Periplasm
Cytosol
Pseudomonas sp.
Periplasm
AlgI
AlgJ
AlgX
AlgF
Cytosol
Bacillus sp.
Periplasm
OatA
PatA
PatB2
PatB1
Cytosol

Figure 1.6

Amino acid sequence alignment showing the conserved blocks Ⅰ, Ⅱ, Ⅲ and Ⅴ in the SGNH-hydrolase family. The catalytic triad-forming residues are indicated by red-filled down triangles, while the oxyanion hole residues are indicated by blue-filled circles. The putative residues specific for acid moiety are labeled with magenta triangles. (TAP, *Escherichia coli* thioesterase I; PAF-AH, bovine brain platelet-activating factor acetylhydrolase; RGAH, *Aspergillus aculeatus* rhamnogalacturonan acetylesterase; SsEst, *Streptomyces scabies* esterase; EtpA, *Vibrio mimicus* arylesterase; GCAT, *Aeromonas hydrophila* lipase/acyltransferase; EstA, *Lactobacillus helveticus* CNRZ32 arylesterase; Sourced from ref. [128])

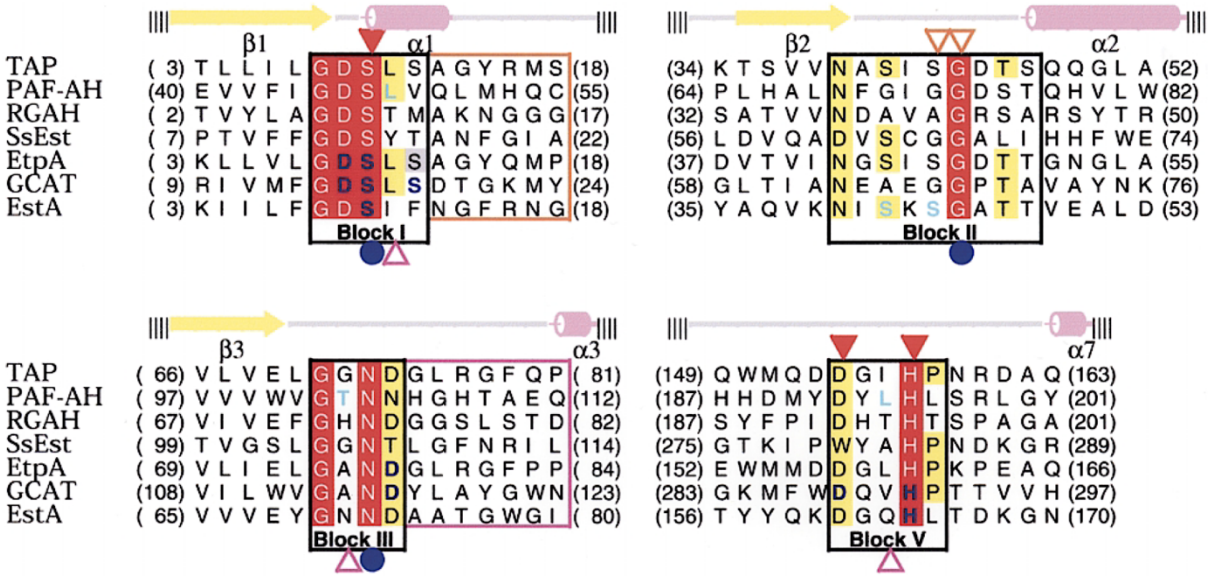
β1
α1
TAP (3) T L L I L G D S L S A G Y R M S (18)
PAF-AH (40) E V V F I G D S L V Q L M H Q C (55)
RGAH (2) T V Y L A G D S T M A K N G G G (17)
SsEst (7) P T V F F G D S Y T A N F G I A (22)
EtpA (3) K L L V L G D S L S A G Y Q M P (18)
GCAT (9) R I V M F G D S L S D T G K M Y (24)
EstA (3) K I I L F G D S I F N G F R N G (18)
Block I
β2
α2
(34) K T S V V N A S I S G D T S Q Q G L A (52)
(64) P L H A L N F G I G G D S T Q H V L W (82)
(32) S A T V V N D A V A G R S A R S Y T R (50)
(56) L D V Q A D V S C G G A L I H H F W E (74)
(37) D V T V I N G S I S G D T T G N G L A (55)
(58) G L T I A N E A E G G P T A V A Y N K (76)
(35) Y A Q V K N I S K S G A T T V E A L D (53)
Block II
β3
α3
TAP (66) V L V E L G G N D G L R G F Q P (81)
PAF-AH (97) V V V WV G T N N H G H T A E Q (112)
RGAH (67) V I V E F G H N D G G S L S T D (82)
SsEst (99) T V G S L G G N T L G F N R I L (114)
EtpA (69) V L I E L G A N D G L R G F P P (84)
GCAT (108) V I L WV G A N D Y L A Y G WN (123)
EstA (65) V V V E Y G N N D A A T G WG I (80)
Block III
α7
(149) Q WM Q D D G I H P N R D A Q (163)
(187) H H D M Y D Y L H L S R L G Y (201)
(187) S Y F P I D H T H T S P A G A (201)
(275) G T K I P WY A H P N D K G R (289)
(152) E WM M D D G L H P K P E A Q (166)
(283) G K M F WD Q V H P T T V V H (297)
(156) T Y Y Q K D G Q H L T D K G N (170)
Block V

Figure 1.7

Proposed ping-pong bi-bi mechanism of peptidoglycan *O*-acetylation catalyzed by OatA.

(Sourced from ref. [88])

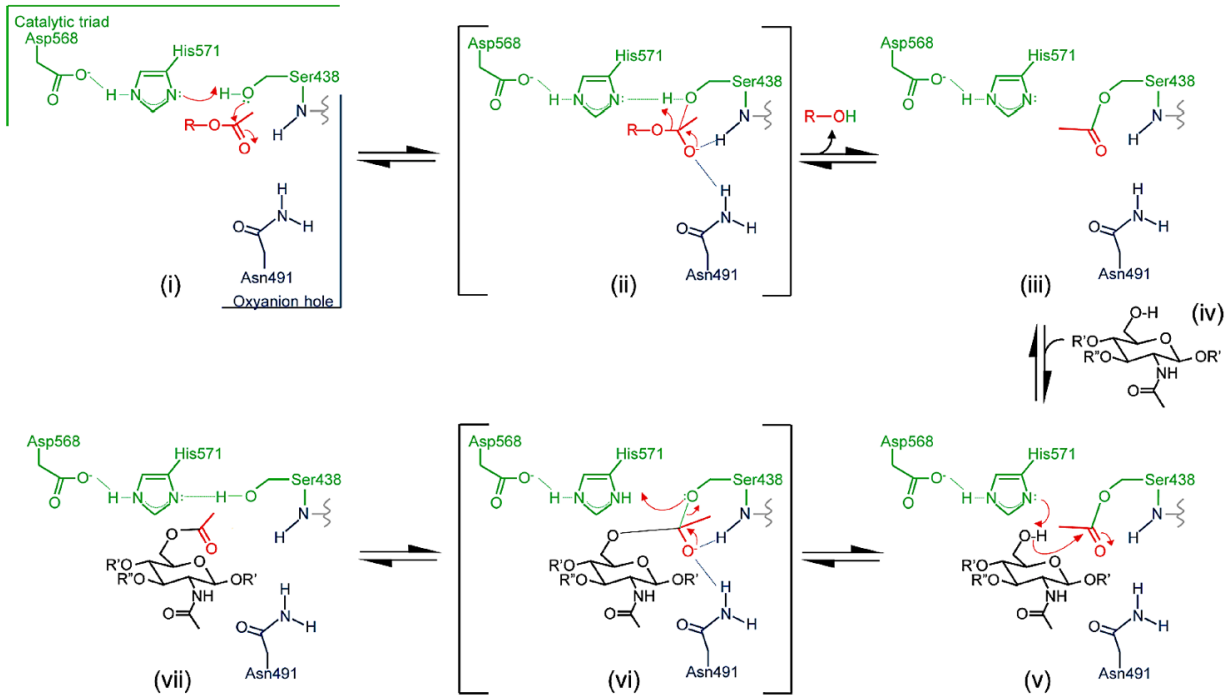
Catalytic triad
Asp568
His571
Ser438
Asn491
Oxyanion hole
(i)
(ii)
(iii)
(iv)
(v)
(vi)
(vii)
R—OH

Figure 1.8

Scheme of the proposed GNA1 catalytic mechanism. (Sourced from ref. [133])

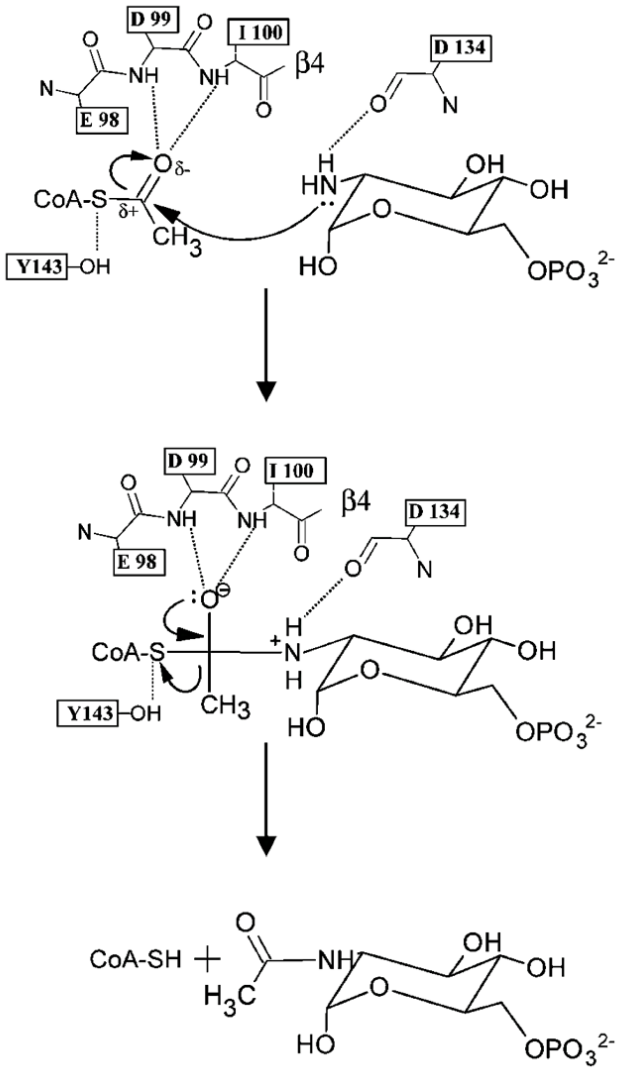
D 99
I 100
β4
D 134
E 98
CoA-S
δ-
δ+
CH3
Y143–OH
HO
OH
OPO3 2-
CoA-SH
H3C

Figure 1.9

Ternary complex mechanism of *N*-acetylation used by the GNAT family members. (Sourced from ref. [167])

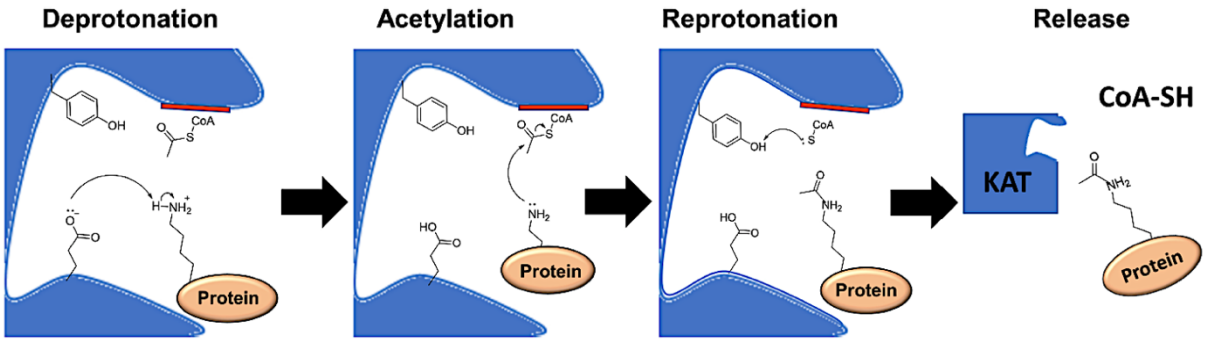
Deprotonation
Acetylation
Reprotonation
Release
CoA-SH
KAT
Protein
Protein
Protein
Protein

CHAPTER 2

MOLECULAR MECHANISM OF POLYSACCHARIDE ACETYLATION BY THE ARABIDOPSIS XYLAN *O*-ACETYLTRANSFERASE XOAT1

Hsin-Tzu Wang[*], Vladimir V. Lunin[*], Vivek S. Bharadwaj[*], Markus Alahuhta[*], Maria J. Peña, Jeong Yeh Yang, Stephanie A. Archer-Hartmann, Parastoo Azadi, Michael E. Himmel, Kelley W. Moremen, William S. York, Yannick J. Bomble, and Breeanna R. Urbanowicz. Plant Cell. 2020 July; 32(7):2367-2382. ([*]Co-first author) Reprinted here with permission of publisher.

Abstract

Xylans are a major component of plant cell walls. *O*-Acetyl moieties are the dominant backbone substituents of glucuronoxylan in dicots and play a major role in the polymer-polymer interactions that are crucial for wall architecture and normal plant development. Here, we describe the biochemical, structural, and mechanistic characterization of Arabidopsis (*Arabidopsis thaliana*) xylan *O*-acetyltransferase 1 (XOAT1), a member of the plant-specific Trichome Birefringence Like (TBL) family. Detailed characterization of XOAT1-catalyzed reactions by real-time NMR confirms that it exclusively catalyzes the 2-*O*-acetylation of xylan, followed by nonenzymatic acetyl migration to the *O*-3 position, resulting in products that are monoacetylated at both *O*-2 and *O*-3 positions. In addition, we report the crystal structure of the catalytic domain of XOAT1, which adopts a unique conformation that bears some similarities to the $\alpha/\beta/\alpha$ topology of members of the GDSL-like lipase/acylhydrolase family. Finally, we use a combination of biochemical analyses, mutagenesis, and molecular simulations to show that XOAT1 catalyzes xylan acetylation through formation of an acyl-enzyme intermediate, Ac-Ser216, by a double displacement bi-bi mechanism involving a Ser-His-Asp catalytic triad and unconventionally uses an Arg residue in the formation of an oxyanion hole.

Introduction

The plant cell wall provides a structural scaffold that surrounds each plant cell, defining the size and shape of the resultant cells and tissues. The plant cell wall is a composite material comprised of cellulose microfibrils, hemicellulosic polysaccharides, pectins, proteins, glycoproteins, and aromatic molecules (including lignins). Xylans are one of the most abundant plant polysaccharides on earth and are hence considered to be key targets for biomass modification to enhance the production of biofuels, bioproducts, and biomaterials [1]. Most cell wall polysaccharides, with the exception of (1,3;1,4)-β-glucan and cellulose, are *O*-acetylated [2]. All xylans produced by vascular plants are substituted with glycosyl, or acyl groups on an identical backbone structure composed of 1,4-linked β-D-xylopyranosyl (Xyl) residues. The nature and pattern of these substituents vary depending on the plant tissue and species [1]. For example, in dicots, *O*-acetylated glucuronoxylan (AcGX) is the most abundant hemicellulosic polysaccharide, whose backbone is substituted with 1,2-linked α-D-glucuronic acid (GlcA) and/or its 4-*O*-methyl derivative (MeGlcA). Approximately 60% of the backbone residues are *O*-acetylated, making it the most abundant substituent of xylan. More detailed analysis of xylan acetylation in Arabidopsis (Col-0) showed that 44% of the Xyl residues are monoacetylated at *O*-2 or *O*-3, 6% are bisubstituted at both *O*-2 and *O*-3, and approximately 75% of the (Me)GlcA substituted backbone residues are also acetylated at the *O*-3 position [3]. Furthermore, MS/MS analysis of enzymatically released neutral xylooligosaccharides revealed acetyl residues are present on every alternate Xyl along the backbone, while a similar systematic, alternating patterning of (Me)GlcA and acetyl moieties is also observed on the released acidic xylooligosaccharides [3]. This data suggests that acetylation may play a key role in the systematic addition of substituents along the polymer backbone.

While the specific structural and biological roles of polysaccharide acetylation in the plant cell wall remain unclear, *O*-acetylation is thought to be a determinant of AcGX hydrophobicity, partially dictating interactions between xylan and other wall polymers, including cellulose and lignin [4, 5]. For example, the presence of *O*-acetyl substituents decreases adsorption of xylan to cellulosic surfaces, indicating that xylan-cellulose and xylan-lignin interactions could be modulated by the degree and patterning of substituents [6, 7]. The effect of acetylation patterning on xylan interactions is unknown, but a similar pattern can be found in xylans from the primary cell wall of grasses, which are heavily substituted with arabinosyl residues at *O*-2 or *O*-3 or at both *O*-2 and *O*-3 [1]. Recent studies on Populus genotypes with different cell wall compositions suggest that there is a close interaction between lignin and xylan, and that the degree of xylan acetylation influences the interaction between these major cell wall polymers, thus impacting pretreatment efficiencies [4]. Furthermore, acetyl groups might sterically hinder some hydrolytic enzymes, and thus decrease the accessibility of those enzymes to their polysaccharide targets [8]. Taken together, it is evident that xylan acetylation affects cell wall architecture and mechanical strength. Therefore, insights into acetylation mechanisms in plants form the basis for a deeper understanding into the interplay between polysaccharide primary structure and cell wall architecture, growth, and development. Advances in this area may be used to overcome biomass recalcitrance to enzymatic saccharification, leading to the development of improved design schema for engineering efforts or targeted genomics approaches for the conversion of cell wall rich plant biomass into sustainable bioproducts.

Until recently, little was known about the process of plant cell wall polysaccharide *O*-acetylation. Despite the importance of this modification in both cell wall structure and organization, the identity of the acetyl donor substrates or the existence of donor intermediates and

the exact roles of many of the proteins involved in polysaccharide acetylation remain unknown. So far, it has been shown that at least four protein families are involved in the acetylation pathway in plants, including the TRICHOME BIREFRINGENCE-LIKE (TBL) protein family, REDUCED WALL ACETYLATION (RWA) proteins [9], the ALTERED XYLOGLUCAN 9 (AXY9) protein [10], and a newly described GDSL acetylesterase family [2].

Members of the TBL family have been shown to function as polysaccharide *O*-acetyltransferases and catalyze *O*-acetylation of specific cell wall polymers [11-15]. ESKIMO1/TBL29 (At3g55990) is one of the most well characterized members of this family. Mutation of this gene in Arabidopsis (*eskimo1*, *tbl29-1*, *tbl29-2*) results in plants that produce xylan with 50-60% less *O*-acetylation, have collapsed xylem vessels [16, 17], that are tolerant to salt, drought and freezing stresses. Our earlier studies on this enzyme provided direct biochemical evidence showing that TBL29/ESK1 is an xylan specific *O*-acetyltransferase that catalyzes the addition of *O*-acetyl groups to the 2-position of xylosyl backbone residues *in vitro*, establishing the precise molecular function of this enzyme [18], and lead to the proposed name XYLAN *O*-ACETYLTRANSFERASE 1 (XOAT1). Recently, an eloquent report by Grantham and coworkers showed that the even pattern of xylan acetylation is absent in the *esk1* mutant, indicating that AtXOAT1 is necessary for patterning of acetyl esters on xylan in *Arabidopsis* [19]. Since the initial biochemical analysis of AtXOAT1, several other members of the TBL family have also been shown to play a role in the regiospecific acetylation of xylan in Arabidopsis, including TBL3 (XOAT4), TBL28 (XOAT2), TBL30 (XOAT3), TBL31 (XOAT5), TBL32 (XOAT6), TBL33 (XOAT7), TBL34 (XOAT8), and TBL35 (XOAT9) [11-13, 20].

In plants, acetyl-CoA cannot readily cross membranes and is independently produced in plastids, mitochondria, peroxisomes and the cytosol, but not in the Golgi apparatus. Members of

the RWA family function non-specifically in polysaccharide *O*-acetylation at a biosynthetic step prior to TBLs and have been proposed to transport an activated form of acetate into the Golgi using cytosolic acetyl-CoA pools [9]. However, no known polysaccharide *O*-acetylating systems, including RWA, OatA, and AlgI have been shown to function as acetyl-CoA transporters (recently reviewed by [2, 21]. Currently, they are proposed to function by translocating acetyl groups derived from cytosolic acetyl-CoA or an unknown donor in both plants and microbes, but not acetyl-CoA itself, across membranes [21].

Understanding the precise function of enzymes involved in plant polysaccharide biosynthesis, including glycosyltransferases, acetyltransferases, and methyltransferase at the molecular level is essential for gaining fundamental insight into how these biocatalysts work together to build architecturally complex structures such as the cell wall. Structural information of enzymes involved in polysaccharide biosynthesis, especially those involved in the addition of methyl and acetyl substituents present in plant cell wall polysaccharides, are completely absent in structural databases despite their significant roles in plant growth and development. Recently, mammalian cell expression has been successfully used to express plant glycosyltransferases involved in xyloglucan biosynthesis in sufficient quantities for structural and biochemical characterization, including *Arabidopsis thaliana* FUCOSYLTRANSFERASE 1 (AtFUT1) and XYLOGLUCAN XYLOSYLTRANSFERASE (AtXXT) [22, 23]. Herein, we applied this strategy for structural characterization of the xylan *O*-acetyltransferase AtXOAT1. We showed that the structure of AtXOAT1 is characterized by a deep cleft on the surface of the protein separating the molecule into two unequal lobes and a Ser216-His465-Asp462 catalytic triad is located at the bottom of this cleft. Molecular simulations of AtXOAT1 in its substrate bound states and

experimental characterization of the acyl-enzyme intermediate provide evidence for a double-displacement mechanism.

Results and Discussion

Biochemical Insights into XOAT1 Catalysis

Members of the plant-specific DOMAIN OF UNKNOWN FUNCTION (DUF) 231 family, also referred to as the TRICHOME BIREFRINGENCE-LIKE (TBL) family are Golgi-localized polysaccharide O-acetyltransferases [2]. AtXOAT1 is comprised of a single NH_2-terminal transmembrane (T) domain followed by an NH_2-terminal variable region (NV), an N-terminal Cys-rich PMR5 domain (PF14416) that is part of the plant-specific TBL region, the DUF231 domain, and contains six predicted N-glycosylation sites (Fig. 2.1a). Previously, we developed a mass spectrometry (MS)-based xylan *O*-acetyltransferase assay (Fig. 2.1b) using acetyl-CoA as the acetyl donor and 2-aminobenzamide β-1,4-xylohexaose (Xyl_6-2AB) to study enzymes involved in polysaccharide O-acetylation *in vitro* [24]. The peptidoglycan O-acetyltransferase from *Neisseria gonorrhoeae* PatB and the secondary cell wall polysaccharide *O*-acetyltransferase from *Bacillus cereus* PatB1 were recently shown to display donor substrate promiscuity and utilize chromogenic acetyl-donor substrates *in vitro* [21, 25]. To determine whether other activated acetyl substrates may function as donor substrates for AtXOAT1, we performed *in vitro* xylan acetylation reactions to compare the ability of *p*-nitrophenyl acetate (*p*NP-Ac), acetylsalicylic acid (ASA), acetyl-CoA and 4-methylumbelliferylacetate (4MU-Ac) to function as donor substrates for AtXOAT1. Matrix-assisted laser desorption ionization time-of-flight mass spectrometry (MALDI-TOF MS) analysis of the reaction products indicated that recombinant AtXOAT1 catalyzes the transfer of *O*-

acetyl moieties from all four substrates to Xyl_6-2AB. Compared to acetyl-CoA, *p*NP-Ac, ASA and 4MU-Ac all serve as better donor substrates *in vitro* (Fig. 2.1c). This is consistent with a recent report by Ye and colleagues that was published during the preparation of this manuscript [26].

The preference for non-acetyl-CoA co-substrates is consistent with what was observed for PatB [27], and calls into question the identity of the natural acetyl donors for this enzyme family in planta. However, the observation that AtXOAT1 is able to utilize surrogate compounds as donor substrates facilitated the development of an *in vitro* xylan acetyltransferase assay utilizing the chromogenic acetyl donor *p*NP-Ac, adapted from methods described for bacterial polysaccharide acetyltransferases [21]. We performed spectrophotometric assays to evaluate the *O*-acetyltransferase activity of AtXOAT1 by using *p*NP-Ac as a donor substrate together with increasing concentrations of xylopentaose (Xyl_5) as an acceptor to validate our assays (Fig. S2.1). The release of *p*NP increased in parallel with the concentration of Xyl_5 added to the reactions, indicating that the presence of Xyl_5 facilitates the activity of AtXOAT1 as a xylan O-acetyltransferase and confirmed that this is an efficient method to determine the biochemical properties of xylan acetyltransferases. Next, we evaluated the ability of AtXOAT1 to use xylobiose and xylooligosaccharides with degrees of polymerization (DP) from two to six as acceptors, and showed that xylotriose is the smallest acceptor that AtXOAT1 is able to *O*-acetylate (Fig. S2.2), consistent with prior biochemical analyses of AtXOAT1 using ^{14}C-labeled acetyl-CoA [13].

AtXOAT1 O-acetylates xylan through the formation of a covalent acetyl-enzyme intermediate

To determine whether an acyl-enzyme intermediate is formed during the reaction, we incubated different donors with AtXOAT1 in the absence of acceptor. The enzyme was then

digested by trypsin and the fragments analyzed by LC-MS/MS. The obtained peptides containing Ser216 (210-MMFVGD**S**LNR-219) appeared as a mixture of the acetylated and unmodified peptides with a difference in molecular weight of 42 Da (shifted by m/z 21 for the doubly charged ion where z = 2; Fig. S2.3) corresponding to an attachment of an acetyl group. The sequences of the peptides were mapped by MS/MS analysis, confirming that the Ser216 was the acetylation site, as shown in the higher energy collisional dissociation (HCD) fragmentation spectra (Fig. S2.4). Further analysis of the peak areas of the extracted ion chromatographs (XIC) indicated that about 59% of the acetylated peptide population was formed when acetyl-CoA was used as a donor substrate for AtXOAT1, while 73%, 74% and 83% of peptide populations were acetylated when *p*NP-Ac, ASA and 4MU-Ac were used as donors, respectively (Fig. 2.1d). It is worth noting that the preferential donor substrates for AtXOAT1, revealed by quantification of the formation of the acyl-enzyme intermediates, is consistent with MALDI-TOF MS analysis of the products of the *in vitro* assays (Fig. 2.1c), revealing that acetyl-CoA is the least preferred donor for AtXOAT1 catalysis. Furthermore, the formation of an acetyl-enzyme intermediate at S216 suggested a double displacement mechanism for AtXOAT1-catalyzed acetyl transfer.

AtXOAT1 is an obligate 2-O-acetyltransferase

The spontaneous migration of acetyl groups has been proven to occur on xylooligosaccharides between the *O*-2 and *O*-3 positions of xylosyl backbone residues [28], and can even rapidly migrate to position 4 on the non-reducing end [29]. This makes it difficult to examine the regiospecificity of *O*-acetyltransferases by solely analyzing the products after the reaction is completed [13]. Therefore, the interpretation of data regarding polysaccharide acetylation can be difficult, and it is unclear whether equilibrium conditions observed are present

in the native plant polysaccharide itself or are established during isolation procedures. Indeed, Kabel et al. have specifically shown that freeze-drying and/or re-dissolving the isolated material promotes acetyl migration on xylooligosaccharides, confirming that the position and distribution of *O*-acetyl moieties cannot be extrapolated to the xylan structures present in the plant. Hence, the phenomenon of acetyl migration complicates determining the enzymatic regiospecificity of AtXOAT1 [28]. In order to unambiguously confirm the regiospecificity of these enzymes, we developed an experimental approach that can rapidly monitor spontaneous changes in the product during catalysis and after product formation. In these assays, we measured product formation 10 min after the enzyme is functioning in real time at 30 min intervals (Fig. 2.1e and f), confirming that the enzyme is an obligate 2-*O*-acetyltransferase. Studies by Ye et al. relied on measuring the final product after long reaction times (16 hrs), which would be highly affected by spontaneous migration [13].

The migration phenomenon of acyl groups and the regiospecificity of acetylesterases have been widely observed and studied [28-31]. AtXOAT1-catalyzed *O*-acetylation of xylohexaose (Xyl_6) was monitored by real-time 1H NMR (RT-NMR) spectroscopy using an optimized protocol to effectively control the pH of the reaction (Fig. 2.1e), and showed that the resonance of the methyl protons of the acetyl groups attached to the *O*-2 position (δ 2.176) appeared at the beginning and dominated throughout the incubation period, confirming that AtXOAT1 catalyzes *O*-acetylation at the *O*-2 position of xylosyl backbone residues. This is a similar trend that we reported in our previous study [18]. The resonance corresponding to 3-*O*-acetyl groups (δ 2.160) showed up after the appearance of that corresponding to the 2-*O*-acetyl resonance, suggesting acetyl group migration possibly occurred in xylopyranose units. To confirm that the acetyl group migration occurring in our reactions is driven by a non-enzymatic mechanism, enzymatic reactions

were allowed to proceed for 6 hrs (bold red line), then AtXOAT1 was removed using a spin filter and the intensities of resonances corresponding to 2-*O* and 3-*O*-acetyl groups were continuously monitored by RT-NMR spectroscopy for an additional 14 hrs (Fig. 2.1f). In contrast to the spectra obtained during the AtXOAT1-catalyzed reaction, a decrease of the resonance of 2-*O*-acetyl groups was observed in parallel to an increase of that of the 3-*O*-acetyl moieties, indicating that spontaneous migration of acetyl groups from the *O*-2 to *O*-3 position occurred after AtXOT1-catalyzed addition of acetyl groups to the *O*-2 position. These results unambiguously confirm the regiospecificity of AtXOAT1 *in vitro* by minimizing the confounding effects of spontaneous acetyl group migration.

Crystal structure reveals atomistic architecture of AtXOAT1

Three truncated forms of AtXOAT1 were generated as fusion proteins containing an NH_2-terminal signal sequence followed by an 8xHis tag, an AviTag, 'superfolder' GFP, and the Tobacco Etch Virus (TEV) protease recognition site followed by truncated coding regions of AtXOAT1 (Fig. S2.5a and b). One construct was designed with a truncation devoid of the NH_2-terminal cytoplasmic tail and predicted transmembrane domain (amino acids 44–487, AtXOAT1-fl), a second encodes the catalytic domain and lacks the N-terminal variable region (amino acids 133-487, AtXOAT1-cat), and the third is solely comprised of the N-terminal variable region (amino acids 44-133, AtXOAT1-nv). Expression and secretion of GFP-AtXOAT1-fl (~121 mg L^{-1}) and GFP-AtXOAT1-cat (~92 mg L^{-1}) in HEK293S (GnTI-) cells yielded high levels of secreted recombinant fusion protein based on GFP fluorescence (Table S1) [32]. The activities of AtXOAT1-fl and AtXOAT1-cat and were virtually the same. Reactions performed with

AtXOAT1-nv did not result in the production acetylated products, as expected (Fig. S2.5c), and AtXOAT1-nv was used as a control protein for comparative analysis using chromogenic substrates in later experiments. Taken together, these data indicate that the core catalytic domain is comprised of the TBL and DUF231 domains, and confirms that the N-terminal variable region does not play a direct role in catalysis.

The crystal structure of the AtXOAT1 catalytic domain (AtXOAT1-cat) was determined by the single wavelength anomalous dispersion method using anomalous signals from sulfur atoms (S-SAD) at CuK_{α} wavelength (1.54 Å). The AtXOAT1-cat domain monomer has approximate dimensions of 45Å × 48Å × 55Å and features an overall fold that is unique based on a search for related structures using PDBeFold (http://www.ebi.ac.uk/msd-srv/ssm/ssmcite.html). Overall there are three β-sheets composed of seven (β4, β5, β6, β3, β9, β12, β13), four (β7, β8, β10, β11) and two (β1 and β2) β-strands, nine α-helices including a 'broken' one, and three α-helical turns (4-residue fragments stabilized by a single H-bond). The protein topology is presented in Fig S2.6. A deep cleft divides the molecule into two unequal lobes. It is worth noting that the larger lobe formed by amino acids 197-366, 403-433 and 470-486 contains almost all secondary structure elements found in the protein – two parallel/antiparallel β-sheets, comprised of seven and four β-strands, respectively, and eight large α-helices (all helices except H8). The smaller lobe includes amino acid residues 133-196, 367-402 and 434-469 and is mostly unstructured with only one short, broken α-helix (H8), three α-helical turns (αT1, αT2 and αT3) and a small two-strand antiparallel β-sheet (β1 and β2). All these unstructured loops are held together by four disulfide bridges (amino acids 140/191, 162/227, 171/467, 384/463). No disulfide bridges are present in the larger, more structured lobe (Fig. 2.2). The deep cleft on the surface of the protein molecule is the most likely substrate binding site, with a putative classic catalytic triad (Ser216-His465-Asp462) characteristic

of serine proteases [33] at the bottom (Fig. 2.2a-c). Accordingly, it has previously been shown that mutation of these residues abolishes AtXOAT1 activity [13], and our structural data now confirms that these residues are part of a classic catalytic triad. The walls of the cleft are formed by two flexible loops comprised of amino acids 443-448 on one side and 273-281 on the other (Fig. 2.2d).

There are six *N*-glycans appended to the surface of AtXOAT1-cat. Four of the glycans are well-defined single *N*-acetylglucosamine (GlcNAc) sugars attached to Nδ atoms of asparagine residues at positions 151, 241, 255 and 393 and 412, as expected after treatment with endo-β-*N*-acetylglucosaminidase F, which cleaves the β-1,4-link between the core *N*-acetylglucosamine residues of *N*-linked glycans. Asparagine 412 showed weak electron density for the fifth single GlcNAc modification and when added to the model it refined to a strained conformation according to Privateer carbohydrate validation program [34]. After modeling and refining this density with and without GlcNAc it was decided to be real but with an unlikely conformation caused by the weak and noisy electron density. The sixth glycan appended to Asn425 is longer, with two GlcNAc units visible in the electron density maps that could be modeled followed by at least one mannose unit visible but not modeled due to weak and scattered electron density. Since most of the glycans are involved in the crystal contacts or are located in the immediate proximity to the crystal contacts, trimming of glycan structures to a single GlcNAc at 4 out of 5 respective sites was critical for successful crystallization of AtXOAT1-cat.

The catalytic triad (Ser-Asp-His) located in the active site cleft of AtXOAT1 was originally identified in serine proteases, and is found in several dissimilar enzymes and protein folds that cleave amide or ester bonds via nucleophilic attack [33]. A search for similar structures using the PDBeFOLD server indicated that the overall fold of AtXOAT1-cat is not present in any previously reported structures in the Protein Data Bank (PDB). However, some subregions of the enzyme,

especially the central β-sheet region in the vicinity of the catalytic triad, have some similarities to known structures despite sharing less than 10% sequence identity. Structural alignments performed with PDBeFold found two structures with a Z-score above six – a putative lipase from *B. thetaiotamicron* (PDB ID 3bzw, Z-score 8.2, RMSD of 2.71 Å over 155 Cα atoms) and peptidoglycan *O*-acetylesterase from *N. meningitidis* (PDB ID 4k3u, Z-score 6.9, RMSD of 2.84 Å over 176 Cα atoms). Both proteins belong to the Pfam GDSL-like lipase/acylhydrolase family and share the α/β/α arrangement of AtXOAT1-cat's larger 'structured' lobe including five of the seven β-strands in the largest β-sheet flanked with seven α-helices on both sides (Fig. 2.3). The central β-sheet region of AtXOAT1-cat and some of the surrounding α-helices also share some similarities upon structural alignment with two functionally similar enzymes - isoamyl acetate hydrolyzing esterase (PDB ID:3mil) [35] and peptidoglycan *O*-acetyltransferase from *B. cerus* (PatB1; PDB ID: 5v8e) [25]. Isoamyl acetate hydrolyzing esterase performs the hydrolysis of acetyl esters, whereas PatB1 transfers an acetyl moiety from acetylated donor molecules, such as *p*NP-Ac onto the C3 hydroxyl of terminal β-GlcNAc residues of peptidoglycan and hence is somewhat related by function to AtXOAT1. Catalytic activity in these four similar proteins is also carried out by a conserved Ser-His-Asp catalytic triad. It is interesting to note that the order of appearance of the secondary structure domains; as well as the catalytic triad in the amino acid sequence is Ser-Asp-His (wherein Ser is closer to the N-terminus and the His is closer to the C-terminus) for the putative lipase, the peptidoglycan *O*-acetyltransferase from *N. meningitidis*, isoamyl acetate hydrolyzing esterase and AtXOAT1. However, even though PatB1 is an acetyltransferase acting on a glycosyl moiety, the arrangement of the secondary structural elements as well as the catalytic triad is shifted to Asp-His-Ser (wherein Asp is closer to the N-terminus while the Ser is closer to the C-terminus). Hence, this structural similarity of PatB1 with AtXOAT1

and the other similar proteins may be evidence of convergent evolution for use of a common catalytic triad, despite low primary sequence similarity among the enzymes (≤10%). This has previously been found for serine proteases containing a similar conserved catalytic triad [36].

Mutagenic analyses implicate the roles key amino acids in AtXOAT function

The C-terminal portion of AtXOAT1, comprised of the latter half of the plant-specific TBL domain and the entire DUF231 domain, is categorized in the PFAM database as a GDSL/SGNH-like acyl-esterase (PF13839) (Fig. S2.7). The SGNH-hydrolase family is characterized by the presence of four invariant residues (Ser-Gly-Asn-His) in conserved blocks (I, II, III, and V). In these enzymes, the Ser in block I and the Asp and His residues in block V form the catalytic triad, while the backbone amide of the Gly and side-chain amides of Asn residues in blocks II and III serve as hydrogen bond donors to stabilize the tetrahedral oxyanion intermediate [37]. Sequence analysis of plant TBL proteins revealed that no conserved motifs characteristic of SGNH blocks II or III were present (Fig. S2.7) in *Arabidopsis* or when compared across all plant species in the Phytozome database (https://phytozome.jgi.doe.gov/; data not shown). The TBL and DUF231 domains contain the conserved GDSL and DxxH motifs of blocks I and V, respectively, that together form the putative Ser216-His465-Asp462 catalytic triad positioned at the bottom of the active site cleft (Fig. S2.7, Fig. 2.2). We observed that the position filled by Leu in the GDSL motif can be occupied by any non-ring forming basic amino acid residue in the plant proteins. Directly downstream of the block I, there is a conserved RNQxxS motif, that we termed plant-specific TBL-block II. In plant TBL proteins, the block V **D**xx**H** motif is part of a larger, highly conserved **D**Cx**H**WCLPGxxD consensus region. We also identified a highly conserved, plant specific RxDxH motif that we termed plant-specific TBL-block III (Fig. S2.7).

To evaluate the involvement of these conserved amino acids in the TBL family that may play an important role in catalysis, we carried out site-directed mutagenesis of these residues in AtXOAT1 by substituting them with alanine. As a control, we also mutated the catalytic residues (S216A, H465A and D462A), and verified that they abolish *O*-acetyltransferase activity as revealed by MALDI-TOF MS analysis of the reaction products (Fig. 2.4a). This confirmed that Ser216A, His465A and Asp462A are loss-of-function mutations that lack both transferase and esterase activity (Fig. 2.4b), and confirm the utility of our *in vitro* assay. It is important to note that the esterase activity discussed here is indicated by release of *p*-nitrophenol in the absence of acceptor, which occurs upon formation of the acyl-enzyme intermediate. Therefore, the combined assays allow us to measure both portions of the reaction: formation of the acyl-intermediate and transfer of the *O*-acetyl moiety from Ac-Ser216 to the xylosyl acceptor. When we incubated AtXOAT1 with four electrophilic mechanism-based inhibitors of serine proteases, *N*-*p*-tosyl-L-phenylalanyl chloromethyl ketone (TPCK), 4-(2-aminoethyl)benzenesulfonyl fluoride hydrochloride (AEBSF), phenylmethylsulfonyl fluoride (PMSF) and methanesulfonyl fluoride (MSF), except for MSF, none of these protease inhibitors abrogated the catalytic activity of AtXOAT1 as an *O*-acetyltransferase as acetylated products had been detected by MALDI-TOF MS after the reaction. Importantly, these data suggest that either AtXOAT1 utilizes a different active site conformation compared to other serine proteases or that the majority of these compounds are unable to access the active site pocket (Fig. S2.8). A similar phenomenon was observed previously, in this case, PMSF was not able to completely inactivate *N. gonorrhoeae* PatB [38], while MSF abrogated both esterase and transferase activities of PatB in *Bacillus cereus* [25].

An important factor for the transition state of the mechanism mediated by the Ser-His-Asp triad is the oxyanion hole that stabilizes the excess negative charge on the oxygen of the acetyl group. The backbone amide of the Gly and side-chain amide of an Asn residue in SGNH blocks II and III stabilize the putative tetrahedral oxyanion through hydrogen bonding in SGNH hydrolases [37]. However, residues that would be characteristic of blocks II and III that are important for formation of the oxyanion hole in the SGNH-hydrolase family are completely absent in the plant TBL family. A recent study suggested that Arg359 of the *O*-acetyltransferase PatB1 from *Bacillus cereus*, is a key component of the oxyanion hole in that enzyme [25]. The conserved RNQxxS motif of TBL-block II contains an arginine (Arg219) that is correctly positioned in the active site and may function to stabilize the negative charges on the acetyl oxyanion during the formation of the tetrahedral reaction intermediates (Fig. 2.3c).

We designed an R219A variant of AtXOAT1 to investigate its role in catalysis. The R219A variant is not capable of catalyzing the transfer of acetyl groups to Xyl_6-2AB (Fig. 2.3a), indicating that Arg219 plays an important role in AtXOAT1 catalysis. The hydrophilic side chain of Arg219 is positioned at the surface of the active site cleft, suggesting that this residue may play a role in forming the correct conformation of the catalytic site, and might be important for the oxyanion hole formation. Furthermore, Arg219 was observed to be an important active site residue involved in binding the donor molecule in the MD simulations. However, it is worth noting that even though transferase activity is abolished in the R219A variant as evidenced by MALDI-TOF MS of the reaction products (Fig. 2.3a), it retains esterase activity indicating that formation of the acyl-enzyme intermediate can still proceed to some extent (Fig. 2.3b). Furthermore, this esterase activity increases when xylo-oligo acceptors are present in the reaction, as revealed by the spectrophotometric assay (Fig. 2.3b), despite its inability to transfer an *O*-acetyl moiety to the

acceptor (Fig. 2.3a). The increased esterase activity of R219A may indicate that the binding of the acceptor substrate stabilizes folding of AtXOAT1 or contributes to formation of the oxyanion hole during the transfer of the acetyl group to the acceptor. Alternatively, in the absence of the guanidinium group of Arg219, the oligosaccharide may bind in an unproductive geometry that directs the movement of a water molecule to a position from which it can attack the serine-bound acetyl group, facilitating its hydrolysis. Thus, the binding of xylo-oligo substrates increases the esterase activity of R219A, and this mutation completely disrupts transferase activity, meaning Arg219 is critical for transferase activity and likely plays a role in limiting ester hydrolysis.

In most SGNH hydrolases, the side-chain amide of a conserved asparagine in SGNH block III is also important to maintain the stability of the oxyanion hole by serving as a hydrogen bond donor for stabilization of the transition state. While we hypothesize that the guanidinium moiety of an arginine residue in AtXOAT1, like PatB1, is a key contributor to formation of the oxyanion hole, we also observe the presence of an asparagine residue (Asn220) that is located close to the Ser-His-Asp catalytic triad (Fig. 2.3c) – with its side chain amide pointing away from the active site. Thus, we evaluated the plausible role of Asn220; however, the N220A variant, despite spatial proximity, retained both acetyltransferase and esterase activity. At the end of the reaction, acetylated oligosaccharide products were detected by MALDI-TOF MS (Fig. 2.3a) and (deacetylated) *p*NP was detected spectrophotometrically (Fig. 2.3b), both in the presence and absence of acceptor substrate. This result indicates that the side chain amide of Asn220 is not involved in stabilizing the intermediate tetrahedral structure of the substrate during xylan *O*-acetylation. In addition, the N220A mutant has significantly more acetylhydrolase activity than either of the catalytically active controls, as indicated by the amount of *p*NP released in the absence of acceptor substrate (Fig. 2.3b). These data suggest that Asn220 might play a role in protecting

the acyl-enzyme intermediate from hydrolysis, which would decrease the efficiency of the enzyme at low acceptor substrate concentrations.

Asp215 resides directly next to the catalytic Ser216, which is the site of nucleophilic attack during both stages of the mechanism (Fig. 2.3c). Mutation of Asp215 to Ala (D215A) abolished both the esterase and transferase activities of AtXOAT1 (Fig. 2.3a) as well as the level of released *p*NP in the hydrolysis assay was similar to that of the catalytically inactive control AtXOAT1-nv (Fig. 2.3b). Since Asp215 lies very close to the catalytic site, it may contribute to stabilizing the active site conformation. Mutation of Asp215 resulted in a ~75% decrease in production of soluble secreted protein (Table S1), indicating that this mutation may also lead to unstable protein folding, as observed previously with AtFUT1 [22]. The RxDxH motif we termed TBL-block III contains a highly conserved His437 residue that may play a role in substrate interactions. Mutation of His437 to Ala (H437A) resulted in the production of no acetylated products based on detection using MALDI-TOF MS; however only 42% and 72% of hydrolysis activities retained in the H437A variant when reactions were respectively carried out with and without the acceptor substrate (Fig. 2.3b).

Computational modelling enables insight into active site characteristics and reaction mechanism

Experimental efforts to obtain substrate bound structures of AtXOAT1 with either a donor molecule (*p*NP-Ac or acetyl-CoA) or an acceptor (xylo-bi/tri/tetra/penta/hexa-oses) were unsuccessful due to complications during the crystallization process (Supplementary Information Section I). Despite numerous attempts to crystallize the longer AtXOAT1-fl construct, the only crystals that grew were formed by the AtXOAT1-cat domain with no space left in the crystal lattice

for the N-terminal variable region, even if it would have been disordered. We hypothesize that this tight packing interfered with our attempts to obtain a XOAT1-xylooligosaccharide co-complex. Given this lack of structural information on the substrate bound states of AtXOAT1, gaining insight into the molecular details of the mechanism and mode of action required alternative strategies. Molecular simulations have previously been used to gain insight into substrate binding poses and the catalytic mechanism in cases where experimental characterization of enzyme-substrate complexes has been unsuccessful [39]. As outlined in the following paragraphs, molecular simulations reveal the putative active site in AtXOAT1 and the ability of its substrate binding groove to stabilize acceptor and donor substrates.

It has also been experimentally shown that AtXOAT1 demonstrates increased activity with longer xylan oligosaccharides (>DP3) and catalyzes the addition of multiple acetyl moieties onto a single acceptor necessitating an active site that can accommodate larger acceptors (Fig. S2.2). MD simulations of AtXOAT1 in the absence of substrates reveal significant flexibility in loops surrounding the putative substrate binding groove. The presence of a Ser-His-Asp triad at the base of this loop further strengthens the hypothesis that the cleft is an extension of the active site and enables binding oligosaccharide substrates. By analogy to serine proteases and esterases [37], the Ser residue acts as a nucleophile assisted by the His residue, which acts as a base whose excess positive charge is stabilized by a hydrogen bond with the Asp residue. Figure S2.9 depicts the two key hydrogen bonds that are necessary for the proper functioning of this catalytic triad. In the absence of substrates, it is observed that the acid-base distance (Asp462 O to His465 H) is within 2 Å throughout the MD simulation, whereas the base-nucleophile distance is frequently (22% of the simulation time) within 3 Å (Fig. 2.6). It must be noted that Asp462 and His465 are a part of the same minor lobe of AtXOAT1, whereas the nucleophile is situated on an α-helix that is part of

the major lobe (Fig. 2.2c). This may explain the observation that the acid-base distances are shorter than the base-nucleophile distances.

Separate MD simulations of AtXOAT1 in the donor and acceptor bound states revealed the ability of the active site and the putative binding groove to accommodate the surrogate donor molecule (*p*NP-Ac) and the acceptor xylodecaose substrate over simulation times in excess of 50ns. These observations of substrate bound configurations from unbiased MD simulations combined with data from mutagenesis experiments enables insight into the catalytic mode of action of AtXOAT1. Structural alignments of sub-regions of the AtXOAT1 crystal structure with other proteins revealed conservation of important structural domains; as well as the putative catalytic triad amongst these enzymes (Fig. 2.3). Furthermore, MD simulations of AtXOAT1 in the absence of substrates, and in the donor- and acceptor-bound states established the stability of the catalytic triad; as well as the ability of the active site to bind the acceptor and donor molecules. The mutagenesis experiments further substantiated the indispensable role of the Ser216-His465-Asp462 catalytic triad and helped identify residues that may contribute to formation of an oxyanion hole. Based on these observations we propose that AtXOAT1 utilizes a double displacement bi-bi reaction to catalyze xylan 2-*O*-acetylation consisting of two stages as illustrated in Figure 2.5. The first stage of catalysis involves acetylation of Ser216 upon binding of the acetyl donor, in this case the surrogate donor *p*NP-Ac is depicted. Coordination of His465 with the unprotonated Asp462 allows His465 to act as a general base, facilitating the nucleophilic attack of the acetyl group of the donor by Ser216. Arg219, contributes to formation of an oxyanion hole that stabilizes the putative tetrahedral transition state. The transfer (via His465) of the Ser216-proton (red font) onto the phenolic oxygen of the donor facilitates release of the deacylated donor (*p*-nitrophenol as shown) and acetylated Ser216 (acyl-enzyme intermediate), which is supported by the LC-MS/MS

data (Fig. 2.1d, Fig. S2.3 and Fig. S2.4) showing that AtXOAT is able to utilize all acetyl donors investigated in formation of the acyl-enzyme intermediate.

Summary

Unraveling the identity, selectivity, and catalytic mechanisms of plant biocatalysts involved in cell wall formation is vital to understanding the roles these enzymes play in generating structures critical to the composite nature of the plant cell wall, which is fundamental to exploiting wall structural plasticity in agronomically productive crops. Xylan forms an integral part of the wall and defines its architecture and structural properties. Enzymes that catalyze the addition of substituents, such as acetyl groups to the xylan backbone (e.g., AtXOAT1), are of significant interest as they play key roles in shaping the polysaccharide's physical properties. The importance of this single enzyme in plant growth and development is substantiated by the fact that mutation of AtXOAT1 in *Arabidopsis* results in plants with a 40% reduction in xylan *O*-acetylation that exhibit collapsed xylem vessels that manifest several pleiotropic phenotypes related to stress responses [2].

Expression of the soluble catalytic domain of AtXOAT1 (AtXOAT-cat, AtXOAT133-487) for structural analysis was achieved by transient transfection of suspension culture HEK293S cells using a fusion protein strategy similar to our prior studies on mammalian and plant GTs [22, 32]. The catalytic domain of AtXOAT1 adopts a unique structure, bearing some similarities the α/β/α topology of members of the GDSL-like lipase/acylhydrolase family, and is comprised of three β-sheets composed of seven, four and two β-strands, nine α-helices and three α-helical turns. A deep cleft divides the molecule into two unequal lobes that open to accommodate the mono O-

acetylation of linear β-1,4-xylan and contains a Ser216-His465-Asp462 catalytic triad at its base. Real time NMR experiments confirm AtXOAT1 specifically transfers O-acetyl moieties solely to the 2-position of the xylan backbone. Further, this technique was applied to study post-synthesis acetyl migration in real time, and showed that the *O*-acetyl at the 2-position migrates spontaneously to the 3-position in the absence of enzyme. A double displacement bi-bi mechanism involving the Ser216-His465-Asp462 triad is proposed and substantiated by both molecular simulation results and biochemical experiments confirming the formation of the acyl-enzyme intermediate, Ac-Ser216. In addition, we propose that AtXOAT1 likely unconventionally employs an arginine (Arg219) residue to conduct the role of an oxyanion hole in the mechanism.

These mechanistic insights into an enzyme involved in plant polysaccharide acetylation and the biosynthesis of the predominant hemicellulosic polysaccharide xylan represent a major leap forward in understanding the biochemical mechanisms used by plants to synthesize their cell walls. This work lays the basis for further studies exploring the nature of enzymes involved in polysaccharide acetylation, including the interplay between glycosyl and non-glycosyl substituent patterning along glycopolymer backbones and how the regiospecificity of O-acetyltransferases impacts plant cell wall properties.

Materials and Methods

Expression and purification of fusion proteins

Fusion protein expression and purification was accomplished as described previously [18]. Briefly, total RNAs extracted from inflorescence stems of wild-type *A. thaliana* (Col-0) were used to generate cDNAs using RevertAid First Strand cDNA Synthesis Kit (Thermo Scientific), and the

sequences of the truncated coding-region of XOAT1 were then amplified from the cDNAs by using the following primer pairs: TBL29/ESK1, 5'-AACTTGTACTTTCAAGGCTCAAAACCTCACGACGTC-3' and 5'-ACAAGAAAGCTGGGTCCTAACGGGAAATGATACGTGT-3'. The resulting PCR product was cloned into a mammalian expression vector, pGEn2-DEST [32], as described previously [22]. The expression plasmids were purified and transformed into HEK cells (FreeStyle™ 293-F cell line, Life Technologies) as previously described [32].

Recombinant proteins were secreted into the culture media by HEK293 cells, and were purified using HisTrap HP column and ÄKTA protein purification system (GE Healthcare Life Sciences). For crystallization ESK1 samples were further purified using Source 15Q anion exchange chromatography with 20 mM Tris pH 7.5 and 0 to 0.35 M NaCl gradient. Finally, Superdex 75 pg (26/60) size exclusion chromatography column in 20 mM Tris pH 7.5, 100 mM NaCl was used to complete the purification. SDS-PAGE followed by Coomassie Brilliant Blue R-250 (Bio-Rad) staining was carried out to confirm the purity of the proteins. For the activity assays, proteins were dialyzed in HEPES sodium salt-HCl (75 mM, pH 7.0) with Chelex-100 resin (5 g/L, Bio-Rad) to remove any divalent metal contaminants. After dialysis, the proteins were concentrated using Amicon Ultra centrifugal filter devices (30 kDa molecular weight cut-off, EMD Millipore), and were quantified by Pierce™ BCA Protein Assay Kit (Thermo Scientific). The resulting fusion proteins comprise NH_2-terminal signal peptides, 8×His-tags, AviTag recognition sites, Green fluorescent proteins, TEV protease recognition sites, and the catalytic domains of the corresponding enzymes.

Mutated variants of AtXOAT1 were generated by site-directed mutagenesis using the Q5® Site-Directed Mutagenesis Kit (New England Biolabs) according to the manufacturer's instructions

using pGEN2-DEST-AtXOAT1 as a template. Oligonucleotide primers used to generate the base changes and expression levels of the wild-type and mutant variants are listed in Table S1. The introduction of mutations was confirmed by sequencing (Eurofins, USA).

Crystallization

AtXOAT1-cat crystals were initially obtained with sitting drop vapor diffusion using a 96-well plate with PEG ion HT screen from Hampton Research (Aliso Viejo, CA). Fifty µL of well solution was added to the reservoir and drops were made with 0.2 µL of well solution and 0.2 µL of protein solution using a Phoenix crystallization robot (Art Robbins Instruments, Sunnyvale, CA). The crystals were grown at 20°C using an optimization screen containing 0.1 M MES pH 6.0 to 7.0 and 15% to 22% w/v PEG 3350, 0.02 M Calcium chloride dihydrate, 0.02 M Cadmium chloride hydrate and 0.02 M Cobalt (II) chloride hexahydrate. The protein solutions contained 5.62 mg/mL of protein, 20 mM Tris pH 7.5, 100 mM NaCl and 20 mM 4-Nitrophenyl acetate. Crystals were soaked in well solution with additional 10% glycerol and 5% ethylene glycol for additional cryo protection.

Data collection and processing

The AtXOAT1-cat crystals were flash frozen in a nitrogen gas stream at 100 K before home source data collection using an in-house Bruker X8 MicroStar X-Ray generator with Helios mirrors and Bruker Platinum 135 CCD detector. Data were indexed and processed with the Bruker Suite of programs version 2014.9 (Bruker AXS, Madison, WI).

Structure solution and refinement

Intensities were converted into structure factors and 5% of the reflections were flagged for Rfree calculations using programs F2MTZ, Truncate, CAD and Unique from the CCP4 package of programs [40]. Crank2 [41] was used to solve the structure utilizing sulfur Single-wavelength anomalous dispersion [42]. Refinement and manual correction was performed using REFMAC5 [43] version 5.8.135 and Coot [44] version 0.8.2. The MOLPROBITY method [45] was used to analyze the Ramachandran plot and root mean square deviations (rmsd) of bond lengths and angles were calculated from ideal values of Engh and Huber stereo chemical parameters [46]. Carbohydrate structures were validated using Privateer [34]. Wilson B-factor was calculated using CTRUNCATE version 1.15.10 [40]. The data collection and refinement statistics are shown in Table S2.

Donor and acceptor substrate specificities of AtXOAT1

To determine the activity of acetyltransferase on different donor substrates, the standard assays (15 µL) were performed using acetylsalicylic acid (1 mM), acetyl-CoA (1 mM), or *p*NP-Ac (1 mM) as donors, and Xyl_6-2AB (0.25 mM) as acceptor substrates in HEPES sodium salt-HCl (75 mM, pH 6.8) with purified proteins (4 µM). The reactions were incubated at room temperature for indicated periods of time, and the products were then analyzed by Matrix-assisted laser desorption/ionization mass spectrometry (MALDI-TOF MS) using a Microflex LT spectrometer (Bruker) as described previously [22]. Briefly, aliquots (5 µL) of the reactions were mixed with Dowex-50 cation exchanger resin (1 µL suspension in water), and the mixture was incubated at room temperature for 30 min. Resin was pelleted by centrifugation and 1 µL of the supernatant

was directly mixed with 1 μL of DHB matrix solution (20 mg/mL 2,5-dihydroxybenzoic acid in 50% MeOH), on a stainless steel MALDI target plate then concentrated to dryness using a hair dryer. Each positive ion spectrum was generated by summation of 200 laser shots.

Xylooligosaccharides (Xyl_2, Xyl_3, Xyl_4, Xyl_5, and Xyl_6) were purchased from Megazyme. The acceptor substrate specificities were determined by the similar assays mentioned above but with increased amount of acetylsalicylic acid (5 mM) as the donor and non-labeled xylo-oligosaccharides (3 mM), Xyl_2, Xyl_3, Xyl_4, Xyl_5 and Xyl_6, as the acceptor substrates, and acetylated products were analyzed by MALDI-TOF MS. On the other hand, the acetyltransferase activity of AtXOAT1 on xylo-oligosaccharide was examined by the hydrolysis assays using *p*NP-Ac (5 mM) as the donor, and xylopentaose (Xyl_5) with different concentrations (0, 1, 5 and 25 mM) as the acceptor substrate in HEPES sodium salt-HCl (75 mM, pH6.8) with purified proteins (5 μM). The reactions were incubated for an hour, and the hydrolysis of *p*NP-Ac in the reaction was determined by measuring the absorbance of the released *para*-nitrophenol (*p*NP) at 350 nm, using Epoch Microplate Spectrometer (BioTek®) every minute during the reaction period.

Determination of catalytic activity of AtXOAT1 constructs and variants

To evaluate the *O*-acetyltransferase activities of different AtXOAT1 constructs and its mutated variants, the activity assays were performed by incubating the purified enzymes (4 μM) with acetylsalicylic acid (1 mM) and Xyl_6-2AB (0.25 mM) in HEPES sodium salt-HCl (75 mM, pH 6.8) for 2 h. The acetylated products were analyzed by MALDI-TOF MS as described previously. To further investigate whether AtXOAT1 variants possess xylan *O*-acetyltransferase and/or *O*-acetylesterase activities, assays were carried out by incubating the enzymes (5 μM) with

or without non-labeled Xyl_4 (5 mM) as the acceptor and *p*NP-Ac (5 mM) as the donor substrate for 60 min. The amount of released *p*NP in the reaction was quantified by measuring the absorbance at 350 nm using Epoch Microplate Spectrometer (BioTek®) as the same described above. The non-catalytic truncated protein containing only the N-terminal variable region and lacking the catalytic domain, AtXOAT1-nv (Fig. S2.5b and c), was used as a control. Each transferase and esterase activity of the AtXOAT1 variants was obtained by subtracting the amount of *p*NP released in the control sample containing AtXOAT1-nv from each standard reaction containing different AtXOAT1 variants with or without the acceptor.

Peptide analysis of acyl-AtXOAT1 by LC-MS/MS

In vitro assays were carried out by incubating AtXOAT1 (4 µM) with four different acetyl donors (1 mM): acetyl-CoA, acetyl salicylic acid, *para*-nitrophenyl acetate and 4-methylumbelliferyl acetate in HEPES sodium salt buffer (pH 6.8; 75 mM) for 4 min at room temperature. The reactions were then stopped immediately by flash freezing in a dry ice/ethanol cooling bath (-78 °C). All the donor substrate stocks were prepared in DMSO, and the final percentage of DMSO in all reactions was 5% (v/v). Control reactions were identical, but no donor substrate was added.

The prepared samples were reduced, alkylated, and then digested with trypsin (sequencing grade; Promega) in Tris-HCl (50 mM, pH 8.2) buffer overnight. After protease digestion, samples were desalted and filtered prior to LC-MS analysis. NanoLC-MS/MS was performed on an Orbitrap Fusion Tribrid Mass Spectrometer (ThermoFisher Scientific) coupled to an Ultimate3000 RSLCnano low flow liquid chromatography system (ThermoFisher Scientific), and equipped with

a nanospray ion source. Prepared peptide samples were injected onto a loading column (ThermoFisher Scientific, C18, volume 2 μL) before being transferred to the separation column (Acclaim PepMap 100 C18 – 0.075 × 150 mm with 3 μm particle size). The separation was performed under a linear gradient from 5% to 100% B (80% Acetonitrile, 0.1% formic acid) at a flow rate of 0.3 μL/min. The analysis was run in automatic mode collecting an MS scan (full FTMS at 150-2000 m/z; resolution 120 000) followed by data dependent MS/MS scans (CID) at a cycle time of 3 sec. The data was manually processed using QualBrowser (ThermoFisher Scientific).

RT-NMR analysis of acetyl group migration

To verify the positional specificity of AtXOAT1-cat, the reaction of *O*-acetylation of Xyl_6 was monitored using real-time ^1H NMR spectroscopy. 200 μg Xyl_6 was mixed with 4 mM Ac-CoA and 9 μM purified enzyme in 100 mM potassium phosphate buffer (pH 6.8) in D_2O (99.9%; Cambridge Isotope Laboratories), and the reaction (110 uL total volume) was rapidly transferred to the NMR spectrometer. Previously, we employed potassium bicarbonate as a buffer in our real-time NMR experiments (18); however, biocarbonate buffers are unstable and become alkaline upon exposure to atmospheric CO_2, increasing the rate of acetyl migration in solution. Due to this observation, we have now optimized our real-time NMR conditions and used phosphate buffer, which is a more stable buffer. Data acquisition started 10 min after the reaction was initiated, and data were recorded at 298 K with an Agilent-NMR spectrometer operating at 600 MHz equipped with a 5-mm NMR cold probe. The 1D ^1H spectra consist of 16 transients and were acquired with water presaturation every 30 min over a 20-hour period. The spectral array generated represents the reaction progress. The amount of acetylated xylosyl residues generated during the reaction were quantified by integrating the resonance peaks corresponding to the methyl protons of the

acetyl groups attached to *O*-2 and *O*-3 of the xylosyl residues, and the calculation was based on the initial concentration of Ac-CoA added into the reaction. Data processing was performed using MestReNova software (Mestrelab Research S.L., Universidad de Santiago de Compostela, Spain).

Non-enzymatic acetyl group migration was monitored in real-time by ^{1}H NMR. To generate an adequate amount of acetylated Xyl_6 that meets the sensitivity of the NMR spectrometer, scaled up reactions were performed in parallel to those prepared for real-time NMR analysis of catalysis. Briefly, acetylated Xyl_6 was generated by incubating AtXOAT1 (9 μM) with non-labeled Xyl_6 (200 μg) and Ac-CoA (4 mM) in 100 mM potassium phosphate buffer in D_2O (99.9%; Cambridge Isotope Laboratories) for 6 h at room temperature. The enzyme was then removed via diafiltration by passing the mixture through a 30 kDa centrifugal filter device (Amicon®, Merck Millipore Ltd., Ireland). The absence of AtXOAT1 in the filtrate, and its complete retention in the filter device, was confirmed by both SDS-PAGE using a precast Mini-PROTEIN® TGX Stain-Free™ Gel (Bio-Rad Laboratories, Inc.) and by measuring the direct absorbance at 280 nm using a NanoDrop™ Spectrophotometer (Thermo Fisher Scientific). The filtrate was immediately transferred to the NMR spectrometer, and the signals that correspond to the CH_3 of the *O*-acetyl substituents at different positions were monitored by arrayed ^{1}H NMR according to the following process. Data were recorded at 298 K with an Agilent-NMR spectrometer equipped with a 5-mm NMR cold probe operating at 600 MHz. Each 1D ^{1}H spectra consists of 16 transients, and were acquired with water presaturation every 30 min for 14 hrs overnight. The spectral array generated represents the reaction progress. Samples were never subjected to lyophilization.

In vitro assays of AtXOAT1 with protease Inhibitors

The in vitro assays with protease inhibitors were carried out as the standard assays mentioned previously but with addition of 80 μM *N*-*p*-tosyl-L-phenylalanyl chloromethyl ketone (TPCK), 0.8 mM 4-(2-aminoethyl)benzenesulfonyl fluoride hydrochloride (AEBSF), 4 mM phenylmethylsulfonyl fluoride (PMSF) or 5 mM methanesulfonyl fluoride (MSF) in the reaction. Acetylsalicylic acid at a final concentration of 1 mM was used as the donor substrate in the assays. After overnight incubation, the acetylated products were analyzed by MALDI-TOF MS.

Computational Modeling

Docking and molecular dynamics simulations have been successful in gaining insight into plausible substrate binding poses and identify the important active site residues that aid substrate binding [22, 39]. AutoDock4 and AutoDockTools4 software package was used for the docking the acceptor (xylodecaose) and donor (*p*NP-Ac) molecules to the 1.85 Å AtXOAT1 structure [47]. Plausible binding poses were identified as starting points for molecular dynamics simulations. The four disulfide bonds identified in the crystal structure, between residues 465-386, 469-173, 229-164 and 142-193 were incorporated and the protonation states of titratable amino acid residues was estimated using the H++ web server [48]. Fully solvated systems were generated for the protein in its apo and bound states. The CHARMM36 forcefield was used for the protein [49], xylodecaose substrate [50], the CGENFF force field for *p*NP-Ac [51], and the TIP3P forcefield for modelling water [52]. Three systems of AtXOAT in different states were built - (i) apo state (no substrate bound) (ii) donor bound state (AtXOAT1 with six *p*NP-Ac molecules bound) and (iii) acceptor bound state (AtXOAT1 with acetylated Ser216 and a xylodecaose substrate bound). The

CGENFF protocol was used to obtain parameters for the acetylated serine residue in the acceptor bound state [51]. The system set-ups for the bound states was obtained based on preliminary docking studies and hence the simulation procedure for the protein-substrate complexes involved multiple minimizations and short equilibration runs with restraints on the substrate. The short equilibration runs involved sequential runs starting with a fixed substrate, followed by restraints on the substrate which were gradually released for unrestrained production runs. The production runs for data analysis involved 60 ns unbiased runs with all H-atoms restrained using the SHAKE algorithm, a 2 fs time step, periodic boundary conditions, a non-bonded cutoff of 11 Å, the particle mesh Ewald for long range electrostatics and frames saved every 100 ps [53, 54]. All MD simulations utilized the domdec MD engine that is part of the CHARMM MD package [55, 56]. The trajectories were analyzed for root mean square fluctuations, interaction energies, catalytically important distances and volumetric occupancies. The RMSF and distance calculations were performed with pytraj (python version of CPPTRAJ [57]) and the volumetric occupancies were calculated using the volmap tool in VMD [58].

Statistical Analysis

All data are present as mean ± SD except for Fig. S2.1 (the quantitative data of the duplicates and their average are displayed). Statistical significance was determined with the two-tailed Student's t-test through Microsoft® Excel Version 15.32 (2017). *, $p < 0.05$; **, $p < 0.01$. The number of replicates is provided in the figure legend for each experiment.

Accession Numbers

The atomic coordinates of XOAT1cat have been deposited into the Protein DataBank (accession code 6CCI; http://www.rcsb.org/pdb). Sequence data for the genes that were described in this article can be found in the Arabidopsis Genome Initiative or GenBank/EMBL databases under the following Arabidopsis AGI locus identifiers: At5g06700 (AtTBR); At3g12060 (AtTBL1); At1g60790 (AtTBL2); At5g01360 (AtTBL3/AtXOAT4); At5g49340 (AtTBL4); At5g20590 (AtTBL5); At3g62390 (AtTBL6); At1g48880 (AtTBL7); At3g11570 (AtTBL8); At5g06230 (AtTBL9); At3g06080 (AtTBL10); At5g19160 (AtTBL11); At5g64470 (AtTBL12); At2g14530 (AtTBL13); At5g64020 (AtTBL14); At2g37720 (AtTBL15); At5g20680 (AtTBL16); At5g51640 (AtTBL17/AtYLS7); At4g25360 (AtTBL18); At5g15900 (AtTBL19); At3g02440 (AtTBL20); At5g15890 (AtTBL21); At3g28150 (AtTBL22/AtAXY4L); At4g11090 (AtTBL23/AtMOAT1); (AtTBL24/AtMOAT2); At1g01430 (AtTBL25/AtMOAT3); At4g01080 (AtTBL26/AtMOAT4); At1g70230 (AtTBL27/AtAXY4); At2g40150 (AtTBL28/AtXOAT2); At3g55990(AtTBL29/AtXOAT1/AtESK1); At2g40160 (AtTBL30/AtXOAT3); At1g73140 AtTBL31/AtXOAT5); At3g11030 (AtTBL32/AtXOAT6); At2g40320 (AtTBL33/AtXOAT7); At2g38320 (AtTBL34/AtXOAT8); At5g01620 (AtTBL35/AtXOAT9); At3g54260 (AtTBL36); At2g34070 (AtTBL37); At1g29050 (AtTBL38); At2g42570 (AtTBL39); At2g31110 (AtTBL40); At3g14850 (AtTBL41); At1g78710 (AtTBL42); At2g30900 (AtTBL43); At5g58600 (AtTBL44/AtPMR5); At2g30010 (AtTBL45).

Funding

Funding was provided in part by the BioEnergy Science Center (BESC) and the Center for Bioenergy Innovation (CBI), from the U.S. Department of Energy Bioenergy Research Centers supported by the Office of Biological and Environmental Research in the DOE Office of Science. This work was also supported by the Laboratory Directed Research and Development (LDRD) Program at NREL. This work was authored in part by Alliance for Sustainable Energy, LLC, the Manager and Operator of the National Renewable Energy Laboratory for the U.S. Department of Energy (DOE) under Contract No. DE-AC36-08GO28308. The views expressed in the article do not necessarily represent the views of the DOE or the U.S. Government. The U.S. Government and the publisher, by accepting the article for publication, acknowledges that the U.S. Government retains a nonexclusive, paid-up, irrevocable, worldwide license to publish or reproduce the published form of this work, or allow others to do so, for U.S. Government purposes. This research was also supported by NIH grants P41GM103390, P01GM107012 and 1S10OD018530.

References

1. Smith PJ, Wang H-T, York WS, Peña MJ, Urbanowicz BR: Designer biomass for next-generation biorefineries: leveraging recent insights into xylan structure and biosynthesis. Biotechnology for biofuels 2017, 10(1):286.
2. Pauly M, Ramírez V: New Insights Into Wall Polysaccharide O-Acetylation. Frontiers in plant science 2018, 9.
3. Chong S-L, Virkki L, Maaheimo H, Juvonen M, Derba-Maceluch M, Koutaniemi S, Roach M, Sundberg B, Tuomainen P, Mellerowicz EJ: O-Acetylation of glucuronoxylan in Arabidopsis thaliana wild type and its change in xylan biosynthesis mutants. Glycobiology 2014, 24(6):494-506.
4. Johnson AM, Kim H, Ralph J, Mansfield SD: Natural acetylation impacts carbohydrate recovery during deconstruction of Populus trichocarpa wood. Biotechnology for biofuels 2017, 10(1):48.
5. Busse-Wicher M, Gomes TC, Tryfona T, Nikolovski N, Stott K, Grantham NJ, Bolam DN, Skaf MS, Dupree P: The pattern of xylan acetylation suggests xylan may interact with cellulose microfibrils as a twofold helical screw in the secondary plant cell wall of Arabidopsis thaliana. The Plant journal : for cell and molecular biology 2014, 79(3):492-506.
6. Köhnke T, Östlund Å, Brelid H: Adsorption of Arabinoxylan on Cellulosic Surfaces: Influence of Degree of Substitution and Substitution Pattern on Adsorption Characteristics. Biomacromolecules 2011, 12(7):2633-2641.

7. Kang X, Kirui A, Widanage MCD, Mentink-Vigier F, Cosgrove DJ, Wang T: Lignin-polysaccharide interactions in plant secondary cell walls revealed by solid-state NMR. Nat Commun 2019, 10(1):347.

8. Biely P: Microbial carbohydrate esterases deacetylating plant polysaccharides. Biotechnology Advances 2012, 30(6):1575-1588.

9. Manabe Y, Verhertbruggen Y, Gille S, Harholt J, Chong S-L, Pawar PM, Mellerowicz E, Tenkanen M, Cheng K, Pauly M: RWA proteins play vital and distinct roles in cell wall O-acetylation in Arabidopsis thaliana. Plant physiology 2013:pp. 113.225193.

10. Schultink A, Naylor D, Dama M, Pauly M: The role of the plant-specific AXY9 protein in Arabidopsis cell wall polysaccharide O-acetylation. Plant physiology 2015:pp. 114.256479.

11. Yuan Y, Teng Q, Zhong R, Ye Z-H: TBL3 and TBL31, two Arabidopsis DUF231 domain proteins, are required for 3-O-monoacetylation of xylan. Plant and Cell Physiology 2015, 57(1):35-45.

12. Yuan Y, Teng Q, Zhong R, Ye ZH: Roles of Arabidopsis TBL34 and TBL35 in xylan acetylation and plant growth. Plant science : an international journal of experimental plant biology 2016, 243:120-130.

13. Zhong R, Cui D, Ye Z-H: Regiospecific Acetylation of Xylan is Mediated by a Group of DUF231-Containing O-Acetyltransferases. Plant and Cell Physiology 2017, 58(12):2126-2138.

14. Zhong R, Cui D, Ye Z-H: Xyloglucan O-acetyltransferases from Arabidopsis thaliana and Populus trichocarpa catalyze acetylation of fucosylated galactose residues on xyloglucan side chains. Planta 2018, 248(5):1159-1171.

15. Stranne M, Ren Y, Fimognari L, Birdseye D, Yan J, Bardor M, Mollet JC, Komatsu T, Kikuchi J, Scheller HV: TBL 10 is required for O-acetylation of pectic rhamnogalacturonan-I in Arabidopsis thaliana. The Plant Journal 2018, 96(4):772-785.

16. Xiong G, Cheng K, Pauly M: Xylan O-acetylation impacts xylem development and enzymatic recalcitrance as indicated by the Arabidopsis mutant tbl29. Molecular plant 2013, 6(4):1373-1375.

17. Lefebvre V, Fortabat M-N, Ducamp A, North HM, Maia-Grondard A, Trouverie J, Boursiac Y, Mouille G, Durand-Tardif M: ESKIMO1 disruption in Arabidopsis alters vascular tissue and impairs water transport. PLoS One 2011, 6(2):e16645.

18. Urbanowicz BR, Peña MJ, Moniz HA, Moremen KW, York WS: Two Arabidopsis proteins synthesize acetylated xylan in vitro. The Plant Journal 2014, 80(2):197-206.

19. Grantham NJ, Wurman-Rodrich J, Terrett OM, Lyczakowski JJ, Stott K, Iuga D, Simmons TJ, Durand-Tardif M, Brown SP, Dupree R: An even pattern of xylan substitution is critical for interaction with cellulose in plant cell walls. Nature plants 2017, 3(11):859.

20. Yuan Y, Teng Q, Zhong R, Haghighat M, Richardson EA, Ye Z-H: Mutations of Arabidopsis TBL32 and TBL33 affect xylan acetylation and secondary wall deposition. PLoS One 2016, 11(1):e0146460.

21. Brott AS, Sychantha D, Clarke AJ: Assays for the Enzymes Catalyzing the O-Acetylation of Bacterial Cell Wall Polysaccharides. In: Bacterial Polysaccharides. Springer; 2019: 115-136.

22. Urbanowicz BR, Bharadwaj VS, Alahuhta M, Peña MJ, Lunin VV, Bomble YJ, Wang S, Yang JY, Tuomivaara ST, Himmel ME et al: Structural, mutagenic and in silico studies of

xyloglucan fucosylation in Arabidopsis thaliana suggest a water-mediated mechanism. The Plant Journal 2017, 91(6):931-949.

23. Culbertson AT, Ehrlich JJ, Choe J-Y, Honzatko RB, Zabotina OA: Structure of xyloglucan xylosyltransferase 1 reveals simple steric rules that define biological patterns of xyloglucan polymers. Proceedings of the National Academy of Sciences 2018, 115(23):6064-6069.

24. Urbanowicz B, Peña M, Moniz H, Moremen K, York W: Two Arabidopsis Proteins Synthesize Acetylated Xylan in Vitro. The Plant Journal 2014, 80.

25. Sychantha D, Little DJ, Chapman RN, Boons G-J, Robinson H, Howell PL, Clarke AJ: PatB1 is an O-acetyltransferase that decorates secondary cell wall polysaccharides. Nature chemical biology 2018, 14(1):79.

26. Zhong R, Cui D, Richardson EA, Phillips DR, Azadi P, Lu G, Ye Z-H: Cytosolic Acetyl-CoA Generated by ATP-Citrate Lyase Is Essential for Acetylation of Cell Wall Polysaccharides. Plant and Cell Physiology 2019.

27. Moynihan PJ, Clarke AJ: Assay for peptidoglycan O-acetyltransferase: a potential new antibacterial target. Analytical biochemistry 2013, 439(2):73-79.

28. Kabel MA, de Waard P, Schols HA, Voragen AG: Location of O-acetyl substituents in xylo-oligosaccharides obtained from hydrothermally treated Eucalyptus wood. Carbohydrate research 2003, 338(1):69-77.

29. Biely P, Mastihubová M, La Grange DC, Van Zyl WH, Prior BA: Enzyme-coupled assay of acetylxylan esterases on monoacetylated 4-nitrophenyl β-d-xylopyranosides. Analytical biochemistry 2004, 332(1):109-115.

30. Lassfolk R, Rahkila J, Johansson MP, Ekholm FS, Wärnå J, Leino R: Acetyl group migration across the saccharide units in oligomannoside model compound. Journal of the American Chemical Society 2018, 141(4):1646-1654.

31. Michalak L, La Rosa SL, Leivers S, Lindstad LJ, Røhr ÅK, Aachmann FL, Westereng B: A pair of esterases from a commensal gut bacterium remove acetylations from all positions on complex β-mannans. Proceedings of the National Academy of Sciences 2020, 117(13):7122-7130.

32. Moremen KW, Ramiah A, Stuart M, Steel J, Meng L, Forouhar F, Moniz HA, Gahlay G, Gao Z, Chapla D: Expression system for structural and functional studies of human glycosylation enzymes. Nature chemical biology 2018, 14(2):156.

33. Dodson G, Wlodawer A: Catalytic triads and their relatives. Trends in biochemical sciences 1998, 23(9):347-352.

34. Agirre J, Iglesias-Fernández J, Rovira C, Davies GJ, Wilson KS, Cowtan KD: Privateer: software for the conformational validation of carbohydrate structures. Nature structural & molecular biology 2015, 22(11):833-834.

35. Ma J, Lu Q, Yuan Y, Ge H, Li K, Zhao W, Gao Y, Niu L, Teng M: Crystal structure of isoamyl acetate-hydrolyzing esterase from Saccharomyces cerevisiae reveals a novel active site architecture and the basis of substrate specificity. Proteins: Structure, Function, and Bioinformatics 2011, 79(2):662-668.

36. Buller AR, Townsend CA: Intrinsic evolutionary constraints on protease structure, enzyme acylation, and the identity of the catalytic triad. Proceedings of the National Academy of Sciences of the United States of America 2013, 110(8):E653-E661.

37. Akoh CC, Lee G-C, Liaw Y-C, Huang T-H, Shaw J-F: GDSL family of serine esterases/lipases. Progress in Lipid Research 2004, 43(6):534-552.

38. Moynihan PJ, Clarke AJ: Mechanism of action of peptidoglycan O-acetyltransferase B involves a Ser-His-Asp catalytic triad. Biochemistry 2014, 53(39):6243-6251.

39. Bharadwaj VS, Dean AM, Maupin CM: Insights into the Glycyl Radical Enzyme Active Site of Benzylsuccinate Synthase: A Computational Study. Journal of the American Chemical Society 2013, 135(33):12279-12288.

40. Winn MD, Ballard CC, Cowtan KD, Dodson EJ, Emsley P, Evans PR, Keegan RM, Krissinel EB, Leslie AG, McCoy A et al: Overview of the CCP4 suite and current developments. Acta Crystallogr D Biol Crystallogr 2011, 67(Pt 4):235-242.

41. Skubak P, Pannu NS: Automatic protein structure solution from weak X-ray data. Nat Commun 2013, 4.

42. Hendrickson WA, Teeter MM: Structure of the hydrophobic protein crambin determined directly from the anomalous scattering of sulphur. Nature 1981, 290(5802):107-113.

43. Murshudov GN, Skubak P, Lebedev AA, Pannu NS, Steiner RA, Nicholls RA, Winn MD, Long F, Vagin AA: REFMAC5 for the refinement of macromolecular crystal structures. Acta Crystallogr D Biol Crystallogr 2011, 67(Pt 4):355-367.

44. Emsley P, Lohkamp B, Scott WG, Cowtan K: Features and development of Coot. Acta Crystallogr D Biol Crystallogr 2010, 66(Pt 4):486-501.

45. Chen VB, Arendall WB, 3rd, Headd JJ, Keedy DA, Immormino RM, Kapral GJ, Murray LW, Richardson JS, Richardson DC: MolProbity: all-atom structure validation for macromolecular crystallography. Acta Crystallogr D Biol Crystallogr 2010, 66(Pt 1):12-21.

46. Engh RA, Huber R: Accurate Bond and Angle Parameters for X-Ray Protein-Structure Refinement. Acta Crystallographica Section A 1991, 47:392-400.

47. Morris GM, Huey R, Lindstrom W, Sanner MF, Belew RK, Goodsell DS, Olson AJ: AutoDock4 and AutoDockTools4: Automated Docking with Selective Receptor Flexibility. Journal of Computational Chemistry 2009, 30(16):2785-2791.

48. Anandakrishnan R, Aguilar B, Onufriev AV: H++3.0: automating pK prediction and the preparation of biomolecular structures for atomistic molecular modeling and simulations. Nucleic Acids Research 2012, 40(W1):W537-W541.

49. Huang J, MacKerell AD: CHARMM36 all-atom additive protein force field: validation based on comparison to NMR data. Journal of Computational Chemistry 2013, 34(25):2135-2145.

50. Guvench O, Hatcher E, Venable RM, Pastor RW, MacKerell AD: CHARMM Additive All-Atom Force Field for Glycosidic Linkages between Hexopyranoses. J Chem Theory Comput 2009, 5(9):2353-2370.

51. Vanommeslaeghe K, Hatcher E, Acharya C, Kundu S, Zhong S, Shim J, Darian E, Guvench O, Lopes P, Vorobyov I et al: CHARMM General Force Field (CGenFF): A force field for drug-like molecules compatible with the CHARMM all-atom additive biological force fields. Journal of computational chemistry 2010, 31(4):671-690.

52. Jorgensen WL, Chandrasekhar J, Madura JD, Impey RW, Klein ML: Comparison of simple potential functions for simulating liquid water. The Journal of chemical physics 1983, 79(2):926-935.

53. Darden T, York D, Pedersen L: Particle mesh Ewald: An N· log (N) method for Ewald sums in large systems. The Journal of chemical physics 1993, 98(12):10089-10092.

54. Ryckaert J-P, Ciccotti G, Berendsen HJC: Numerical integration of the cartesian equations of motion of a system with constraints: molecular dynamics of n-alkanes. Journal of Computational Physics 1977, 23(3):327-341.

55. Brooks BR, Brooks CL, MacKerell AD, Nilsson L, Petrella RJ, Roux B, Won Y, Archontis G, Bartels C, Boresch S: CHARMM: the biomolecular simulation program. Journal of computational chemistry 2009, 30(10):1545-1614.

56. Hynninen AP, Crowley MF: New faster CHARMM molecular dynamics engine. Journal of computational chemistry 2014, 35(5):406-413.

57. Roe DR, Cheatham TE: PTRAJ and CPPTRAJ: Software for Processing and Analysis of Molecular Dynamics Trajectory Data. J Chem Theory Comput 2013, 9(7):3084-3095.

58. Humphrey W, Dalke A, Schulten K: VMD: Visual molecular dynamics. Journal of Molecular Graphics 1996, 14(1):33-38.

Table S2.1 Primer sequences for gene cloning and site-directed mutagenesis for generation of the expression constructs

Enzyme form	Amino acid length	Primer sequence 5' → 3'	GFP fluorescence*
AtXOAT1-fl	44-487	AACTTGTACTTTCAAGGCGAAGACGTCAAGTCCAT ACAAGAAAGCTGGGTCCTACGAACGGGAAATGATAC	1590
AtXOAT1-cat	133-487	AACTTGTACTTTCAAGGCGAAGACGTGGAATTGCC ACAAGAAAGCTGGGTCCTACGAACGGGAAATGATAC	2120
AtXOAT1-nv	44-133	AACTTGTACTTTCAAGGCGAAGACGTCAAGTCCAT ACAAGAAAGCTGGGTCCTACACGTCTTCTTCATCCT	1865
AtXOAT1-aa57-486	57-486	AACTTGTACTTTCAAGGCTCAAAACCTCACGACGTC ACAAGAAAGCTGGGTCCTAACGGGAAATGATACGTGT	2198
D215A†	133-486	GTTCGTTGGAGCTTCCCTAAACC ATCATTCTCTTGTTCCTTAGCTTC	569
S216A†	133-486	CGTTGGAGATGCCCTAAACCGGA AACATCATTCTCTTGTTCCTTAGCTTC	3071
R219A†	133-486	ATTCCCTAAACGCGAACCAATGGG CTCCAACGAACATCATTCTCTTGT	947
N220A†	133-486	CCCTAAACCGGGCCCAATGGGAAT AATCTCCAACGAACATCATTCTCT	2604
H437A†	133-486	GGAAAGATGCTGCCACTTCGGTTC GGTATTCGGAGAGTTTGGTAATGT	1639
D462A†	57-486	ACTTACGCCGCTTGTATCCATTG GTTGGGATCGGCTTGTTG	2356
H465A†	133-486	CGATTGTATCGCTTGGTGTCTTCCCGG GCGTAAGTGTTGGGATCG	2926

*Expression and secretion of the recombinant GFP-AtXOAT1 protein and its variants in transiently transfected HEK293F cells. The expression levels are determined by measuring the relative fluorescence of the secreted proteins in the media.

† The underlined nucleotides in the primer sequences represent the bases corresponding to the mutated residues used for site-directed mutagenesis.

Figure 2.1

Biochemical properties of *At*XOAT1. (**a**) The scaled domain architecture of *At*XOAT1 described in this study. T, NH_2-terminal transmembrane domain; NV, NH_2-terminal variable region; TBL, TBL domain; DUF231, DUF231 domain. The transmembrane helix was predicted using TMHMM Server v. 2.0 (http://www.cbs.dtu.dk/services/TMHMM/). Prediction of the *N*-glycosylation sites (red diamonds) were carried out using the NetNGlyc 1.0 Server (http://www.cbs.dtu.dk/services/NetNGlyc/). Scale bar represents 100 amino acids. (**b**) The *in vitro* reaction scheme of xylan *O*-acetylation catalyzed by *At*XOAT1. (**c**) The donor substrate promiscuity of *At*XOAT revealed by MALDI-TOF MS analysis of acetylated Xyl_6-2AB generated by incubating *At*XOAT1 with Xyl_6-2AB acceptors and different acetyl-donors, acetyl-CoA, *para*-nitrophenyl acetate (*p*NP-Ac), acetylsalicylic acid (ASA) and 4-methylumbelliferylacetate (4MU-Ac) for 6 h. Each transfer of *O*-acetyl group increases the mass of Xyl_6-2AB by 42 Da as indicated by annotating $[M+H]^+$ ions. (**d**) The percentage of acyl-*At*XOAT1 formed upon reaction with different acetyl donors. The error bars indicate mean ± s.d. from three independent assays. Statistical significance was determined with the two-tailed Student's *t*-test. *, $p < 0.05$; **, $p < 0.01$. (**e**) Real-time ^{1}H NMR analysis of *At*XOAT1-catalyzed reaction by using acetyl-CoA and xylohexaose (Xyl_6) as the substrates. The thickened green line corresponds to the spectrum of the reaction at the 6 h time point, while the thickened purple line indicates the end of the 20-hour reaction. (**f**) Acetyl group migration analysis through real-time ^{1}H NMR after removal of *At*XOAT1. The thickened red line corresponds to the starting point for monitoring acetyl group migration after removal of AtXOAT1 after a 6-hour reaction, while the thickened purple line represents the end point of monitoring the migration (14 hours after transfer).

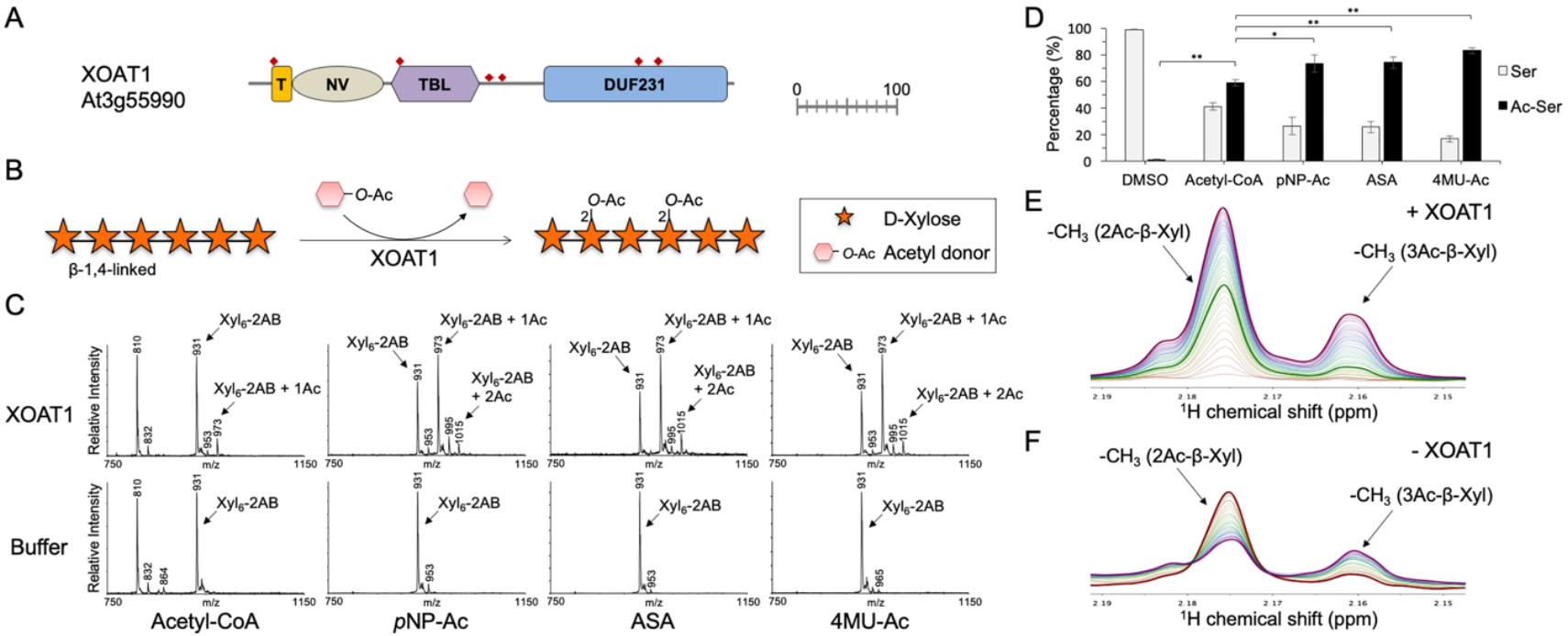
A
XOAT1
At3g55990
T
NV
TBL
DUF231
0
100
B
O-Ac
XOAT1
β-1,4-linked
D-Xylose
O-Ac Acetyl donor
C
XOAT1
Buffer
Relative Intensity
m/z
Xyl6-2AB
Xyl6-2AB + 1Ac
Xyl6-2AB + 2Ac
Acetyl-CoA
pNP-Ac
ASA
4MU-Ac
D
Percentage (%)
Ser
Ac-Ser
DMSO
Acetyl-CoA
pNP-Ac
ASA
4MU-Ac
E
+ XOAT1
-CH3 (2Ac-β-Xyl)
-CH3 (3Ac-β-Xyl)
1H chemical shift (ppm)
F
- XOAT1
-CH3 (2Ac-β-Xyl)
-CH3 (3Ac-β-Xyl)
1H chemical shift (ppm)

Figure 2.2

Overall structure of *At*XOAT1: (**a**) Cartoon representation of the *At*XOAT1-cat fold. Pink loops, cyan α-helices and magenta β-strands are shown for the major lobe and green loops, red α-helices and yellow β-strands are shown for the minor lobe. Disulfides are shown as spheres. The sidechains of the catalytic triad Asp462-His465-Ser216 are shown in stick representation. (**b**) Surface representation reveals a putative substrate binding groove. The major lobe is shown in cyan and the minor lobe is colored green. A xylodecaose bound in the groove in MD simulations is shown in stick representation. (**c**) Zoomed in active site. (**d**) Cartoon representation of the XOAT1-cat colored by flexibility of the protein regions based on MD simulations.

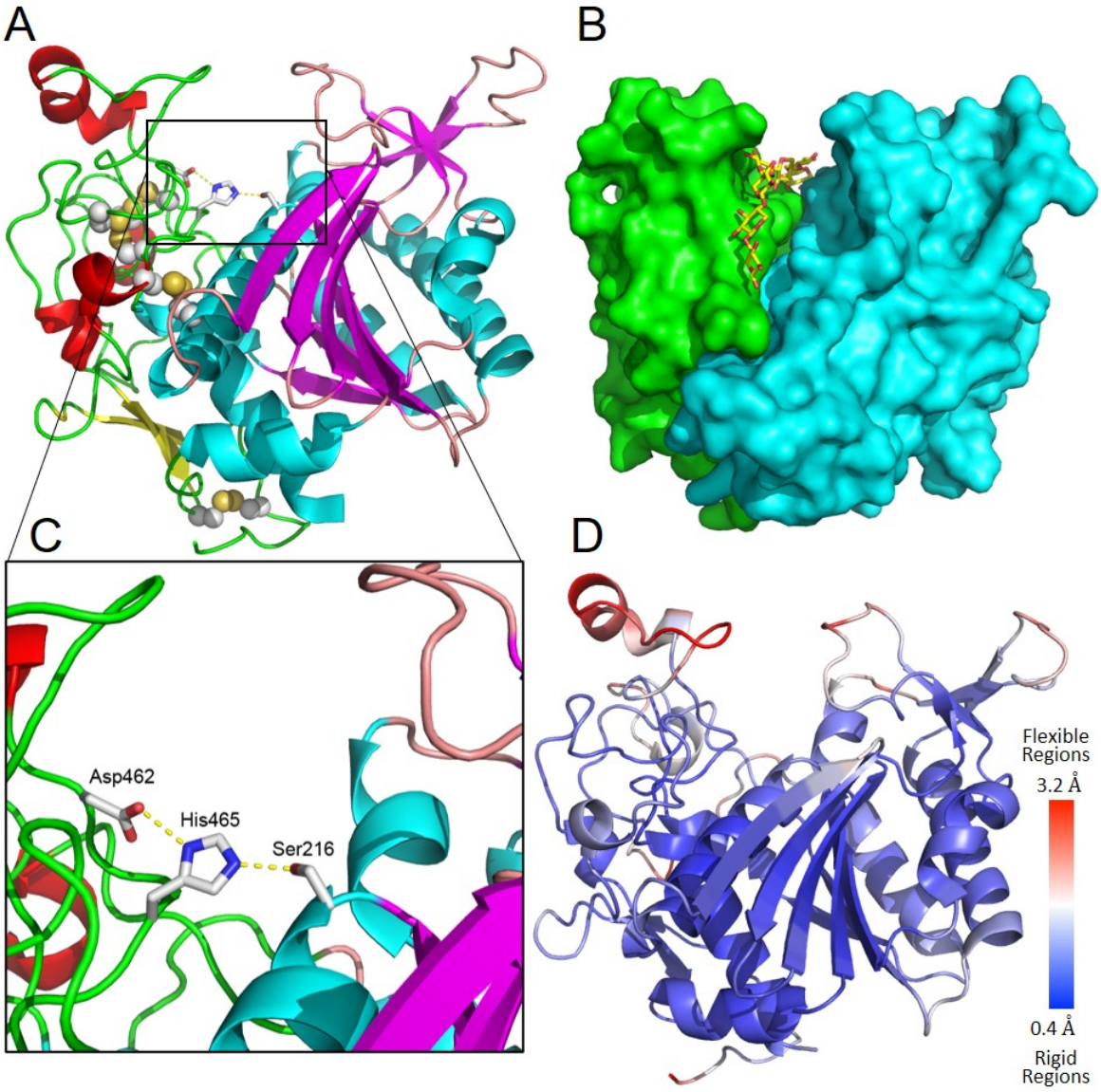
A
B
C
D
Asp462
His465
Ser216
Flexible
Regions
3.2 Å
0.4 Å
Rigid
Regions

Figure 2.3

Active site and partial conservation of structural domains in A*t*XOAT1. Structural alignment of *At*XOAT1 (**a** - Center) with (**b** – Top Left) peptidoglycan *O*-acetyltransferase from *B. cerus* (PATB1) (PDB ID: 5V8E), (**c** – Top Right) Isoamyl acetate hydrolyzing esterase (PDB ID:3MIL), (**d** – Bottom Left) a putative lipase from *B. thetaiotamicron* (PDB ID 3BZW) and (**e** – Bottom right) peptidoglycan *O*-acetylesterase from *N. meningitidis* (PDB ID 4K3U). The secondary structure domains that demonstrate good alignment with *At*XOAT1 are depicted in solid colors while the non-aligned parts are greyed out. All structures share the Ser-His-Asp catalytic triad, which is shown in licorice representation with the carbons, oxygen and nitrogen atoms are colored yellow, red and blue, respectively.

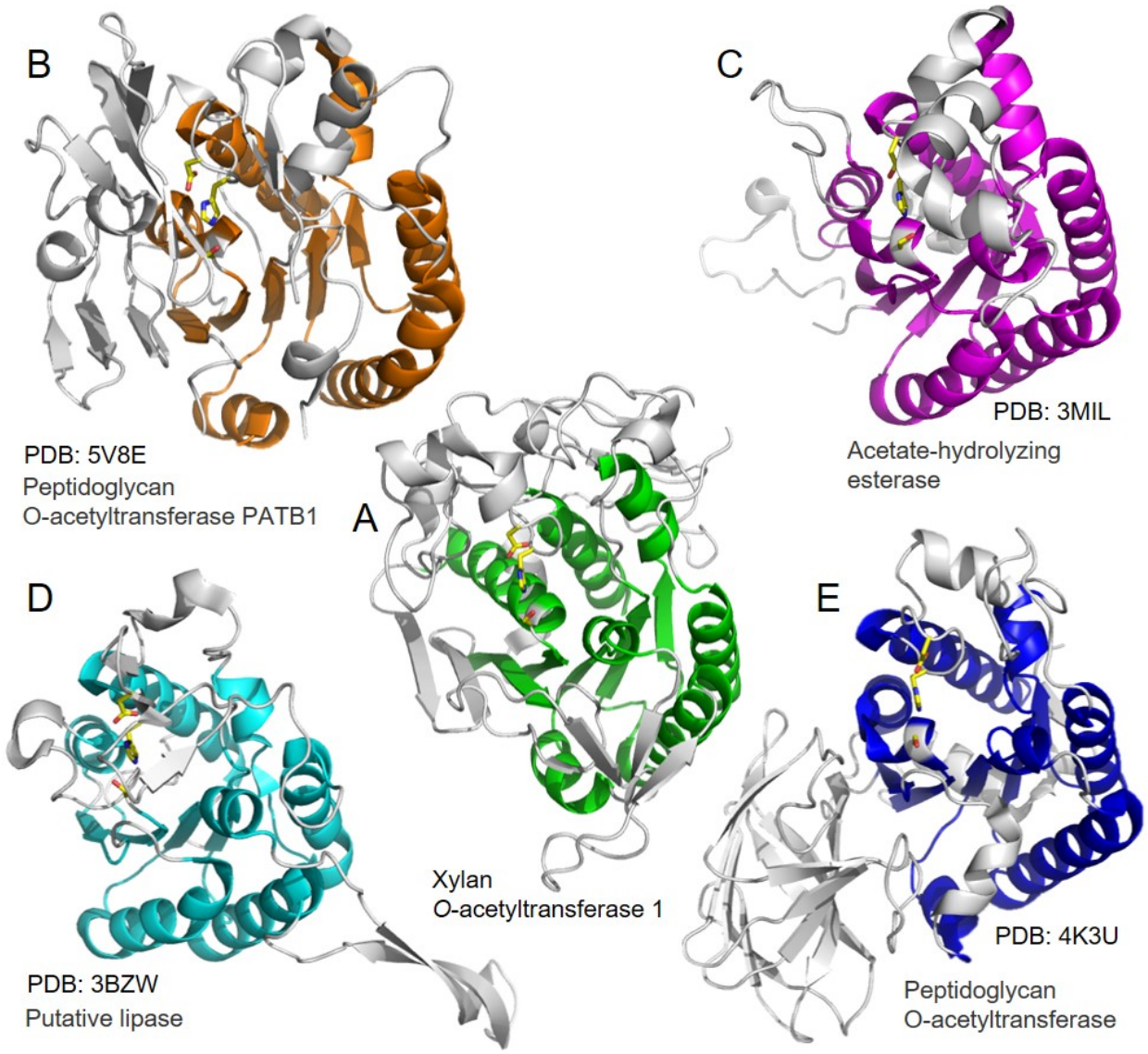
B
PDB: 5V8E
Peptidoglycan
O-acetyltransferase PATB1
C
PDB: 3MIL
Acetate-hydrolyzing
esterase
A
Xylan
O-acetyltransferase 1
D
PDB: 3BZW
Putative lipase
E
PDB: 4K3U
Peptidoglycan
O-acetyltransferase

Figure 2.4

Enzymatic activity of *At*XOAT1 mutant variants compared with the wild type *At*XOAT1. (**a**) MALDI-TOF MS of the reaction products produced by *At*XOAT1 and its mutant variants. Each transfer of an acetyl group (Ac) increases the mass of the Xyl_6-2AB acceptor by 42 Da as annotated $[M+H]^+$ ions. (**b**) Comparative analysis of the esterase and transferase activities of of *At*XOAT1 and its variants determined by measuring the release of *p*NP from *p*NP-Ac (5 mM) formed in the absence (grey) or in the presence (black) of the acceptor substrate Xyl_4 (5 mM), respectively. The error bars indicate mean ± s.d. from four independent assays. Statistical significance of each variant compared to the corresponding wild-typed constructs (*At*XOAT1-cat and $AtXOAT1^{aa57\text{-}486}$) was determined with the two-tailed Student's *t*-test. **, $p < 0.01$. (**c**) Close-up view of the mutated residues at the *At*XOAT1 active site.

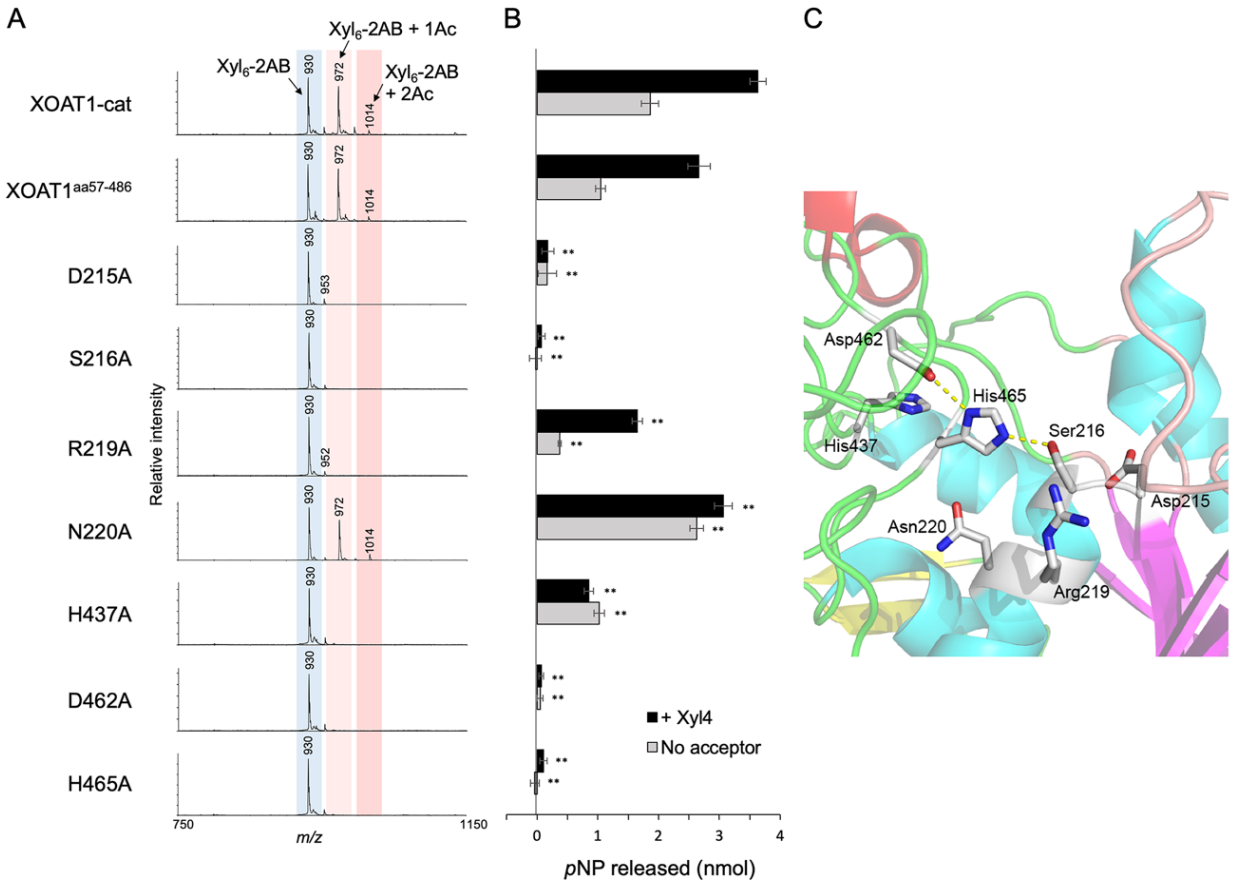
A
Xyl6-2AB + 1Ac
Xyl6-2AB
Xyl6-2AB
+ 2Ac
XOAT1-cat
XOAT1aa57-486
D215A
S216A
R219A
N220A
H437A
D462A
H465A
930
972
1014
953
952
Relative intensity
750
m/z
1150
B
+ Xyl4
No acceptor
0
1
2
3
4
pNP released (nmol)
C
Asp462
His465
His437
Ser216
Asp215
Asn220
Arg219

Figure 2.5

Reaction mechanism of *At*XOAT1. (**a**) Proposed reaction mechanism for acetylation of xylan oligosaccharides by *At*XOAT1. Rearrangement of the pi electrons within the His residue are not shown.

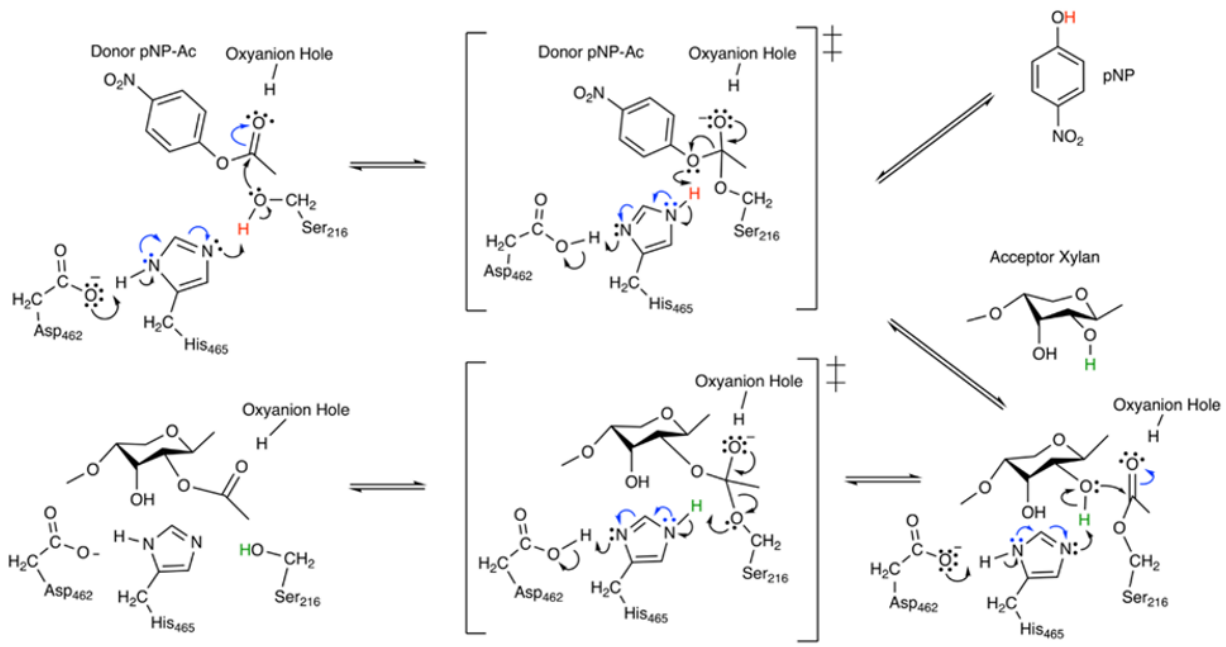
Donor pNP-Ac
Oxyanion Hole
Asp462
His465
Ser216
pNP
Acceptor Xylan

Figure 2.6

Molecular Dynamics simulation results corroborate reaction: (**a**) A snapshot from unbiased simulations of *At*XOAT1 in its donor bound state reveals catalytically competent configurations for the 1st stage of the reaction mechanism. The donor molecule is shown in licorice representation with carbons colored magenta along with the important residues stabilizing it. Distances for the proton transfer and nucleophilic attack are shown with dashed lines. (**b**) Distances between protons on *O*-2 (magenta) and *O*-3 (blue) of the xylose ring closest to the catalytic triad indicate that the *O*-2 proton is consistently closer to the His465 Nitrogen. (**c**) A snapshot from an unbiased simulation of *At*XOAT1 in its acceptor (xylodecaose) bound state. Three xylose units closest to the active site are shown in licorice representation with the carbons colored yellow along with the important residues stabilizing it. The distance for proton transfer to generate the nucleophile on the xylose unit is shown with dashed lines. Note that snapshots depicted in A and C are pre-reaction stationary states observed in MD simulations.

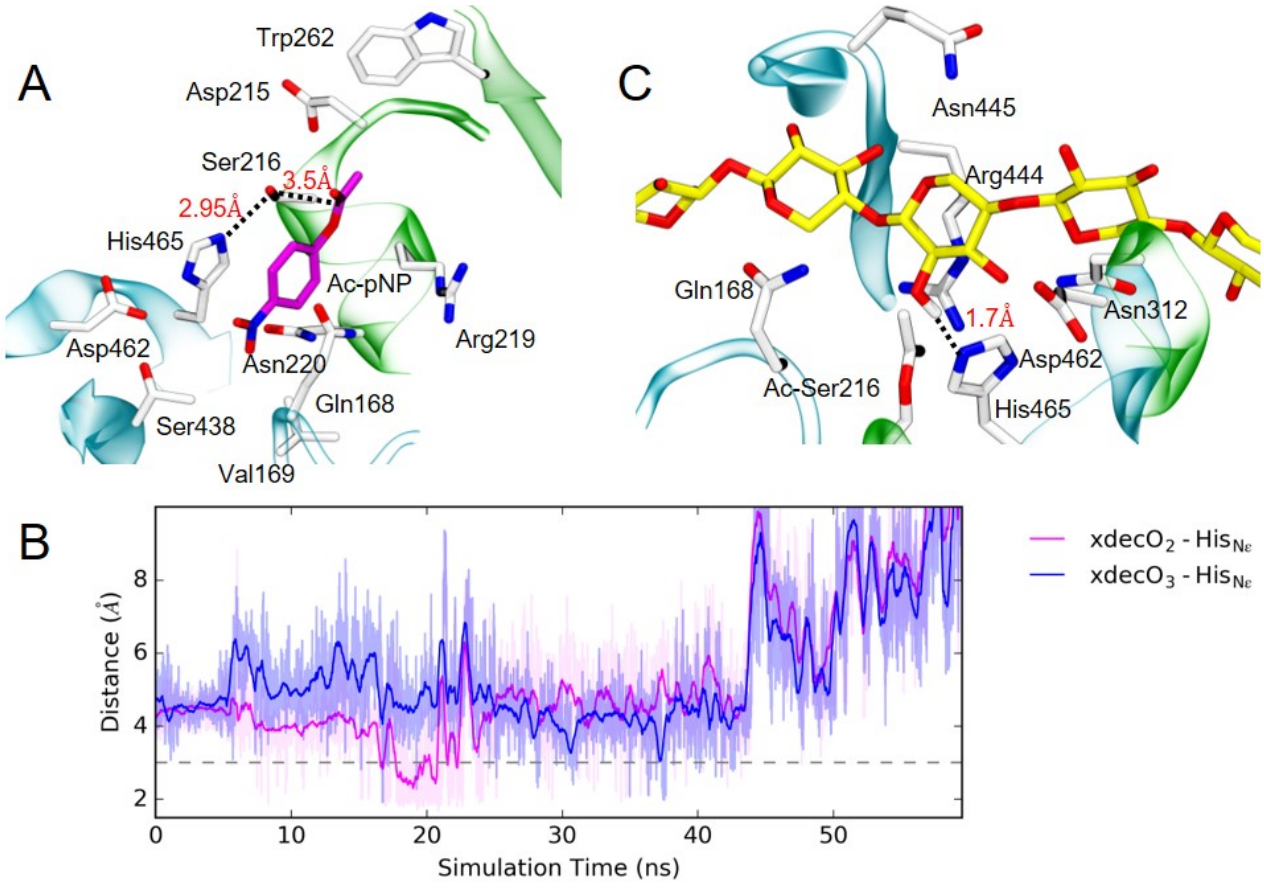
A
Trp262
Asp215
Ser216
3.5Å
2.95Å
His465
Ac-pNP
Arg219
Asp462
Asn220
Gln168
Ser438
Val169
C
Asn445
Arg444
Gln168
1.7Å
Asn312
Asp462
Ac-Ser216
His465
B
Distance (Å)
Simulation Time (ns)
xdecO2 - HisNε
xdecO3 - HisNε

Figure S2.1

Activity curves of *At*XOAT1 as an *O*-acetyltransferase. The release of *p*NP was measured in the reaction with 5 μM *At*XOAT1 incubated with 5 mM *p*NP-Ac as the donor substrate and xylopentaose (Xyl5) with various concentrations as the acceptor. The solid filled markers represent the average from duplicate measurements at each time point, and empty markers indicate the values of each replicate.

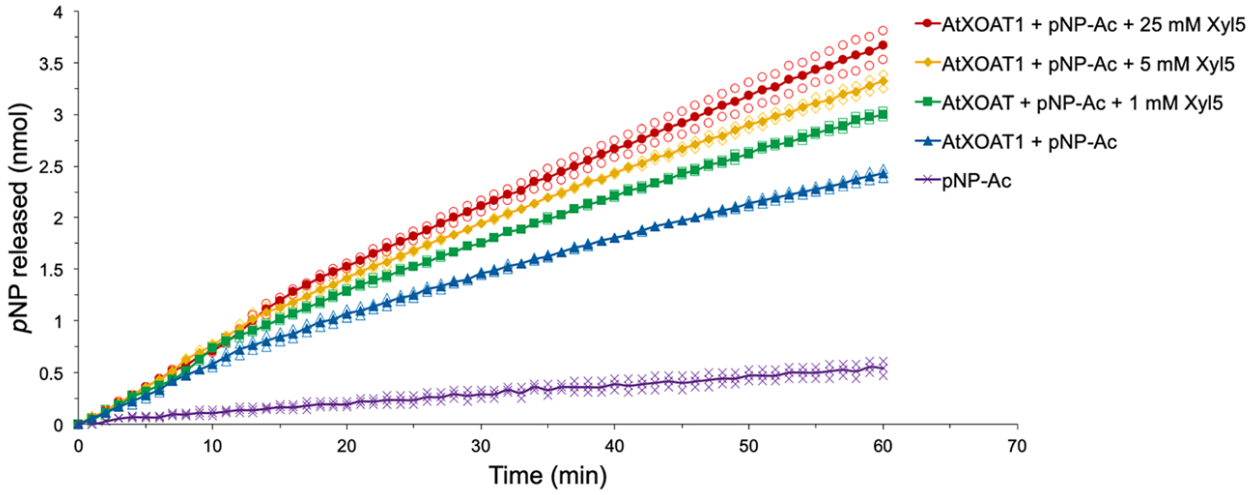
pNP released (nmol)
Time (min)
AtXOAT1 + pNP-Ac + 25 mM Xyl5
AtXOAT1 + pNP-Ac + 5 mM Xyl5
AtXOAT + pNP-Ac + 1 mM Xyl5
AtXOAT1 + pNP-Ac
pNP-Ac

Figure S2.2

MALDI-TOF MS of the acetylated xylo-oligosacharides generated by *At*XOAT1. The *O*-acetyltransferase activity of *At*XOAT1 toward xylo-oligosaccharides with different DPs was assayed using 5 mM acetylsalicylic acid as the donor substrate. The reaction products were analyzed by MALDI-TOF MS. Each transfer of the *O*-acetyl group (Ac) increases the mass of the xylo-oligo acceptors by 42 Da as the annotated $[M+H]^+$ ions. Xyl2, xylobiose; Xyl3, xylotriose; Xyl4, xylotetraose; Xyl5, xylopentaose; Xyl6, xylohexaose.

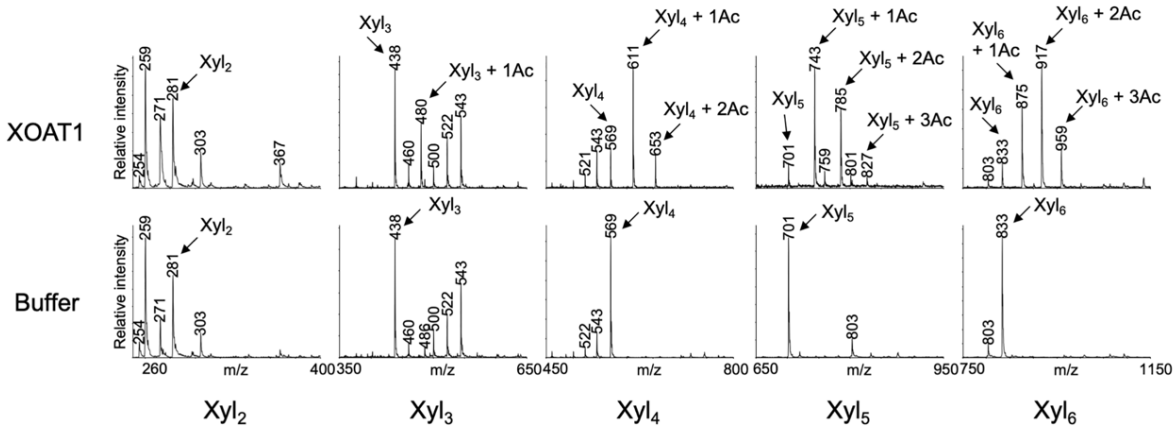
XOAT1
Buffer
Relative intensity
Xyl2
Xyl3
Xyl3 + 1Ac
Xyl4
Xyl4 + 1Ac
Xyl4 + 2Ac
Xyl5
Xyl5 + 1Ac
Xyl5 + 2Ac
Xyl5 + 3Ac
Xyl6
Xyl6 + 1Ac
Xyl6 + 2Ac
Xyl6 + 3Ac
m/z
Xyl2
Xyl3
Xyl4
Xyl5
Xyl6

Figure S2.3

Quantitation of the XOAT1 acyl-enzyme intermediate. Combined extracted ion chromatographs (XIC) of m/z corresponding to the peptide MMFVGDSLNR (m/z 585.2728 z=2) and the acetylated peptide MMFVGD**S**LNR (m/z 606.2840 z=2), where **S** indicates the Ser residue of modification. Extracted data was collected within 5.0 ppm mass tolerance.

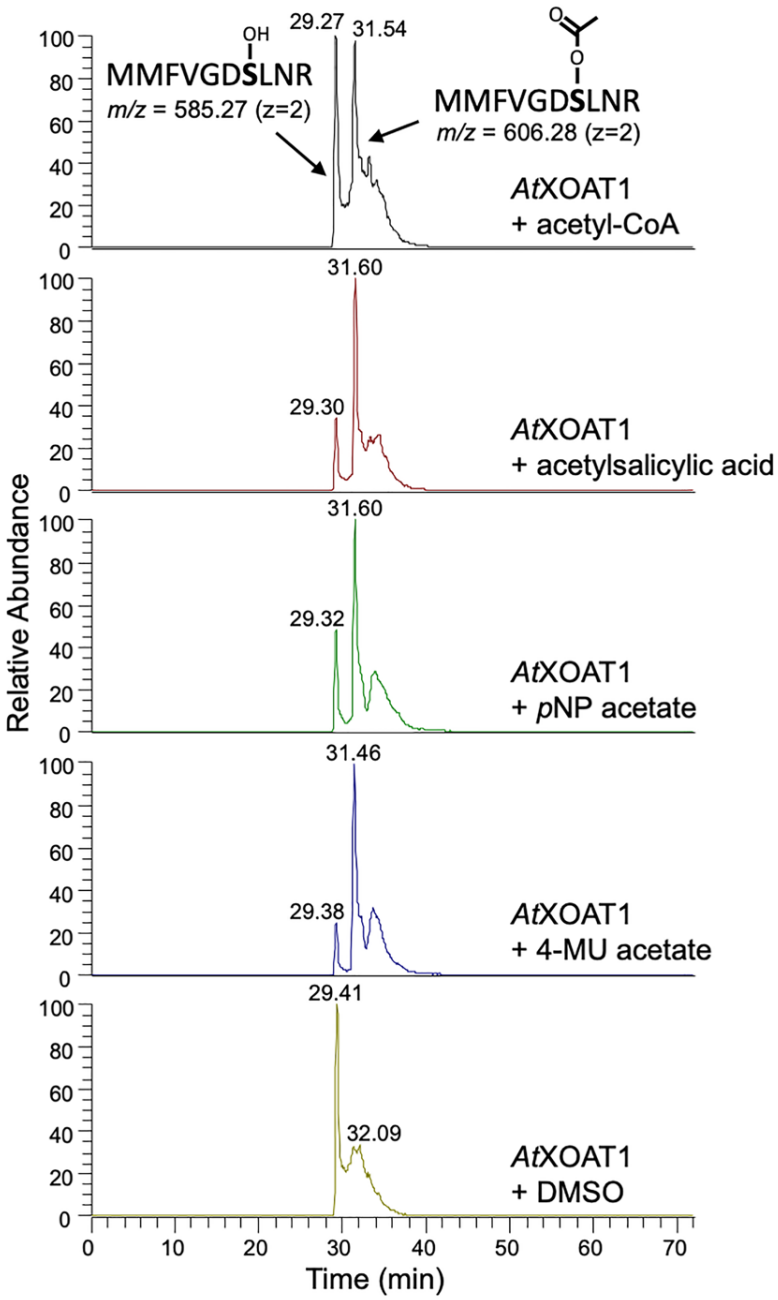
OH
MMFVGDSLNR
m/z = 585.27 (z=2)
29.27
31.54
O
O
MMFVGDSLNR
m/z = 606.28 (z=2)
AtXOAT1
+ acetyl-CoA
31.60
29.30
AtXOAT1
+ acetylsalicylic acid
31.60
29.32
AtXOAT1
+ pNP acetate
31.46
29.38
AtXOAT1
+ 4-MU acetate
29.41
32.09
AtXOAT1
+ DMSO
Relative Abundance
Time (min)

Figure S2.4

MS/MS Fragmentation Spectra (HCD) of m/z corresponding to the acetylated peptide MMFVGDSLNR (m/z 606.2840 z=2), where S indicates the site of modification.

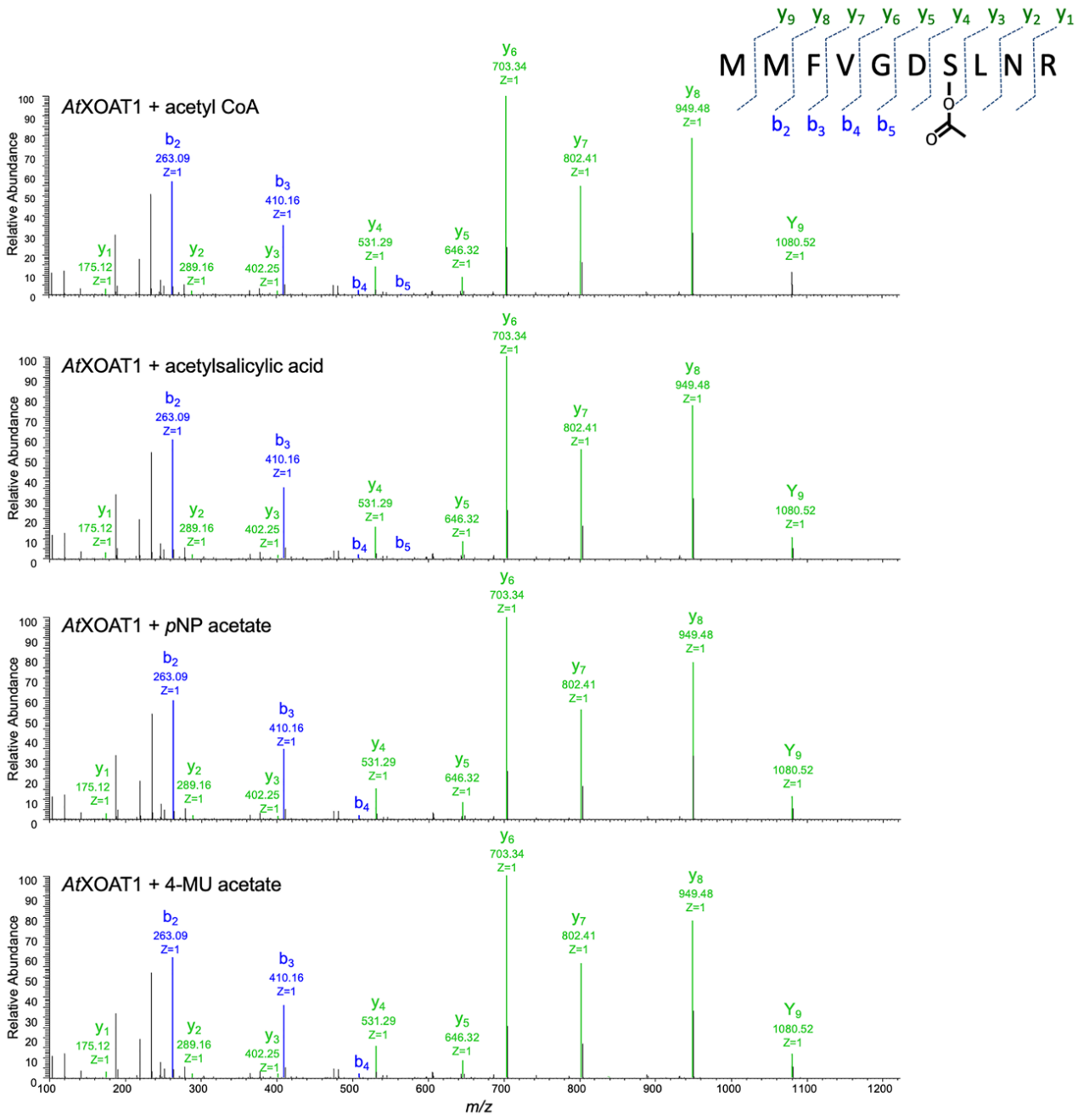
M M F V G D S L N R
y9 y8 y7 y6 y5 y4 y3 y2 y1
b2 b3 b4 b5
AtXOAT1 + acetyl CoA
AtXOAT1 + acetylsalicylic acid
AtXOAT1 + pNP acetate
AtXOAT1 + 4-MU acetate
Relative Abundance
m/z
y6 703.34 Z=1
y8 949.48 Z=1
y7 802.41 Z=1
b2 263.09 Z=1
b3 410.16 Z=1
y4 531.29 Z=1
y5 646.32 Z=1
Y9 1080.52 Z=1
y1 175.12 Z=1
y2 289.16 Z=1
y3 402.25 Z=1
b4
b5

Figure S2.5

Domain architectures of the designed expression constructs of *At*XOAT1 and their corresponding *O*-acetyltransferase activities. Domain structures of the *At*XOAT1 (**A**) and the designed expression constructs (**B**) used in this study. SS, signal sequence; H, 8XHis Tag; A, AviTag; sfGFP, Superfolder GFP; TEV, cleavage site for the cysteine protease from Tobacco Etch Virus (TEV); T, NH_2-terminal transmembrane domain; NV, NH_2-terminal variable region; TBL, TBL domain; DUF321, DUF231 domain. Predicted *N*-glycosylation sites are labeled with the red diamonds. Scale bar represents 100 amino acids. (c) MALDI-TOF MS of the reaction products generated by the *At*XOAT1 expression constructs, *At*XOAT1-fl, *At*XOAT1-cat and *At*XOAT1-nv. Each transfer of the *O*-acetyl group (Ac) increases the mass of the acceptor Xyl6-2AB by 42 Da as indicated by the annotated $[M+H]^+$ ions.

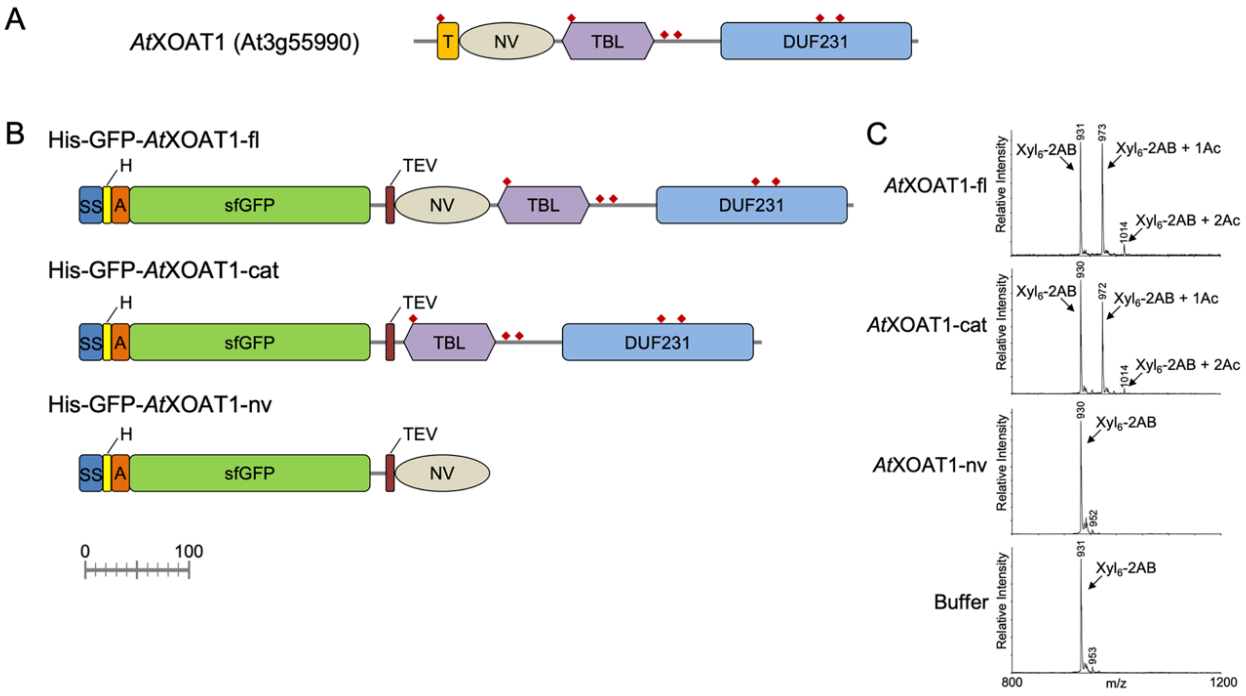
A
AtXOAT1 (At3g55990)
T
NV
TBL
DUF231
B
His-GFP-AtXOAT1-fl
H
TEV
SS
A
sfGFP
NV
TBL
DUF231
His-GFP-AtXOAT1-cat
His-GFP-AtXOAT1-nv
0
100
C
AtXOAT1-fl
AtXOAT1-cat
AtXOAT1-nv
Buffer
Relative Intensity
Xyl6-2AB
Xyl6-2AB + 1Ac
Xyl6-2AB + 2Ac
931
973
1014
930
972
962
953
800
m/z
1200

Figure S2.6

Protein topology diagram for *At*XOAT1-cat. Alpha-helices are shown as cylinders and marked as ‘H’, alpha-turns (helical fragments with a single H-bond) marked as ‘αT’ and beta-strands as ‘β’. Secondary structure elements belonging to the major ‘structured’ lobe are shaded in blue and outlined with the blue dashed line. Secondary structure elements belonging to the minor ‘unstructured’ lobe are shaded in green and outlined with the green dashed line. Amino acid residue numbers for the beginning and end of each secondary structure element are indicated.

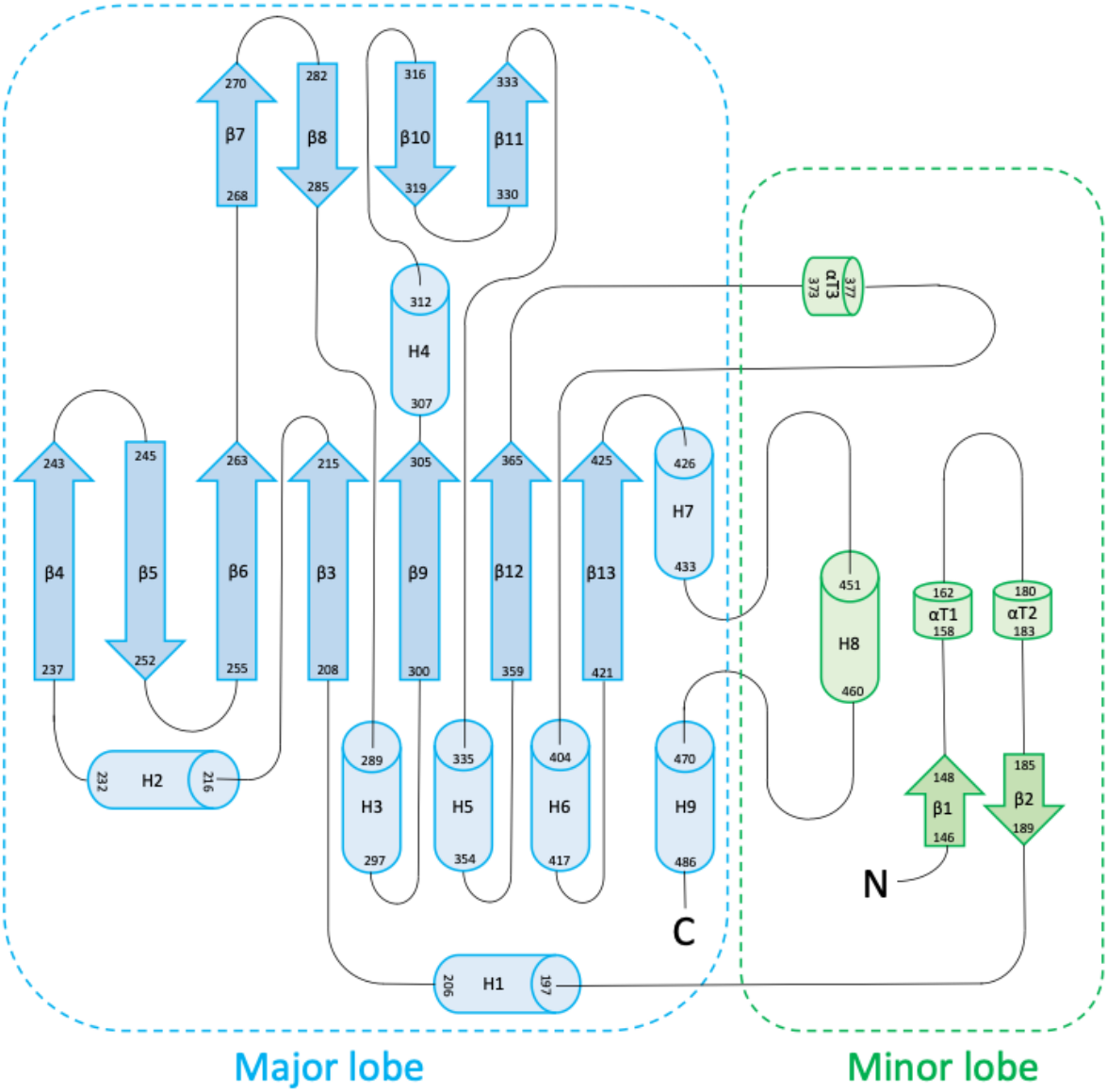
β7
270
268
β8
282
285
β10
316
319
β11
333
330
H4
312
307
αT3
373
377
β4
243
237
β5
245
252
β6
263
255
β3
215
208
β9
305
300
β12
365
359
β13
425
421
H7
426
433
H8
451
460
αT1
162
158
αT2
180
183
β1
148
146
β2
185
189
N
C
H2
232
216
H3
289
297
H5
335
354
H6
404
417
H9
470
486
H1
206
197
Major lobe
Minor lobe

Figure S2.7

Sequence alignment of the *Arabidopsis* TBL protein family. The name of each TBL protein is shown on the left. The number of the last amino acid residue for each protein is indicated in the end of each line. The consensus GDS and DXXH motifs are boxed in red, while the newly identified plant-specific TBL-block II, RNQxxS, and block III, RxDxH, are boxed in blue. Catalytic residues are denoted by the red asterisks. *N*-glycosylation sites are pointed in the domain structure by the red diamonds. The hypothesized oxyanion hole-forming residues and substrate-stabilizing residues are indicated by the arrowheads and empty arrowheads.

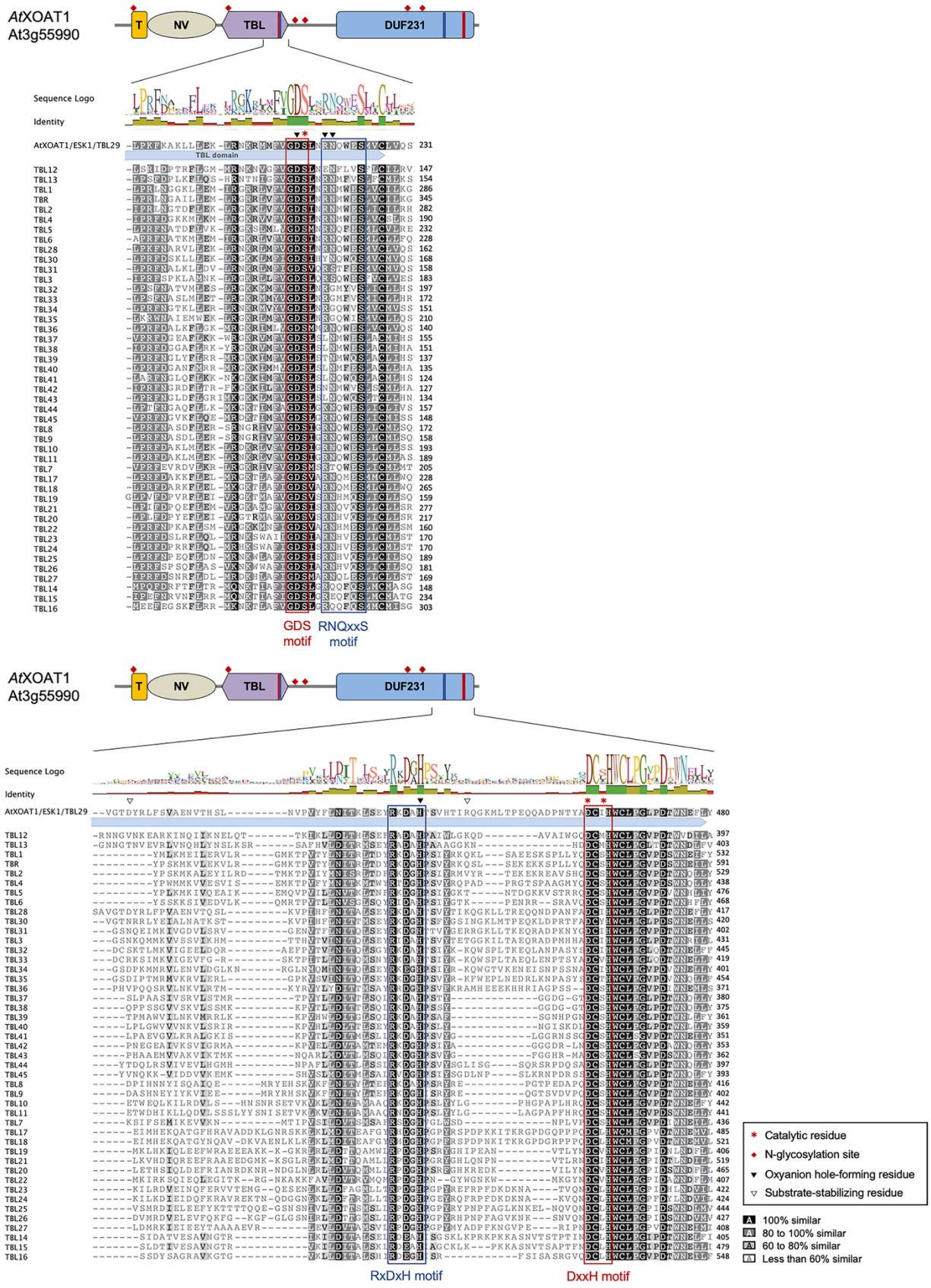
AtXOAT1
At3g55990
T
NV
TBL
DUF231
Sequence Logo
Identity
AtXOAT1/ESK1/TBL29
TBL domain
GDS motif
RNQxxS motif
RxDxH motif
DxxH motif
Catalytic residue
N-glycosylation site
Oxyanion hole-forming residue
Substrate-stabilizing residue
100% similar
80 to 100% similar
60 to 80% similar
Less than 60% similar

Figure S2.8

MALDI-TOF MS of the reaction products produced by *At*XOAT1 with serine protease inhibitors. The acetylated Xyl_6-2AB produced by *At*XOAT1 incubating with serine protease inhibitors, TPCK (80 μM), AEBSF (800 μM), PMSF (4 mM) and MSF (5 mM) in the reaction were analyzed by MALDI-TOF MS. DMSO was used in the reaction as a control. Each transfer of an acetyl group (Ac) increases the mass of Xyl_6-2AB acceptor by 42 Da as indicated by the annotated $[M+H]^+$ ions.

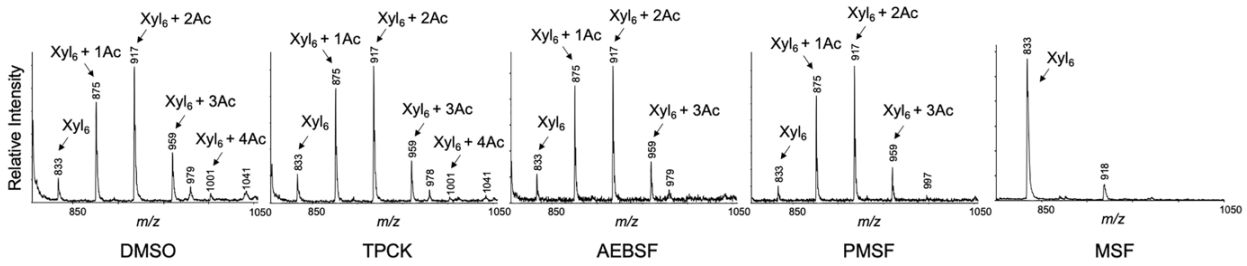
Relative Intensity
Xyl6
Xyl6 + 1Ac
Xyl6 + 2Ac
Xyl6 + 3Ac
Xyl6 + 4Ac
833
875
917
959
979
1001
1041
978
997
918
850
1050
m/z
DMSO
TPCK
AEBSF
PMSF
MSF

Figure S2.9

Stability of the Catalytic Triad. Hydrogen bonding distances observed for the catalytic triad over a 60 ns unbiased simulation of *At*XOAT1 in the apo state. The Ser216 H to His465 N distance is shown in pink and the shortest Asp O to His H distance is depicted in blue. The dark lines indicate the moving average value while the lighter lines indicate values of the distance at this time step.

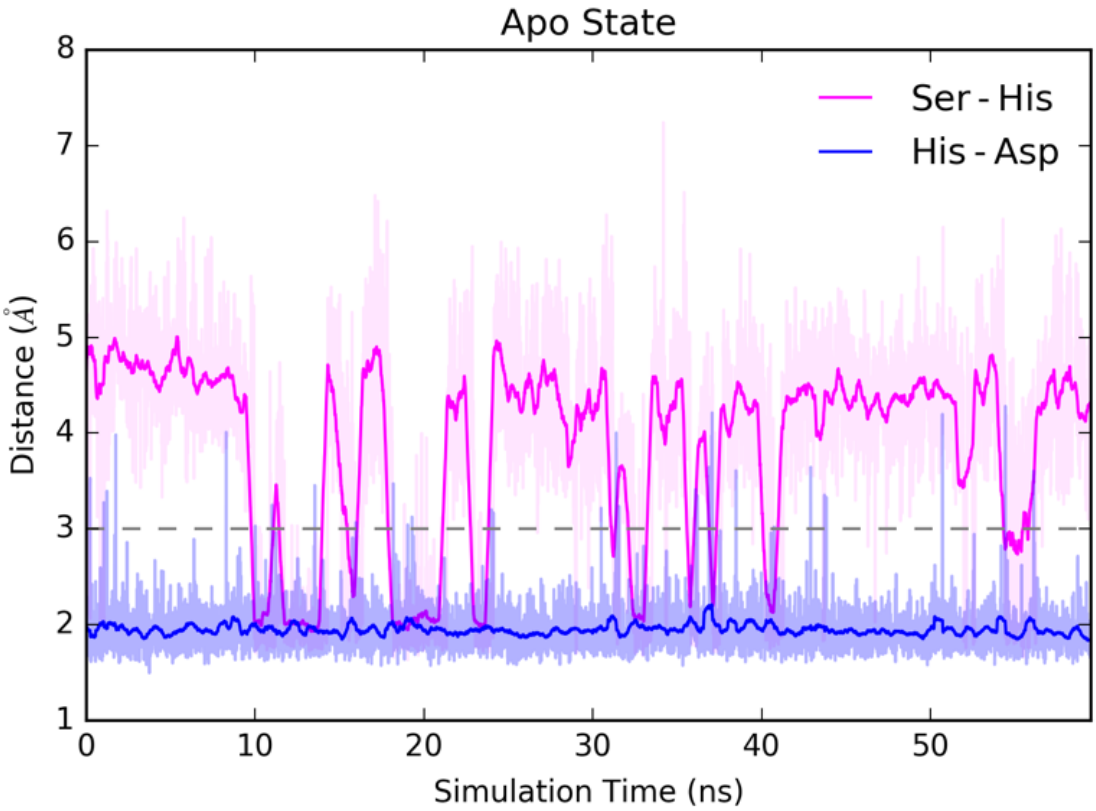
Apo State
Ser - His
His - Asp
Distance (Å)
Simulation Time (ns)
1
2
3
4
5
6
7
8
0
10
20
30
40
50

CHAPTER 3

RATIONAL ENZYME DESIGN FOR CONTROLLED FUNCTIONALIZATION OF ACETYLATED XYLAN FOR CELL-FREE POLYMER BIOSYNTHESIS.

Hsin-Tzu Wang, Vivek S. Bharadwaj, Jeong Yeh Yang, Thomas M. Curry, Kelley W. Moremen, Yannick J. Bomble, and Breeanna R. Urbanowicz. Submitted to *Carbohydrate Polymers* on July 2nd, 2021

Abstract

Xylan *O*-acetyltransferase 1 (XOAT1) is involved in biosynthesis of the hemicellulose xylan, adding *O*-acetyl moieties to the backbone. Recent structural analysis of XOAT1 showed a heart-shaped enzyme characterized by two unequal lobes that form a cleft predicted to be involved in positioning xylan acceptors into proximity with the catalytic triad localized at the bottom. Here, we used docking and molecular dynamics simulations to investigate the optimal orientation of xylan in the binding cleft of XOAT1 and identify putative key residues (Gln445 and Arg444 on Minor lobe & Asn312, Met311 and Asp403 on Major lobe) involved in acceptor substrate interactions. Site-directed mutagenesis coupled with biochemical analyses revealed residues located on the major lobe of XOAT1 are important for xylan binding. Mutation of single key residues on the major and minor lobe yielded XOAT1 variants with decreased or increased enzymatic efficiency, respectively. One-pot in vitro synthesis of xylan polymers with different degrees of *O*-acetylation confirmed that single amino acid substitutions are effective in modulating xylan acetylation levels during active synthesis. Taken together, our results demonstrate the effectiveness of computational modeling in guiding experimental protein design strategies by revealing important residues crucial for substrate-binding. This combined approach will play an important role in future enzyme engineering efforts aimed at redesigning the plant cell wall.

Introduction

Acetylation of biomolecules is an important chemical modification employed in nature observed across all domains of life. These modifications have significant implications to myriad biological functions and self-assembly of molecular architectures in biopolymers, including proteins, polysaccharides and polyphenolics. Plant secondary cell walls, which constitute the majority of the primary biomass resources harvested for valorization into fuels, chemicals, textiles and materials, are principally composed of cellulose, hemicelluloses, and lignin [1]. Xylan is the most abundant hemicellulose in these walls and on Earth, making up to 20-30% of the dry weight of most secondary cell walls [2]. Glucuronoxylan present in dicots consists of a backbone that is formed by 1,4-linked β-D-xylopyranosyl (Xyl) residues that is further substituted by 1,2-linked α-D-glucuronic acid (GlcA) and/or its 4-*O*-methyl derivative (MeGlcA). In addition, more than half of the Xyl residues are *O*-acetylated at the *O*-2 or *O*-3 position, or can also be di-acetylated at both the *O*-2 and *O*-3 positions [3-4]. The level of acetylation has been shown to affect the physical properties of polysaccharides such as hydrophobicity [5], may also interfere with the interaction between xylan and other cell wall polymers [6], and perturbs various physiological functions, including freezing tolerance and pathogen resistance [7-11].

Recent advances using solid-state nuclear magnetic resonance (NMR) spectroscopy have begun to reveal detailed, molecular-level information about the organization of the supramolecular networks formed, and the roles specific polymer structures play, within the 3D architecture of secondary cell walls. These groundbreaking studies indicate that xylans play a more important role than previously thought, and the *O*-acetyl moieties along the xylan backbone form intermolecular interactions with lignin aromatics or cellulose microfibrils in a conformation dependent manner. Using mass spectrometry and NMR, it has been observed that substituents are evenly attached to

the xylan backbone in an alternating pattern in *Arabidopsis*, suggesting that this xylan glycoform adopts a twofold helical screw conformation (a 360° twist every two glycosidic bonds) where the unsubstituted side forms hydrogen bonds with the hydrophilic surface of cellulose microfibrils [12-14]. This hypothetical model was later experimentally substantiated by solid-state magic-angle spinning (MAS) NMR spectroscopy of fresh Arabidopsis stems, and supported by in silico predictions, which reveal an induced assembly of xylan on cellulose fibrils as a rigid twofold screw from a flexible threefold conformation (a 360° twist every three glycosidic bonds) in solution [15]. Moreover, a recent study of acetylated xylan rearrangement via unrestrained molecular dynamics simulations further indicates that not only evenly spaced substituents but also the position on xylosyl residues play key roles in tuning xylan-cellulose interactions. It has been shown that 2-*O*-acetylated xylan is required to trigger the transition from a threefold to twofold screw conformation on cellulose surface through specific O-O contacts [16], while 3-*O*-acetylated xylan maintains a threefold screw that preferentially binds lignin and only interacts weakly with cellulose [12, 16]. Taken together, these data suggest that *O*-acetyl substituents along the backbone may be one of the key chemical determinants of xylan confirmation, and thus lignin-cellulose packing, *in muro* [12-14].

From an industrial perspective, acetic acid derived from innate acetylation of lignocellulosic materials could have both positive and negative impacts on biomass conversion. During biomass pretreatment processes, it has been shown that acetic acid itself could be effectively used for delignification [17-18] and fractionation of cell wall components [19-20]. A recent study further shows that acetic acid that is liberated from acetylated cell wall polysaccharides in *Populus trichocarpa* are able to catalyze the breakdown of wood and thus

increase sugar release during biomass pretreatment [21]. In addition to that, the downstream fermentative microorganisms were shown to be inhibited by the released acetic acid [22-23].

Overall, understanding the process of plant polysaccharide acetylation at the molecular level is essential to not only elucidating this crucial modification, but also promotes our ability to develop targeted genomics or genome engineering approaches to design plant cell walls that can be more efficiently valorized into food, materials and products. Nine members of the TRICHOME-BIREFRINGENCE-LIKE (TBL) family in *Arabidopsis* have been shown to possess xylan *O*-acetyltransferase activities, and differ in their regiospecificity for the *O*-2 and/or *O*-3 positions on xylosyl residues [24-28]. XYLAN *O*-ACETYLTRANSFERASE 1 (XOAT1) has been shown to specifically catalyze the 2-*O*-acetylation of xylan using an NMR spectroscopy technique that allows the reaction to be monitored in real time [8, 29], diminishing the ambiguity caused by non-enzymatic acetyl migration observed in end-point analyses [30-34]. The *esk1* mutant is a null mutant in the *XOAT1* gene that has collapsed xylem vessels, a ~60% reduction of xylan *O*-acetylation [35-36], and is more tolerant to freezing, drought and salt stress [37-38]. Further, it has been shown that the even-pattern of acetyl and Me(GlcA) substituents on alternate xylosyl residues along the backbone is disrupted in *esk1* mutants, suggesting a role of XOAT1 in patterning xylan decorations [39]. However, it is unclear how polysaccharide *O*-acetyltransferases interact with specific acceptor substrates to potentially control acetyl distribution.

A recent crystallographic study of XOAT1 revealed a heart shaped enzyme formed by two unequal lobes, referred to as major and minor, with a catalytic triad formed by Ser216-His465-Asp462 localized at the bottom of the cleft [29]. One of the key challenges in gaining insight into the enzymatic mechanisms of plant biopolymer synthesis and modification in general, and in XOAT1 in particular, is the paucity of experimentally characterized enzyme-substrate co-crystal

structures. Molecular modelling techniques involving docking and molecular dynamics (MD) simulations have been effective in successfully bridging this crucial gap [29, 40]. In our previous study, a combination of biochemical analyses and molecular simulations indicated that XOAT1 utilizes a double displacement/Ping Pong Bi Bi mechanism [29]. In addition to revealing the root mean square fluctuations of the various domains of the protein, the molecular simulations also enabled the identification of donor and substrate binding sites on XOAT1. While the substrate bound simulations revealed that the active site and substrate binding groove were able to stabilize the bound states of XOAT1 over timescales relevant for the catalytic mechanism, identification of the specific residues involved in substrate binding remained to be explored. In this study, we extend our analyses to investigate key residues involved in enzyme-acceptor substrate interactions through a combination of computational modeling followed by site-directed mutagenesis (SDM), kinetic analysis, and in vitro synthesis of *O*-acetylated xylan. Taken together, our results show that the major lobe of XOAT1 interacts more with the substrate, and two of the major lobe residues, M311 and D403, are crucial for hydrolysis of the acetyl donors to form the acyl-enzyme intermediate.

The use of computational techniques greatly speeds up the exploration of protein design space, facilitating the identification of key residues for protein engineering. We envisage that our study lays the foundations to provide insight into the relationships between the conformation of TBL proteins and their corresponding substrate specificities, allowing catalytic parameters to be precisely modulated to synthesize xylan with different degrees of *O*-acetylation and/or substitution patterns. Understanding the molecular levers that can be used to control a key modification such as polysaccharide *O*-acetylation opens the door towards new synthetic biology strategies aimed at fine tuning 3-D cell wall architecture. Post-synthetic modification of plant cell walls through *in*

muro expression of acetyl xylan esterases (AXE) has been shown to reduce biomass recalcitrance without perturbing plant growth, the obtained transgenic lines exhibited reduced xylan acetylation and are more susceptible to β-1,4-endoxylanase during saccharification, which further results in increased sugar yields [41-43]. In addition to modification of cell walls via post-synthesis, our research provides candidates for direct replacement of synthetic genes involved in pathways of xylan acetylation to improve lignocellulosic materials for benefits in industrial applications including valorization into food, fuels, and chemicals.

Materials and Methods

Molecular Dynamics Simulations

The recently published protein structure of XOAT1 (PDB ID: 6CCI) in its apo state was used to develop the donor (*p*-nitrophenyl acetate, *p*NP-Ac) and acceptor (xylodecaose) bound complexes of XOAT1. A combined docking and molecular dynamics protocol was employed to predict binding poses for donor-XOAT1 and acceptor-XOAT1 complexes. The detailed set-up for docking and molecular dynamics simulations of this complex are outlined in our previous publication [29]. For this publication, only simulations of the acceptor-bound XOAT1 complex were considered. Briefly, the production run consisted of an unbiased 50 ns trajectory of a fully solvated acceptor-bound (xylodecaose) XOAT1 complex. The MD trajectory was analyzed to quantify interaction energies between XOAT1 amino acid residues and the xylodecaose substrate using CHARMM44-45 and VMD46. These per-residue interaction energies were used as the metric to rank all the amino-acid interactions stabilizing acceptor binding to XOAT1 and identify targets for experimental mutagenesis.

Fusion protein expression and purification

Briefly, the truncated XOAT1 coding-region was cloned into a mammalian expression vector, pGEn2-DEST, as previously described [47]. A truncated form of XOAT1 (amino acids 133-487) was used in all experiments that encodes the catalytic domain and lacks the N-terminal variable region. Specifically, the fusion proteins contain an NH_2-terminal signal sequence followed by an 8xHis tag, an AviTag, 'superfolder' GFP, and the Tobacco Etch Virus (TEV) protease recognition site followed by amino acids 133-487 of *Arabidopsis* XOAT1 [48]. XOAT1 variants mutated at the predicted substrate-binding residue(s) were generated using the Q5 Site-Directed Mutagenesis Kit (New England Biolabs) and the aforementioned plasmid construct, pGEn2-DEST-XOAT1, as a template. Oligonucleotide primers (Eurofins, USA) used to generate the base changes were designed using NEBaseChanger (http://nebasechanger.neb.com/) and are listed in Supplemental Table S3.1. The introduction of mutations into pGEn2-DEST-XOAT1 was confirmed by DNA sequencing (Eurofins, USA). Fusion proteins were expressed in HEK cells (FreeStyle™ 293-F cell line, Life Technologies) and purified from the culture media using HisTrap HP columns (Cytiva, USA) using an ÄKTA Pure 25L protein purification system (GE Healthcare Life Sciences) as described previously [49]. Purification of XOAT1 and each variant was carried out on individual 1-ml HisTrap HP columns (Cytiva, USA) to exclude the risk of protein cross-contamination.

The purity of proteins was confirmed by sodium dodecyl sulfate-polyacrylamide gel electrophoresis (SDS-PAGE) followed by Coomassie Brilliant Blue R-250 (Bio-Rad) staining. The obtained fusion proteins were concentrated by using Amicon Ultra centrifugal filter devices (30-kD molecular weight cutoff, EMD Millipore), then buffer exchanged into 75 mM HEPES sodium salt-HCl (pH 7.0) via dialysis. The dialysis buffer was supplemented with Chelex-100

resin (0.5 g/L, Bio-Rad) to remove any potential contamination by divalent metal ions for activity assays. The concentrations of the dialyzed proteins were measured by Pierce™ BCA Protein Assay Kit (Thermo Fisher Scientific) using bovine serum albumin (BSA) as a standard. Protein expression levels of wild-type XOAT1 and the mutant variants, together with the primers used for generating mutations, are listed in Supplemental Table S3.1.

In vitro activity assay

To monitor the ability of each enzyme to catalyze the transfer of *O*-acetyl moieties to xylan, each variant was evaluated using the standard *in vitro* acetyltransferase assay that was described previously [48]. Briefly, reactions (20 µL) consisted of 4 µM purified enzyme, 1 mM acetyl donor substrate and 0.1 mM 2-aminobenzamide-labeled xylohexaose (Xyl_6-2AB) as an acceptor substrate, unless otherwise indicated, in 75 mM HEPES sodium salt-HCl (pH 6.8). All reactions were carried out at room temperature. Acetyl donor substrate used in this study is acetylsalicylic acid. After overnight incubation, a 5 µL aliquot of the reaction was mixed with 1 µL Dowex-50 (Bio-Rad, USA) cation exchange resin (suspended in water), and incubated at room temperature for 30 min. The mixture was then centrifuged at 2000 × g for a minute to pellet the resin, and 1 µL of the supernatant was mixed with 1 µL of matrix solution (2% (w/v) 2,5-dihydroxybenzoic acid (DHB) in 50% (v/v) methanol) directly on a stainless steel MALDI target plate. The mixture was dried under a stream of warm air by a hair dryer (Conair) and analyzed by matrix-assisted laser desorption/ionization-time of flight mass spectrometry (MALDI-TOF MS) using a Microflex LT spectrometer (Bruker). Positive ion spectra of the reaction products were generated by summation of 200 laser shots at a frequency of 10 shots/sec.

Kinetic analysis

To determine the kinetic parameters, assays were carried out in 75 mM HEPES sodium salt-HCl (pH 6.8) with enzyme concentrations at 1 μM (WT, N312A, R444A, Q445A, N312A/R444A, N312A/Q445A and R444A/Q445A), 2 μM (D403A), 3 μM (M311A and D403A/Q445A) or 6 μM (M311A/R444A, M311A/Q445A and D403A/R444A), depending on the catalytic performance of each variant. The concentration of the acceptor substrate, xylohexaose (Xyl_6, Megazyme, Ireland), used in the assays ranged from 0 to 400 μM (WT, R444A, Q445A and R444A/Q445A), 0 to 2 mM (N312A, D403A, N312A/R444A, N312A/Q445A, D403A/R444A and D403A/Q445A) or 0 to 3 mM (M311A, M311A/R444A and M311A/Q445A) according to each variant's catalytic velocity with a constant concentration of 1.5 mM 4MU-Ac as the donor substrate. Reactions were initiated with addition of 4MU-Ac, and the hydrolysis of 4MU-Ac by each variant was determined by measuring the emission of blue fluorescence from the released 4MU at 460 nm (excitation at 360 nm) using Synergy LX Multi-Mode Microplate Spectrometer (BioTek, USA) every minute during the 20-min reaction period at room temperature. Reaction rates with different Xyl_6 concentrations were calculated from the linear portion of each variant's hydrolysis curve. Steady-state parameters (k_{cat}, K_M and V_{max}) were calculated by fitting the initial reaction velocities to the Michaelis–Menten equation with nonlinear curve fitting using GraphPad Prism version 7.0d Macintosh Version (GraphPad Software Inc., USA; www.graphpad.com). All kinetic parameters were obtained through Michaelis-Menten Analysis performed by the same program.

Hydrolytic activity determination

Previously, we confirmed an acetyl-enzyme intermediate is formed at Ser-216 of XOAT1 using 4MU-Ac as an acetyl donor [29, 48]. To monitor the ability of each enzyme to form the acyl enzyme intermediate, the esterase activity of acetyltransferases can be measured by quantification of the released deacylated donor, which indicates their ability to form the acyl-enzyme intermediate in the absence of acceptor. The ability of each variant to hydrolyze 4MU-Ac in the absence of acceptor substrate was determined through the aforementioned method described by Lunin et al., without adding Xyl_6 or any other acceptor substrates in the reaction [29]. The autohydrolytic background of 4MU-Ac was determined by measuring the released 4MU from the incubation of 1.5 mM 4MU-Ac in 75 mM HEPES sodium salt-HCl (pH 6.8), and was subtracted from the value obtained from each enzyme-containing hydrolytic assay.

Protein thermal shift assays

Thermal shift analysis of the protein stability of XOAT1 and its variants was compared using SYPRO Orange Fluorescent Dye [50]. Protein thermal shift assays were carried out using a CFX96™ Real-Time System (Bio-Rad, USA) to detect fluorescent dye-bound denatured proteins according to the protocol from the manufacturer (https://www.biorad.com/webroot/web/pdf/lsr/literature/Bulletin_7180.pdf). In brief, 45 µL of protein (2 µM) in 75 mM HEPES-sodium salt buffer (pH 6.8) was mixed with 5 µL of 100× SYPRO Orange Protein Gel Stain (diluted from 5000× stock supplied by Sigma-Aldrich, USA; λ_{ex} 470 nm /λ_{em} 570 nm) in 96-well Hard-Shell® PCR plates (Bio-Rad, USA) and sealed with PCR Sealers™ Microseal® 'B' Film (Bio-Rad, USA). Controls contain an equal volume of 75 mM

HEPES-sodium salt buffer (pH 6.8) in lieu of protein. The program included an initial temperature hold of 10°C for 31 seconds, followed by a temperature ramp from 10°C to 95°C at 0.5°C increments with a 30-second hold at each temperature. Fluorescence reads using the "FRET" channel to measure the SYPRO Orange fluorescence signal were taken at the end of each hold, and the obtained data were processed using CFX Maestro™ Software for calculation of the melting temperature (T_m) of each XOAT1 variant.

In vitro synthesis of acetylated xylan

For cell-free, *in vitro* synthesis of acetylated xylo-oligosaccharides with adjusted acetylation levels, we carried out a one-pot reaction by co-incubating heterologously expressed xylan synthase from *Klebsormidium flaccidum* (KfXYS1)51 and XOAT1 or its variants at an enzyme concentration of 3 μM each in the presence of 60 mM uridine 5'-diphosphate (UDP)-xylose as an activate nucleotide sugar donor, 2 mM xylobiose (Xyl_2) as an acceptor for the xylan synthase, 3.5 mM acetylsalicylic acid as an acetyl donor in 75 mM HEPES-sodium salt (pH6.8). After overnight incubation, the products were analyzed by MALDI-TOF MS according to the method described above.

Results and Discussion

In our previous study, we provided several lines of evidence that suggest XOAT1 uses a double displacement Bi-Bi reaction to catalyze 2-*O*-acetylation of xylan that occurs in two stages. First, Ser-216 of the catalytic triad is acetylated, forming an acyl-enzyme intermediate that has been experimentally confirmed by LC-MS/MS [48]. The transfer of the proton from Ser-216 to

the phenolic oxygen of the donor results in release of deacylated donor, which can be measured spectrophotometrically when *p*NP-Ac or 4MU-Ac are used. After formation of the acyl-enzyme intermediate, the xylan substrate binds to the substrate binding groove to get into alignment with the active site. Next, the acetyl group is transferred from Ser216 onto the acceptor xylan substrate [29]. The main objective of this study is to understand mechanisms of acceptor substrate recognition and the residues dictating the acetylation propensities of XOAT1. Thus, we started by identifying the key residues involved in acceptor binding followed by detailed biochemical characterization of the impact of mutations on the overall acetylation mechanism, kinetic parameters, and finally the ability of putative acceptor binding mutants to synthesize xylan with different degrees of O-acetyl substitution that could be potentially applied in planta to generate xylan with different physicochemical properties to modulate lignin-carbohydrate interactions *in muro*.

In-silico studies enable identification of mutagenesis targets

Molecular dynamics simulations of the XOAT1-xylodecaose complex revealed important residues involved in stabilizing the binding of the acceptor substrate. Table S3.2 in the supplemental information lists these amino acid residues ranked according to the strength of their interaction energies. The amino acids identified to be interacting with the substrate span the whole binding groove and involve residues on both the major and the minor lobes. The residues that were observed to have the highest binding energies were situated closest to the catalytic triad. Amongst the top-five ranked residues involved in interacting with xylodecaose, two are part of the minor lobe (R444 and Q445), and the other three residues are part of the more structured major lobe (M311, N312 and D403) (Figure 3.1). Interestingly, the two distinct lobes interact with different

sections of xylodecaose, with residues localized on the major lobe (M311, N312 and D403) binding to the terminal (non-reducing) region, while the residues on the minor lobe (R444 and Q445) interacting with the reducing end of xylodecaose (Figure 3.1).

Biochemical analysis of XOAT1 variants

Although molecular simulations enable the identification of putative residues in substrate binding, the roles played by these residues in governing the acetylation mechanism still needs to be established. Thus, we generated a series of XOAT1 variants using site-directed mutagenesis, determined kinetic parameters and analyzed the reaction products to investigate their potential role in xylan acetylation. This was executed by substituting each of the five hypothesized binding residues to alanine in various combinations resulting in five single mutants (M311A, N312A, D403A, R444A and Q445A) and nine double mutants (M311A/D403A, M311A/R444A, M311A/Q445A, N312A/D403A, N312A/R444A, N312A/Q445A, D403A/R444A, D403A/Q445A and R444A/Q445A). Kinetic parameters were determined by measuring the initial reaction rates using the fluorogenic substrate 4MU-Ac in the presence and absence of acceptor. The ability of the enzymes to transfer an acetyl group onto a saccharide acceptor was measured using and an *in vitro* acetyltransferase assay that is based on the same principles as β-(1,4)-xylosyltransferase assays, comprised of acetylsalicylic acid as an acetyl donor and 2-aminobenzamide β-(1,4)-xylohexaose (Xyl_6-2AB) as an acceptor [8].

The wild-type XOAT1 enzyme and the R444A, Q445A and R444A/Q445A variants show similar acetyltransferase activity and are able to transfer up to four acetyl groups to Xyl_6-2AB (Figure 3.2a and b). On the other hand, mutants of the major lobe residues showed decreased

acetyltransferase activities, with the single mutants M311A, N312A and D403A generating xylooligosaccharides with up to 2 (M311A) or 3 (N312A and D403A) *O*-acetyl substituents (Figure 3.2a). It is worth noting that substrate-binding residues on the two distinct lobes are in close proximity to the opposite ends of the xylosyl chain as observed in simulations, where major lobe residues are near the terminal non-reducing end while interactions with the minor lobe occur closer to the reducing end. Double substitutions of the major lobe residues also resulted in drastic reductions of enzyme activity, with N312A/D403A only producing mono-acetylated xylohexaose after overnight incubation, and M311A/D403A demonstrating no acetyltransferase activity (Figure 3.2b). The thermal stability of the mutants was compared with that of the wild-type XOAT1 protein by measuring temperature-induced changes in the fluorescence SYPRO® Orange. Wild-type XOAT1 exhibited a melting temperature (T_m) of 53 ± 0.5 °C where 50% of the protein is unfolded. Analysis of the mutant variants showed that M311A and N312A showed decreases (-1.7 and -2.0, respectively) compared to the wild type (Figure 3.2a), indicating mutation of residues causes loss of acetyltransferase activities without significantly affecting protein stability. D403A, R444A, and Q445A did not show significant changes in T_m in comparison with wild type. Taken together, mutation of different residues on the major lobe reduced XOAT1's acetyltransferase activity to a greater or lesser extent, while substituting minor lobe residues, in contrast, allowed the enzyme to retain an activity that is comparable to the wild type, suggesting a more important role for the major lobe in substrate binding and the acetylation mechanism.

The *in vitro* analysis reveals the overall effect of the mutations on XOAT1 activity which could be manifested via the impact on binding or catalysis or a combination of the two. In order to probe this further, we determined the kinetic parameters of XOAT and its variants for the acceptor by generating a substrate saturation curve for each variant. The impact of mutations on

xylohexaose binding affinity to XOAT1 variants was quantified by determining the Michaelis constant (K_M) for each XOAT1 variant. The minor lobe mutants (R444A, Q445A and R444A/Q445A) showed a similar or slightly higher K_M compared to the wild type (Table 3.1), indicating that they maintained a comparable xylohexaose-binding affinity to that of the wild type. Contrarily, all the major lobe mutants demonstrated highly impaired xylohexaose-binding abilities as shown by the significantly higher K_M, and which is consistent with the results of the acetyltransferase assays that showed the reduced acetylation levels of the products generated by these variants (Figure 3.2a and b). Taken together, these data suggest that the major lobe plays an important role in interacting with the xylan acceptor.

Intriguingly, the turnover number (k_{cat}) of each variant varies, and does not correspond to their localizations on the major or minor lobe of XOAT1. For example, point mutation of N312 residue on the major lobe resulted in a low affinity (high K_M) for xylohexaose, while the k_{cat} values of the N312-related mutants, on the contrary, were dramatically increased, especially for the single mutant N312A (Table 3.1). The increased k_{cat} of N312-related mutants satisfied a catalytic efficiency (k_{cat}/K_M) that allows those variants, although with low substrate binding affinities, to still be able to generate multi-acetylated xylohexaoses as shown in the in vitro assays (Figure 3.2b. MALDI - major). Besides N312, mutating other two putative substrate-binding residues localized on the major lobe, M311 and D403, significantly decreased k_{cat}, especially for M311-related single and double mutants. The reduced turnover numbers (low k_{cat}) and decreased substrate-binding affinities (high K_M) resulted in low catalytic efficiencies of the M311 and D403-related mutants. On the other hand, substituting the two residues R444 and Q445 on the minor lobe to alanine caused the k_{cat} to increase. R444A, Q445A and R444A/Q445A all presented higher k_{cat}, demonstrating that switching from bulky to small and non-polar side chains on the residues at these

positions promotes the number of reactions that the enzyme catalyzes per unit time. Without losing the substrate-binding affinity, R444A, Q445A and R444A/Q445A variants revealed much improved catalytic efficiencies compared to the wild type.

It has been shown that targeting substrate-binding residues along the active site cleft based on computational modeling is an efficient strategy to evaluate the protein design space to mediate enzymatic activities of TBL proteins. An example of such rationally designed enzymes has been reported in a previous study of Candida Antarctica lipase A (CAL-A), which generates fatty acid esters that are useful in the biodiesel, cosmetic, and food industries [52]. The *in silico* designed CAL-A mutant D122L, showed lower hydrolysis activity that reduces the production of unwanted fatty acid by-products, while retaining the process-relevant acyltransferase activity and thermostability [52]. Another example of targeting binding pocket residues based on sequence alignment and 3D modeling to improve enzymatic activities has been reported in lipases/acyltransferases in Candida species [53]. In addition to enhancing enzyme activities, switching substrate specificity through mutating key residues in binding channels is an effective enzyme engineering strategy. Substituting small amino acids with the ones that contain bulky side chains inside the tunnel of Candida rugose lipase resulted in shifting the substrate preference from long chain fatty acids toward those with shorter acyl groups [54].

Overall, our research on the substrate-binding mode of XOAT1 revealed the important residues involved in binding the xylo-oligosaccharides that were initially suggested by computational modeling and then confirmed by SDM and activity assays. The kinetic parameters strongly revealed that mutating the hypothesized binding residues on the major lobe, M311, N312 and D403, critically interferes with XOAT1's ability to interact with to xylohexaose, suggesting that the major lobe is critical for effective substrate binding and can be used as a future target for

generation of modified lignocellulosic materials with reduced acetylation levels through transgenic biotechnology. It has been recently shown that heterologously expressed fungal acetyl xylan esterase from *Hypocrea jecorina* (HjAXE) in hybrid aspen using wood-specific promoter helped reduce recalcitrance for enzymatic saccharification and thus improved sugar yield by 27% in transgenic lines [43]. A similar strategy of expressing a fugal AXE *in muro* has also been applied in *Arabidopsis* and aspen wood, and the resulting transgenic lines showed increased susceptibility to hydrolytic enzymes that led to improved yields of reducing sugars [41-42], suggesting that it is a promising approach to optimize lignocellulosic biomass for biofuel production through changing cell wall architecture but without interfering with plant growth. The major lobe of XOAT1 has been shown to be determinant in binding the substrate in our research, and could be a potential transgenic target to reduce recalcitrant acetyl content in biomass through up-stream modification of xylan structures in the cell wall biosynthetic pathway.

Although the residues chosen for mutagenesis were identified to be involved in acceptor binding and are most likely to be involved in the second stage (acetyl transfer) of the XOAT1 catalytic mechanism, it is important to recognize that they could plausibly also be involved or impact the first stage i.e. the esterase activity of XOAT1. To study if mutations of the hypothesized binding residues affects XOAT1's hydrolytic activity, the variants were examined using 4MU-Ac as the donor substrate and measuring the release of 4MU in the absence of any acceptor substrates. All mutant variants were capable of releasing 4MU from 4MU-Ac *in vitro*. However, M311A and D403A single mutants presented significantly reduced hydrolytic activities compared to other single mutants, and all the M311 and D403-related double mutants, except N312A/D403A, showed decreased hydrolytic rates (Figure S2). The obtained esterase activities of the XOAT1 variants demonstrated that the two residues, M311 and D403, on the major lobe are not only critical

to binding the acceptor substrate, xylohexaose, but decrease the rate that the enzyme forms an acyl-enzyme intermediate using the donor substrate, 4MU-Ac. The third major lobe residue, N312 and its related double mutants displayed hydrolytic activities at a similar level as the wild type, despite its close proximity to the catalytic triad. It's worth noticing that the double mutant N312A/D403A maintains a hydrolysis rate comparable to the wild type while the single mutant D403A does not, suggesting that the loss of activity by mutating D403 can somehow be compensated by mutation of N312. Finally, mutating the two residues on the minor lobe R444 and Q445 showed no difference in hydrolysis activity relative to wild-type.

XOAT1 variants are able to synthesis xyloigosaccharides with different degrees of O-acetylation

Previously, we have identified a highly active xylan synthase from *Klebsormidium flaccidum*, designated *K. flaccidum* XYLAN SYNTHASE 1 (KfXYS1), which is able to synthesize xylan polymers with a degree of polymerization of up to 29 Xyl residues [51]. We have taken advantage of the highly active nature of KfXYS1 to use as a model in vitro xylan synthesis platform to evaluate XOAT1 variants. Mutants with different enzymatic efficiencies were reacted together with KfXYS1 to evaluate production of xylo-oligosaccharides (XOS) with adjusted degrees of acetylation *in vitro*, to more closely mimic the long chain acceptors that the enzymes would encounter *in vivo*. One-pot reactions were carried out by co-incubating KfXYS1 and XOAT1 or its variants in reactions comprised of uridine 5'-diphosphate-xylose (UDP-Xyl) and xylobiose (Xyl_2) as the donor and acceptor for xylan synthesis, respectively, together with and acetylsalicylic acid as an acetyl donor. MALDI-TOF MS analysis of the products from the overnight reaction shows that KfXYS1 was able to generate XOS with degree of polymerization (DP) ranging from 8 to around 20, and up to 2 to 4 acetyl groups were attached to the XOS

depending on their DP (Figure 3.3). Consistent with our hypothesis, the acetylation levels of the xylo-oligo products produced by different XOAT1 variants differ according to their enzymatic efficiencies, suggesting a potential strategy to synthesize XOS *in vitro* or going further and replacing XOAT1 in planta with mutant variants to produce plant secondary cell walls with tuned properties through adjusted acetylation levels.

XOS are non-digestible in human guts and have been shown to exhibit prebiotic effects of stimulating a limited number of beneficial bacteria in gastrointestinal microbiota such as *Bifidobacterium*, which can beneficially affect the hosts' health [55-56]. Besides exhibiting prebiotic effects, XOS have also been shown to help prevent diabetes and colon cancer [57-58], and other properties such as antioxidant, anti-inflammatory, and thermal (up to 100°C) and pH (pH 2.5 - 8) stability have made XOS suitable for applications in various marketable areas such as cosmetic, pharmaceutical, and food industries [59-60]. Moreover, XOS have been applied in microencapsulation techniques used in the field of dietary and medical supplements for microbiota balancing through improvement of digestion resistance and viability of the encapsulated probiotic organisms under gastrointestinal conditions [61-62]. Different from traditional methods using lignocellulose as raw materials for XOS production [56, 60, 63], the results of one-pot XOS synthesis shown in this study provide a different strategy that allows us to finely adjust the acetylation level, which could have significant impacts on the physiochemical property of xylan [5], of XOS during synthesis, and could thus generate modified features of XOS to meet the requirement for different purposes in various areas mentioned above.

Conclusions

The ability to modulate the acetylation activity of XOAT1 presents unique opportunities for the engineering of plant biomass with highly controlled degrees of acetylation without compromising on plant growth and stature. This will yield unique insights into the role of acetylated biopolymers in enabling healthy plant cell wall architectures that could also be easily deconstructed. Additionally, this capability to exploiting natural plant enzymatic pathways would also open doors for the development of biosynthetic technologies directed towards the tailored biosynthesis of glycopolymers. In this study, we used computational molecular simulations to bridge gaps in the structural biology of XOAT1 enzyme-substrate complexes. The simulations identified key residues involved in acceptor substrate binding and provided targets for directed mutagenesis of XOAT1. The detailed biochemical characterizations conducted here enabled insights into the role of these residues in substrate binding, esterase and transferase activities.

Amongst the five amino-acid residues identified to play an important role in substrate binding from simulations, two of them are present on the minor lobe (R444, Q445) and three on the major lobe (M311, N312 and D403). The single and double mutant variants of XOAT1 are observed to have differing impacts on substrate binding, esterase and transferase activities. XOAT1 variants of the minor lobe residues (R444A, Q445A, R444A/Q445A) are observed to have the least detrimental impact on acceptor binding affinities, esterase activity and turnover rates for transferase activities. In fact, the R444A variant demonstrates improved catalytic efficiency for substrate acetylation. On the other hand, XOAT1 variants of the major lobe had a far more detrimental impact on acceptor substrate binding and kinetic parameters. All single and double mutants involving any of the major lobe residues, M311A, D403A and N312A showed highly diminished binding affinities for the acceptor xylan substrate. XOAT1 variants involving M311A

and D403A also demonstrate highly reduced esterase activities indicating that the transfer of the acetyl group may also hindered in these cases. Interestingly, all XOAT1 variants involving the N312A mutation seemed to demonstrate restored esterase activity. However, all single and double mutants involving the major lobe residues show impaired xylan acetylation activities. Finally, by combining the xylan synthase enzyme with specific XOAT1 variants described above, we demonstrate a biochemical pathway for the production of xylo-oligomers with highly controlled degrees of acetylation.

This study forms the basis for the quest to gain a detailed and complete understanding of the impact of acetylation on the assembly of biopolymers in the plant cell wall as well as the development of engineered acetylated biopolymers for a circular economy.

Acknowledgements: Funding was provided by the Center for Bioenergy Innovation (CBI), a U.S. Department of Energy Bioenergy Research Center supported by the Office of Biological, Environmental Research in the DOE Office of Science and National Institutes of Health (P41GM103390 and R01GM130915). This work was authored in part by Alliance for Sustainable Energy, LLC, the manager and operator of the National Renewable Energy Laboratory for the U.S. Department of Energy (DOE) under Contract No. DE-AC36-08GO28308. The views expressed in the article do not necessarily represent the views of the DOE or the U.S. Government. The U.S. Government retains and the publisher, by accepting the article for publication, acknowledges that the U.S. Government retains a nonexclusive, paid-up, irrevocable, worldwide license to publish or reproduce the published form of this work, or allow others to do so, for U.S. Government purposes.

Author Contributions: H.T.W., V.S.B., J.Y.Y., Y.J.B, T.M.C., and B.R.U designed experiments, performed experiments, and analyzed data. V.S.B. performed computational simulations. K.W.M. and J.Y.Y. expressed recombinant proteins in HEK cells. K.W.M, Y.J.B and B.R.U designed experiments, analyzed and interpreted data and edited the manuscript. H.T.W., V.S.B., and B.R.U wrote the manuscript. Y.J.B. and B.R.U. conceived and led the project.

References

1. Carpita, N. C.; McCann, M. C., Redesigning plant cell walls for the biomass-based bioeconomy. Journal of Biological Chemistry 2020, 295 (44), 15144-15157.
2. Scheller, H. V.; Ulvskov, P., Hemicelluloses. Annu Rev Plant Biol 2010, 61, 263-89.
3. Teleman, A.; Lundqvist, J.; Tjerneld, F.; Stalbrand, H.; Dahlman, O., Characterization of acetylated 4-O-methylglucuronoxylan isolated from aspen employing 1H and 13C NMR spectroscopy. Carbohydrate research 2000, 329 (4), 807-15.
4. Teleman, A.; Tenkanen, M.; Jacobs, A.; Dahlman, O., Characterization of O-acetyl-(4-O-methylglucurono)xylan isolated from birch and beech. Carbohydrate Research 2002, 337 (4), 373-377.
5. Biely, P., Microbial carbohydrate esterases deacetylating plant polysaccharides. Biotechnology Advances 2012, 30 (6), 1575-1588.
6. Busse-Wicher, M.; Gomes, T. C.; Tryfona, T.; Nikolovski, N.; Stott, K.; Grantham, N. J.; Bolam, D. N.; Skaf, M. S.; Dupree, P., The pattern of xylan acetylation suggests xylan may interact with cellulose microfibrils as a twofold helical screw in the secondary plant cell wall of Arabidopsis thaliana. The Plant journal : for cell and molecular biology 2014, 79 (3), 492-506.
7. Xin, Z.; Mandaokar, A.; Chen, J.; Last, R. L.; Browse, J., Arabidopsis ESK1 encodes a novel regulator of freezing tolerance. The Plant journal : for cell and molecular biology 2007, 49 (5), 786-99.
8. Urbanowicz, B. R.; Peña, M. J.; Moniz, H. A.; Moremen, K. W.; York, W. S., Two Arabidopsis proteins synthesize acetylated xylan in vitro. The Plant Journal 2014, 80 (2), 197-206.

9. Manabe, Y.; Nafisi, M.; Verhertbruggen, Y.; Orfila, C.; Gille, S.; Rautengarten, C.; Cherk, C.; Marcus, S. E.; Somerville, S.; Pauly, M.; Knox, J. P.; Sakuragi, Y.; Scheller, H. V., Loss-of-Function Mutation of REDUCED WALL ACETYLATION2 in Arabidopsis Leads to Reduced Cell Wall Acetylation and Increased Resistance to Botrytis cinerea. Plant Physiology 2011, 155 (3), 1068-1078.

10. Vogel, J. P.; Raab, T. K.; Somerville, C. R.; Somerville, S. C., Mutations in PMR5 result in powdery mildew resistance and altered cell wall composition. The Plant journal : for cell and molecular biology 2004, 40 (6), 968-78.

11. Diener, A. C.; Ausubel, F. M., RESISTANCE TO FUSARIUM OXYSPORUM 1, a dominant Arabidopsis disease-resistance gene, is not race specific. Genetics 2005, 171 (1), 305-21.

12. Kang, X.; Kirui, A.; Widanage, M. C. D.; Mentink-Vigier, F.; Cosgrove, D. J.; Wang, T., Lignin-polysaccharide interactions in plant secondary cell walls revealed by solid-state NMR. Nat Commun 2019, 10 (1), 347.

13. Gao, Y.; Lipton, A. S.; Wittmer, Y.; Murray, D. T.; Mortimer, J. C., A grass-specific cellulose–xylan interaction dominates in sorghum secondary cell walls. Nature communications 2020, 11 (1), 1-10.

14. Duan, P.; Kaser, S. J.; Lyczakowski, J. J.; Phyo, P.; Tryfona, T.; Dupree, P.; Hong, M., Xylan Structure and Dynamics in Native Brachypodium Grass Cell Walls Investigated by Solid-State NMR Spectroscopy. ACS Omega 2021.

15. Simmons, T. J.; Mortimer, J. C.; Bernardinelli, O. D.; Poppler, A. C.; Brown, S. P.; deAzevedo, E. R.; Dupree, R.; Dupree, P., Folding of xylan onto cellulose fibrils in plant cell walls revealed by solid-state NMR. Nat Commun 2016, 7, 13902.

16. Gupta, M.; Rawal, T. B.; Dupree, P.; Smith, J. C.; Petridis, L., Spontaneous rearrangement of acetylated xylan on hydrophilic cellulose surfaces. Cellulose 2021, 28 (6), 3327-3345.

17. Simon, M.; Brostaux, Y.; Vanderghem, C.; Jourez, B.; Paquot, M.; Richel, A., Optimization of a formic/acetic acid delignification treatment on beech wood and its influence on the structural characteristics of the extracted lignins. Journal of Chemical Technology & Biotechnology 2014, 89 (1), 128-136.

18. Young, R. A.; Davis, J. L.; Wiesmann, E.-B., Organic Acid Pulping of Wood - Part II. Acetic Acid Pulping of Aspen. 1986, 40 (2), 99-108.

19. Vásquez, D.; Lage, M. A.; Parajó, J. C.; Vázquez, G., Fractionation of Eucalyptus wood in acetic acid media. Bioresource Technology 1992, 40 (2), 131-136.

20. Parajó, J. C.; Alonso, J. L.; Santos, V., Kinetics of Eucalyptus wood fractionation in actic acid-HCl-water media. Bioresource Technology 1995, 51 (2), 153-162.

21. Johnson, A. M.; Kim, H.; Ralph, J.; Mansfield, S. D., Natural acetylation impacts carbohydrate recovery during deconstruction of Populus trichocarpa wood. Biotechnology for biofuels 2017, 10 (1), 48.

22. Olsson, L.; Hahn-Hägerdal, B., Fermentation of lignocellulosic hydrolysates for ethanol production. Enzyme and Microbial Technology 1996, 18 (5), 312-331.

23. Larsson, S.; Palmqvist, E.; Hahn-Hägerdal, B.; Tengborg, C.; Stenberg, K.; Zacchi, G.; Nilvebrant, N.-O., The generation of fermentation inhibitors during dilute acid hydrolysis of softwood. Enzyme and microbial technology 1999, 24 (3), 151-159.

24. Yuan, Y.; Teng, Q.; Zhong, R.; Haghighat, M.; Richardson, E. A.; Ye, Z.-H., Mutations of Arabidopsis TBL32 and TBL33 Affect Xylan Acetylation and Secondary Wall Deposition. PLOS ONE 2016, 11 (1), e0146460.

25. Yuan, Y.; Teng, Q.; Zhong, R.; Ye, Z.-H., The Arabidopsis DUF231 Domain-Containing Protein ESK1 Mediates 2-O- and 3-O-Acetylation of Xylosyl Residues in Xylan. Plant and Cell Physiology 2013, 54 (7), 1186-1199.

26. Yuan, Y.; Teng, Q.; Zhong, R.; Ye, Z.-H., TBL3 and TBL31, two Arabidopsis DUF231 domain proteins, are required for 3-O-monoacetylation of xylan. Plant and Cell Physiology 2015, 57 (1), 35-45.

27. Yuan, Y.; Teng, Q.; Zhong, R.; Ye, Z. H., Roles of Arabidopsis TBL34 and TBL35 in xylan acetylation and plant growth. Plant Sci 2016, 243, 120-30.

28. Zhong, R.; Cui, D.; Ye, Z.-H., Regiospecific acetylation of xylan is mediated by a group of DUF231-containing O-acetyltransferases. Plant and Cell Physiology 2017, 58 (12), 2126-2138.

29. Lunin, V. V.; Wang, H.-T.; Bharadwaj, V. S.; Alahuhta, M.; Peña, M. J.; Yang, J.-Y.; Archer-Hartmann, S. A.; Azadi, P.; Himmel, M. E.; Moremen, K. W.; York, W. S.; Bomble, Y. J.; Urbanowicz, B. R., Molecular Mechanism of Polysaccharide Acetylation by the Arabidopsis Xylan O-acetyltransferase XOAT1. The Plant Cell 2020, 32 (7), 2367-2382.

30. Brecker, L.; Mahut, M.; Schwarz, A.; Nidetzky, B., In situ proton NMR study of acetyl and formyl group migration in mono-O-acyl D-glucose. Magn Reson Chem 2009, 47 (4), 328-32.

31. Lassfolk, R.; Rahkila, J.; Johansson, M. P.; Ekholm, F. S.; Warna, J.; Leino, R., Acetyl Group Migration across the Saccharide Units in Oligomannoside Model Compound. Journal of the American Chemical Society 2019, 141 (4), 1646-1654.

32. Roslund, M. U.; Aitio, O.; Warna, J.; Maaheimo, H.; Murzin, D. Y.; Leino, R., Acyl group migration and cleavage in selectively protected beta-d-galactopyranosides as studied by NMR spectroscopy and kinetic calculations. Journal of the American Chemical Society 2008, 130 (27), 8769-72.

33. Yoshimoto, K.; Tsuda, Y., General Path of O-Acyl Migration in D-Glucose Derivatives : Acyl Migration of Methyl Mono-O-myristoyl-α- and β-D-Glucopyranosides and Mono-O-myristoyl-D-glucopyranoses. CHEMICAL & PHARMACEUTICAL BULLETIN 1983, 31 (12), 4324-4334.

34. Mastihubová, M.; Biely, P., Lipase-catalysed preparation of acetates of 4-nitrophenyl β-d-xylopyranoside and their use in kinetic studies of acetyl migration. Carbohydrate research 2004, 339 (7), 1353-1360.

35. Lefebvre, V.; Fortabat, M.-N.; Ducamp, A.; North, H. M.; Maia-Grondard, A.; Trouverie, J.; Boursiac, Y.; Mouille, G.; Durand-Tardif, M., ESKIMO1 disruption in Arabidopsis alters vascular tissue and impairs water transport. PLoS One 2011, 6 (2), e16645.

36. Xiong, G.; Cheng, K.; Pauly, M., Xylan O-acetylation impacts xylem development and enzymatic recalcitrance as indicated by the Arabidopsis mutant tbl29. Mol Plant 2013, 6 (4), 1373-5.

37. Xin, Z.; Browse, J., Eskimo1 mutants of Arabidopsis are constitutively freezing-tolerant. Proceedings of the National Academy of Sciences of the United States of America 1998, 95, 7799-7804.

38. Bouchabke-Coussa, O.; Quashie, M.-L.; Seoane-Redondo, J.; Fortabat, M.-N.; Gery, C.; Yu, A.; Linderme, D.; Trouverie, J.; Granier, F.; Téoulé, E.; Durand-Tardif, M., ESKIMO1 is a key gene involved in water economy as well as cold acclimation and salt tolerance. Bmc Plant Biol 2008, 8 (1), 125.

39. Grantham, N. J.; Wurman-Rodrich, J.; Terrett, O. M.; Lyczakowski, J. J.; Stott, K.; Iuga, D.; Simmons, T. J.; Durand-Tardif, M.; Brown, S. P.; Dupree, R., An even pattern of xylan substitution is critical for interaction with cellulose in plant cell walls. Nature plants 2017, 3 (11), 859.

40. Urbanowicz, B. R.; Bharadwaj, V. S.; Alahuhta, M.; Peña, M. J.; Lunin, V. V.; Bomble, Y. J.; Wang, S.; Yang, J.-Y.; Tuomivaara, S. T.; Himmel, M. E.; Moremen, K. W.; York, W. S.; Crowley, M. F., Structural, mutagenic and in silico studies of xyloglucan fucosylation in Arabidopsis thaliana suggest a water-mediated mechanism. The Plant Journal 2017, 91 (6), 931-949.

41. Pawar, P. M.; Derba-Maceluch, M.; Chong, S. L.; Gandla, M. L.; Bashar, S. S.; Sparrman, T.; Ahvenainen, P.; Hedenstrom, M.; Ozparpucu, M.; Ruggeberg, M.; Serimaa, R.; Lawoko, M.; Tenkanen, M.; Jonsson, L. J.; Mellerowicz, E. J., In muro deacetylation of xylan affects lignin properties and improves saccharification of aspen wood. Biotechnology for biofuels 2017, 10, 98.

42. Pawar, P. M.; Derba-Maceluch, M.; Chong, S. L.; Gomez, L. D.; Miedes, E.; Banasiak, A.; Ratke, C.; Gaertner, C.; Mouille, G.; McQueen-Mason, S. J.; Molina, A.; Sellstedt, A.; Tenkanen, M.; Mellerowicz, E. J., Expression of fungal acetyl xylan esterase in Arabidopsis thaliana improves saccharification of stem lignocellulose. Plant biotechnology journal 2016, 14 (1), 387-97.

43. Wang, Z.; Pawar, P. M.; Derba-Maceluch, M.; Hedenström, M.; Chong, S. L.; Tenkanen, M.; Jönsson, L. J.; Mellerowicz, E. J., Hybrid Aspen Expressing a Carbohydrate Esterase Family 5 Acetyl Xylan Esterase Under Control of a Wood-Specific Promoter Shows Improved Saccharification. Front Plant Sci 2020, 11, 380.

44. Brooks, B. R.; Brooks Iii, C. L.; Mackerell Jr, A. D.; Nilsson, L.; Petrella, R. J.; Roux, B.; Won, Y.; Archontis, G.; Bartels, C.; Boresch, S.; Caflisch, A.; Caves, L.; Cui, Q.; Dinner, A. R.; Feig, M.; Fischer, S.; Gao, J.; Hodoscek, M.; Im, W.; Kuczera, K.; Lazaridis, T.; Ma, J.; Ovchinnikov, V.; Paci, E.; Pastor, R. W.; Post, C. B.; Pu, J. Z.; Schaefer, M.; Tidor, B.; Venable, R. M.; Woodcock, H. L.; Wu, X.; Yang, W.; York, D. M.; Karplus, M., CHARMM: The biomolecular simulation program. Journal of Computational Chemistry 2009, 30 (10), 1545-1614.

45. Hynninen, A.-P.; Crowley, M. F., New faster CHARMM molecular dynamics engine. Journal of Computational Chemistry 2014, 35 (5), 406-413.

46. Humphrey, W.; Dalke, A.; Schulten, K., VMD: Visual molecular dynamics. Journal of Molecular Graphics 1996, 14 (1), 33-38.

47. Moremen, K. W.; Ramiah, A.; Stuart, M.; Steel, J.; Meng, L.; Forouhar, F.; Moniz, H. A.; Gahlay, G.; Gao, Z.; Chapla, D., Expression system for structural and functional studies of human glycosylation enzymes. Nature chemical biology 2018, 14 (2), 156.

48. Lunin, V. V.; Wang, H.-T.; Bharadwaj, V. S.; Alahuhta, M.; Peña, M. J.; Yang, J.-Y.; Archer-Hartmann, S. A.; Azadi, P.; Himmel, M. E.; Moremen, K. W.; York, W. S.; Bomble, Y. J.; Urbanowicz, B. R., Molecular Mechanism of Polysaccharide Acetylation by the Arabidopsis Xylan O-acetyltransferase XOAT1. The Plant cell 2020, 32 (7), 2367-2382.

49. Prabhakar, P. K.; Wang, H. T.; Smith, P. J.; Yang, J. Y.; Barnes, W. J.; Peña, M. J.; Moremen, K. W.; Urbanowicz, B. R., Heterologous expression of plant glycosyltransferases for biochemistry and structural biology. Methods Cell Biol 2020, 160, 145-165.

50. Huynh, K.; Partch, C. L., Analysis of protein stability and ligand interactions by thermal shift assay. Current protocols in protein science 2015, 79 (1), 28.9. 1-28.9. 14.

51. Jensen, J. K.; Busse-Wicher, M.; Poulsen, C. P.; Fangel, J. U.; Smith, P. J.; Yang, J. Y.; Pena, M. J.; Dinesen, M. H.; Martens, H. J.; Melkonian, M.; Wong, G. K.; Moremen, K. W.; Wilkerson, C. G.; Scheller, H. V.; Dupree, P.; Ulvskov, P.; Urbanowicz, B. R.; Harholt, J., Identification of an algal xylan synthase indicates that there is functional orthology between algal and plant cell wall biosynthesis. New Phytol 2018, 218 (3), 1049-1060.

52. Müller, J.; Sowa, M. A.; Fredrich, B.; Brundiek, H.; Bornscheuer, U. T., Enhancing the Acyltransferase Activity of Candida antarctica Lipase A by Rational Design. Chembiochem 2015, 16 (12), 1791-6.

53. Jan, A. H.; Subileau, M.; Deyrieux, C.; Perrier, V.; Dubreucq, É., Elucidation of a key position for acyltransfer activity in Candida parapsilosis lipase/acyltransferase (CpLIP2) and in Pseudozyma antarctica lipase A (CAL-A) by rational design. Biochimica et biophysica acta 2016, 1864 (2), 187-94.

54. Schmitt, J.; Brocca, S.; Schmid, R. D.; Pleiss, J., Blocking the tunnel: engineering of Candida rugosa lipase mutants with short chain length specificity. Protein Eng 2002, 15 (7), 595-601.

55. Mussatto, S. I.; Mancilha, I. M., Non-digestible oligosaccharides: A review. Carbohydrate Polymers 2007, 68 (3), 587-597.

56. Samanta, A. K.; Jayapal, N.; Jayaram, C.; Roy, S.; Kolte, A. P.; Senani, S.; Sridhar, M., Xylooligosaccharides as prebiotics from agricultural by-products: Production and applications. Bioactive Carbohydrates and Dietary Fibre 2015, 5 (1), 62-71.

57. Aachary, A. A.; Gobinath, D.; Srinivasan, K.; Prapulla, S. G., Protective effect of xylooligosaccharides from corncob on 1,2-dimethylhydrazine induced colon cancer in rats. Bioactive Carbohydrates and Dietary Fibre 2015, 5 (2), 146-152.

58. Yang, J.; Summanen, P.; Henning, S.; Hsu, M.; Lam, H. M.; Huang, J.; Tseng, C.-H.; Dowd, S.; Finegold, S.; Heber, D.; Li, Z., Xylooligosaccharide supplementation alters gut bacteria in both healthy and prediabetic adults: a pilot study. Frontiers in Physiology 2015, 6 (216).

59. Vázquez, M. J.; Alonso, J. L.; Domínguez, H.; Parajó, J. C., Xylooligosaccharides: manufacture and applications. Trends in Food Science & Technology 2000, 11 (11), 387-393.

60. Amorim, C.; Silvério, S. C.; Prather, K. L. J.; Rodrigues, L. R., From lignocellulosic residues to market: Production and commercial potential of xylooligosaccharides. Biotechnology Advances 2019, 37 (7), 107397.

61. Liao, N.; Luo, B.; Gao, J.; Li, X.; Zhao, Z.; Zhang, Y.; Ni, Y.; Tian, F., Oligosaccharides as co-encapsulating agents: effect on oral Lactobacillus fermentum survival in a simulated gastrointestinal tract. Biotechnol Lett 2019, 41 (2), 263-272.

62. Martins, M.; Silva, K. C. G.; Ávila, P. F.; Sato, A. C. K.; Goldbeck, R., Xylo-oligosaccharide microparticles with synbiotic potential obtained from enzymatic hydrolysis of sugarcane straw. Food Research International 2021, 140, 109827.

63. Carvalho, A. F. A.; Neto, P. d. O.; da Silva, D. F.; Pastore, G. M., Xylo-oligosaccharides from lignocellulosic materials: Chemical structure, health benefits and production by chemical and enzymatic hydrolysis. Food Research International 2013, 51 (1), 75-85.

Table 3.1 Kinetic parameters for XOAT1 variants

XOAT1 variant	K_M (uM)	V_{max} (pmol·min^{-1}·nmol^{-1})	k_{cat} (S^{-1})	k_{cat}/K_M ($M^{-1}\cdot S^{-1}$)
WT	51.45 ± 6.54	211.50 ± 8.62	0.0035 ± 0.00014	68.51
M311A	414.00 ± 144.50	29.58 ± 3.20	0.00049 ± 0.000053	1.19
N312A	493.30 ± 49.55	389.90 ± 13.86	0.0065 ± 0.00023	13.17
D403A	250.10 ± 34.56	110.90 ± 4.88	0.0018 ± 0.000081	7.39
R444A	51.48 ± 5.83	304.30 ± 11.07	0.0051 ± 0.00018	98.52
Q445A	56.87 ± 5.78	261.90 ± 8.77	0.0044 ± 0.00015	76.75
M311A/D403A	n.d.	n.d.	n.d.	n.d.
M311A/R444A	497.80 ± 266.30	26.07 ± 4.80	0.00043 ± 0.000080	0.87
M311A/Q445A	575.40 ± 260.30	24.59 ± 3.98	0.00041 ± 0.000066	0.71
N312A/D403A	n.d.	n.d.	n.d.	n.d.
N312A/R444A	447.50 ± 23.68	279.30 ± 5.54	0.0047 ± 0.000092	10.40
N312A/Q445A	445.20 ± 25.53	251.70 ± 5.40	0.0042 ± 0.000090	9.42
D403A/R444A	890.90 ± 264.30	56.63 ± 7.80	0.00094 ± 0.00013	1.06
D403A/Q445A	420.50 ± 125.80	87.15 ± 9.60	0.0015 ± 0.00016	3.45
R444A/Q445A	75.79 ± 9.25	279.90 ± 12.19	0.0047 ± 0.00020	61.55

n.d., not detected

Table S3.1 Primer sequences for *XOAT1* cloning and site-directed mutagenesis for building the expression constructs

XOAT1 variant	**Primer pair sequences[*] (5' → 3')**	**GFP fluorescence[†]**
Wild type	AACTTGTACTTTCAAGGCGAAGACGTGGAATTGCC; ACAAGAAAGCTGGGTCCTACGAACGGGAAATGATAC	2120.1
M311A	ACATTTGGTGGGCGAACACATTCG; AAGTGTTGAAAACAAGAAAGTCAA	1009.9
N312A	TTTGGTGGATGGCCACATTCGCTA; TGTAAGTGTTGAAAACAAGAAAGT	832.36
D403A	CGTAGGAACAGCCTACAGACTGT; CTGAATGGCATTGACATGTTTAG	1611.6
R444A	TTCACACAATCGCACAAGGCAAAA; CCGAAGTGTGAGCATCTTTCCGGT	1591.8
Q445A	ACACAATCCGAGCAGGCAAAATGC; GAACCGAAGTGTGAGCATCTTTC	2002.5
M311A/D403A	ACATTTGGTGGGCGAACACATTCG; AAGTGTTGAAAACAAGAAAGTCAA (Template: D403A)	798.6
M311A/R444A	ACATTTGGTGGGCGAACACATTCG; AAGTGTTGAAAACAAGAAAGTCAA (Template: R444A)	1003.4

M311A/Q445A	ACATTTGGTGGGCGAACACATTCG; AAGTGTTGAAAACAAGAAAGTCAA (Template: Q445A)	922.28
N312A/D403A	TTTGGTGGATGGCCACATTCGCTA; TGTAAGTGTTGAAAACAAGAAAGT (Template: D403A)	413.4
N312A/R444A	TTTGGTGGATGGCCACATTCGCTA; TGTAAGTGTTGAAAACAAGAAAGT (Template: R444A)	717.33
N312A/Q445A	TTTGGTGGATGGCCACATTCGCTA; TGTAAGTGTTGAAAACAAGAAAGT (Template: Q445A)	693.98
D403A/R444A	CGTAGGAACAGCCTACAGACTGT; CTGAATGGCATTGACATGTTTAG (Template: R444A)	778.58
D403A/Q445A	CGTAGGAACAGCCTACAGACTGT; CTGAATGGCATTGACATGTTTAG (Template: Q445A)	1026.4
R444A/Q445A	TTCACACAATCGCAGCAGGCAAAA; CCGAAGTGTGAGCATCTTTCCGGT	1964.3

* Nucleotides in the primer sequences corresponding to the mutated amino acid residues are underlined.

† Recombinant protein expression levels of XOAT1 and its variants were determined by the relative GFP fluorescence of the secreted proteins in the media.

Table S3.2 Interaction energies for XOAT1 residues involved in xylodecaose binding evaluated from unbiased MD simulations of the docked acceptor substrate averaged over 50 ns.

Residue Number	Total Interaction Energy (kcal/mol)	Van der Waals Interactions (kcal/mol)	Electrostatic Interactions (kcal/mol)
D403	-19.4	-2.1	-17.3
R444	-12.6	-2.9	-9.7
H465	-10.6	-0.7	-9.9
N312	-7.7	-3.6	-4.2
Q445	-6.1	-1.8	-4.3
M311	-5.5	-4.0	-1.5
Y404	-4.3	-1.4	-2.9
R335	-3.4	-0.3	-3.1
G401	-3.4	-2.1	-1.4
Q168	-3.1	-2.0	-1.1
I464	-2.7	-2.4	-0.3
I443	-2.6	-1.9	-0.8

Figure 3.1

Surface topology of XOAT1 in the substrate bound state: (a,b) The major and minor lobes colored in cyan and green respectively with the substrate show in Licorice representation with carbons colored yellow. The substrate residues have been labeled with increasing numbers from the non-reducing end to the reducing end with the residue at the active site being labeled 0. (c) A close-up view of the bound substrate, the catalytic triad (Ser216-His465-Asp462 depicted in VDW representation) and the residues identified to be having the highest binding energies from MD represented in licorice representation with the carbons colored gray.

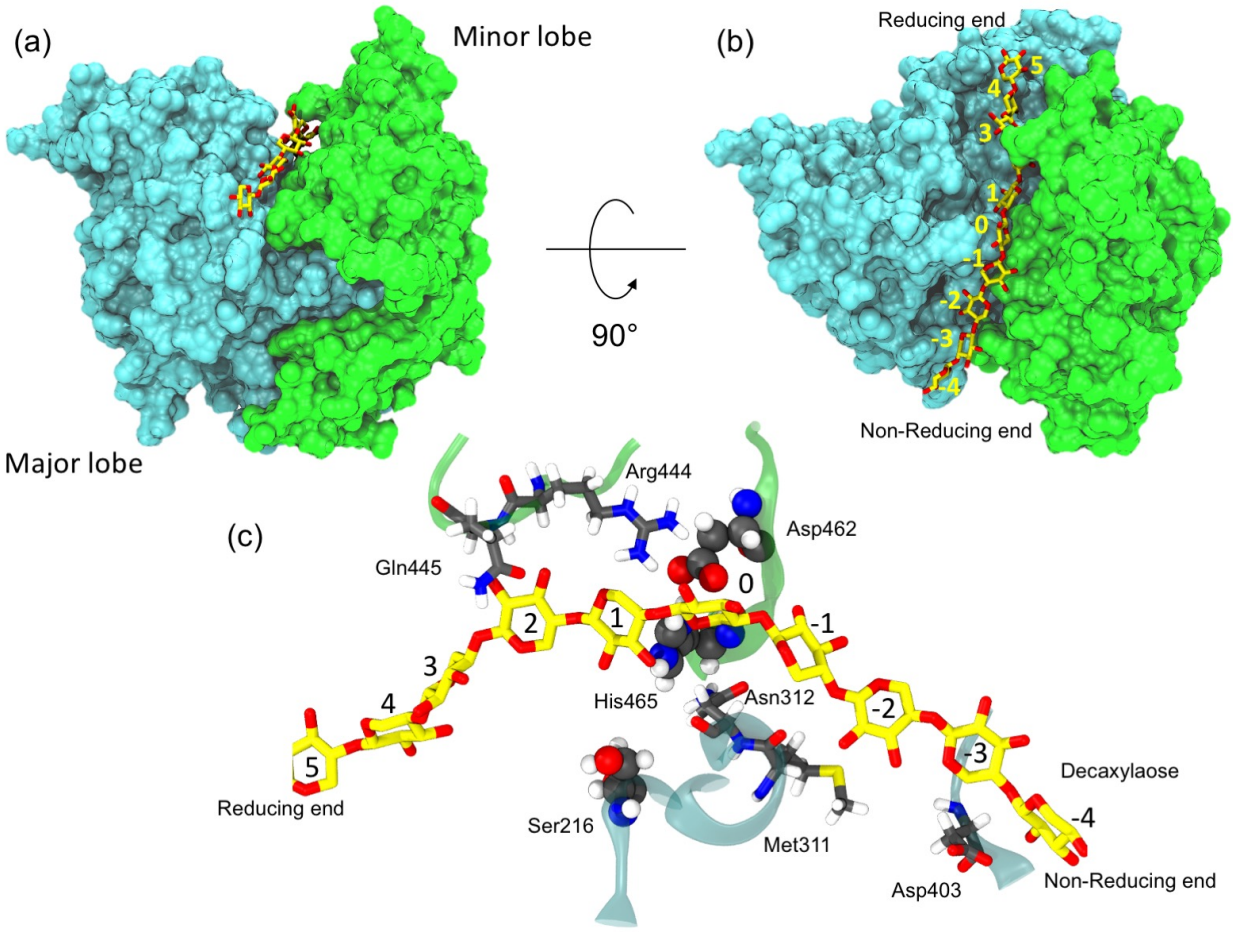
(a)
Minor lobe
Major lobe
90°
(b)
Reducing end
Non-Reducing end
(c)
Arg444
Asp462
Gln445
His465
Asn312
Ser216
Met311
Asp403
Reducing end
Decaxylaose
Non-Reducing end

Figure 3.2

Analysis of acetyltransferase activity of XOAT1 variants. (a) Single mutants of XOAT1 are sorted by increasing enzymatic efficiency (k_{cat}/K_M) from left to right. Protein thermal stability (T_m) and k_{cat}/K_M of each variant are shown in the top panel. For reference, the T_m and k_{cat}/K_M of wild-type XOAT1 are 53 ± 0.5 ℃ and 68.51 $M^{-1} \cdot S^{-1}$, respectively. In the second panel, sequence logos showing conservation of amino acids are depicted based on an alignment of nine xylan-specific TBLs, and the location of each mutated residues is marked by an asterisk. In the third panel, local areas inside the binding pocket of XOAT1 with point mutations and the docked xylodecaose are shown. Xylosyl residues are numbered according to the proximity to the catalytic site, the closest residue is assigned as 0, and the number increases towards reducing end. The major lobe is colored in cyan, while the minor lobe is in green. In the bottom panel, MALDI-TOF MS spectra of acetylated Xyl_6-2AB products generated by XOAT1 variants after overnight reactions are shown. (b) MALDI-TOF MS spectra of acetylated products generated by the double mutants of XOAT1. M311A/D403A variant generated no acetylated products, and the spectrum is shown in Figure S1. An addition of one acetyl group increases the mass of Xyl_6-2AB by 42 Da as indicated by $[M+H]^+$ ions.

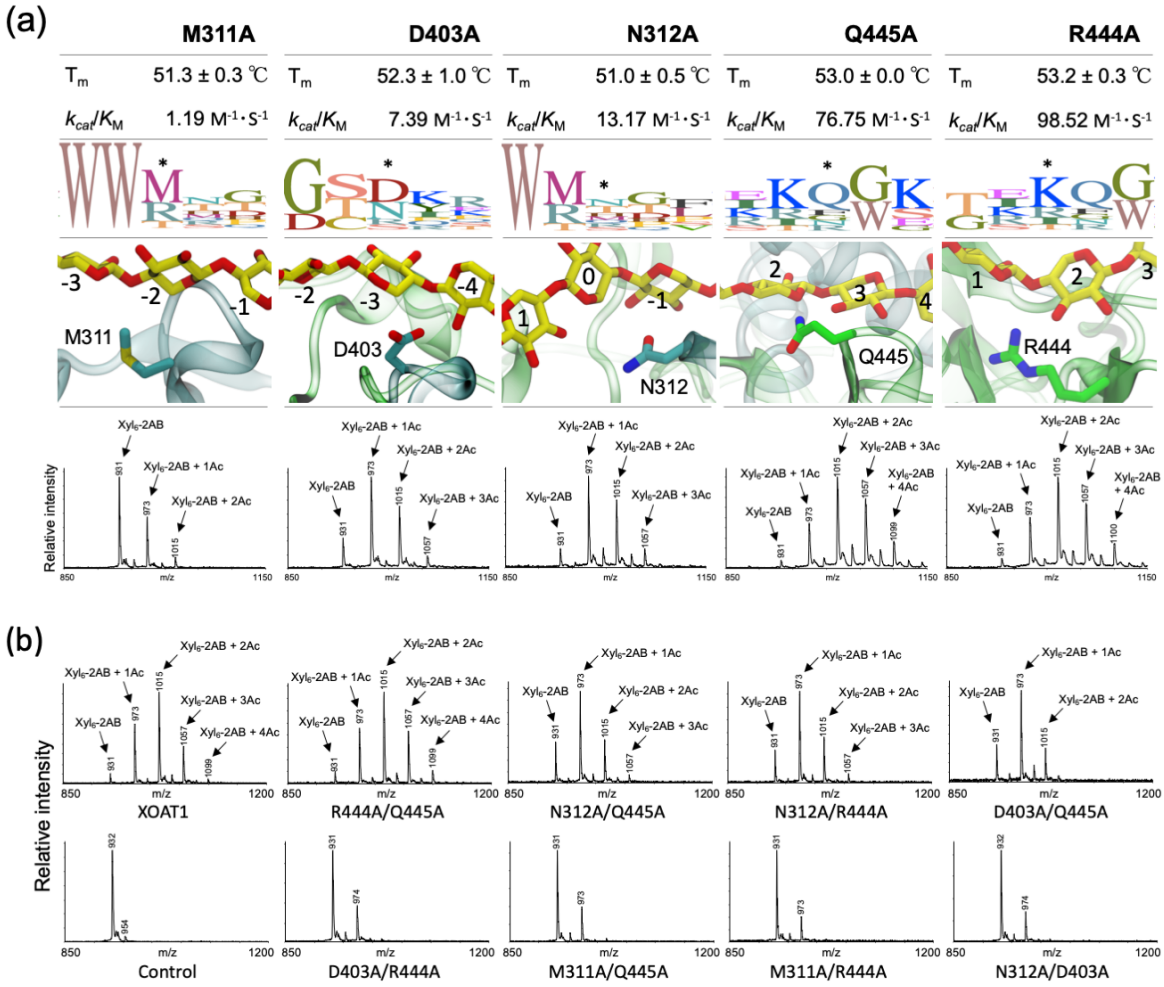
(a)
M311A
T$_m$ 51.3 ± 0.3 ℃
k_{cat}/K_M 1.19 M^{-1}·S^{-1}
D403A
T$_m$ 52.3 ± 1.0 ℃
k_{cat}/K_M 7.39 M^{-1}·S^{-1}
N312A
T$_m$ 51.0 ± 0.5 ℃
k_{cat}/K_M 13.17 M^{-1}·S^{-1}
Q445A
T$_m$ 53.0 ± 0.0 ℃
k_{cat}/K_M 76.75 M^{-1}·S^{-1}
R444A
T$_m$ 53.2 ± 0.3 ℃
k_{cat}/K_M 98.52 M^{-1}·S^{-1}
M311
D403
N312
Q445
R444
Relative intensity
m/z
(b)
XOAT1
R444A/Q445A
N312A/Q445A
N312A/R444A
D403A/Q445A
Control
D403A/R444A
M311A/Q445A
M311A/R444A
N312A/D403A

Figure 3.3

MALDI-TOF MS of acetylated xylo-oligosaccharides (XOS) synthesized through one-pot reaction catalyzed by xylan synthase and XOAT1 or its variants. Spectra of acetylated products generated by five variants (M311A, N312A, D403A, R444A, and Q445A) are shown and sorted from top to bottom by decreasing enzymatic efficiency. Control contains no XOAT1 or its variants. Degree of polymerization (DP) of XOS are labeled on top of the signals, and an asterisk represents one acetyl group attached to the xylosyl species. An addition of one acetyl group increases the mass of xylo-oligomers by 42 Da as indicated by $[M+H]^+$ ions.

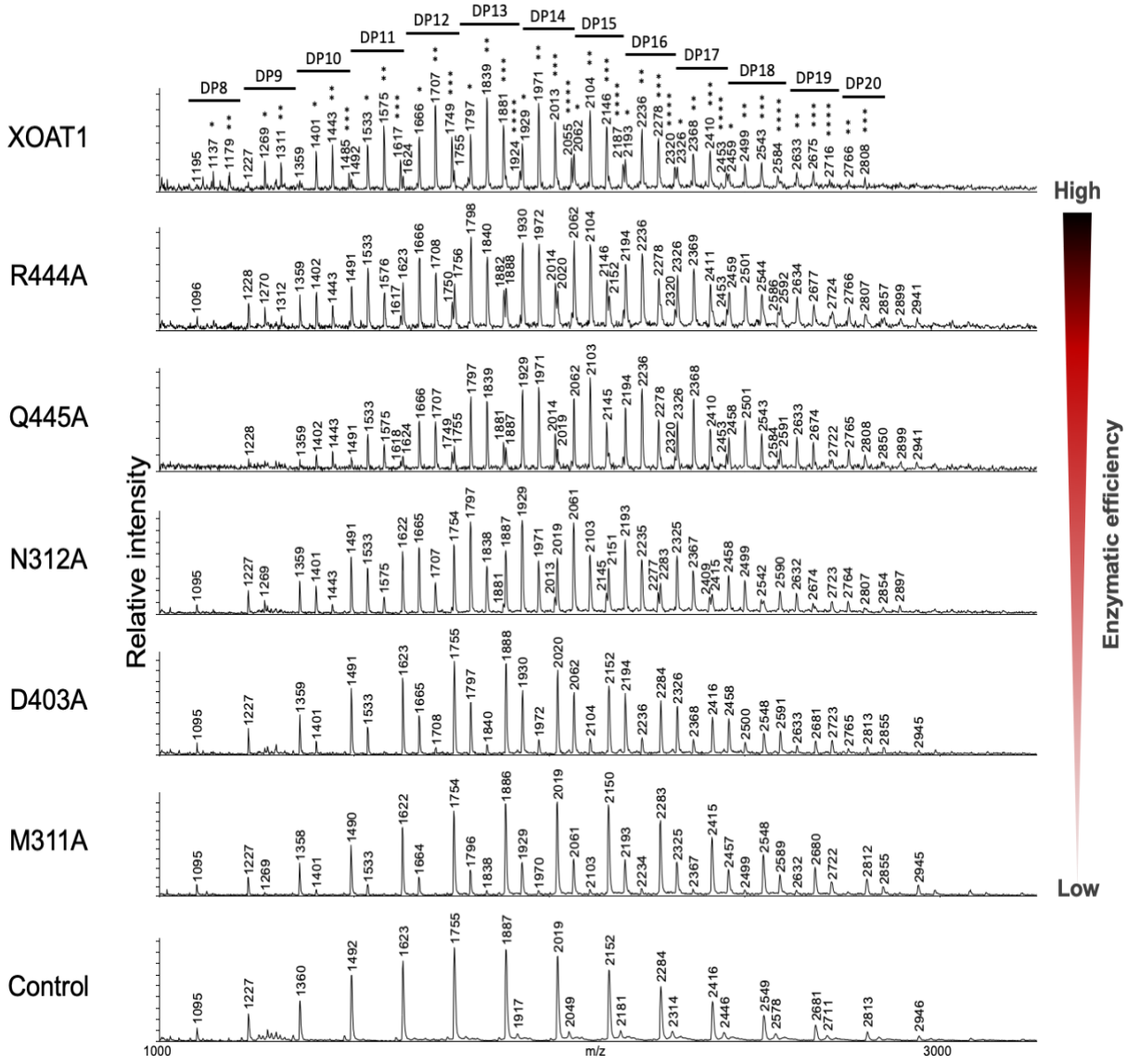
DP8
DP9
DP10
DP11
DP12
DP13
DP14
DP15
DP16
DP17
DP18
DP19
DP20
XOAT1
R444A
Q445A
N312A
D403A
M311A
Control
Relative intensity
m/z
1000
3000
High
Low
Enzymatic efficiency

Figure S3.1

MALDI-TOF MS analysis of the overnight products generated by M311A/D403A. The acetyltransferase activity of the double mutant M311A/D403A was assessed using 1 mM acetylsalicylic acid and 0.1 mM 2-aminobenzamide-labeled xylohexaose (Xyl_6-2AB) as the donor and accepter substrate, respectively. The products from the overnight reaction were analyzed through MALDI-TOF MS. Wild type XOAT1 was used as a positive control, while control contained equal volume of buffer to substitute enzymes. Each transfer of the *O*-acetyl group (Ac) increases the mass of the xylo-oligo acceptors by 42 Da as the annotated [M+H]+ ions.

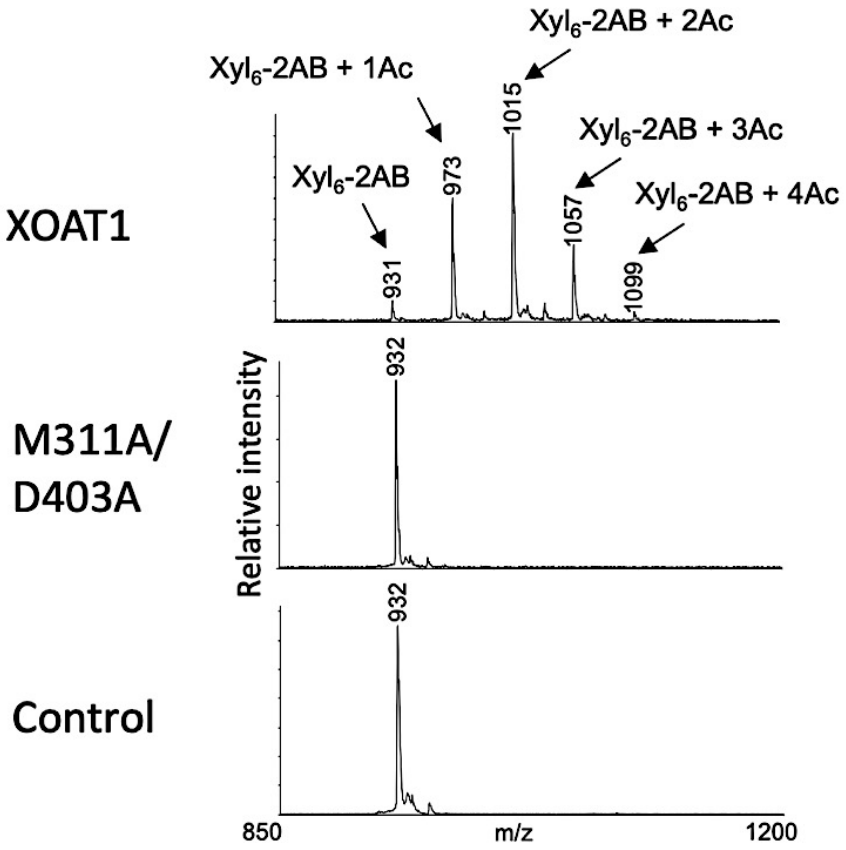
XOAT1
M311A/
D403A
Control
Xyl6-2AB + 2Ac
Xyl6-2AB + 1Ac
Xyl6-2AB + 3Ac
Xyl6-2AB + 4Ac
Xyl6-2AB
931
973
1015
1057
1099
932
932
Relative intensity
850
m/z
1200

Figure S3.2

Hydrolysis rates of 4MU-Ac by XOAT1 variants without acceptor substrates in the reaction. Statistical significance of each variant to the wild-type (WT) was determined through two-tailed Student's t test. **, $p < 0.01$.

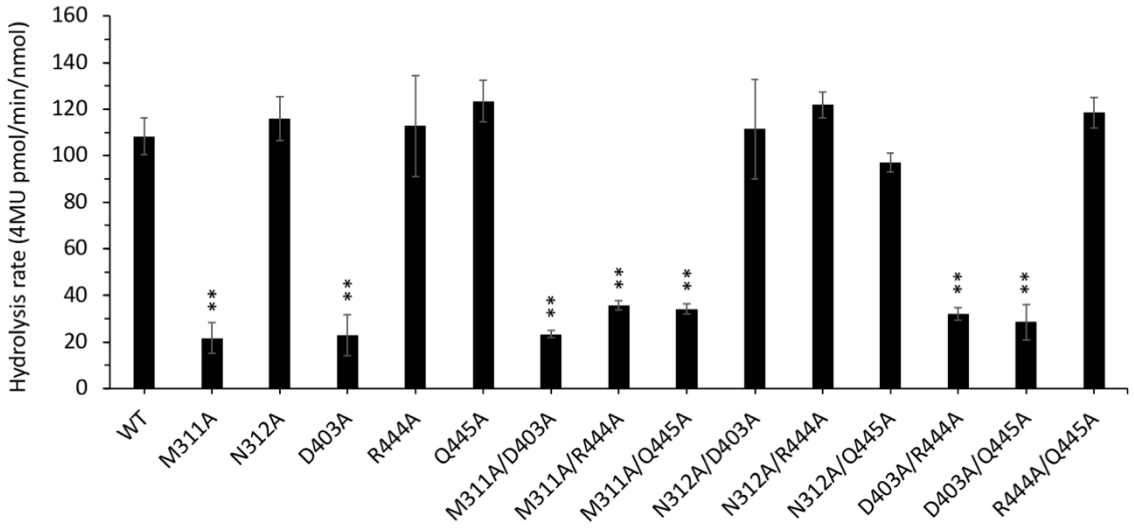
Hydrolysis rate (4MU pmol/min/nmol)
160
140
120
100
80
60
40
20
0
**
**
**
**
**
**
WT
M311A
N312A
D403A
R444A
Q445A
M311A/D403A
M311A/R444A
M311A/Q445A
N312A/D403A
N312A/R444A
N312A/Q445A
D403A/R444A
D403A/Q445A
R444A/Q445A

CHAPTER 4

CHARACTERIZATION OF A NOVEL TRANSACETYLASE: TRICHOME BIREFRINGENCE-LIKE3 (TBL3) IN *ARABIDOPSIS THALIANA*

Hsin-Tzu Wang, Maria J. Peña, Jeong Yeh Yang, Kelley W. Moremen, William S. York, and Breeanna R. Urbanowicz. To be submitted to *Frontiers in Plant Science*

Abstract

Xylan, the most abundant hemicellulose in dicots, is heavily *O*-acetylated. The *O*-acetylation levels on xylan and other cell wall polymers can be crucial to maintaining cell wall architecture and plant growth, and thus need to be finely mediated. Despite the importance of polysaccharide *O*-acetylation, the detailed mechanism of how cell wall polysaccharides are *O*-acetylated remains to be understood. The TRICHOME BIREFRINGENCE-LIKE (TBL) protein family is involved in *O*-acetylation of different wall polysaccharides. TBL3 has been previously shown to function as a xylan *O*-acetyltransferase. Here, we present a novel biochemical activity of TBL3, and show that this enzyme is a bifunctional xylan transacetylase, which catalyzes both deacetylation and acetylation of xylan and is able to use acetylated xylan as an acetyl donor substrate. Real-time NMR analysis to investigate the regiospecificity of TBL3 demonstrates that it substitutes xylose at *O*-2 for both acetylation and deacetylation, suggesting that TBL3 may play a role in regulating the *O*-acetylation levels and/or patterning on the xylan backbone. Taken together, our study reveals previously undescribed function possessed by the TBL proteins, which provides insights into the mechanism of xylan *O*-acetylation during cell wall biosynthesis.

Introduction

Xylans are highly abundant hemicellulosic polysaccharides in plant cell walls and have been widely applied in different industries in human society. In food industry, for example, xylooligosaccharides (XOS) obtained from plant biomass have been used as prebiotics to stimulate growth and activity of beneficial bacteria in the human gut [1, 2]. Moreover, xylans are not broken down by mammalian-encoded enzymes and display pH stability in the gastrointestinal track, making XOS ideal materials for microencapsulation of probiotic organisms, which are used as dietary supplements for increasing beneficial microbiota [3, 4]. In addition to that, their antioxidant, anti-inflammatory, and thermal stability properties have advanced interest in utilization of XOS as sustainable and biocompatable feedstock for production of cosmetic, food, and pharmaceutical products [5, 6]. In addition, due to their abundance in agricultural biomass, xylans have garnered momentum as targets for crop improvement and biofuel production.

The structures of xylans vary depending on the species and the type of cell wall containing them [7]. In dicots, *O*-acetylglucuronoxylans (AcGX) are the most common xylan structures in secondary walls and are composed of 1,4-linked β-D-xylopyranosyl (Xyl) backbones, which are further substituted with 1,2-linked α-D-glucuronic acid (GlcA) and/or its 4-O-methyl derivative (MeGlcA) [8]. The most abundant substituents attached to the xylan backbone are *O*-acetyl moieties, which decorate more than half of the xylosyl residues in secondary walls of dicots [9]. *O*-acetylation is not only a key determinant of the polysaccharide hydrophobicity but also affects their interactions with other polysaccharides. For example, the viscosity of mixtures of xanthan and guar galactomannan increases when the xanthan is de-*O*-acetylated, demonstrating that the stability of xanthan-guar interactions increases as the degree of acetylation decreases [10]. Similar behavior is observed for the interaction of xylans with cellulose [11], where the presence of *O*-

acetyl substituents on the xylan decreases the adsorption of xylan to cellulose, indicating that xylan substituent type, amount and possibly patterning influence xylan-cellulose interactions. Moreover, a close relationship between xylans and cellulose has been revealed by precipitation of native xylans at the cellulose microfibril surface observed through electron microscopy [12]. Based on the aforementioned studies, we postulate that acetylation of xylans can affect cell wall architecture and mechanical strength by modulating its interaction with other polymers in the wall.

O-Acetylation of xylans is known to play an important role in both cell growth and biomass conversion into fuels and products, but the precise roles of the proteins involved in this process remains poorly understood. It has been suggested that at least three protein families are involved in xylan acetylation in the model plant *Arabidopsis thaliana*. The REDUCED WALL ACETYLATION (RWA) proteins are proposed to function in translocating acetyl-donors into the Golgi prior to *O*-acetylation of the polymers [13]. ALTERED XYLOGLUCAN 9 (AXY9) has not been shown to function as an acetyltransferase; however, *axy9* null mutants have lower overall levels of cell wall *O*-acetylation [14, 15]. The TRICHOME BIREFRINGENCE-LIKE (TBL) proteins are polysaccharide *O*-acetyltransferases directly involved in the addition of substituents to cell wall polysaccharides [16]. Plant-specific TBLs are Golgi-localized type 2 transmembrane proteins that have two conserved domains: the TBL domain and the DOMAIN OF UNKNOWN FUNCTION 231 (DUF231). The Gly-Asp-Ser (GDS) motif in the TBL domain has also been found in some carbohydrate esterases and lipases, and forms a catalytic triad composed of the Ser of the GDS motif together with Asp and His within the DXXH motif in the C-terminal DUF231 domain [17, 18].

Phylogenetic analysis of the *Arabidopsis* TBL family reveals that proteins present in different subclades display distinct substrate specificities (Figure 4.1a). TBLs in the xylan-specific

subclade, termed XOATs, share a high degree of amino acid sequence identity (Table 4.1 and Figure 4.2). However, XOATs have been shown to possess very specific regio-selectivity, indicating there are key factors present in both the active site and substrate-binding cleft that determine this specificity. Within the xylan-specific subclade, biochemical and or genetic evidence suggests that nine XOATs are regiospecific, including enzymes involved in 2-*O*- and 3-*O*-monoacetylation (TBL30); 2,3-di-*O*-acetylation (TBL35); both 2-*O*-, 3-*O*-mono- and 2,3-di-*O*-acetylation of linear xylan (TBL3, TBL28, TBL29/ESK1/XOAT1, TBL31, and TBL34); or 3-*O*-acetylation of 2-*O*-GlcA-substituted xylosyl residues (TBL32 and TBL33) (Figure 4.1b) [19-23]. Understanding the molecular determinants of selectivity are prime future targets for enzyme engineering and synthetic biology efforts aimed to develop lignocellulosic materials with precisely altered acetylation levels and/or patterning.

In recent years, the fourth class of Golgi-localized enzymes involved in modulating xylan *O*-acetylation has been identified [24, 25]. The rice (*Oryza sativa*) protein BRITTLE LEAF SHEATH1 (BS1) has been shown to catalyze deacetylation at the *O*-2 and *O*-3 positions of xylosyl backbone residues based on a combination of *in vitro* activity assays and mutant analysis [24]. Moreover, the *bs1* null mutant has altered patterning of secondary walls in vessels, indicating the importance of BS1 in secondary cell wall formation. Another recently reported deacetylase, DEACETYLASE ON ARABINOSYL SIDECHAIN OF XYLAN1 (DARX1) is arabinoxylan-specific enzyme that cleaves acetyl moieties from arabinosyl substituents attached to the xylan backbone. Analysis of the *darx1* mutant revealed plants were shorter and with reduced cell wall mechanical strength [25]. These enzymes are distinct from the previously identified PECTIN ACETYLESTERASE 1 (PAE1) in *Populus trichocarpa* that is cell wall-localized and is a member of carbohydrate esterase family 13 (CE13) [26]. BS1 and DARX1 are localized in Golgi apparatus,

where hemicellulose synthesis occurs, and have been categorized as members of the GDSL esterase/lipase family. Taken together, data suggested they are involved in upstream manipulation of acetylation levels in the pathway of xylan synthesis, prior to deposition of the polymer in the cell wall.

The identification of new catalysts in the polysaccharide acetylation pathway in plants demonstrates that there may be an antagonistic mechanism employing acetyltransferase and deacetylase activities to meet certain biological and/or structural requirements in plants during the biosynthesis process, akin to post-deposition cell wall remodeling, to tightly control wall properties. Cell wall remodeling occurs when plant cells are expanding or in response to abiotic stresses such as heat, cold, drought, or salt to adapt to the environment by modulating wall structures and/or components. A variety of enzymes have been shown to play a role in this process, such as peroxidases, xyloglucan endo-β-transglucosylases/hydrolases (XTHs; GH16), expansins (GH45), and pectin-modifying enzymes including pectin methylesterases (PME; CE8) and pectin acetylesterases (PAE; CE13) [27-30]. The latter two enzymes are involved in controlling the degrees of pectin methylesterification and acetylation, respectively, to regulate stiffness and elasticity of plant cell walls during growth and in response to biotic and abiotic stresses [26, 31], suggesting that these substituents play central roles in affecting physiochemical properties of cell wall polysaccharides.

Biochemical analysis of the extensively studied TBL protein, XYLAN *O*-ACETYLTRANSFERASE 1 (XOAT1), showed that it is a xylan-specific 2-*O*-acetyltransferase, and established the precise molecular function of this protein and the TBL family [13]. TBL3 is phylogenetically close to XOAT1, and is also highly expressed during secondary wall synthesis, suggesting it plays a role in the complex mechanism of xylan *O*-acetylation. Analysis of plant cell

wall material isolated from *tbl3* mutants showed they contain lower levels of crystalline cellulose and esterified pectins in trichomes and stems, indicating that TBL3 contributes to the deposition of secondary wall cellulose, possibly through altering esterification of pectic polysaccharides [16]. A reduced level of 3-*O*-acetylation on xylans has been observed in the *tbl3 tbl31* double mutant, suggesting TBL3 and TBL31 enzymes are involved in xylan 3-*O*-acetylation [21]. The enzymatic activity of TBL3 as a xylan *O*-acetyltransferase has been determined through *in vitro* assays [19], in addition to its homologs in *Populus trichocarpa* and *Oryza sativa*, PtrXOAT7 and OsXOAT8 [32, 33]. However, the endpoint assays used in these studies involving product analysis after reactions lasting 16 h or more are not sufficient for determination of regiospecificity due to non-enzymatic, spontaneous acetyl migration observed in acetylated XOS [18].

Previously, we showed that *A. thaliana* XOAT1 is able to utilize several surrogate compounds as donor substrates, including *p*-nitrophenyl acetate (*p*NPA), acetylsalicylic acid, acetyl coenzyme A (acetyl-CoA), and 4-methylumbelliferylacetate (4MU-Ac) [18]. Here, we investigated the substrate specificities of *A. thaliana* TBL3, and determined that TBL3 can barely use acetyl-CoA as a donor in *vitro*, which is hypothesized to be the native acetyl-donor in plants [34]. Instead, TBL3 has a strong preference for the synthetic donor substrate, *p*NPA. This is distinct from XOAT1, which can readily use both acetyl-CoA and *p*NPA. Furthermore, we found that the level of XOS O-acetylation was reduced when TBL3 was co-incubated with XOAT1 in acetyltransferase reactions, relative to products formed by XOAT1 alone, suggesting that TBL3 may not be an obligate *O*-acetyltransferase. Indeed, we show that TBL3 is able to utilize acetyl-xylooligosaccharides (Ac-XOS) as acetyl-donor substrates to catalyze the transfer of *O*-acetyl groups to xylan acceptors. Real-time analysis through 1-dimensional proton nuclear magnetic resonance (1D ^{1}H NMR) spectroscopy of the transacetylation reaction revealed the unbiased

regiospecificity of TBL3, and show that the enzyme adds or removes *O*-acetyl groups at the *O*-2 position on xylosyl residues. Taken together, our data suggests that acetyl substituents may be transferred between cell wall polymers in a regiospecific manner, expanding our understanding of *O*-acetylation machinery of cell wall polysaccharides.

Results

Insights into TBL3 donor substrate selectivity

To identify the catalytic activity and substrate specificity of TBL3, a recombinant form of this enzyme was expressed in human embryonic kidney (HEK) 293 cells and purified from the culture medium. Recombinant *A. thaliana* xylan acetyltransferase, XOAT1, was expressed as previously described [18, 23]. XOAT1 has been shown to display donor substrate promiscuity, and is able to utilize multiple acetyl-donor substrates *in vitro* [18, 35]. Other TBLs such as TBL22/ALTERED XYLOGLUCAN 4-LIKE (AXY4L), TBL26/MANNAN O-ACETYLTRANSFERASE 4 (MOAT4), and TBL27/ ALTERED XYLOGLUCAN 4 (AXY4) were also able to hydrolyze various pseudo-substrates, such as *p*NPA and 4MU-Ac in esterase/deacetylase assays [14, 35]. To investigate the donor substrate selectivity of TBL3, a mass spectrometry (MS)-based xylan *O*-acetyltransferase assay with 2-aminobenzamide-labeled 1,4-β-xylohexaose (Xyl_6-2AB) as a fluorescently labeled acceptor substrate and acetyl-CoA, acetylsalicylic acid, or *p*NPA as acetyl-donor substrates was used [23]. After a 2h incubation at room temperature, the reaction products were analyzed by matrix-assisted laser desorption/ionization time-of-flight mass spectrometry (MALDI-TOF MS). The results showed that TBL3 can barely utilize acetyl-CoA (a naturally occurring acetyl-donor) or acetylsalicylic acid

as donor substrates (Figure 4.3). It has been previously reported that acetylated products could be detected after TBL3 has been incubated with acetyl-CoA as a donor for extended time periods (16 h) [19]. However, our data shows TBL3 was able to readily use chromogenic substrate *p*NPA, frequently used to measure acetylesterase activity of enzymes, as an *O*-acetyl donor. In contrast, XOAT1 used here as a control, is known to be much less selective [18], and is capable of catalyzing the transfer of acetyl groups to Xyl_6-2AB acceptor substrate using all the three donors (Figure 4.3), even though the amino acid sequences of XOAT1 and TBL3 are similar (Figure 4.2).

Biochemical Characterization of TBL3

Xylan backbone residues found in plants can be 2-*O*- and 3-*O*-monoacetylated, 2,3-di-*O*-acetylated, and 3-*O*-acetylated on those that are (Me)GlcA-substituted. Because of this complexity, acetyltransferases are thought to act cooperatively to synthesize structures found in nature. Previously, analysis of xylan isolated from *A. thaliana* knockout mutants suggested TBL3 plays a role in xylan 3-*O*-acetylation [19], whereas XOAT1 specifically catalyzes 2-*O*-acetylation of xylan. Thus, our initial experiments sought to determine whether XOAT1 and TBL3 can act cooperatively in 'co-synthesis' reactions to generate xylan that is more complex than that decorated by XOAT1 alone, i.e., by 2-*O*- and 3-*O*-monoacetylated or di-substituted. First, the two enzymes were incubated at equimolar concentrations together with Xyl_6-2AB and the donor substrate, *p*NPA, which we have shown can be utilized by both enzymes. Surprisingly, MALDI-TOF MS analysis of the reaction products showed that these initial co-synthesis reactions did not result in an increased amount of Ac-XOS. Rather than that, the acetylation level of the products produced via co-synthesis using the two enzymes was lower than that produced by XOAT1 alone (Figure 4.4a).

Next, we sought to examine whether TBL3 preferentially catalyzes acetyl hydrolysis/deacetylation over acetyl transfer. In order to investigate this, we took advantage of XOAT1 and used it to synthesize acetylated Xyl_6-2AB oligosaccharides (Ac-Xyl_6-2AB) using acetylsalicylic acid as a donor substrate, and is not a donor for TBL3 (Figure 4.4b, upper lane). After 4 hrs, TBL3 or an equal volume of buffer was added to the reaction mixture, and they were allowed to continue for another hour at room temperature. MALDI-TOF MS analysis of the products showed that less Ac-Xyl_6-2AB were present in reactions containing TBL3, indicating that acetyl groups attached to Xyl_6-2AB were potentially removed due to hydrolysis of esters by TBL3 (Figure 4.4b, lower lane). This acetylesterase/deacetylase (here after called deacetylase) activity initially suggested that TBL3 might function primarily to de-acetylate wall polysaccharides during cell wall biogenesis, similarly to BS1 and DARX1.

TBL3 can function as a transacetylase

Our initial donor substrate selectively screen did indicate that TBL3 can transfer *O*-acetyl groups to XOS. Specifically, TBL3 does not prefer the native acetyl-donor, acetyl-CoA (Figure 4.3), suggesting that there might be other donors present in plants which can be utilized by this enzyme. Our revised hypothesis suggests that Ac-XOS generated during synthesis of cell wall xylans by TBL proteins such as XOAT1 could potentially be TBL3's acetyl-donors. To test the hypothesis, acetylated Xyl_6 (Ac-Xyl_6) was used as the donor in another two-step experiment (schematically described in Figure 4.5a) to determine whether TBL3 can use Ac-XOS to catalyze acetylation of non-acetylated, chemically labelled Xyl_6-2AB. In the first reaction, non-labeled Ac-XOS were synthesized using XOAT1, unlabeled Xyl6, and acetylsalicylic acid as the donor substrate and incubated overnight (Figure 4.5b). To eliminate subsequent acetylation catalyzed by

XOAT1, the reaction was treated at 85°C for 15 min to inactivate XOAT1. Then, TBL3 and chemically labeled (but not acetylated) Xyl_6-2AB was added to the sample containing Ac-Xyl_6 from the first reaction. The labeling of 2AB allowed acceptor molecules in the TBL3-catalyzed reaction to be distinguished from donor molecules. After incubation at room temperature for 2h, the products were analyzed by MALDI-TOF MS. As shown in Figure 4.5c, acetylation of Xyl_6-2AB was observed under these conditions. Ac-Xyl_6 was thus almost certainly acting as the acetyl donor for TBL3, as no active XOAT1 was present at this stage and TBL3 cannot use acetylsalicylic acid as an acetyl donor, suggesting that TBL3 catalyzes the transfer of acetyl groups from one XOS to another. No Ac-Xyl_6-2AB was detected in control reactions (Figure 4.5d). In addition to using in vitro synthesized Ac-Xyl_6 as TBL3 donor substrates, the transacetylase assay was carried out using naturally Ac-XOS extracted from poplar as the donor substrates (the preparation procedure of poplar Ac-XOS is schematically demonstrated in Figure 4.6a). The results show that TBL3 can also transfer acetyl groups from poplar Ac-XOS to Xyl_6-2AB (Figure 4.6b), confirming the transacetylase activity of TBL3.

The regiospecificity analysis of TBL3

A previous study of TBL3 regiospecificity was carried out through an acetyltransferase assay using Xyl_6 as the acceptor substrate, and final acetylated products were analyzed by ^{1}H NMR spectroscopy to examine the position attached with acetyl moieties on xylosyl residues [19]. However, this data was an endpoint assay where reaction products were analyzed after a long incubation period of 16 h, where non-enzymatically driven acetyl migration is known to occur [18, 36-38]. To unambiguously characterize the regiospecificity of TBL3 as an acetyltransferase, we used 1D ^{1}H NMR spectroscopy to monitor a 17-hour reaction of *O*-acetylation catalyzed by TBL3

in real-time using methods previously developed to study XOAT1 [18]. The pseudo-substrate, *p*NPA, was used as the acetyl donor, and Xyl_6 was used as the acceptor in the TBL3 reaction. A XOAT1 reaction containing equal amounts of the same substrates under the same conditions was carried out as a positive control. Dimethyl sulfoxide (DMSO) is included in both TBL3 and XOAT1 reactions as an internal standard for quantification. The results are shown in Figure 4.7a, the proton signal of $-CH_3$ in the 2-*O*-acetylated xylose appeared followed by the *O*-3 signal in 30 min after the reaction initiated, and both signals increased at similar rates. These data are distinct from the XOAT1 reaction, suggesting that TBL3 is a 2-*O*-acetyltransferase, and might be involved in 3-*O*-acetylation. However, the amount of acetic acid released by TBL3 is much more (at a rate of 3.62 nmol/hour) than that produced by XOAT1 (at a rate of 2.60 nmol/hour). Quantification of 2-*O* and 3-*O*-acetylated xylosyl residues produced in each reaction is shown in Figure 4.7b, which reveals that 2-*O* and 3-*O*-acetylated xyloses reached the approximately equal amounts at 17-hour time point.

To further analyze the regiospecificity of the deacetylase activity of TBL3, we again used real-time NMR technique to carry out and monitor another two-step experiment. In the first reaction, we incubated XOAT1 with acetylsalicylic acid and Xyl_6 to generate a significant amount of mono-acetylated Xyl_6 at *O*-2 position (Figure 4.8a). After the reaction was allowed to proceed for 2 hrs, XOAT1 was removed by diafiltration using a 3 kDa spin filter. The resulting filtrate enriched in 2-*O*-acetylated Xyl6 was then used as the substrate in a second reaction, which was initiated by adding TBL3 and monitored for 20 hours. Control reactions were performed by adding an equal amount of buffer to monitor the non-enzymatic, spontaneous migration of acetyl groups according to prior methods [18]. Reactions containing TBL3 (Figure 4.8b), a faster and higher decrease of the signals corresponding to the 2-*O*-acetyl CH_3 decreased at a higher rate compared

to the control, while similar increments of the 3-*O*-acetyl CH_3 signals from both mixtures with and without TBL3 were observed (Figure 4.8b and c), indicating that the spontaneous migration of acetyl groups occurred. The ratio of 3-*O* to 2-*O*-acetylated xylosyl residues (*O*-3 : *O*-2) during the reaction period is shown in Figure 4.8d, and due to the deacetylase activity catalyzed by TBL3 at *O*-2 position, the amount of 2-*O*-acetylated xylosyl residues was lower than 3-*O*-acetylation at the end of the reaction, resulting in a *O*-3 : *O*-2 ratio that is higher than 1. On the contrary, although *O*-3 : *O*-2 ratio in the control slowly increased due to the spontaneous migration of acetyl groups, the ratio remained below 1 during the entire 20-h reaction period (Figure 4.8d). The results suggest that TBL3 is a bifunctional enzyme with xylan acetyltransferase and deacetylase activities that catalyzes both *O*-acetylation and deacetylation, respectively, at *O*-2 position on xylosyl residues, but more evidences are needed to evaluate whether if TBL3 is also involved in 3-*O*-acetylation.

Discussion

The proteins in the TBL family in Arabidopsis are acetyltransferases that catalyze *O*-acetylation on non-cellulosic polysaccharides [39]. Here, we present a newly discovered biochemical function of one of the TBL proteins, TBL3, which shows that it is a bifunctional xylan transacetylase that possesses both xylan acetyltransferase and deacetylase activities. As a member of the TBL family, TBL3 shows a comparatively narrow donor substrate selectivity relative to XOAT1 or other GDS motif-containing lipases/esterases, which exhibit a broad substrate specificity as one of their well-known characteristics [17]. Our data shows that acetyl-CoA is not a preferred substrate for TBL3 to catalyze *O*-acetylation of xylan and is sparingly able to utilize acetyl-CoA, which is unexpected since acetyl-CoA is often considered as a universal acetyl-donor substrate for *O*-acetylation of wall polysaccharides in plants and sialic acids in mammalian cells

[34, 40]. Bacterial systems have also been postulated to use acetyl-CoA as a donor substrate to catalyze O-acetylation on peptidoglycan [41]. Rather than using acetyl-CoA as a donor substrate, TBL3 is capable of hydrolyzing acetyl moieties from the xylan backbone and transferring them to other and/or the same XOS as indicated by both the two-step in vitro assay and the activity assay using naturally acetylated poplar Ac-XOS as the donor (Figures 4.5 and 4.6), suggesting that Ac-XOS could possibly be the native acetyl-donor substrates for TBL3 *in vivo*.

The regiospecificity of TBL3 was analyzed through monitoring the transfer of acetyl groups on Xyl_6 in the reaction by using 1D ^1H NMR, which indicated that TBL3 catalyzes acetylation at *O*-2 position (and possibly *O*-3) on xylosyl residues. Further analysis of the regiospecificity of TBL3 as a deacetylase was carried out by using the same real-time NMR technique to monitor TBL3 hydrolyzing the in vitro-synthesized 2-*O*-monoacetylated Xyl6 produced by XOAT1, which confirms a 2-*O*-deacetylase activity possessed by TBL3. Taken together, the results of regiospecificity analysis of TBL3 suggest that it is an enzyme with both acetyltransferase and deacetylase activities at the *O*-2 position (but possibly not limited to) on xylan. Previously, it has been suggested that TBL3 is able to catalyze both *O*-2 and *O*-3-monoacetylation as well as 2,3-di-*O*-acetylation with a preference of *O*-3-monoacetylation on xylan based on the ratio of *O*-2 and *O*-3-acetyl signals in the NMR spectrum of the products generated from a long-incubated reaction [42], which could involve spontaneous migration of acetyl groups transferring from *O*-2 and *O*-3 position on xylosyl residues that might be overlooked in the study. Similar distributions of *O*-2 and *O*-3-acetyl groups on xylosyl residues produced by poplar and rice TBL3 homologs through a similar assay but with an even higher incubation temperature that could trigger more non-enzymatic acetyl migration were also reported [32, 33]. The phenomenon of spontaneous acetyl group migration could lead to ambiguous results of the

acetyltransferase assay, and should be carefully dealt with when carrying out experiments. In our previous study on the regiospecificity of XOAT1, the acetyl group migration was monitored after removal of the enzyme from the reaction, confirming the exclusive 2-*O*-acetyltransfersase activity possessed by XOAT1 [18]. In this study, XOAT1 was used as a control, and a similar result was observed that *O*-2 signal appeared in the beginning of the XOAT1 reaction (at a rate of 3.85 nmol/hour in the first 5-h linear period; the rates mentioned hereafter are based on calculations from the same period) followed by the slowly increasing *O*-3 signal (0.46 nmol/hour), which is caused by spontaneous migration from *O*-2 to *O*-3 position (Figure 4.7b). In comparison, TBL3 showed a slower production rate of the initially appeared *O*-2 signal (2.09 nmol/hour), but presented a higher rate of the follow-up *O*-3 signal generation (1.30 nmol/hour) compared with XOAT1 (Figure 4.7b), suggesting that TBL3 might be potentially involved in 3-*O*-acetylation as well, but direct evidence is needed to validate this activity. Based on our results, the confirmed and potential paths for xylan *O*-acetylation and deacetylation catalyzed by TBL3, and acetyl group migration and hydrolysis driven by non-enzymatic reactions or possibly catalyzed by TBL3 are summarized in Figure 4.9.

Compared to the GDSL lipases/esterases in other kingdoms, very few GDSL members in plants have been characterized [43, 44]. Recently, a GDSL protein in rice, BS1, has been identified as an acetyl-xylan deacetylase, which removes acetyl groups from the xylan backbone in the Golgi [24]. BS1 is the first reported polysaccharide deacetylase in the plant GDSL family, and the existence of BS1 together with a latterly identified deacetylase, DARX1 [25], demonstrates an antagonistic mechanism employing both acetyltransferase and deacetylase activities is needed in plants to properly adjust *O*-acetylation of cell wall polysaccharides. In this study, we biochemically characterized a TBL family member, TBL3, which not only possesses xylan acetyltransferase

activity, but also contains deacetylase activity. The enzymes involved in cell wall *O*-acetylation can play crucial roles in plant growth including pathogen resistance, freezing tolerance and cell wall architecture as revealed by the studies on mutants [13, 24, 45-47]. It has also been proposed that patterning of acetyl group on xylan backbones affects the interactions with cellulose microfibrils based on molecular dynamics simulation [48]. Since xylan *O*-acetylation is important to plants in many different aspects, the quantity as well as the distribution of acetyl moieties on xylans need to be finely adjusted through both acetylation and deacetylation. We thus propose that the xylan transacetylase, TBL3, characterized in this study could serve as a secondary mediator in the process that manipulates the fine structure of xylans through controlling degree of acetylation as well as distribution of acetyl groups after XOAT1 primarily transfers acetyl groups from acetyl-CoA or other acetyl donors to xylosyl residues. Different from the apoplast-resident pectin acetylesterases involved in polysaccharide modification *in muro* [26, 49, 50], the subcellular localization of TBL3 is in the Golgi apparatus [51], where non-cellulosic polysaccharides are synthesized [52], suggesting its involvement in mediating acetyl substitutions during xylan biosynthesis, which possibly aims to keep the solubility of xylans during intracellular transport prior to deposition in plant cell walls.

The biochemical evidence showing that TBL3 possesses the xylan transacetylase activity also brings up other intriguing questions related to the mechanism of xylan *O*-acetylation, such as what are the determinants for the catalytic promiscuity of TBL3? How do plants control the activity of TBL3 during cell wall development, and how it relates to the acetylation levels, substitution patterns, and physicochemical properties of cell wall polysaccharides? These questions remain to be answered by future research. The transacetylase activity of TBL3 identified in this study may provide insights into the mechanism of xylan *O*-acetylation during cell wall biosynthesis, which

may also be applied to enzyme engineering and manipulating cell wall acetylation in biomass for improving bioconversion into fuel and agricultural products.

Experimental Procedures

Expression and purification of fusion proteins

Fusion protein expression and purification was accomplished as described previously [53]. Briefly, total RNAs extracted from inflorescence stems of wild-type *A. thaliana* (Col-0) were used to generate cDNA using the RevertAid First Strand cDNA Synthesis Kit (Thermo Scientific). The sequences of the truncated coding-region of XOAT1 (aa57-486) and TBL3 (aa36-434) were then amplified from the cDNAs using the following primer pairs: XOAT1, 5'-AACTTGTACTTTCAAGGCTCAAAACCTCACGACGTC-3' and 5'-ACAAGAAAGCTGGGTCCTAACGGGAAATGATACGTGT-3'; TBL3, 5'-AACTTGTACTTTCAAGGCGAAAGAATCAGCTTGTTGTCT-3' and 5'-AC AAGAAAGCTGGGTCCTAGATTCCATGTATCGGGTAGT-3'. A second round of PCR was used to generate a tobacco etch virus (TEV) protease cleavage site and an attB recombination region by using the universal primer pairs: 5'- GGGGACAAGTTTGTACAAAAAAGCAGGCTC TGAAAACTTGTACTTTCAAGGC-3' and 5'-GGGGACC ACTTTGTACAAGAAAGCTGGG TC-3'. The PCR products were gel purified using AxyPrep™ DNA Gel Extraction Kit (Corning), subcloned into Gateway pDONR221 vector (Life Technologies) and recombined into a mammalian expression vector, pGEn2-DEST [54]. The expression plasmids were purified using the PureLink™ HiPure Plasmid Filter Maxiprep Kit (Life Technologies), and transformed into HEK cells (FreeStyle™ 293-F cell line, Life Technologies) as previously described [54].

Recombinant proteins secreted into the culture media by HEK293 cells were purified using HisTrap HP (Cytiva) column and ÄKTA protein purification system (Cytiva). SDS-PAGE following by Coomassie Brilliant Blue R-250 (Bio-Rad) staining was carried out to confirm the purity of the proteins. For the activity assays, proteins were dialyzed against HEPES sodium salt-HCl (75 mM, pH7.0) buffer supplemented with Chelex-100 resin (0.5 g/L, Bio-Rad) to remove any interfering metal ions. After dialysis, the proteins were concentrated using Amicon Ultra centrifugal filters (30 kDa molecular weight cut-off, EMD Millipore), and quantified by the Pierce™ BCA Protein Assay Kit (Thermo Scientific). The resulting fusion proteins consist of the NH2-terminal signal peptides, 8×His-tags, AviTag recognition sites, Green fluorescent proteins, TEV protease recognition sites, and the catalytic domains of the corresponding enzymes.

Determination of acetyltransferase/transacetylase activity

To determine the acetyltransferase activity of TBL3, standard assays (15 μL) were performed using acetylsalicylic acid (0.5 mM), acetyl-CoA (0.5 mM) or pNPA (0.5 mM) as donors, and 2-aminobenzamide (2AB)-labeled xylohexaose (Xyl_6-2AB) (0.1 mM) as an acceptor substrate in HEPES sodium salt-HCl (75 mM, pH7.0) and were initiated by the addition of purified protein (4 μM). The procedure of 2AB-labeling of Xyl_6 is according to Cumpstey et al. The reactions were incubated at room temperature for 2h, and the products were then analyzed by matrix assisted laser desorption ionization-time of flight mass spectrometry (MALDI-TOF MS) as described in detail below. For co-incubation experiments of TBL3 with XOAT1, *p*NPA (0.5 mM) and Xyl_6-2AB (0.1 mM) were used as the donor and acceptor substrates, respectively, with a final concentration of each protein at 4 μM in the same conditions described above. Reactions were incubated for 4h and then the reaction products were analyzed by MALDI-TOF MS. Acetylated

Xyl_6-2AB (Ac-Xyl6-2AB) oligosaccharides were enzymatically synthesized by reacting XOAT1 (4 μM) with acetylsalicylic acid (0.5 μM) as a donor substrate and Xyl_6-2AB (0.1 mM) as an acceptor for 4h. Solutions (15 μL) of enzymatically acetylated Xyl_6-2AB were treated with TBL3 (4 μM) or an equal volume of HEPES sodium salt-HCl (75 mM, pH7.0) as a control, incubated for 1 hr, and the products analyzed by MALDI-TOF MS.

Two-step experiments were carried out to further investigate potential transacetylase activity. Acetylated Xyl_6 (Ac-Xyl_6) oligosaccharides were synthesized *in vitro* in reactions (15 μL) containing xylohexaose (Xyl_6, 1 mM), acetylsalicylic acid (4 mM) and purified XOAT1 (4 μM) in HEPES sodium salt-HCl (75 mM, pH7.0) at room temperature overnight for use as donors in subsequent reactions. XOAT1 was inactivated by by heating samples at 85°C for 15 min. The resulting Ac-Xyl_6 oligosaccharides (0.1 mM) were used as donor substrates in a reaction (15 μL) containing Xyl_6-2AB (0.1 mM) and purified TBL3 (4 μM) in HEPES sodium salt-HCl (75 mM, pH7.0). After 2h incubation at room temperature, the products were analyzed by MALDI-TOF MS. Samples without proteins were set up as negative controls. On the other hand, to test if the naturally acetylated xylo-oligosaccharides (Ac-XOS) can be used as the donor for TBL3, Ac-XOS were prepared from ball-milled and endo-1,4-β-xylanase M1 (Megazyme, Cat. No. E-XYTR1)-digested alcohol-insoluble residue (AIR) from poplar stem tissues, and after purification by using Superdex™ 75 Increase 10/300 GL column (Sigma-Aldrich, Cat. No. GE29-1487-21), 1.5 μL of the obtained AcXOS was added into the second reaction as described above and followed by the same analytic procedure.

MALDI-TOF MS analysis of acetylated products

Aliquots (5 µL) of reactions product were mixed with Dowex-50 cation exchanger resin (1 µL suspension in water), and the mixture was incubated at room temperature for 30 min. After centrifugation, the supernatant was directly mixed with matrix solution (20 mg/mL 2,5-dihydroxybenzoic (DHB) acid in 50% MeOH) at a ratio of 1:1, and dried directly on the ground steel MALDI target plate. The samples were then analyzed by MALDI-TOF MS using a Bruker microflex™ LT/SH spectrometer. Each positive ion spectrum was generated by 200 laser shots.

NMR analysis of (de)acetylated products

1D ^{1}H NMR spectroscopy was used for the structural analysis of the acetylated Xyl_6 synthesized in vitro. To analyze the regiospecificity of TBL3, reactions were performed by incubating pNPA (4 mM) and Xyl_6 (200 µg) with TBL3 (5 µM) in 100 mM potassium phosphate buffer (pH 6.7) prepared in D_2O (99.9%; Cambridge Isotope Laboratories) for 17h (200 µL total volume). DMSO (0.005% v/v) was included in reactions as an internal standard. Data acquisition started 10 min after the reaction was initiated. Data was recorded at 298 K using an Agilent-NMR spectrometer equipped with a 5-mm NMR cold probe operating at 600 MHz. Each 1D ^{1}H spectrum consists of 16 transients, and was acquired with water presaturation every 30 min for 17h. A positive control was set up by substituting TBL3 with XOAT1 in reactions described above. The amount of acetylated xylosyl residues generated during the course of the reactions were quantified by integrating the resonance peaks corresponding to the methyl protons (δ ^{1}H 2.721) of the DMSO (0.005% v/v). Data processing was done using MestReNova software (Mestrelab Research S.L., Universidad de Santiago de Compostela, Spain).

To examine the regiospecificity of TBL3 as an esterase, Ac-Xyl_6 oligosaccharides were synthesized in vitro in reactions containing XOAT1 (10 μM), unlabeled Xyl_6 (400 μg), and acetylsalicylic acid (4 mM) in potassium phosphate buffer (100 mM, pH 6.7) prepared in D_2O (99.9%; Cambridge Isotope Laboratories) for 2h (400 μL total volume). XOAT1 was removed via diafiltration through a 3 kDa spin filter (Amicon, Merck Millipore) as described previously (add Lunin et al., 2020). Ac-Xyl_6 oligosaccharides were then reacted with TBL3 (5 μM), or an equivalent amount of phosphate buffer, and extensively incubated for another 20h, and the progress of the reaction was monitored by real-time NMR as described above. 1D ^1H spectra consisting of 16 transients were acquired with water presaturation every 20 min over a 20-h period at 298 K with an Agilent-NMR spectrometer operating at 600 MHz and equipped with a 5 mm NMR cold probe. DMSO (0.005% (v/v)) was added to all reactions as an internal standard for determination of chemical shifts and for quantification of acetylated xylosyl residues.

Phylogenetic tree construction

Phylogenetic tree of TBL/DUF231 proteins were generated by Geneious Prime® 2019.2.3. Global alignment with free end gaps was used to align amino acid sequences following by calculation of similarity scores using Blosum62 matrix. UPGMA (Unweighted Pair Group Method using Arithmetic averages) clustering algorithm and Jukes-Cantor genetic distance model were used for building the trees.

References

1. Samanta AK, Jayapal N, Jayaram C, Roy S, Kolte AP, Senani S, Sridhar M: Xylooligosaccharides as prebiotics from agricultural by-products: Production and applications. Bioactive Carbohydrates and Dietary Fibre 2015, 5(1):62-71.
2. Mussatto SI, Mancilha IM: Non-digestible oligosaccharides: A review. Carbohydrate Polymers 2007, 68(3):587-597.
3. Liao N, Luo B, Gao J, Li X, Zhao Z, Zhang Y, Ni Y, Tian F: Oligosaccharides as co-encapsulating agents: effect on oral Lactobacillus fermentum survival in a simulated gastrointestinal tract. Biotechnol Lett 2019, 41(2):263-272.
4. Martins M, Silva KCG, Ávila PF, Sato ACK, Goldbeck R: Xylo-oligosaccharide microparticles with synbiotic potential obtained from enzymatic hydrolysis of sugarcane straw. Food Research International 2021, 140:109827.
5. Vázquez MJ, Alonso JL, Domínguez H, Parajó JC: Xylooligosaccharides: manufacture and applications. Trends in Food Science & Technology 2000, 11(11):387-393.
6. Amorim C, Silvério SC, Prather KLJ, Rodrigues LR: From lignocellulosic residues to market: Production and commercial potential of xylooligosaccharides. Biotechnology Advances 2019, 37(7):107397.
7. York WS, O'Neill MA: Biochemical control of xylan biosynthesis - which end is up? Curr Opin Plant Biol 2008, 11(3):258-265.
8. Aspinall GO: Chemistry of cell wall polysaccharides. The Biochemistry of Plants 1980, 3:473-500.

9. Teleman A, Tenkanen M, Jacobs A, Dahlman O: Characterization of O-acetyl-(4-O-methylglucurono)xylan isolated from birch and beech. Carbohydrate Research 2002, 337(4):373-377.

10. Lopes L, Andrade CT, Milas M, Rinaudo M: Role of conformation and acetylation of xanthan on xanthan-guar interaction. Carbohydrate Polymers 1992, 17(2):121-126.

11. Kabel MA, van den Borne H, Vincken J-P, Voragen AGJ, Schols HA: Structural differences of xylans affect their interaction with cellulose. Carbohydrate Polymers 2007, 69(1):94-105.

12. Mora F, Ruel K, Comtat J, Joseleau J-P: Aspect of Native and Redeposited Xylans at the Surface of Cellulose Microfibrils. In: Holzforschung - International Journal of the Biology, Chemistry, Physics and Technology of Wood. vol. 40; 1986: 85.

13. Manabe Y, Nafisi M, Verhertbruggen Y, Orfila C, Gille S, Rautengarten C, Cherk C, Marcus SE, Somerville S, Pauly M et al: Loss-of-Function Mutation of REDUCED WALL ACETYLATION2 in Arabidopsis Leads to Reduced Cell Wall Acetylation and Increased Resistance to Botrytis cinerea. Plant Physiology 2011, 155(3):1068-1078.

14. Zhong R, Cui D, Ye ZH: Xyloglucan O-acetyltransferases from Arabidopsis thaliana and Populus trichocarpa catalyze acetylation of fucosylated galactose residues on xyloglucan side chains. Planta 2018, 248(5):1159-1171.

15. Schultink A, Naylor D, Dama M, Pauly M: The role of the plant-specific ALTERED XYLOGLUCAN9 protein in Arabidopsis cell wall polysaccharide O-acetylation. Plant Physiol 2015, 167(4):1271-1283.

16. Bischoff V, Nita S, Neumetzler L, Schindelasch D, Urbain A, Eshed R, Persson S, Delmer D, Scheible W-R: TRICHOME BIREFRINGENCE and Its Homolog AT5G01360 Encode

Plant-Specific DUF231 Proteins Required for Cellulose Biosynthesis in Arabidopsis. Plant Physiology 2010, 153(2):590-602.

17. Akoh CC, Lee G-C, Liaw Y-C, Huang T-H, Shaw J-F: GDSL family of serine esterases/lipases. Progress in Lipid Research 2004, 43(6):534-552.

18. Lunin VV, Wang H-T, Bharadwaj VS, Alahuhta M, Peña MJ, Yang J-Y, Archer-Hartmann SA, Azadi P, Himmel ME, Moremen KW et al: Molecular Mechanism of Polysaccharide Acetylation by the Arabidopsis Xylan O-acetyltransferase XOAT1. The Plant cell 2020, 32(7):2367-2382.

19. Zhong R, Cui D, Ye ZH: Regiospecific Acetylation of Xylan is Mediated by a Group of DUF231-Containing O-Acetyltransferases. Plant & cell physiology 2017, 58(12):2126-2138.

20. Yuan Y, Teng Q, Zhong R, Haghighat M, Richardson EA, Ye Z-H: Mutations of Arabidopsis TBL32 and TBL33 Affect Xylan Acetylation and Secondary Wall Deposition. PLOS ONE 2016, 11(1):e0146460.

21. Yuan Y, Teng Q, Zhong R, Ye Z-H: TBL3 and TBL31, two Arabidopsis DUF231 domain proteins, are required for 3-O-monoacetylation of xylan. Plant and Cell Physiology 2015, 57(1):35-45.

22. Yuan Y, Teng Q, Zhong R, Ye ZH: Roles of Arabidopsis TBL34 and TBL35 in xylan acetylation and plant growth. Plant Sci 2016, 243:120-130.

23. Urbanowicz BR, Peña MJ, Moniz HA, Moremen KW, York WS: Two Arabidopsis proteins synthesize acetylated xylan in vitro. Plant J 2014, 80(2):197-206.

24. Zhang B, Zhang L, Li F, Zhang D, Liu X, Wang H, Xu Z, Chu C, Zhou Y: Control of secondary cell wall patterning involves xylan deacetylation by a GDSL esterase. Nat Plants 2017, 3:17017.

25. Zhang L, Gao C, Mentink-Vigier F, Tang L, Zhang D, Wang S, Cao S, Xu Z, Liu X, Wang T et al: Arabinosyl Deacetylase Modulates the Arabinoxylan Acetylation Profile and Secondary Wall Formation. The Plant cell 2019, 31(5):1113-1126.

26. Gou JY, Miller LM, Hou G, Yu XH, Chen XY, Liu CJ: Acetylesterase-mediated deacetylation of pectin impairs cell elongation, pollen germination, and plant reproduction. Plant Cell 2012, 24(1):50-65.

27. Le Gall H, Philippe F, Domon J-M, Gillet F, Pelloux J, Rayon C: Cell Wall Metabolism in Response to Abiotic Stress. Plants 2015, 4(1):112-166.

28. Tenhaken R: Cell wall remodeling under abiotic stress. Frontiers in Plant Science 2015, 5(771).

29. Seale M: Cell Wall Remodeling during Wood Development. Plant Physiology 2020, 182(4):1800-1801.

30. Coutinho FS, Rodrigues JM, Lima LL, Mesquita RO, Carpinetti PA, Machado JPB, Vital CE, Vidigal PM, Ramos MES, Maximiano MR et al: Remodeling of the cell wall as a drought-tolerance mechanism of a soybean genotype revealed by global gene expression analysis. aBIOTECH 2021.

31. Sénéchal F, Wattier C, Rustérucci C, Pelloux J: Homogalacturonan-modifying enzymes: structure, expression, and roles in plants. J Exp Bot 2014, 65(18):5125-5160.

32. Zhong R, Cui D, Ye ZH: A group of Populus trichocarpa DUF231 proteins exhibit differential O-acetyltransferase activities toward xylan. PLoS One 2018, 13(4):e0194532.

33. Zhong R, Cui D, Dasher RL, Ye ZH: Biochemical characterization of rice xylan O-acetyltransferases. Planta 2018, 247:1489-1498.

34. Pauly M, Scheller HV: O-Acetylation of plant cell wall polysaccharides: identification and partial characterization of a rhamnogalacturonan O-acetyl-transferase from potato suspension-cultured cells. Planta 2000, 210:659-667.

35. Zhong R, Cui D, Richardson EA, Phillips DR, Azadi P, Lu G, Ye ZH: Cytosolic Acetyl-CoA Generated by ATP-Citrate Lyase Is Essential for Acetylation of Cell Wall Polysaccharides. Plant & cell physiology 2020, 61(1):64-75.

36. Reicher F, Corrêa JBC, Gorin PAJ: Location of O-acetyl groups in the acidic d-xylan of mimosa scabrella (bracatinga). A study of O-acetyl group migration. Carbohydrate research 1984, 135(1):129-140.

37. Lassfolk R, Rahkila J, Johansson MP, Ekholm FS, Warna J, Leino R: Acetyl Group Migration across the Saccharide Units in Oligomannoside Model Compound. Journal of the American Chemical Society 2019, 141(4):1646-1654.

38. Brecker L, Mahut M, Schwarz A, Nidetzky B: In situ proton NMR study of acetyl and formyl group migration in mono-O-acyl D-glucose. Magn Reson Chem 2009, 47(4):328-332.

39. Gille S, Pauly M: O-acetylation of plant cell wall polysaccharides. Front Plant Sci 2012, 3:12.

40. Vandamme-Feldhaus V, Schauer R: Characterization of the Enzymatic 7-O-Acetylation of Sialic Acids and Evidence for Enzymatic O-Acetyl Migration from C-7 to C-9 in Bovine Submandibular Gland. The Journal of Biochemistry 1998, 124(1):111-121.

41. Laaberki MH, Pfeffer J, Clarke AJ, Dworkin J: O-Acetylation of peptidoglycan is required for proper cell separation and S-layer anchoring in Bacillus anthracis. The Journal of biological chemistry 2011, 286(7):5278-5288.

42. Zhong R, Cui D, Ye Z-H: Regiospecific acetylation of xylan is mediated by a group of DUF231-containing O-acetyltransferases. Plant and Cell Physiology 2017, 58(12):2126-2138.

43. Kikuta Y, Ueda H, Takahashi M, Mitsumori T, Yamada G, Sakamori K, Takeda K, Furutani S, Nakayama K, Katsuda Y et al: Identification and characterization of a GDSL lipase-like protein that catalyzes the ester-forming reaction for pyrethrin biosynthesis in Tanacetum cinerariifolium- a new target for plant protection. The Plant journal : for cell and molecular biology 2012, 71(2):183-193.

44. Clauss K, Baumert A, Nimtz M, Milkowski C, Strack D: Role of a GDSL lipase-like protein as sinapine esterase in Brassicaceae. The Plant journal : for cell and molecular biology 2008, 53(5):802-813.

45. Xin Z, Mandaokar A, Chen J, Last RL, Browse J: Arabidopsis ESK1 encodes a novel regulator of freezing tolerance. The Plant journal : for cell and molecular biology 2007, 49(5):786-799.

46. Lefebvre V, Fortabat MN, Ducamp A, North HM, Maia-Grondard A, Trouverie J, Boursiac Y, Mouille G, Durand-Tardif M: ESKIMO1 disruption in Arabidopsis alters vascular tissue and impairs water transport. PLoS One 2011, 6(2):e16645.

47. Diener AC, Ausubel FM: RESISTANCE TO FUSARIUM OXYSPORUM 1, a dominant Arabidopsis disease-resistance gene, is not race specific. Genetics 2005, 171(1):305-321.

48. Busse-Wicher M, Gomes TC, Tryfona T, Nikolovski N, Stott K, Grantham NJ, Bolam DN, Skaf MS, Dupree P: The pattern of xylan acetylation suggests xylan may interact with cellulose microfibrils as a twofold helical screw in the secondary plant cell wall of Arabidopsis thaliana. Plant J 2014, 79(3):492-506.

49. M B, R G, JC H, JC P: A novel protein from mung bean hypocotyl cell walls with acetyl esterase activity. Phytochemistry 1995, 38(2):315-319.

50. Souza Ad, Hull PA, Gille S, Pauly M: Identification and functional characterization of the distinct plant pectin esterases PAE8 and PAE9 and their deletion mutants. Planta 2014, 240:1123-1138.

51. Yuan Y, Teng Q, Zhong R, Ye ZH: TBL3 and TBL31, Two Arabidopsis DUF231 Domain Proteins, are Required for 3-O-Monoacetylation of Xylan. Plant & cell physiology 2016, 57(1):35-45.

52. Scheller HV, Ulvskov P: Hemicelluloses. Annu Rev Plant Biol 2010, 61:263-289.

53. Urbanowicz BR, Peña MJ, Moniz HA, Moremen KW, York WS: Two Arabidopsis proteins synthesize acetylated xylan in vitro. The Plant Journal 2014, 80(2):197-206.

54. Meng L, Forouhar F, Thieker D, Gao Z, Ramiah A, Moniz H, Xiang Y, Seetharaman J, Milaninia S, Su M et al: Enzymatic basis for N-glycan sialylation: structure of rat alpha2,6-sialyltransferase (ST6GAL1) reveals conserved and unique features for glycan sialylation. J Biol Chem 2013, 288(48):34680-34698.

Table 4.1 Percent identities of the conserved region containing TBL and DUF231 domains between xylan-specific TBLs

	XOAT1	TBL3	TBL28	TBL30	TBL31	TBL32	TBL33	TBL34	TBL35
XOAT1		47.59%	80.61%	58.38%	46.09%	49.58%	47.47%	43.80%	44.38%
TBL3	47.59%		45.38%	41.85%	47.86%	47.31%	47.14%	39.33%	42.49%
TBL28	80.61%	45.38%		57.69%	46.96%	48.21%	47.22%	46.72%	44.85%
TBL30	58.38%	41.85%	57.69%		44.11%	41.00%	41.50%	40.76%	39.00%
TBL31	46.09%	47.86%	46.96%	44.11%		43.94%	45.20%	44.35%	44.35%
TBL32	49.58%	47.31%	48.21%	41.00%	43.94%		72.11%	44.57%	48.31%
TBL33	47.47%	47.14%	47.22%	41.50%	45.20%	72.11%		46.09%	49.15%
TBL34	43.80%	39.33%	46.72%	40.76%	44.35%	44.57%	46.09%		49.86%
TBL35	44.38%	42.49%	44.85%	39.00%	44.35%	48.31%	49.15%	49.86%	

Figure 4.1

Phylogenetic analysis of Arabidopsis TBL/DUF231 proteins. (a) TBL protein sequences were used to construct the phylogenetic tree. Biochemically characterized substrate specificities of TBLs in different clades are colored and labeled aside each clade. XOAT1 and TBL3 in the xylan-specific subclade focused in this study are marked with red asterisks. (b) Phylogenetic tree of nine TBL members in the xylan-specific subclade labeled with their distinguished regio-specificities. Both phylogenetic trees were built with UPGMA (Unweighted Pair Group Method using Arithmetic averages) algorithm, and the 0.2 scale represents 20% differences between two sequences.

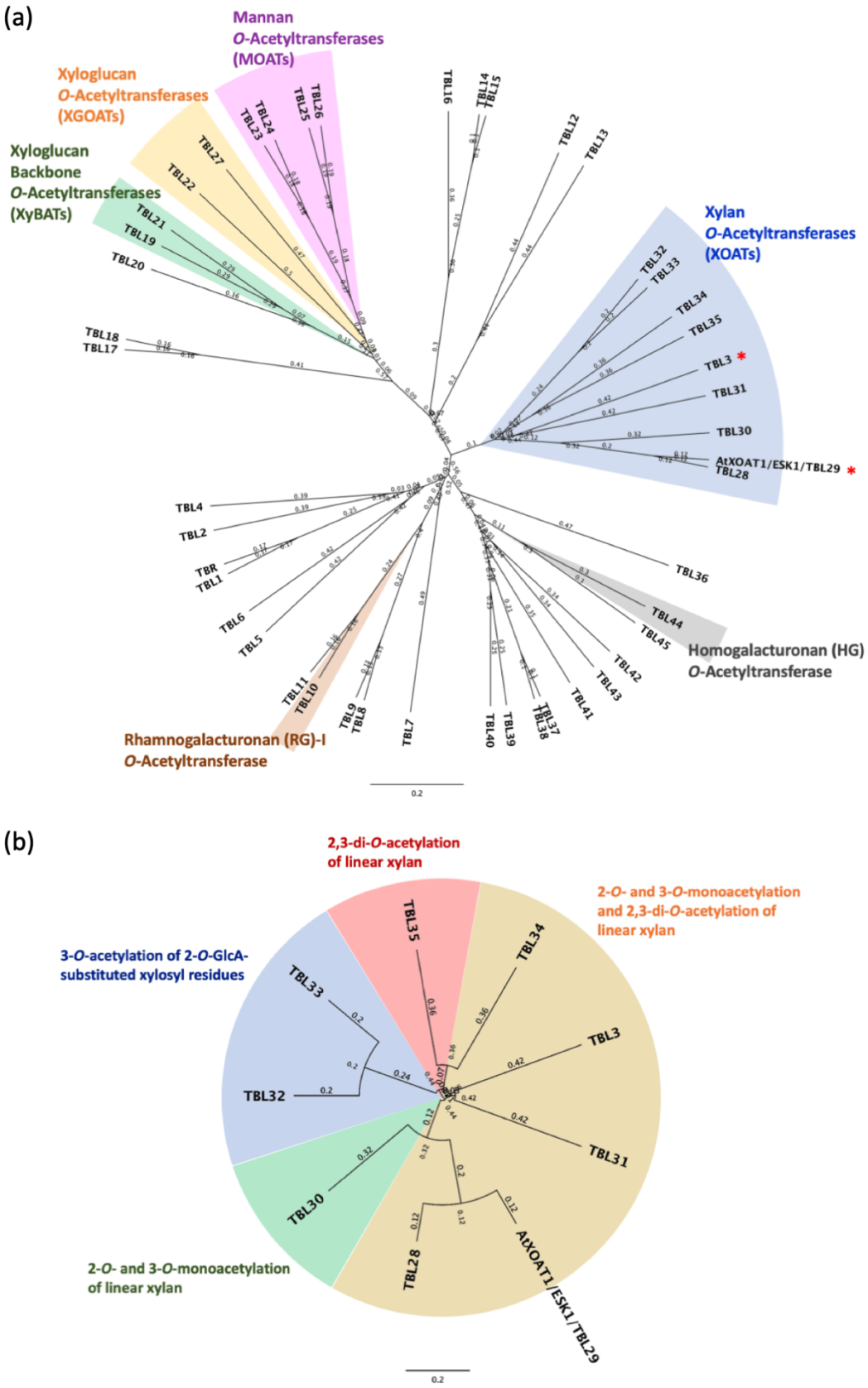
(a)
Mannan
O-Acetyltransferases
(MOATs)
Xyloglucan
O-Acetyltransferases
(XGOATs)
Xyloglucan
Backbone
O-Acetyltransferases
(XyBATs)
Xylan
O-Acetyltransferases
(XOATs)
Homogalacturonan (HG)
O-Acetyltransferase
Rhamnogalacturonan (RG)-I
O-Acetyltransferase
TBL16
TBL14
TBL15
TBL12
TBL13
TBL26
TBL25
TBL24
TBL23
TBL27
TBL22
TBL21
TBL19
TBL20
TBL18
TBL17
TBL32
TBL33
TBL34
TBL35
TBL3 *
TBL31
TBL30
AtXOAT1/ESK1/TBL29 *
TBL28
TBL4
TBL2
TBR
TBL1
TBL6
TBL5
TBL36
TBL44
TBL45
TBL42
TBL43
TBL41
TBL11
TBL10
TBL9
TBL8
TBL7
TBL40
TBL39
TBL37
TBL38
0.2
(b)
2,3-di-O-acetylation
of linear xylan
2-O- and 3-O-monoacetylation
and 2,3-di-O-acetylation of
linear xylan
3-O-acetylation of 2-O-GlcA-
substituted xylosyl residues
2-O- and 3-O-monoacetylation
of linear xylan
TBL35
TBL34
TBL33
TBL3
TBL32
TBL31
TBL30
TBL28
AtXOAT1/ESK1/TBL29
0.2

Figure 4.2

Sequence alignment of the xylan-specific TBLs in Arabidopsis. The name of each TBL protein is shown on the left. The number of the last amino acid residue is indicated in the end of each line for each protein. The transmembrane domain and variable region of XOAT1 are labeled by red and yellow bars, respectively. The catalytic TBL and DUF231 domains are indicated by bars in blue.

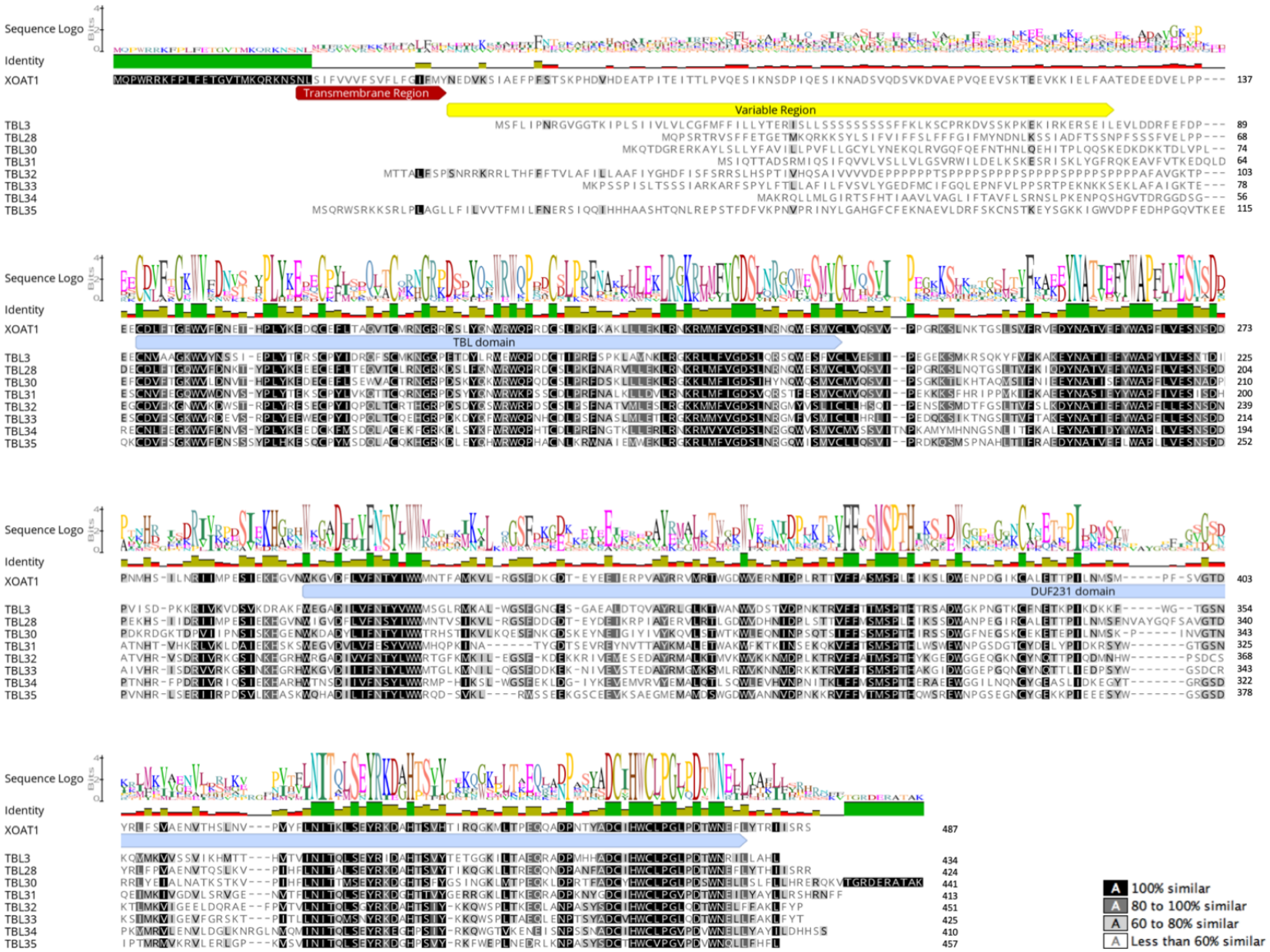
Sequence Logo
Identity
XOAT1
Transmembrane Region
Variable Region
TBL3
TBL28
TBL30
TBL31
TBL32
TBL33
TBL34
TBL35
TBL domain
DUF231 domain
A 100% similar
A 80 to 100% similar
A 60 to 80% similar
A Less than 60% similar

Figure 4.3

MALDI-TOF MS of the products after 2h reactions catalyzed by TBL3 and XOAT1 in the absence and presence of different acetyl-donor substrates: *p*NPA, acetylsalicylic acid, and acetyl-CoA. The annotated $[M + H]^+$ ions are the result of structures with a mass difference of 42 Da, consistent with the addition of one or more *O*-acetyl groups to Xyl_6-2AB acceptor substrate.

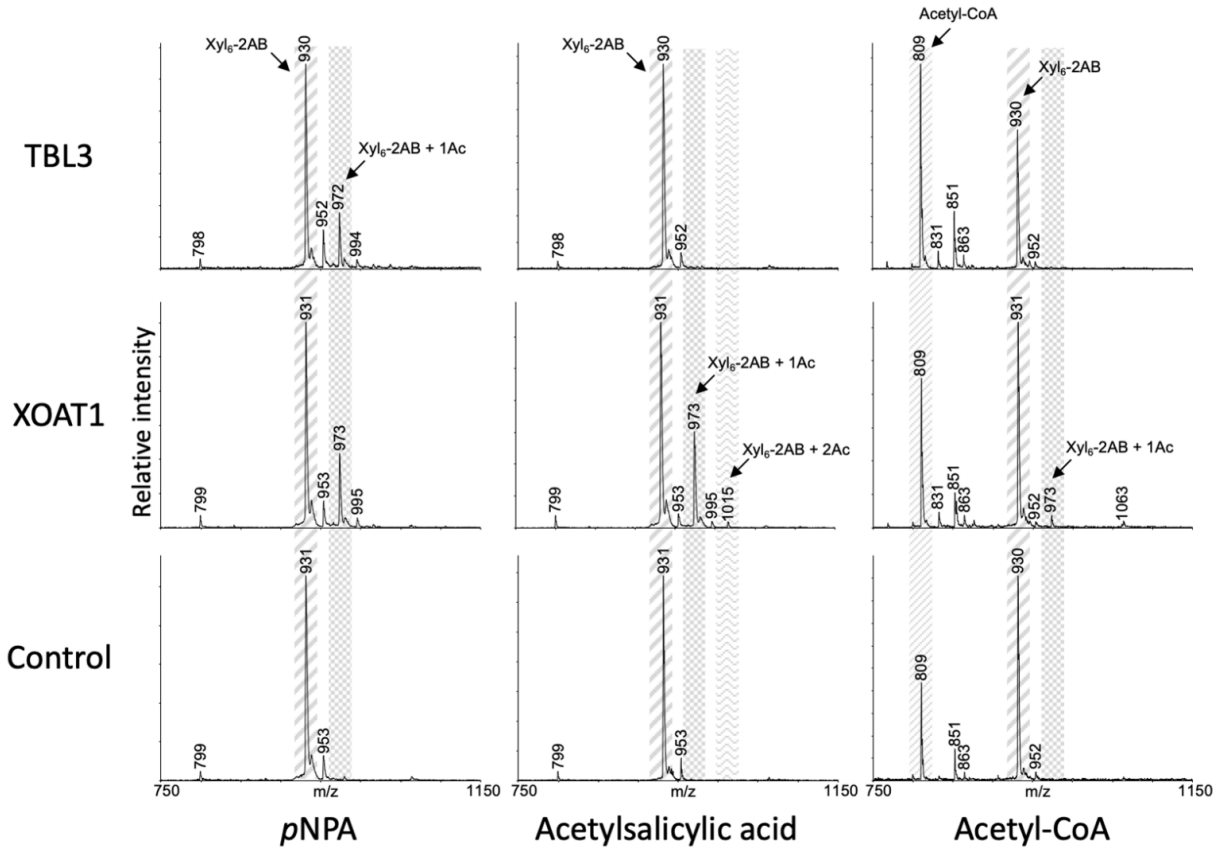
TBL3
XOAT1
Control
Relative intensity
Xyl6-2AB
Xyl6-2AB + 1Ac
Xyl6-2AB + 2Ac
Acetyl-CoA
m/z
750
1150
pNPA
Acetylsalicylic acid
Acetyl-CoA

Figure 4.4

Analysis of TBL3 deacetylase activity through *in vitro* assays. (a) MALDI-TOF-MS analysis of the products catalyzed by the action of TBL3 or XOAT1 alone, or co-incubation of TBL3 or XOAT1 in equimolar amounts using Xyl_6-2AB and *p*NPA as acceptor and donor substrates, respectively, for 4h. (b) Development of a two-step *in vitro* assay to evaluate the deacetylase activity of TBL3. MALDI-TOF MS spectrum of Ac-Xyl_6-2AB oligosaccharides synthesized *in vitro* by XOAT1 using acetylsalicylic acid as a donor is shown in the top panel, while the bottom panel shows the spectra of Ac-Xyl_6-2AB oligosaccharides after incubating with TBL3 (left) or buffer (right) for 1h at room temperature. The annotated [M + H]+ ions are the result of structures with a mass difference of 42 Da, consistent with the addition of one or more *O*-acetyl groups to Xyl_6-2AB acceptor substrate.

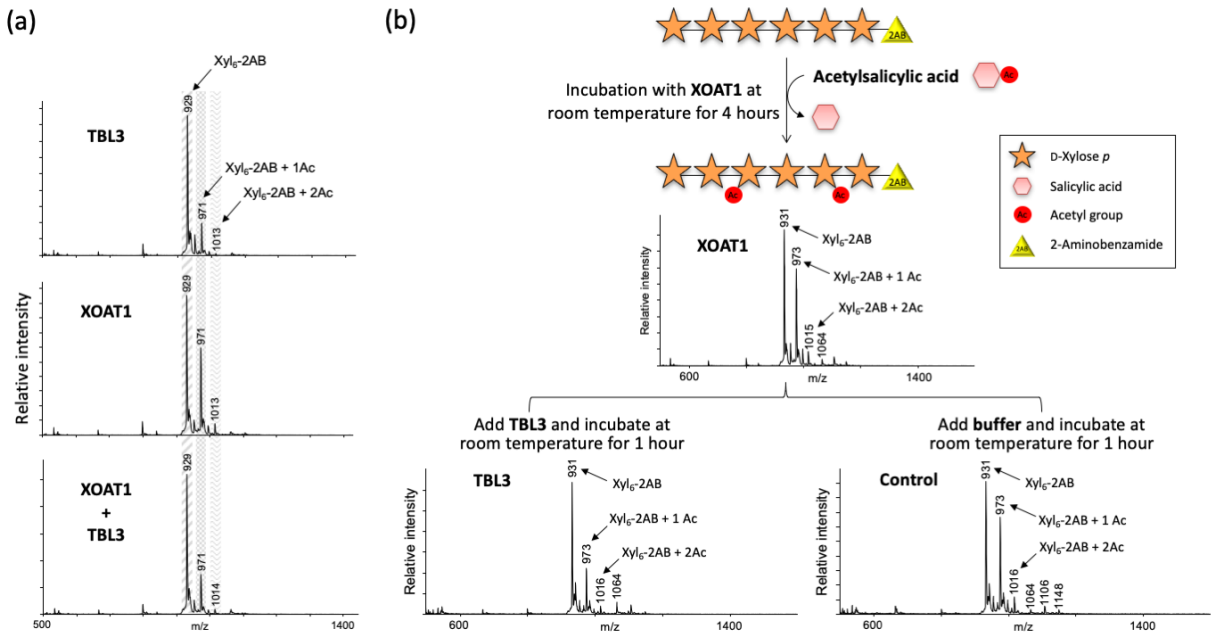
(a)
Xyl6-2AB
TBL3
Xyl6-2AB + 1Ac
Xyl6-2AB + 2Ac
929
971
1013
XOAT1
929
971
1013
XOAT1
+
TBL3
929
971
1014
Relative intensity
500
m/z
1400
(b)
2AB
Incubation with XOAT1 at
room temperature for 4 hours
Acetylsalicylic acid
Ac
D-Xylose p
Salicylic acid
Acetyl group
2-Aminobenzamide
XOAT1
931
973
1015
1064
Xyl6-2AB
Xyl6-2AB + 1 Ac
Xyl6-2AB + 2Ac
Relative intensity
600
m/z
1400
Add TBL3 and incubate at
room temperature for 1 hour
TBL3
931
973
1016
1064
Xyl6-2AB
Xyl6-2AB + 1 Ac
Xyl6-2AB + 2Ac
Relative intensity
600
m/z
1400
Add buffer and incubate at
room temperature for 1 hour
Control
931
973
1016
1064
1106
1148
Xyl6-2AB
Xyl6-2AB + 1 Ac
Xyl6-2AB + 2Ac
Relative intensity
600
m/z
1400

Figure 4.5

Development of a two-step *in vitro* assay to determine if TBL3 can function as a transacetylase (a) Diagram showing the experimental procedure of the two-step *in vitro* assay. (b) MALDI-TOF MS analysis of the Ac-Xyl_6 oligosaccharides synthesized *in vitro* by XOAT1 using acetylsalicylic acid as the donor and Xyl_6 as the acceptor. Reactions were allowed to proceed overnight at room temperature. (c,d) MALDI-TOF MS analysis of the acetylated Xyl_6-2AB products catalyzed by (c)TBL3 or (d) buffer after 2h in the presence of Ac-Xyl_6 and Xyl_6-2AB as the donor and acceptor, respectively. When unlabeled and 2AB-labeled xylo-oligomers are subjected to MALDI-TOF analysis (as in Panel c), ions from the 2AB-labeled oligomers dominate the spectrum, while ions corresponding to unlabeled oligomers are detected only at very low abundance.

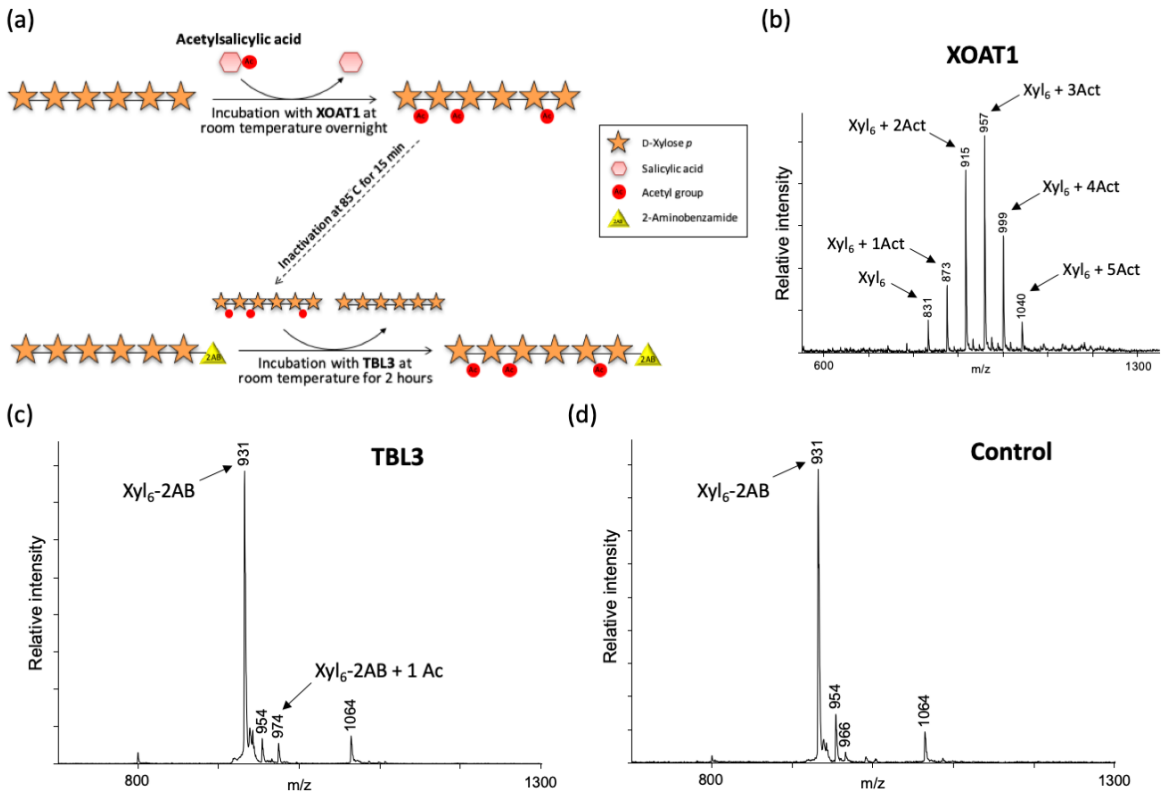
(a)
Acetylsalicylic acid
Incubation with XOAT1 at room temperature overnight
Inactivation at 85°C for 15 min
Incubation with TBL3 at room temperature for 2 hours
D-Xylose p
Salicylic acid
Acetyl group
2-Aminobenzamide
(b)
XOAT1
Xyl6 + 3Act
Xyl6 + 2Act
Xyl6 + 4Act
Xyl6 + 1Act
Xyl6
Xyl6 + 5Act
957
915
999
873
831
1040
Relative intensity
600
m/z
1300
(c)
TBL3
Xyl6-2AB
931
Xyl6-2AB + 1 Ac
954
974
1064
Relative intensity
800
m/z
1300
(d)
Control
Xyl6-2AB
931
954
966
1064
Relative intensity
800
m/z
1300

Figure 4.6

TBL3 catalyzes acetylation of Xyl_6-2AB by using acetylated xylo-oligosaccharides (Ac-XOS) extracted from poplar as the donor substrates. (a) Schematic procedure of the preparation of natural Ac-XOS from poplar stem tissue. A MALDI-TOF MS spectrum of the column-purified Ac-XOS is shown on the far right. (b) MALDI-TOF MS analysis of the Ac-Xyl_6-2AB catalyzed by TBL3 using Xyl_6-2AB as the acceptor, and poplar Ac-XOS (Panel a) as the donor substrates. 2AB-labeled oligosaccharides dominate the spectra in Panel b.

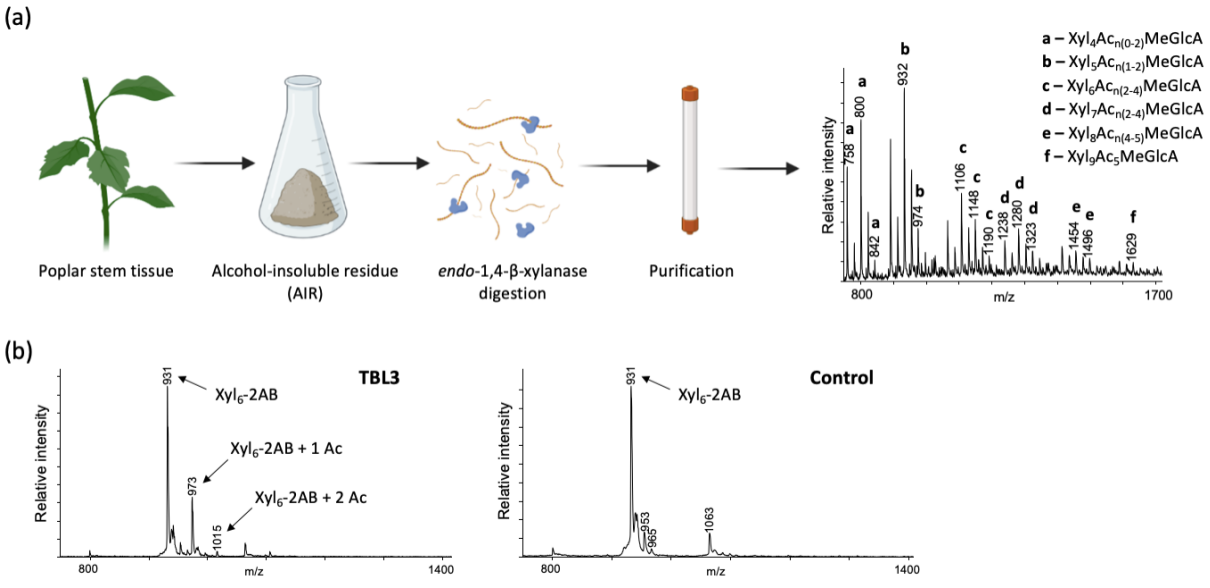
(a)
Poplar stem tissue
Alcohol-insoluble residue (AIR)
endo-1,4-β-xylanase digestion
Purification
Relative intensity
m/z
800
1700
a – Xyl4Acn(0-2)MeGlcA
b – Xyl5Acn(1-2)MeGlcA
c – Xyl6Acn(2-4)MeGlcA
d – Xyl7Acn(2-4)MeGlcA
e – Xyl8Acn(4-5)MeGlcA
f – Xyl9Ac5MeGlcA
(b)
TBL3
Control
Xyl6-2AB
Xyl6-2AB + 1 Ac
Xyl6-2AB + 2 Ac
Relative intensity
m/z
800
1400

Figure 4.7

Regiospecificity analysis of the xylan acetyltransferase activity of XOAT1 and TBL3. (a) Real-time 1D ^{1}H NMR spectra of TBL3 and XOAT1 reactions by using *p*NPA and Xyl_6 as the substrates and incubated for 17 h. The proton signals of the 2-*O* and 3-*O*-acetyl groups are indicated by the arrows. (b) Quantification of the 2-*O* and 3-*O*-acetylated xylosyl residues and the released acetates in the TBL3 and XOAT1 reaction.

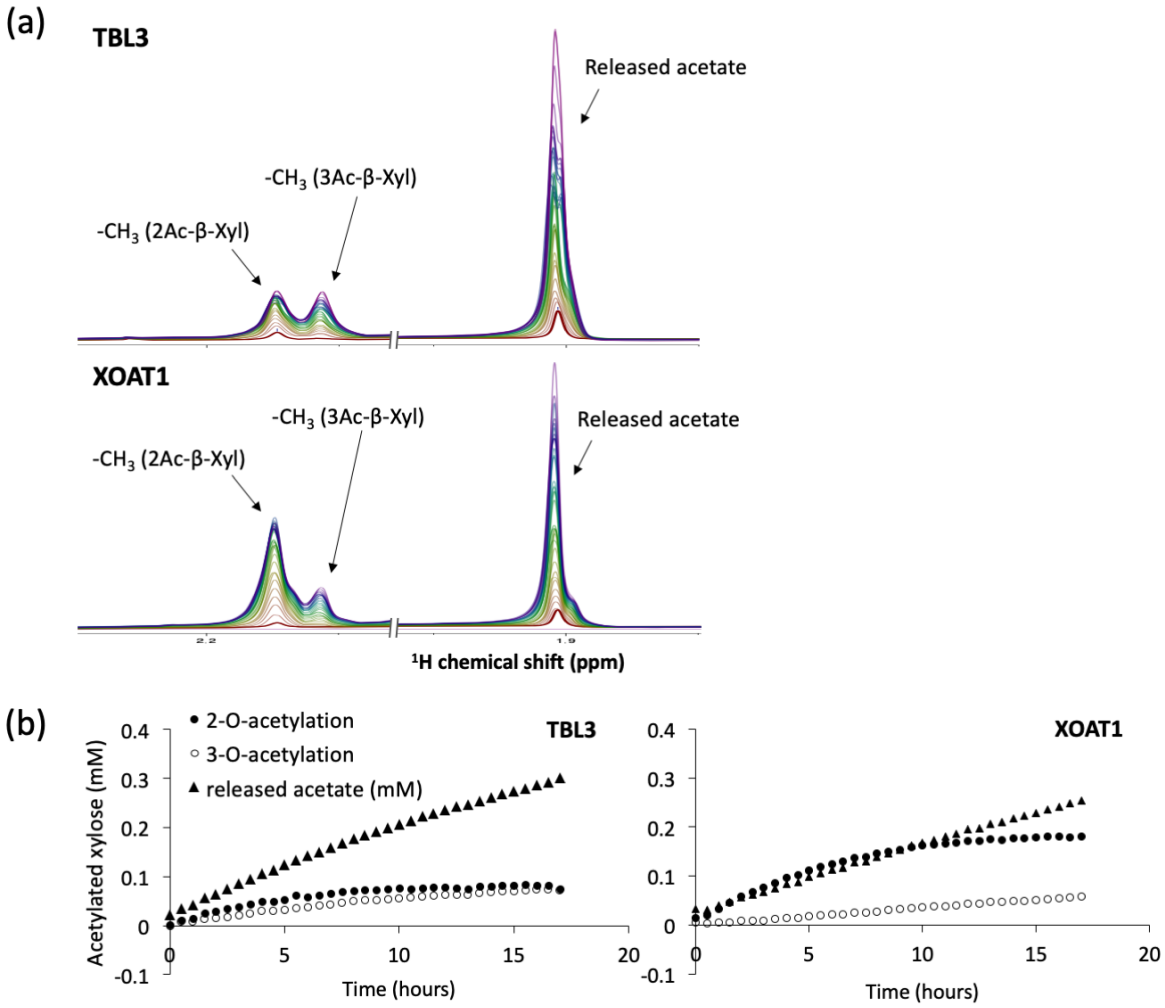
(a)
TBL3
Released acetate
-CH3 (3Ac-β-Xyl)
-CH3 (2Ac-β-Xyl)
XOAT1
-CH3 (3Ac-β-Xyl)
Released acetate
-CH3 (2Ac-β-Xyl)
2.2
1.9
¹H chemical shift (ppm)
(b)
2-O-acetylation
3-O-acetylation
released acetate (mM)
TBL3
XOAT1
Acetylated xylose (mM)
0.4
0.3
0.2
0.1
0
-0.1
0
5
10
15
20
Time (hours)

Figure 4.8

Regiospecificity analysis of the xylan deacetylase activity of TBL3 through a two-step experiment. Real-time 1D ^{1}H NMR spectra recorded every 10 min for 2 hours of xylan acetylation catalyzed by XOAT1 using acetylsalicylic acid and Xyl_6 as the substrates (a), and the resulting 2-*O*-acetylated Xyl_6 was then used as the substrate for the deacetylase assay catalyzed by TBL3. The 1D ^{1}H NMR spectra of the TBL3 reaction was recorded every 20 min during the 20-h reaction (b). The proton signals of the 2-*O* and 3-*O*-acetyl groups are indicated by the black arrows, and the dashed arrows (gray) are used to indicate the increase and decrease of 2-*O*-acetyl CH_3 signals in the XOAT1 and TBL3 reaction, respectively. (c) Quantification of changes in 2-*O* and 3-*O*-acetyl groups attached to xylosyl residues, released acetates, and acetylsalicylic acid in the TBL3 reaction and control. (d) Ratio of 3-*O* to 2-*O*-acetylated xylosyl residues in the 20-h reaction with and without TBL3.

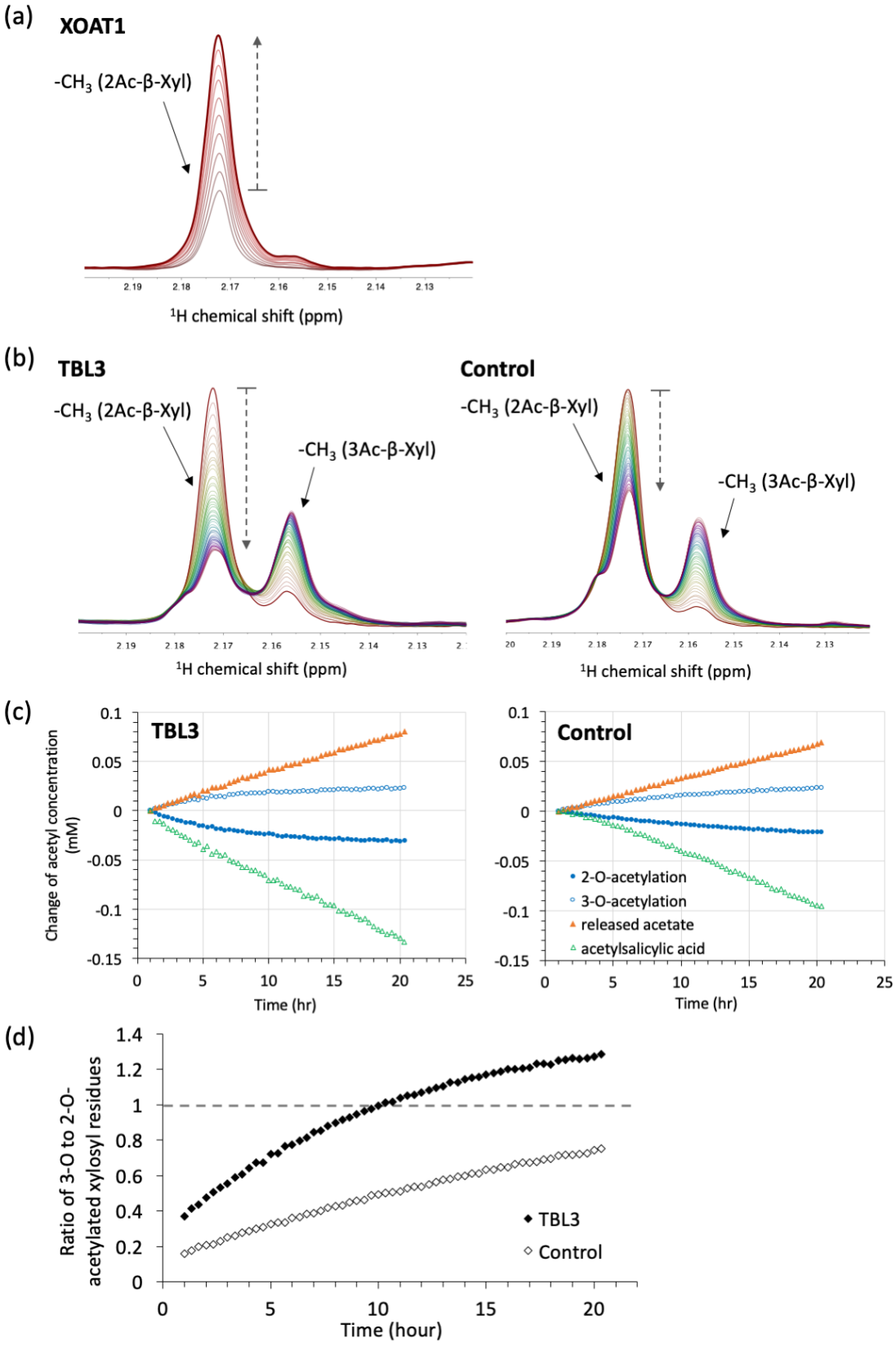
(a)
XOAT1
-CH3 (2Ac-β-Xyl)
2.19 2.18 2.17 2.16 2.15 2.14 2.13
1H chemical shift (ppm)
(b)
TBL3
-CH3 (2Ac-β-Xyl)
-CH3 (3Ac-β-Xyl)
1H chemical shift (ppm)
Control
-CH3 (2Ac-β-Xyl)
-CH3 (3Ac-β-Xyl)
1H chemical shift (ppm)
(c)
TBL3
Control
Change of acetyl concentration (mM)
0.1
0.05
0
-0.05
-0.1
-0.15
0 5 10 15 20 25
Time (hr)
2-O-acetylation
3-O-acetylation
released acetate
acetylsalicylic acid
(d)
Ratio of 3-O to 2-O-acetylated xylosyl residues
1.4
1.2
1
0.8
0.6
0.4
0.2
0
0 5 10 15 20
Time (hour)
TBL3
Control

Figure 4.9

Paths of xylan *O*-acetylation and deacetylation catalyzed by TBL3, and acetyl group migration and hydrolysis driven by non-enzymatic reactions (automigration and autohydrolysis, respectively) or potentially catalyzed by TBL3. The possible but unconfirmed pathways are labeled in gray and indicated by dashed arrows.

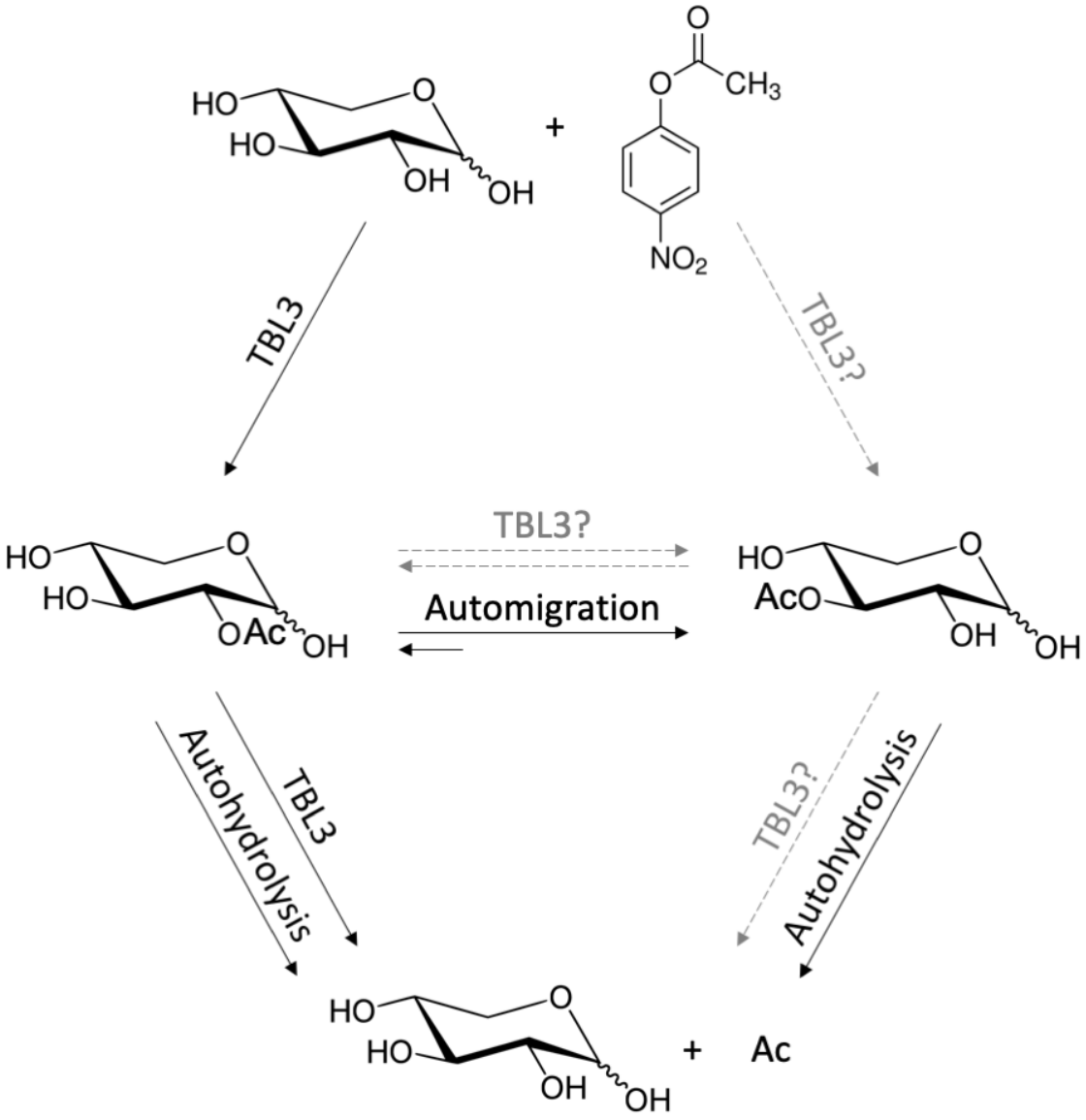
HO
HO
O
OH
OH
+
O
O
CH3
NO2
TBL3
TBL3?
HO
HO
O
OAc
OH
TBL3?
Automigration
HO
AcO
O
OH
OH
Autohydrolysis
TBL3
TBL3?
Autohydrolysis
HO
HO
O
OH
OH
+
Ac

CHAPTER 5

DISCUSSION AND CONCLUSIONS

The GDSL family of serine esterases/lipases is distinguished by a Gly-Asp-Ser-Leu sequence motif located close to the N-terminus of most members of the family, where the Ser serves as the nucleophile during catalysis. Members of the larger GDSL family are often promiscuous due to a flexible active site that changes conformation during substrate binding [127]. Members of the plant-specific TRICHOME BIREFRINGENCE-LIKE (TBL) family share the same catalytic triad with the GDSL proteins and have been shown to be widely involved in *O*-acetylation of polysaccharides [71, 74, 82, 83, 122, 188, 189]. In most species, all plant cell wall polysaccharides present in the cell wall are *O*-acetylated, with the exception of cellulose and mixed-linkage glucans. These modifications not only have a large impact on the physicochemical properties of cell wall polysaccharides [62], but also affect their interactions with other cell wall polymers [16, 17, 39, 63]. Thus, understanding the biochemical characteristics, structural information, and the catalytic mechanisms of TBL *O*-acetyltransferases could help us improve the utilization of lignocellulosic materials via manipulating their acetylation levels. In my research, two highly expressed TBL proteins, XOAT1 and TBL3, were studied. The work described herein details the structural characterization, biochemical analyses, a proposed mechanism, and the potential substrate binding mode for XOAT1. Additionally, a newly discovered transacetylase activity of TBL3 is identified, which is able to utilize *O*-acetylated xylooligosaccharides as acetyl-donor substrates.

Potential in vivo acetyl donors for TBLs

Among all the acetyl-donors that could be utilized by TBL proteins such as XOAT1, acetyl-CoA is considered to be the most likely candidate since it is involved in the process of acetylation and generation of many metabolites in plants, such as isoprenoids, phenolics, flavonoids, alkaloids, malonyl derivatives and fatty acids [190-194]. In addition, acetyl-CoA is used as a critical acetyl donor for lysine acetyl transferase (KAT) that carry out histone acetylation in plants and other organism as reported previously [195-197]. However, more evidence is required to establish whether acetyl-CoA is the direct acetyl-donor for TBL proteins *in vivo*. In plant cells, there are four subcellular compartments in which acetyl-CoA metabolism occurs: plastids, mitochondria, peroxisomes, and the cytosol. Further, each compartment contains distinct enzymes responsible for synthesizing acetyl-CoA [198, 199]. In the cytosol, ATP-citrate lyase (ACL) catalyzes ATP and CoA-dependent cleavage of citrate to form oxaloacetate and acetyl-CoA, which can further undergo carboxylation and condensation to form malonyl-CoA and acetoacetyl-CoA, respectively, as intermediates of a variety of metabolites [190, 200]. In Arabidopsis, ACL is present as a heterooctomer that is composed of two types of subunits, ACLA and ACLB, with an A_4B_4 configuration that is distinct from the homomeric ACLs in animals [199]. The genes encoding ACLA (*ACLA-1*, *ACLA-2*, and *ACLA-3*) and ACLB (*ACLB-1* and *ACLB-2*) are up-regulated during plant development, possibly due to higher physiological needs for acetyl-CoA in the cytosol [199, 201].

Recently, a study of the potential acetyl source for *O*-acetylation of cell wall polysaccharides in Arabidopsis revealed that the expression level of *ACL* genes increases in secondary wall-forming fiber cells compared to parenchyma cells. In addition, this upregulation was driven by secondary wall-associated transcription factors (TFs), including NAC (NAM,

ATAF, and CUC) and MYB, indicating a correlation between ACL expression and biosynthesis of secondary walls [202]. Further analysis of down-regulation of *ACL* genes through RNA interference (RNAi) in the same study indicates that the RNAi lines showed an overall reduction in cell wall acetylation by more than 50% in stems. Interestingly, these observed decreases were not specific to any particular class of cell wall polysaccharide, suggesting that ACLs may play a key role in cell wall polysaccharide acetylation [202]. To act as the initial supply of *O*-acetyl groups used by TBL proteins that catalyze *O*-acetylation of cell wall polysaccharides, acetyl-CoA must be transported from the cytosol into the Golgi apparatus. Since CoA derivatives are membrane-impermeable, enzymatic translocator/transporter machinery is required. This function has been predicted to be carried out by the Golgi-localized multi-transmembrane RWA proteins, as suggested in a previously reported hypothetical model[71, 72]. Indeed, analysis of Arabidopsis *rwa* mutants indicate acetylation of various cell wall polysaccharides is reduced in a nonspecific manner [66, 70], which further demonstrates its potential role in transporting acetyl groups across the Golgi membrane for downstream TBL-catalyzed *O*-acetylation of targeted polysaccharides.

To validate the role of RWAs in the cell wall acetylation pathway, Golgi-enriched membrane vesicles from an Arabidopsis *rwa1/2/3/4* quadruple mutant were isolated, and their acetyl-CoA-transporting activity was analyzed using radiolabeled [acetyl-1-^{14}C]-CoA [202]. In contrast to wild-type vesicles, those isolated from the *rwa1/2/3/4* mutant stems showed a 70% reduction of the transporting activity of acetyl-CoA, indicating an essential role of RWA in cell wall polysaccharide acetylation. It is worth noting that the ability to transport acetyl-CoA was not completely abolished in the *rwa1/2/3/4* mutant, and the overall degree of cell wall acetylation was reduced by 63% compared to wild-type control plants shown in a previous study [70]. Taken together, the data suggests that there could be other translocators and/or potential acetyl donors or

intermediates used *in vivo* by the promiscuous TBL proteins to *O*-acetylate specific cell wall polysaccharides.

Our deep dive into the xylan-specific function of TBL3 revealed a novel characteristic of the TBL protein family. Specifically, our biochemical analysis showed that TBL3 can utilize acetylated xylan as a donor substrate to catalyze *O*-acetylation of xylan. Observation of this apparent transacetylase activity provides additional insights into the process of cell wall polysaccharide *O*-acetylation. First, the degree and distribution of acetylation on xylan might be manipulated after primary acetyl transfer to the saccharide substrate occurs. This suggests that after acetyl groups are transferred from the acetyl donor to xylan, they can be either hydrolyzed or moved from the original site to a new position. Second, some members of the TBL family might, akin to TBL3, play roles that are distinct from the more well studied acetyltransferases, potentially functioning as secondary mediators responsible for patterning, or even proof reading the acetyl groups along saccharide backbones via transacetylation and/or hydrolysis reactions. Based on the esterase and transacetylase activities we observed in TBL3, we thus hypothesize that TBL3 might be a downstream player in the xylan acetylation pathway that plays a role in fine-tuning acetyl substitution (Figure 5.1).

Interestingly, the optimum pH of TBL3 (pH 6.5) is lower than that of XOAT1 (pH 6.8) according to our *in vitro* data (Figure 5.2), which might reflect an *in vivo* localization that is downstream in the Golgi apparatus (the luminal pH of the Golgi stacks closer to the *trans* face is 6.9, while the trans-Golgi network (TGN) is at pH 6.1; Figure 5.3) [35], where a secondary mediation of xylan *O*-acetylation could possibly take place. As the degree and distribution of acetyl groups on xylan are critical to cell wall polymer interactions and can affect the physical strength of cell walls, our hypothetical mechanism of xylan acetylation involving a primary and a secondary

mediation could meet the physiological needs in plants to fine-adjust this sophisticated cell wall modification.

The supportive role of computational modeling in improving enzyme engineering

In XOAT1 studies, we used computational methods to analyze the potential substrate binding mode of XOAT1. Docking the substrate, xylodecaose, at the catalytic pocket following by MD simulation provided information regarding the enzyme-substrate interaction. Based on the simulation results, we carried out site-directed mutagenesis (SDM) of the residues with the most negative contributions to the Gibbs free energy of binding (ΔG_b) present along XOAT1's acceptor substrate binding pocket, and evaluated the variants' acetyltransferase activities biochemically and kinetically. Notably, *in vitro* experiments indicated that the residues in the major lobe of XOAT1 are very important for binding the substrate xylohexaose (Figure 3.2a), which we used in our *in vitro* assays, while mutation of the minor lobe residues did not significantly interfere with the acetyltransferase activity of XOAT1. This result differs from the predictions based on the computational model and may be caused by different lengths of the acceptor substrates used in the two experiments. Xylohexaose is the longest, commercially available xylo-oligosaccharide that we were able to obtain for use in our *in vitro* assays; however, it is much shorter than the xylodecaose used in the *in silico* analyses, and possibly not long enough to reach the mutated sites on the minor lobe. Despite these disadvantages, the computational modeling still precisely predicted residues on the major lobe that were confirmed to be highly critical for binding the acceptor substrate. Although the K_M values for the xylohexaose acceptor of the minor lobe variants were not significantly different from those of the wild type enzyme, which indicates that substrate-binding affinity was not significantly disrupted, these mutant proteins displayed higher turnover

numbers (k_{cat}), resulting in improved enzymatic efficiencies (k_{cat}/K_M). Thus, this work shows that combined biochemical and computational studies can be used to provide targets for enzyme engineering, which could be potentially applied towards developing synthetic biology approaches to engineer plants with altered amounts of *O*-acetylation or patterning.

Enzyme engineering of GDSL family members has been widely applied in the food, beverage, cosmetic, pharmaceutical, biodiesel, chemical, and agricultural industries, with applications to lipases that are engineered to reduce manufacturing costs [203]. The properties obtained by enzyme engineering include enhanced catalytic efficiency, improved thermal or chemical stability, shifted or broadened substrate specificity, regioselectivity, and enantioselectivity [204]. In general, there are two major biotechnological strategies for a modified enzyme to acquire the properties mentioned above, directed evolution and rational design. Directed evolution involves cycles of random mutation and screening the resulting mutant library for variants with improved properties. In contrast, rational design is based on the knowledge and understanding of an enzyme's structure, function, and catalytic mechanism, and uses site-directed mutagenesis (SDM) to introduce amino-acid changes at sites predicted to cause the desired changes. In recent years, computational methods used to analyze inter- and intra-molecular interactions such as docking and MD simulations have been developed and helped us effectively predict the targets for modification. These potential targets can be localized at the catalytic sites, substrate-binding pockets, or flexible regions according to the enzyme engineering goals.

An example of rational design supported by computational modeling that targets a key residue in the binding pocket has been presented in a study of *Candida Antarctica* lipase A (CAL-A), which generates fatty acid esters that are useful in the biodiesel, cosmetic, and food industries [205]. The computational designed CAL-A mutant D122L, showed lower hydrolysis activity that

reduces the production of unwanted fatty acid by-products, while retaining the process-relevant acyltransferase activity and thermostability [205]. Another example of targeting binding pocket residues based on sequence alignment and 3D modeling to improve enzymatic activities has been reported in lipases/acyltransferases in *Candida* species [206]. In addition to enhancing enzyme activities, switching substrate specificity through mutating key residues in binding channels is an effective enzyme engineering strategy. Substituting small amino acids with the ones that contain bulky side chains inside the tunnel of *Candida rugose* lipase resulted in shifting the substrate preference from long chain fatty acids toward shorter chain lengths [207]. Our research on the substrate-binding mode of XOAT1 revealed the important residues involved in binding the xylo-oligosaccharides that were initially suggested by computational modeling and then confirmed by SDM and activity assays. The results indicate that three major lobe-localized amino acids, M311, N312 and D403, play crucial roles in binding the substrate, and could be potential targets for future acetyltransferase engineering. Furthermore, understanding the key, substrate-interacting residues inside the binding cleft of TBL proteins could help us unravel the critical factors that determine the diverse substrate specificities in the TBL family, which shares high similarity in protein sequences between family members.

In addition to focusing on modification of binding pockets, mobile lid regions located over the active site in proteins might also be targeted for mutagenesis to switch substrate specificities, to enhance enzyme activities, or to improve other desired properties. According to Yu et al. [208], substituting the hydrophobic lid in *Rhizopus chinensis* lipase with a hydrophilic lid, shifted the enzyme's specificity toward water-soluble substrates. On the other hand, the replacement of the same lid with a hydrophobic lid in *Rhizomucor miehei* lipase resulted in a 5.4-fold increased catalytic efficiency [208], suggesting that lid areas could be structural targets for efficient enzyme

engineering. The flexible minor lobe in XOAT1 somewhat resembles a lid-like structure which covers approximately half of the substrate-binding cleft. Our kinetic data showed that two variants where bulky residues were replaced with alanine in this region have elevated catalytic efficiencies, providing a future direction of modifying minor lobes as a potential strategy for improving efficiencies of TBL proteins.

In the context of computational methods for studying protein structure-function relationships, AlphaFold is a novel program that has recently garnered considerable attention. This program is used to predict three-dimensional structures of proteins using artificial intelligence (AI) with no need to use existing homologous structures as templates. AlphaFold was developed by DeepMind Technologies, which was acquired by Alphabet Inc. in 2014. The initial version of AlphaFold was evaluated in the Critical Assessment of Protein Structure Prediction (CASP13) competition [209], a worldwide biennial blind assessment for protein prediction held in 2018. The participating groups had to predict the structures of proteins that have been solved using experimental techniques such as X-ray crystallography, nuclear magnetic resonance (NMR), or cryo-electron microscopy (cryo-EM), but have not yet been released in public. To evaluate the accuracy of predictions, the Global Distance Test (GDT) scoring from 0-100 is used as the metric to measure the percentage of amino acids within a reasonable distance from the correct structure [210, 211]. The latest version of AlphaFold performed in CASP14 is based on a neural network system that uses evolutionarily related sequences, multiple sequence alignment (MSA), and representative pairs of amino acid residues to build the models, and has achieved a median score of 87.0 GDT in the category of free-modeling (FM), where no homologous structure is available. This result outperformed all the competitors and was considered to be competitive with the structural results obtained from the experimental techniques [212, 213]. It is worth mentioning that

in early 2020, the company group predicted the unknown protein structure of ORF3a in SARS-CoV-2 virus, which causes coronavirus disease 2019 (COVID-19) and resulted in an ongoing global pandemic. The prediction of ORF3a by AlphaFold turned out to achieve a high degree of accuracy compared to the experimentally solved structure through cryo-EM (PDB ID: 7kjr), which was reported later in June 2020 [214]. Thus AI technology could be applied in the field of drug design and vaccine development to improve human life, but most astonishingly, it might provide an answer to a basic scientific question that hasn't been solved for more than 50 years, that is, "How does protein sequence lead to protein structure and function?' [215].

Conclusions and future directions

To summarize, my research aims are to understand the process and mechanism of polysaccharide acetylation to not only gain insight that is relevant for xylan and other cell wall polysaccharides, but also to improve technologies for lowering the cost for generation of biomaterials and biofuels. The enzymes involved in polysaccharide *O*-acetylation in plants are TBL/DUF231 family members, which act on diverse polysaccharide substrates yet still share many highly conserved sequence motifs. We focus on two highly expressed Arabidopsis xylan *O*-acetyltransferases, XOAT1 and TBL3, and evaluate their biochemical properties through *in vitro* analysis, along with *in silico* studies for XOAT1. In my XOAT1 research, we first analyzed the enzyme's substrate specificity and found that it utilizes multiple acetyl donor substrates, which is a common feature shared by members in the larger GDSL protein family. Further, I investigated the regiospecificity of XOAT1 using real-time NMR spectroscopy to exclude the ambiguity caused by spontaneous (non-enzymatic) migration of acetyl groups, and confirmed the regio-selectivity of XOAT1 to be exclusively at the *O*-2 position of xylosyl residues in the acceptor. Additionally,

our crystallographic study revealed two unequal lobes in the structure of XOAT1 along with a Ser-His-Asp catalytic triad localized at the bottom of the cleft that is formed between them. Tandem mass spectroscopy analysis confirmed that a covalent acetyl-enzyme intermediate (Ac-Ser216) is formed during the reaction. Based on the combined biochemical and structural data, we proposed XOAT1 uses a Ping-Pong Bi-Bi mechanism that is to catalyze *O*-acetylation of xylan. Moreover, analysis of the XOAT1 variants generated by SDM indicated crucial residues involved in catalysis, including an unconventional Arg residue that forms the oxyanion hole to stabilize the negative charge of the tetrahedral intermediate formed during the reaction.

The crystal structure of XOAT1 has been the first protein structure solved in the TBL/DUF231 family, and can now be used as a template for future efforts to engineer XOAT1. In addition, it also represents a new template for structural predictions of other TBL protein family members and could thus expand our understanding of their conformations. In addition to analysis of XOAT1 from the perspective of catalysis, we also studied the substrate-binding mode through docking and MD simulation, and biochemically and kinetically analyzed the XOAT1 variants with mutated substrate-binding residues suggested by the computational modeling. The results indicate that the major lobe residues lining the binding pocket play critical roles in binding the substrates, while minor lobe variants intriguingly showed higher turnover rates and enzymatic efficiencies when using xylohexaose as the acceptor substrate. Both results could provide future directions for acetyltransferase engineering to improve bio-material processing and for understanding the key determinants of substrate specificity in the TBL/DUF231 family.

Finally, we examined another xylan acetyltransferase, TBL3, that is phylogenetically related to XOAT1 (40% identity between their protein sequences), through *in vitro* activity assays. The results showed that TBL3 not only possesses acetyltransferase activity, but also is able to

catalyze transacetylation - i.e., is able to transfer acetyl groups between xylo-oligosaccharides. Further evaluation of the regio-selectivity of TBL3 through NMR spectroscopy revealed an *O*-2-specific preference for xylosyl residues, both during acetyltransferase or esterase-type processes. This novel feature of TBL3 provides a new perspective of the process of cell wall polysaccharide *O*-acetylation, which could involve an enzymatic process for re-distribution or quantitative adjustment of the acetyl groups on polysaccharides after they have been initially transferred from non-carbohydrate acetyl donors. The xylan transacetylase activity revealed by the TBL3 study also suggested that TBL/DUF231 proteins may play an expanded set of roles in the *O*-acetylation process to fine-tune this sophisticated substitution on cell wall polysaccharides. Taken together, I hope the research presented herein will shed light on the process of *O*-acetylation in plant cell walls, and thus contribute to applications resulting in modified lignocellulosic biomass with improved properties for biomaterial and biofuel production.

Figure 5.1

Hypothetical mechanism of xylan *O*-acetylation mediated by XOAT1 and TBL3 in Golgi apparatus

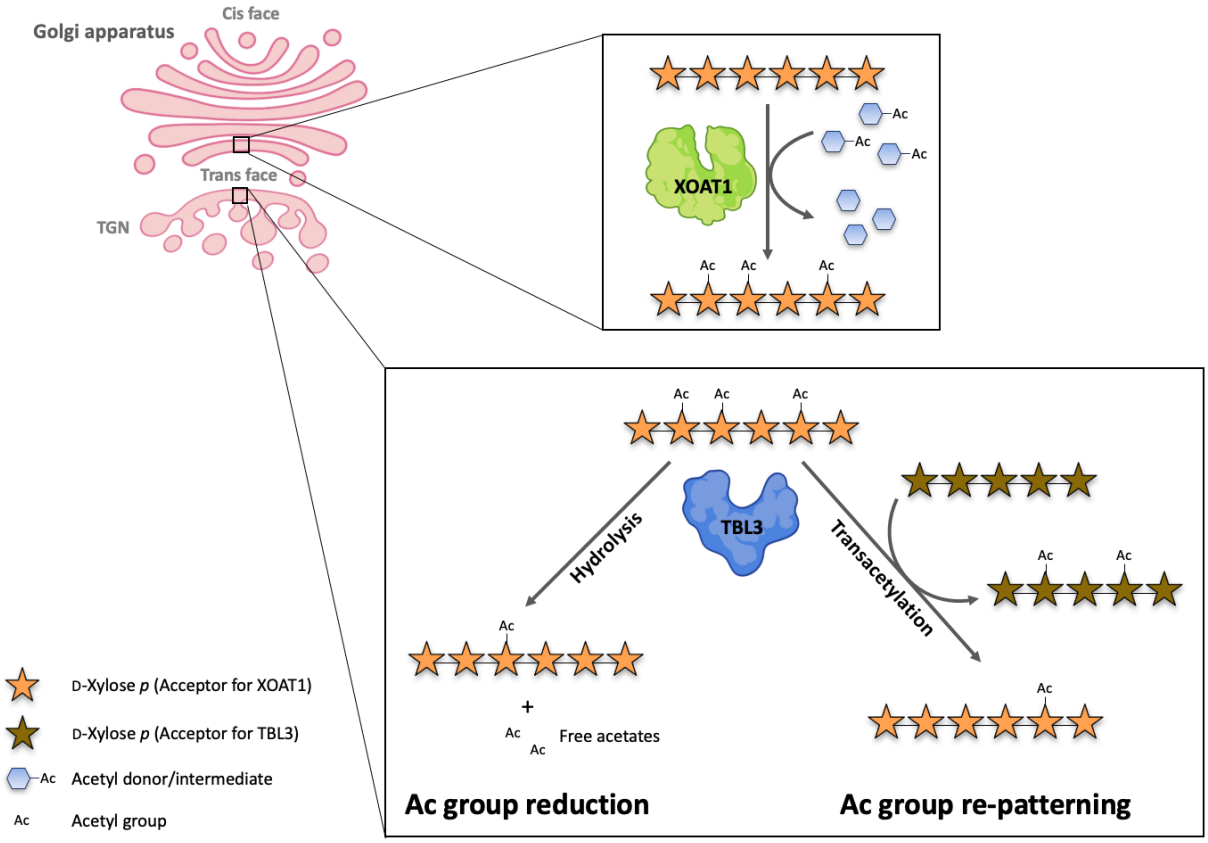
Golgi apparatus
Cis face
Trans face
TGN
XOAT1
Ac
Ac
Ac
Ac
Ac
Ac
Ac
Ac
Ac
TBL3
Hydrolysis
Transacetylation
Ac
Ac
Ac
Ac
Ac
Ac
Free acetates
Ac group reduction
Ac group re-patterning
D-Xylose p (Acceptor for XOAT1)
D-Xylose p (Acceptor for TBL3)
Ac
Acetyl donor/intermediate
Ac
Acetyl group

Figure 5.2

The optimum pH of TBL3 and XOAT1. MALDI-TOF MS spectra of acetylated Xyl_6-2AB produced by TBL3 and XOAT1 at different pH using *p*NPA as the donor substrate. An addition of one acetyl group increases the mass of Xyl_6-2AB by 42 Da as indicated by $[M+H]^+$ ions.

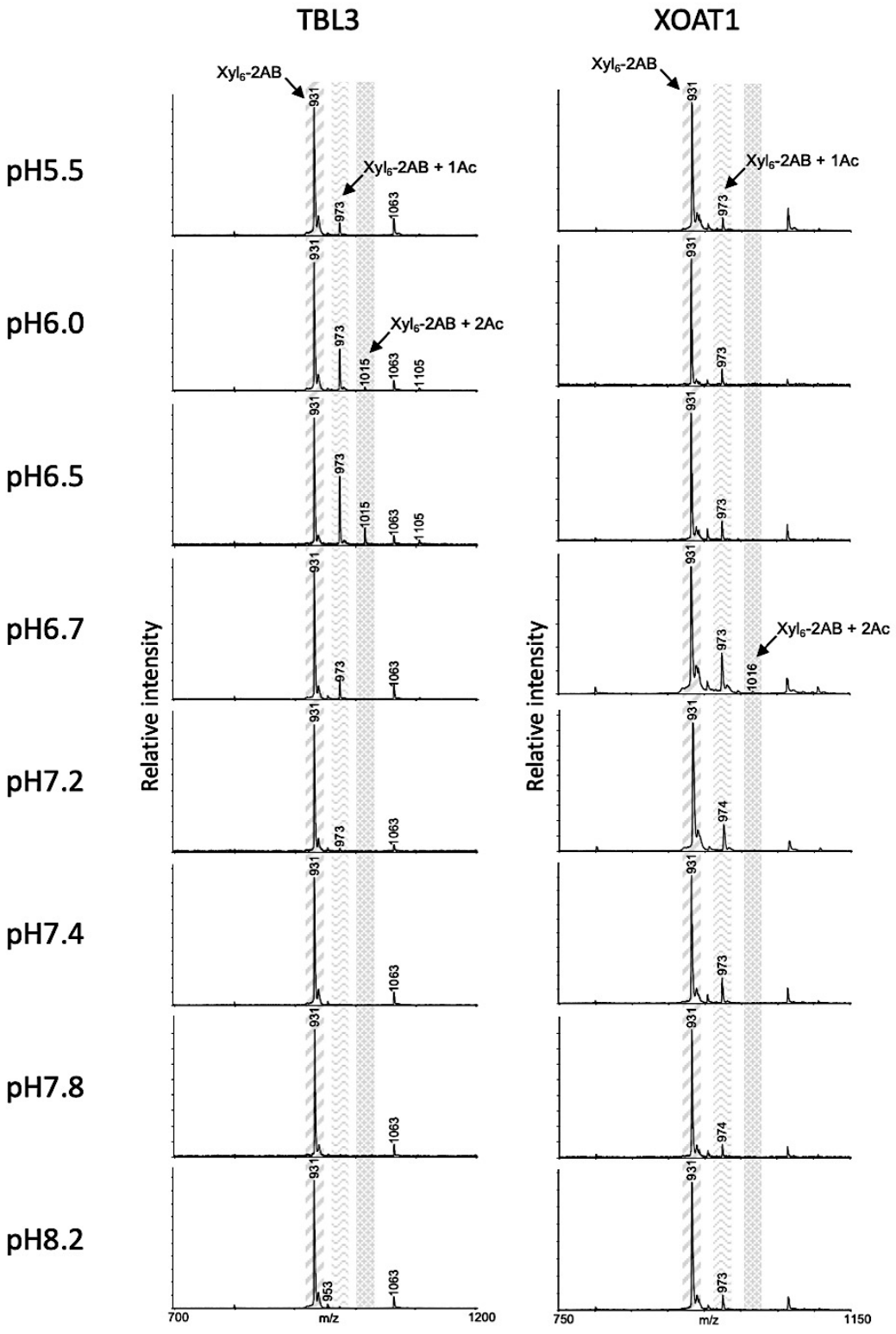
TBL3
XOAT1
pH5.5
pH6.0
pH6.5
pH6.7
pH7.2
pH7.4
pH7.8
pH8.2
Xyl6-2AB
Xyl6-2AB + 1Ac
Xyl6-2AB + 2Ac
Relative intensity
m/z
700
1200
750
1150

Figure 5.3

Intracellular compartments labeled with steady state pH in tobacco epidermal cells. ER, endoplasmic reticulum; LE, late endosome; LPVC, late prevacuolar compartment; PVC, prevacuolar compartment; TGN, trans-Golgi network. (Adopted from Martinière et al. [35])

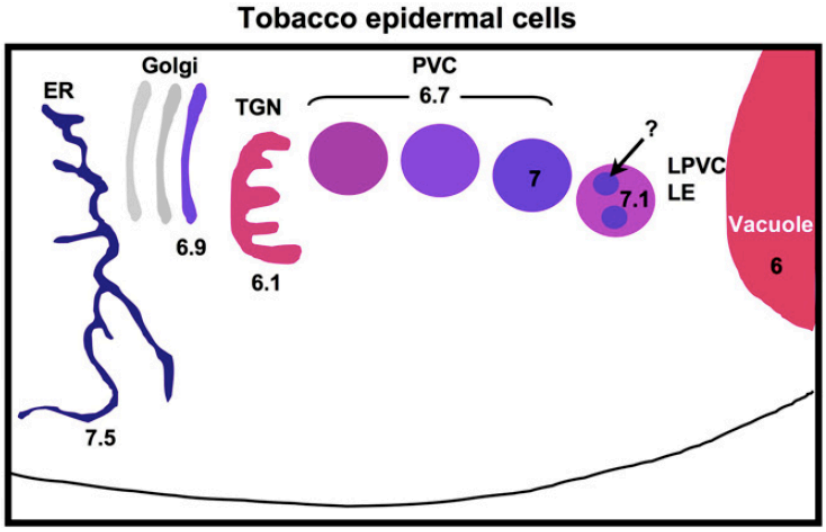
Tobacco epidermal cells
ER
Golgi
TGN
PVC
6.7
?
LPVC
LE
7
7.1
Vacuole
6
6.9
6.1
7.5

REFERENCES

1. Keegstra K: **Plant Cell Walls**. *Plant Physiology* 2010, **154**(2):483-486.
2. Harholt J, Suttangkakul A, Vibe Scheller H: **Biosynthesis of pectin**. *Plant Physiol* 2010, **153**(2):384-395.
3. O'Neill MA, York WS: **The Composition and Structure of Plant Primary Cell Walls**. In: *The Plant Cell Wall.* Edited by Rose JKC, vol. 8. Boca Raton, FL: CRC Press; 2003: 1-54.
4. Mohnen D: **Pectin structure and biosynthesis**. *Curr Opin Plant Biol* 2008, **11**(3):266-277.
5. Vogel J: **Unique aspects of the grass cell wall**. *Curr Opin Plant Biol* 2008, **11**(3):301-307.
6. Scheller HV, Ulvskov P: **Hemicelluloses**. *Annu Rev Plant Biol* 2010, **61**:263-289.
7. Somerville C, Youngs H, Taylor C, Davis SC, Long SP: **Feedstocks for lignocellulosic biofuels**. *Science* 2010, **329**(5993):790-792.
8. Smith PJ, Wang H-T, York WS, Peña MJ, Urbanowicz BR: **Designer biomass for next-generation biorefineries: leveraging recent insights into xylan structure and biosynthesis**. *Biotechnology for biofuels* 2017, **10**(1):286.
9. Chong S-L, Virkki L, Maaheimo H, Juvonen M, Derba-Maceluch M, Koutaniemi S, Roach M, Sundberg B, Tuomainen P, Mellerowicz EJ: **O-Acetylation of glucuronoxylan in Arabidopsis thaliana wild type and its change in xylan biosynthesis mutants**. *Glycobiology* 2014, **24**(6):494-506.

10. Evtuguin DV, Tomas JL, Silva AM, Neto CP: **Characterization of an acetylated heteroxylan from Eucalyptus globulus Labill**. *Carbohydrate research* 2003, **338**(7):597-604.

11. Goncalves VM, Evtuguin DV, Domingues MR: **Structural characterization of the acetylated heteroxylan from the natural hybrid Paulownia elongata/Paulownia fortunei**. *Carbohydrate research* 2008, **343**(2):256-266.

12. Teleman A, Lundqvist J, Tjerneld F, Stalbrand H, Dahlman O: **Characterization of acetylated 4-O-methylglucuronoxylan isolated from aspen employing 1H and 13C NMR spectroscopy**. *Carbohydrate research* 2000, **329**(4):807-815.

13. Teleman A, Tenkanen M, Jacobs A, Dahlman O: **Characterization of O-acetyl-(4-O-methylglucurono)xylan isolated from birch and beech**. *Carbohydrate research* 2002, **337**(4):373-377.

14. Ebringerova A, Heinze T: **Xylan and xylan derivatives– biopolymers with valuable properties, 1. Naturally occurring xylans structures, isolation procedures and properties**. *Macromol Rapid Commun* 2000, **21**(9):542-556.

15. Jacobs A, Dahlman O: **Characterization of the molar masses of hemicelluloses from wood and pulps employing size exclusion chromatography and matrix-assisted laser desorption ionization time-of-flight mass spectrometry**. *Biomacromolecules* 2001, **2**(3):894-905.

16. Grantham NJ, Wurman-Rodrich J, Terrett OM, Lyczakowski JJ, Stott K, Iuga D, Simmons TJ, Durand-Tardif M, Brown SP, Dupree R: **An even pattern of xylan substitution is critical for interaction with cellulose in plant cell walls**. *Nature plants* 2017, **3**(11):859.

17. Busse-Wicher M, Gomes TC, Tryfona T, Nikolovski N, Stott K, Grantham NJ, Bolam DN, Skaf MS, Dupree P: **The pattern of xylan acetylation suggests xylan may interact with cellulose microfibrils as a twofold helical screw in the secondary plant cell wall of Arabidopsis thaliana**. *The Plant journal : for cell and molecular biology* 2014, **79**(3):492-506.

18. Fischer E: **Wanderung von Acyl Bei Den Glyceriden**. *Ber Dtsch Chem Ges* 1920, **53**:1621-1633.

19. Lassfolk R, Rahkila J, Johansson MP, Ekholm FS, Warna J, Leino R: **Acetyl Group Migration across the Saccharide Units in Oligomannoside Model Compound**. *Journal of the American Chemical Society* 2019, **141**(4):1646-1654.

20. Roslund MU, Aitio O, Warna J, Maaheimo H, Murzin DY, Leino R: **Acyl group migration and cleavage in selectively protected beta-d-galactopyranosides as studied by NMR spectroscopy and kinetic calculations**. *Journal of the American Chemical Society* 2008, **130**(27):8769-8772.

21. Brecker L, Mahut M, Schwarz A, Nidetzky B: **In situ proton NMR study of acetyl and formyl group migration in mono-O-acyl D-glucose**. *Magn Reson Chem* 2009, **47**(4):328-332.

22. Yoshimoto K, Tsuda Y: **General Path of O-Acyl Migration in D-Glucose Derivatives : Acyl Migration of Methyl Mono-O-myristoyl-α- and β-D-Glucopyranosides and Mono-O-myristoyl-D-glucopyranoses**. *CHEMICAL & PHARMACEUTICAL BULLETIN* 1983, **31**(12):4324-4334.

23. Akira K, Taira T, Shinohara Y: **Direct detection of the internal acyl migration reactions of benzoic acid 1-O-acylglucuronide by 13C-labeling and nuclear magnetic**

resonance spectroscopy. *Journal of Pharmacological and Toxicological Methods* 1997, **37**(4):237-243.

24. Michalak L, La Rosa SL, Leivers S, Lindstad LJ, Røhr Å K, Lillelund Aachmann F, Westereng B: **A pair of esterases from a commensal gut bacterium remove acetylations from all positions on complex β-mannans**. *Proceedings of the National Academy of Sciences of the United States of America* 2020, **117**(13):7122-7130.

25. Mortensen RW, Sidelmann UG, Tjørnelund J, Hansen SH: **Stereospecific pH-dependent degradation kinetics of R- and S-naproxen-β-l-O-acyl-glucuronide**. *Chirality* 2002, **14**(4):305-312.

26. Smith PC, Hasegawa J, Langendijk PN, Benet LZ: **Stability of acyl glucuronides in blood, plasma, and urine: studies with zomepirac**. *Drug Metabolism and Disposition* 1985, **13**(1):110.

27. Reinhard B, Faillard H: **Regioselective aectylations of sialic acid α-ketosides**. *Liebigs Annalen der Chemie* 1994, **1994**(2):193-203.

28. Hyneck ML, Munafo A, Benet LZ: **Effect of pH on acyl migration and hydrolysis of tolmetin glucuronide**. *Drug Metabolism and Disposition* 1988, **16**(2):322.

29. Schulze O, Bruns S, Voss J, Adiwidjaja G: **The thio-Mitsunobu reaction of d-glucitol, d-mannitol, galactitol and 1-seleno-d-xylitol**. *Carbohydrate research* 2000, **329**(4):781-790.

30. Toshio Y, Ken-ichi S, Hironobu H, Juji Y: **Branched-chain Sugars. XXXVI. A New Synthesis of Methyl 4-O-Benzoyl-3-benzoylamino-2,3,6-trideoxy-3-C-methyl-α-L-xylo-hexopyranoside, a Derivative of the Branched-chain Amino Sugar of Antibiotic A35512B**. *Bulletin of the Chemical Society of Japan* 1984, **57**:2538-2542.

31. Yuan Y, Teng Q, Zhong R, Haghighat M, Richardson EA, Ye Z-H: **Mutations of Arabidopsis TBL32 and TBL33 Affect Xylan Acetylation and Secondary Wall Deposition**. *PLOS ONE* 2016, **11**(1):e0146460.

32. Yuan Y, Teng Q, Zhong R, Ye Z-H: **TBL3 and TBL31, two Arabidopsis DUF231 domain proteins, are required for 3-O-monoacetylation of xylan**. *Plant and Cell Physiology* 2015, **57**(1):35-45.

33. Yuan Y, Teng Q, Zhong R, Ye ZH: **Roles of Arabidopsis TBL34 and TBL35 in xylan acetylation and plant growth**. *Plant science : an international journal of experimental plant biology* 2016, **243**:120-130.

34. Yuan Y, Teng Q, Zhong R, Ye Z-H: **The Arabidopsis DUF231 Domain-Containing Protein ESK1 Mediates 2-O- and 3-O-Acetylation of Xylosyl Residues in Xylan**. *Plant and Cell Physiology* 2013, **54**(7):1186-1199.

35. Martinière A, Bassil E, Jublanc E, Alcon C, Reguera M, Sentenac H, Blumwald E, Paris N: **In Vivo Intracellular pH Measurements in Tobacco and Arabidopsis Reveal an Unexpected pH Gradient in the Endomembrane System**. *The Plant cell* 2013, **25**(10):4028-4043.

36. Reicher F, Corrêa JBC, Gorin PAJ: **Location of O-acetyl groups in the acidic d-xylan of mimosa scabrella (bracatinga). A study of O-acetyl group migration**. *Carbohydrate research* 1984, **135**(1):129-140.

37. Chen XY, Kim JY: **Callose synthesis in higher plants**. *Plant Signal Behav* 2009, **4**(6):489-492.

38. Simmons TJ, Mortimer JC, Bernardinelli OD, Poppler AC, Brown SP, deAzevedo ER, Dupree R, Dupree P: **Folding of xylan onto cellulose fibrils in plant cell walls revealed by solid-state NMR**. *Nat Commun* 2016, **7**:13902.

39. Kabel MA, van den Borne H, Vincken J-P, Voragen AGJ, Schols HA: **Structural differences of xylans affect their interaction with cellulose**. *Carbohydrate Polymers* 2007, **69**(1):94-105.

40. Gao Y, Lipton AS, Wittmer Y, Murray DT, Mortimer JC: **A grass-specific cellulose–xylan interaction dominates in sorghum secondary cell walls**. *Nat Commun* 2020, **11**(1):6081.

41. Minic Z, Rihouey C, Do CT, Lerouge P, Jouanin L: **Purification and Characterization of Enzymes Exhibiting b-D-Xylosidase Activities in Stem Tissues of Arabidopsis**. *Plant Physiology* 2004, **135**:867-878.

42. Derba-Maceluch M, Awano T, Takahashi J, Lucenius J, Ratke C, Kontro I, Busse-Wicher M, Kosik O, Tanaka R, Winzell A *et al*: **Suppression of xylan endotransglycosylase *PtxtXyn10A* affects cellulose microfibril angle in secondary wall in aspen wood**. *The New phytologist* 2015, **205**(2):666-681.

43. Ren Y, Hansen SF, Ebert B, Lau J, Scheller HV: **Site-Directed Mutagenesis of IRX9, IRX9L and IRX14 Proteins Involved in Xylan Biosynthesis: Glycosyltransferase Activity Is Not Required for IRX9 Function in Arabidopsis**. *PLoS One* 2014, **9**:e105014.

44. Wu A-M, Ho¨rnblad E, Voxeur A, Gerber L, Rihouey C, Lerouge P, Marchant A: **Analysis of the Arabidopsis IRX9/IRX9-L and IRX14/IRX14-L Pairs of**

Glycosyltransferase Genes Reveals Critical Contributions to Biosynthesis of the Hemicellulose Glucuronoxylan. *Plant Physiology* 2010, **153**:542-554.

45. Zeng W, Jiang N, Nadella R, Killen TL, Nadella V, Faik A: **A glucurono(arabino)xylan synthase complex from wheat contains members of the GT43, GT47, and GT75 families and functions cooperatively**. *Plant Physiol* 2010, **154**(1):78-97.

46. Zeng W, Lampugnani ER, Picard KL, Song L, Wu A-M, Farion IM, Zhao J, Ford K, Doblin MS, Bacic A: **Asparagus IRX9, IRX10, and IRX14A Are Components of an Active Xylan Backbone Synthase Complex that Forms in the Golgi Apparatus**. *Plant Physiology* 2016, **171**:93-109.

47. Jiang N, Wiemels RE, Soya A, Whitley R, Held M, Faik A: **Composition, assembly, and trafficking of a wheat xylan synthase complex**. *Plant Physiol* 2016, **170**(4):1999-2023.

48. Lee C, Zhong R, Ye Z-H: **Arabidopsis Family GT43 Members are Xylan Xylosyltransferases Required for the Elongation of the Xylan Backbone**. *Plant & cell physiology* 2012, **53**:135-143.

49. Mortimer JC, Faria-Blanc N, Yu X, Tryfona T, Sorieul M, Ng YZ, Zhang Z, Stott K, Anders N, Dupree P: **An unusual xylan in Arabidopsis primary cell walls is synthesised by GUX3, IRX9L, IRX10L and IRX14**. *The Plant Journal* 2015, **83**:413-426.

50. Peña MJ, Zhong R, Zhou GK, Richardson EA, O'Neill MA, Darvill AG, York WS, Ye ZH: **Arabidopsis irregular xylem8 and irregular xylem9: implications for the complexity of glucuronoxylan biosynthesis**. *The Plant cell* 2007, **19**(2):549-563.

51. Brown DM, Goubet F, Wong VW, Goodacre R, Stephens E, Dupree P, Turner SR: **Comparison of five xylan synthesis mutants reveals new insight into the mechanisms of xylan synthesis**. *The Plant journal : for cell and molecular biology* 2007, **52**(6):1154-1168.

52. Ratke C, Terebieniec BK, Winestrand S, Derba-Maceluch M, Grahn T, Schiffthaler B, Ulvcrona T, Özparpucu M, Rüggeberg M, Lundqvist SO *et al*: **Downregulating aspen xylan biosynthetic GT43 genes in developing wood stimulates growth via reprograming of the transcriptome**. *New Phytologist* 2018, **219**:230-245.

53. Konishi T, Takeda T, Miyazaki Y, Ohnishi-Kameyama M, Hayashi T, O'Neill MA, Ishii T: **A plant mutase that interconverts UDP-arabinofuranose and UDP-arabinopyranose**. *Glycobiology* 2007, **17**:345-354.

54. Anders N, Wilkinson MD, Lovegrove A, Freeman J, Tryfona T, Pellny TK, Weimar T, Mortimer JC, Stott K, Baker JM *et al*: **Glycosyl transferases in family 61 mediate arabinofuranosyl transfer onto xylan in grasses**. *Proceedings of the National Academy of Sciences of the United States of America* 2012, **109**(3):989-993.

55. Urbanowicz BR, Peña MJ, Moniz HA, Moremen KW, York WS: **Two Arabidopsis proteins synthesize acetylated xylan *in vitro***. *The Plant journal : for cell and molecular biology* 2014, **80**(2):197-206.

56. Zhong R, Peña MJ, Zhou GK, Nairn CJ, Wood-Jones A, Richardson EA, Morrison WH, 3rd, Darvill AG, York WS, Ye ZH: **Arabidopsis fragile fiber8, which encodes a putative glucuronyltransferase, is essential for normal secondary wall synthesis**. *The Plant cell* 2005, **17**(12):3390-3408.

57. Persson S, Caffall KH, Freshour G, Hilley MT, Bauer S, Poindexter P, Hahn MG, Mohnen D, Somerville C: **The Arabidopsis irregular xylem8 mutant is deficient in glucuronoxylan and homogalacturonan, which are essential for secondary cell wall integrity**. *The Plant cell* 2007, **19**(1):237-255.

58. Kreuger J, Kjellén L: **Heparan sulfate biosynthesis: regulation and variability**. *J Histochem Cytochem* 2012, **60**(12):898-907.

59. Bromley JR, Busse-Wicher M, Tryfona T, Mortimer JC, Zhang Z, Brown DM, Dupree P: **GUX1 and GUX2 glucuronyltransferases decorate distinct domains of glucuronoxylan with different substitution patterns**. *The Plant Journal* 2013, **74**(3):423-434.

60. Lee C, Teng Q, Zhong R, Ye Z-H: **Arabidopsis GUX Proteins Are Glucuronyltransferases Responsible for the Addition of Glucuronic Acid Side Chains onto Xylan**. *Plant and Cell Physiology* 2012, **53**(7):1204-1216.

61. Mortimer JC, Miles GP, Brown DM, Zhang Z, Segura MP, Weimar T, Yu X, Seffen KA, Stephens E, Turner SR *et al*: **Absence of branches from xylan in Arabidopsis gux mutants reveals potential for simplification of lignocellulosic biomass**. *Proceedings of the National Academy of Sciences* 2010, **107**(40):17409-17414.

62. Biely P: **Microbial carbohydrate esterases deacetylating plant polysaccharides**. *Biotechnology Advances* 2012, **30**(6):1575-1588.

63. Kang X, Kirui A, Widanage MCD, Mentink-Vigier F, Cosgrove DJ, Wang T: **Lignin-polysaccharide interactions in plant secondary cell walls revealed by solid-state NMR**. *Nat Commun* 2019, **10**(1):347.

64. Xin Z, Mandaokar A, Chen J, Last RL, Browse J: **Arabidopsis ESK1 encodes a novel regulator of freezing tolerance**. *The Plant journal : for cell and molecular biology* 2007, **49**(5):786-799.

65. Urbanowicz BR, Peña MJ, Moniz HA, Moremen KW, York WS: **Two Arabidopsis proteins synthesize acetylated xylan in vitro**. *The Plant Journal* 2014, **80**(2):197-206.

66. Manabe Y, Nafisi M, Verhertbruggen Y, Orfila C, Gille S, Rautengarten C, Cherk C, Marcus SE, Somerville S, Pauly M *et al*: **Loss-of-Function Mutation of REDUCED WALL ACETYLATION2 in Arabidopsis Leads to Reduced Cell Wall Acetylation and Increased Resistance to Botrytis cinerea**. *Plant Physiology* 2011, **155**(3):1068-1078.

67. Vogel JP, Raab TK, Somerville CR, Somerville SC: **Mutations in PMR5 result in powdery mildew resistance and altered cell wall composition**. *The Plant journal : for cell and molecular biology* 2004, **40**(6):968-978.

68. Diener AC, Ausubel FM: **RESISTANCE TO FUSARIUM OXYSPORUM 1, a dominant Arabidopsis disease-resistance gene, is not race specific**. *Genetics* 2005, **171**(1):305-321.

69. Olsson L, Hahn-Hägerdal B: **Fermentation of lignocellulosic hydrolysates for ethanol production**. *Enzyme and microbial technology* 1996, **18**(5):312-331.

70. Manabe Y, Verhertbruggen Y, Gille S, Harholt J, Chong SL, Pawar PM, Mellerowicz EJ, Tenkanen M, Cheng K, Pauly M *et al*: **Reduced Wall Acetylation proteins play vital and distinct roles in cell wall O-acetylation in Arabidopsis**. *Plant Physiol* 2013, **163**(3):1107-1117.

71. Pauly M, Ramírez V: **New Insights Into Wall Polysaccharide O-Acetylation**. *Frontiers in plant science* 2018, **9**.

72. Schultink A, Naylor D, Dama M, Pauly M: **The role of the plant-specific ALTERED XYLOGLUCAN9 protein in Arabidopsis cell wall polysaccharide O-acetylation**. *Plant Physiol* 2015, **167**(4):1271-1283.

73. Zhong R, Cui D, Ye Z-H: **Regiospecific Acetylation of Xylan is Mediated by a Group of DUF231-Containing O-Acetyltransferases**. *Plant and Cell Physiology* 2017, **58**(12):2126-2138.

74. Lunin VV, Wang H-T, Bharadwaj VS, Alahuhta M, Peña MJ, Yang J-Y, Archer-Hartmann SA, Azadi P, Himmel ME, Moremen KW *et al*: **Molecular Mechanism of Polysaccharide Acetylation by the Arabidopsis Xylan O-acetyltransferase XOAT1**. *The Plant cell* 2020, **32**(7):2367-2382.

75. Mastihubová M, Biely P: **Lipase-catalysed preparation of acetates of 4-nitrophenyl β-d-xylopyranoside and their use in kinetic studies of acetyl migration**. *Carbohydrate research* 2004, **339**(7):1353-1360.

76. Lefebvre V, Fortabat M-N, Ducamp A, North HM, Maia-Grondard A, Trouverie J, Boursiac Y, Mouille G, Durand-Tardif M: **ESKIMO1 disruption in Arabidopsis alters vascular tissue and impairs water transport**. *PLoS One* 2011, **6**(2):e16645.

77. Xiong G, Cheng K, Pauly M: **Xylan O-acetylation impacts xylem development and enzymatic recalcitrance as indicated by the Arabidopsis mutant tbl29**. *Molecular plant* 2013, **6**(4):1373-1375.

78. Z X, J B: **Eskimo1 mutants of Arabidopsis are constitutively freezing-tolerant**. *Proceedings of the National Academy of Sciences of the United States of America* 1998, **95**:7799-7804.

79. Bouchabke-Coussa O, Quashie M-L, Seoane-Redondo J, Fortabat M-N, Gery C, Yu A, Linderme D, Trouverie J, Granier F, Téoulé E *et al*: **ESKIMO1 is a key gene involved in water economy as well as cold acclimation and salt tolerance**. *Bmc Plant Biol* 2008, **8**(1):125.

80. Bischoff V, Nita S, Neumetzler L, Schindelasch D, Urbain A, Eshed R, Persson S, Delmer D, Scheible W-R: **TRICHOME BIREFRINGENCE and Its Homolog AT5G01360 Encode Plant-Specific DUF231 Proteins Required for Cellulose Biosynthesis in Arabidopsis**. *Plant Physiology* 2010, **153**(2):590-602.

81. Yuan Y, Teng Q, Zhong R, Ye ZH: **TBL3 and TBL31, Two Arabidopsis DUF231 Domain Proteins, are Required for 3-O-Monoacetylation of Xylan**. *Plant & cell physiology* 2016, **57**(1):35-45.

82. Zhong R, Cui D, Ye ZH: **Regiospecific Acetylation of Xylan is Mediated by a Group of DUF231-Containing O-Acetyltransferases**. *Plant & cell physiology* 2017, **58**(12):2126-2138.

83. Zhong R, Cui D, Ye ZH: **A group of Populus trichocarpa DUF231 proteins exhibit differential O-acetyltransferase activities toward xylan**. *PLoS One* 2018, **13**(4):e0194532.

84. Zhong R, Cui D, Dasher RL, Ye ZH: **Biochemical characterization of rice xylan O-acetyltransferases**. *Planta* 2018, **247**:1489-1498.

85. Janbon G, Himmelreich U, Moyrand F, Improvisi L, Dromer F: **Cas1p is a membrane protein necessary for the O-acetylation of the Cryptococcus neoformans capsular polysaccharide**. *Molecular microbiology* 2001, **42**(2):453-467.

86. Arming S, Wipfler D, Mayr J, Merling A, Vilas U, Schauer R, Schwartz-Albiez R, Vlasak R: **The human Cas1 protein: a sialic acid-specific O-acetyltransferase?** *Glycobiology* 2011, **21**(5):553-564.

87. Baumann AM, Bakkers MJ, Buettner FF, Hartmann M, Grove M, Langereis MA, de Groot RJ, Mühlenhoff M: **9-O-Acetylation of sialic acids is catalysed by CASD1 via a covalent acetyl-enzyme intermediate**. *Nat Commun* 2015, **6**:7673.

88. Sychantha D, Jones CS, Little DJ, Moynihan PJ, Robinson H, Galley NF, Roper DI, Dowson CG, Howell PL, Clarke AJ: **In vitro characterization of the antivirulence target of Gram-positive pathogens, peptidoglycan O-acetyltransferase A (OatA)**. *PLoS Pathog* 2017, **13**(10):e1006667.

89. Bera A, Herbert S, Jakob A, Vollmer W, Götz F: **Why are pathogenic staphylococci so lysozyme resistant? The peptidoglycan O-acetyltransferase OatA is the major determinant for lysozyme resistance of Staphylococcus aureus**. *Molecular microbiology* 2005, **55**(3):778-787.

90. Jones CS, Sychantha D, Howell PL, Clarke AJ: **Structural basis for the O-acetyltransferase function of the extracytoplasmic domain of OatA from Staphylococcus aureus**. *The Journal of biological chemistry* 2020, **295**(24):8204-8213.

91. Bernard E, Rolain T, Courtin P, Guillot A, Langella P, Hols P, Chapot-Chartier M-P: **Characterization of O-Acetylation of N-Acetylglucosamine: A NOVEL**

STRUCTURAL VARIATION OF BACTERIAL PEPTIDOGLYCAN. *Journal of Biological Chemistry* 2011, **286**(27):23950-23958.

92. Aubry C, Goulard C, Nahori M-A, Cayet N, Decalf J, Sachse M, Boneca IG, Cossart P, Dussurget O: **OatA, a Peptidoglycan O-Acetyltransferase Involved in Listeria monocytogenes Immune Escape, Is Critical for Virulence**. *The Journal of Infectious Diseases* 2011, **204**(5):731-740.

93. Hébert L, Courtin P, Torelli R, Sanguinetti M, Chapot-Chartier MP, Auffray Y, Benachour A: **Enterococcus faecalis constitutes an unusual bacterial model in lysozyme resistance**. *Infect Immun* 2007, **75**(11):5390-5398.

94. Bernard E, Rolain T, David B, André G, Dupres V, Dufrêne YF, Hallet B, Chapot-Chartier MP, Hols P: **Dual role for the O-acetyltransferase OatA in peptidoglycan modification and control of cell septation in Lactobacillus plantarum**. *PLoS One* 2012, **7**(10):e47893.

95. Veiga P, Bulbarela-Sampieri C, Furlan S, Maisons A, Chapot-Chartier M-P, Erkelenz M, Mervelet P, Noirot P, Frees D, Kuipers OP *et al*: **SpxB Regulates O-Acetylation-dependent Resistance of Lactococcus lactis Peptidoglycan to Hydrolysis**. *Journal of Biological Chemistry* 2007, **282**(27):19342-19354.

96. Moynihan PJ, Clarke AJ: **O-acetylation of peptidoglycan in gram-negative bacteria: identification and characterization of peptidoglycan O-acetyltransferase in Neisseria gonorrhoeae**. *The Journal of biological chemistry* 2010, **285**(17):13264-13273.

97. Franklin MJ, Nivens DE, Weadge JT, Howell PL: **Biosynthesis of the Pseudomonas aeruginosa Extracellular Polysaccharides, Alginate, Pel, and Psl**. *Front Microbiol* 2011, **2**:167.

98. Pier GB, Coleman F, Grout M, Franklin M, Ohman DE: **Role of alginate O acetylation in resistance of mucoid Pseudomonas aeruginosa to opsonic phagocytosis**. *Infect Immun* 2001, **69**(3):1895-1901.

99. Baker P, Ricer T, Moynihan PJ, Kitova EN, Walvoort MT, Little DJ, Whitney JC, Dawson K, Weadge JT, Robinson H *et al*: **P. aeruginosa SGNH hydrolase-like proteins AlgJ and AlgX have similar topology but separate and distinct roles in alginate acetylation**. *PLoS Pathog* 2014, **10**(8):e1004334.

100. Riley LM, Weadge JT, Baker P, Robinson H, Codée JD, Tipton PA, Ohman DE, Howell PL: **Structural and functional characterization of Pseudomonas aeruginosa AlgX: role of AlgX in alginate acetylation**. *The Journal of biological chemistry* 2013, **288**(31):22299-22314.

101. Franklin MJ, Ohman DE: **Mutant analysis and cellular localization of the AlgI, AlgJ, and AlgF proteins required for O acetylation of alginate in Pseudomonas aeruginosa**. *J Bacteriol* 2002, **184**(11):3000-3007.

102. Franklin MJ, Ohman DE: **Identification of algI and algJ in the Pseudomonas aeruginosa alginate biosynthetic gene cluster which are required for alginate O acetylation**. *J Bacteriol* 1996, **178**(8):2186-2195.

103. Franklin MJ, Ohman DE: **Identification of algF in the alginate biosynthetic gene cluster of Pseudomonas aeruginosa which is required for alginate acetylation**. *J Bacteriol* 1993, **175**(16):5057-5065.

104. Chanasit W, Gonzaga ZJC, Rehm BHA: **Analysis of the alginate O-acetylation machinery in Pseudomonas aeruginosa**. *Appl Microbiol Biotechnol* 2020, **104**(5):2179-2191.

105. Sychantha D, Brott AS, Jones CS, Clarke AJ: **Mechanistic Pathways for Peptidoglycan O-Acetylation and De-O-Acetylation**. *Front Microbiol* 2018, **9**:2332.

106. Weadge JT, Pfeffer JM, Clarke AJ: **Identification of a new family of enzymes with potential O-acetylpeptidoglycan esterase activity in both Gram-positive and Gram-negative bacteria**. *BMC Microbiol* 2005, **5**:49.

107. Dillard JP, Hackett KT: **Mutations affecting peptidoglycan acetylation in Neisseria gonorrhoeae and Neisseria meningitidis**. *Infect Immun* 2005, **73**(9):5697-5705.

108. Laaberki MH, Pfeffer J, Clarke AJ, Dworkin J: **O-Acetylation of peptidoglycan is required for proper cell separation and S-layer anchoring in Bacillus anthracis**. *The Journal of biological chemistry* 2011, **286**(7):5278-5288.

109. Leoff C, Choudhury B, Saile E, Quinn CP, Carlson RW, Kannenberg EL: **Structural elucidation of the nonclassical secondary cell wall polysaccharide from Bacillus cereus ATCC 10987. Comparison with the polysaccharides from Bacillus anthracis and B. cereus type strain ATCC 14579 reveals both unique and common structural features**. *The Journal of biological chemistry* 2008, **283**(44):29812-29821.

110. Choudhury B, Leoff C, Saile E, Wilkins P, Quinn CP, Kannenberg EL, Carlson RW: **The structure of the major cell wall polysaccharide of Bacillus anthracis is species-specific**. *The Journal of biological chemistry* 2006, **281**(38):27932-27941.

111. Lunderberg JM, Nguyen-Mau SM, Richter GS, Wang YT, Dworkin J, Missiakas DM, Schneewind O: **Bacillus anthracis acetyltransferases PatA1 and PatA2 modify the secondary cell wall polysaccharide and affect the assembly of S-layer proteins**. *J Bacteriol* 2013, **195**(5):977-989.

112. Sychantha D, Little DJ, Chapman RN, Boons G-J, Robinson H, Howell PL, Clarke AJ: **PatB1 is an O-acetyltransferase that decorates secondary cell wall polysaccharides**. *Nature chemical biology* 2018, **14**(1):79.

113. Zhong R, Cui D, Ye Z-H: **Evolutionary origin of O-acetyltransferases responsible for glucomannan acetylation in land plants**. *New Phytologist* 2019, **224**(1):466-479.

114. Soria V, Martínez-Amorós E, Escaramís G, Valero J, Crespo JM, Gutiérrez-Zotes A, Bayés M, Martorell L, Vilella E, Estivill X *et al*: **Resequencing and association analysis of arylalkylamine N-acetyltransferase (AANAT) gene and its contribution to major depression susceptibility**. *J Pineal Res* 2010, **49**(1):35-44.

115. Wang GY, Lee CG, Lee EJ: **Genetic variability of arylalkylamine-N-acetyl-transferase (AA-NAT) gene and human sleep/wake pattern**. *Chronobiol Int* 2004, **21**(2):229-237.

116. Tiwari P, Dwivedi S, Singh MP, Mishra R, Chandy A: **Basic and modern concepts on cholinergic receptor: A review**. *Asian Pac J Trop Dis* 2013, **3**(5):413-420.

117. Schwarz S, Kehrenberg C, Doublet B, Cloeckaert A: **Molecular basis of bacterial resistance to chloramphenicol and florfenicol**. *FEMS Microbiol Rev* 2004, **28**(5):519-542.

118. Biswas T, Houghton JL, Garneau-Tsodikova S, Tsodikov OV: **The structural basis for substrate versatility of chloramphenicol acetyltransferase CATI**. *Protein Sci* 2012, **21**(4):520-530.

119. Shaw WV: **Chloramphenicol acetyltransferase: enzymology and molecular biology**. *CRC Crit Rev Biochem* 1983, **14**(1):1-46.

120. Ragland SA, Criss AK: **From bacterial killing to immune modulation: Recent insights into the functions of lysozyme**. *PLoS Pathog* 2017, **13**(9):e1006512-e1006512.

121. Ralph J, Lapierre C, Boerjan W: **Lignin structure and its engineering**. *Current Opinion in Biotechnology* 2019, **56**:240-249.

122. Zhong R, Cui D, Ye ZH: **Members of the DUF231 Family are O-Acetyltransferases Catalyzing 2-O- and 3-O-Acetylation of Mannan**. *Plant & cell physiology* 2018, **59**(11):2339-2349.

123. Zhong R, Cui D, Ye ZH: **Evolutionary origin of O-acetyltransferases responsible for glucomannan acetylation in land plants**. *The New phytologist* 2019, **224**(1):466-479.

124. Stranne M, Ren Y, Fimognari L, Birdseye D, Yan J, Bardor M, Mollet JC, Komatsu T, Kikuchi J, Scheller HV *et al*: **TBL10 is required for O-acetylation of pectic rhamnogalacturonan-I in Arabidopsis thaliana**. *The Plant journal : for cell and molecular biology* 2018, **96**(4):772-785.

125. Zhong R, Cui D, Phillips DR, Richardson EA, Ye ZH: **A Group of O-Acetyltransferases Catalyze Xyloglucan Backbone Acetylation and Can Alter Xyloglucan Xylosylation Pattern and Plant Growth When Expressed in Arabidopsis**. *Plant & cell physiology* 2020, **61**(6):1064-1079.

126. Gille S, de Souza A, Xiong G, Benz M, Cheng K, Schultink A, Reca IB, Pauly M: **O-acetylation of Arabidopsis hemicellulose xyloglucan requires AXY4 or AXY4L, proteins with a TBL and DUF231 domain**. *The Plant cell* 2011, **23**(11):4041-4053.

127. Akoh CC, Lee G-C, Liaw Y-C, Huang T-H, Shaw J-F: **GDSL family of serine esterases/lipases**. *Progress in Lipid Research* 2004, **43**(6):534-552.

128. Lo YC, Lin SC, Shaw JF, Liaw YC: **Crystal structure of Escherichia coli thioesterase I/protease I/lysophospholipase L1: consensus sequence blocks constitute the catalytic center of SGNH-hydrolases through a conserved hydrogen bond network**. *Journal of molecular biology* 2003, **330**(3):539-551.

129. Upton C, Buckley JT: **A new family of lipolytic enzymes?** *Trends in biochemical sciences* 1995, **20**(5):178-179.

130. Milewski S, Gabriel I, Olchowy J: **Enzymes of UDP-GlcNAc biosynthesis in yeast**. *Yeast* 2006, **23**(1):1-14.

131. Sternglanz R, Schindelin H: **Structure and mechanism of action of the histone acetyltransferase Gcn5 and similarity to other N-acetyltransferases**. *Proceedings of the National Academy of Sciences of the United States of America* 1999, **96**(16):8807-8808.

132. Mio T, Yamada-Okabe T, Arisawa M, Yamada-Okabe H: **Saccharomyces cerevisiae GNA1, an Essential Gene Encoding a Novel Acetyltransferase Involved in UDP-N-acetylglucosamine Synthesis**. *Journal of Biological Chemistry* 1999, **274**(1):424-429.

133. Peneff C, Mengin-Lecreulx D, Bourne Y: **The crystal structures of Apo and complexed Saccharomyces cerevisiae GNA1 shed light on the catalytic mechanism of an amino-sugar N-acetyltransferase**. *The Journal of biological chemistry* 2001, **276**(19):16328-16334.

134. Del Río JC, Marques G, Rencoret J, Martínez AT, Gutiérrez A: **Occurrence of naturally acetylated lignin units**. *J Agric Food Chem* 2007, **55**(14):5461-5468.

135. Pawar PM, Koutaniemi S, Tenkanen M, Mellerowicz EJ: **Acetylation of woody lignocellulose: significance and regulation**. *Front Plant Sci* 2013, **4**:118.

136. Sarkanen KV, Chang H-M, Allan GG: **Species variation in lignins. III. Hardwood lignins**. *Tappi* 1967, **50**:587-590.

137. Ralph J, Lu F: **The DFRC Method for Lignin Analysis. 6. A Simple Modification for Identifying Natural Acetates on Lignins**. *Journal of Agricultural and Food Chemistry* 1998, **46**(11):4616-4619.

138. Lu F, Ralph J: **Preliminary evidence for sinapyl acetate as a lignin monomer in kenaf**. *Chem Commun (Camb)* 2002(1):90-91.

139. Smith DCC: **Ester Groups in Lignin**. *Nature* 1955, **176**(4475):267-268.

140. Klein DC, Coon SL, Roseboom PH, Weller JL, Bernard M, Gastel JA, Zatz M, Iuvone PM, Rodriguez IR, Bégay V *et al*: **The melatonin rhythm-generating enzyme: molecular regulation of serotonin N-acetyltransferase in the pineal gland**. *Recent Prog Horm Res* 1997, **52**:307-357; discussion 357-308.

141. Hickman AB, Namboodiri MAA, Klein DC, Dyda F: **The Structural Basis of Ordered Substrate Binding by Serotonin N-Acetyltransferase: Enzyme Complex at 1.8 A Resolution with a Bisubstrate Analog**. *Cell* 1999, **97**(3):361-369.

142. Carbini LA, Hersh LB: **Functional analysis of conserved histidines in choline acetyltransferase by site-directed mutagenesis**. *J Neurochem* 1993, **61**(1):247-253.

143. Hersh LB, Peet M: **Re-evaluation of the kinetic mechanism of the choline acetyltransferase reaction**. *The Journal of biological chemistry* 1977, **252**(14):4796-4802.

144. Kim A-R, Rylett RJ, Shilton BH: **Substrate Binding and Catalytic Mechanism of Human Choline Acetyltransferase**. *Biochemistry* 2006, **45**(49):14621-14631.

145. Bulkley D, Innis CA, Blaha G, Steitz TA: **Revisiting the structures of several antibiotics bound to the bacterial ribosome**. *Proceedings of the National Academy of Sciences of the United States of America* 2010, **107**(40):17158-17163.

146. Shaw WV: **The enzymatic acetylation of chloramphenicol by extracts of R factor-resistant Escherichia coli**. *The Journal of biological chemistry* 1967, **242**(4):687-693.

147. Day PJ, Shaw WV: **Acetyl coenzyme A binding by chloramphenicol acetyltransferase. Hydrophobic determinants of recognition and catalysis**. *The Journal of biological chemistry* 1992, **267**(8):5122-5127.

148. Murray IA, Lewendon A, Shaw WV: **Stabilization of the imidazole ring of His-195 at the active site of chloramphenicol acetyltransferase**. *The Journal of biological chemistry* 1991, **266**(18):11695-11698.

149. Leslie AG, Moody PC, Shaw WV: **Structure of chloramphenicol acetyltransferase at 1.75-A resolution**. *Proceedings of the National Academy of Sciences of the United States of America* 1988, **85**(12):4133-4137.

150. Lee KK, Workman JL: **Histone acetyltransferase complexes: one size doesn't fit all**. *Nat Rev Mol Cell Biol* 2007, **8**(4):284-295.

151. Aksnes H, Ree R, Arnesen T: **Co-translational, Post-translational, and Non-catalytic Roles of N-Terminal Acetyltransferases**. *Mol Cell* 2019, **73**(6):1097-1114.

152. Drazic A, Myklebust LM, Ree R, Arnesen T: **The world of protein acetylation**. *Biochimica et biophysica acta* 2016, **1864**(10):1372-1401.

153. Polevoda B, Sherman F: **N-terminal acetyltransferases and sequence requirements for N-terminal acetylation of eukaryotic proteins**. *Journal of molecular biology* 2003, **325**(4):595-622.

154. Brown CW, Sridhara V, Boutz DR, Person MD, Marcotte EM, Barrick JE, Wilke CO: **Large-scale analysis of post-translational modifications in E. coli under glucose-limiting conditions**. *BMC Genomics* 2017, **18**(1):301.

155. Kentache T, Jouenne T, Dé E, Hardouin J: **Proteomic characterization of Nα- and Nε-acetylation in Acinetobacter baumannii**. *J Proteomics* 2016, **144**:148-158.

156. Ouidir T, Jarnier F, Cosette P, Jouenne T, Hardouin J: **Characterization of N-terminal protein modifications in Pseudomonas aeruginosa PA14**. *J Proteomics* 2015, **114**:214-225.

157. Allfrey VG, Mirsky AE: **Structural Modifications of Histones and their Possible Role in the Regulation of RNA Synthesis**. *Science* 1964, **144**(3618):559.

158. Allis CD, Berger SL, Cote J, Dent S, Jenuwien T, Kouzarides T, Pillus L, Reinberg D, Shi Y, Shiekhattar R *et al*: **New nomenclature for chromatin-modifying enzymes**. *Cell* 2007, **131**(4):633-636.

159. Paquette N, Conlon J, Sweet C, Rus F, Wilson L, Pereira A, Rosadini CV, Goutagny N, Weber AN, Lane WS *et al*: **Serine/threonine acetylation of TGFβ-activated kinase (TAK1) by Yersinia pestis YopJ inhibits innate immune signaling**. *Proceedings of the National Academy of Sciences of the United States of America* 2012, **109**(31):12710-12715.

160. Lee J, Manning AJ, Wolfgeher D, Jelenska J, Cavanaugh KA, Xu H, Fernandez SM, Michelmore RW, Kron SJ, Greenberg JT: **Acetylation of an NB-LRR Plant Immune-Effector Complex Suppresses Immunity**. *Cell Rep* 2015, **13**(8):1670-1682.

161. Birhanu AG, Yimer SA, Holm-Hansen C, Norheim G, Aseffa A, Abebe M, Tønjum T: **N(ε)- and O-Acetylation in Mycobacterium tuberculosis Lineage 7 and Lineage 4**

Strains: Proteins Involved in Bioenergetics, Virulence, and Antimicrobial Resistance Are Acetylated. *J Proteome Res* 2017, **16**(11):4045-4059.

162. VanDrisse CM, Escalante-Semerena JC: **In Streptomyces lividans, acetyl-CoA synthetase activity is controlled by O-serine and N(ε) -lysine acetylation**. *Molecular microbiology* 2018, **107**(4):577-594.

163. Vetting MW, LP SdC, Yu M, Hegde SS, Magnet S, Roderick SL, Blanchard JS: **Structure and functions of the GNAT superfamily of acetyltransferases**. *Arch Biochem Biophys* 2005, **433**(1):212-226.

164. Mizzen CA, Yang XJ, Kokubo T, Brownell JE, Bannister AJ, Owen-Hughes T, Workman J, Wang L, Berger SL, Kouzarides T *et al*: **The TAF(II)250 subunit of TFIID has histone acetyltransferase activity**. *Cell* 1996, **87**(7):1261-1270.

165. Bannister AJ, Kouzarides T: **The CBP co-activator is a histone acetyltransferase**. *Nature* 1996, **384**(6610):641-643.

166. Marmorstein R, Zhou MM: **Writers and readers of histone acetylation: structure, mechanism, and inhibition**. *Cold Spring Harb Perspect Biol* 2014, **6**(7):a018762.

167. Christensen DG, Xie X, Basisty N, Byrnes J, McSweeney S, Schilling B, Wolfe AJ: **Post-translational Protein Acetylation: An Elegant Mechanism for Bacteria to Dynamically Regulate Metabolic Functions**. *Frontiers in Microbiology* 2019, **10**(1604).

168. Yuan H, Marmorstein R: **Histone acetyltransferases: Rising ancient counterparts to protein kinases**. *Biopolymers* 2013, **99**(2):98-111.

169. Salah Ud-Din AI, Tikhomirova A, Roujeinikova A: **Structure and Functional Diversity of GCN5-Related N-Acetyltransferases (GNAT)**. *Int J Mol Sci* 2016, **17**(7).

170. Yan Y, Harper S, Speicher DW, Marmorstein R: **The catalytic mechanism of the ESA1 histone acetyltransferase involves a self-acetylated intermediate**. *Nat Struct Biol* 2002, **9**(11):862-869.

171. Berndsen CE, Albaugh BN, Tan S, Denu JM: **Catalytic mechanism of a MYST family histone acetyltransferase**. *Biochemistry* 2007, **46**(3):623-629.

172. Liu X, Wang L, Zhao K, Thompson PR, Hwang Y, Marmorstein R, Cole PA: **The structural basis of protein acetylation by the p300/CBP transcriptional coactivator**. *Nature* 2008, **451**(7180):846-850.

173. Ulusu NN: **Evolution of Enzyme Kinetic Mechanisms**. *J Mol Evol* 2015, **80**(5-6):251-257.

174. Aksnes H, Van Damme P, Goris M, Starheim KK, Marie M, Støve SI, Hoel C, Kalvik TV, Hole K, Glomnes N *et al*: **An organellar nα-acetyltransferase, naa60, acetylates cytosolic N termini of transmembrane proteins and maintains Golgi integrity**. *Cell Rep* 2015, **10**(8):1362-1374.

175. Aksnes H, Goris M, Strømland Ø, Drazic A, Waheed Q, Reuter N, Arnesen T: **Molecular determinants of the N-terminal acetyltransferase Naa60 anchoring to the Golgi membrane**. *Journal of Biological Chemistry* 2017, **292**(16):6821-6837.

176. Aksnes H, Drazic A, Marie M, Arnesen T: **First Things First: Vital Protein Marks by N-Terminal Acetyltransferases**. *Trends in Biochemical Sciences* 2016, **41**(9):746-760.

177. Dinh TV, Bienvenut WV, Linster E, Feldman-Salit A, Jung VA, Meinnel T, Hell R, Giglione C, Wirtz M: **Molecular identification and functional characterization of the first Nα-acetyltransferase in plastids by global acetylome profiling**. *PROTEOMICS* 2015, **15**(14):2426-2435.

178. Drazic A, Aksnes H, Marie M, Boczkowska M, Varland S, Timmerman E, Foyn H, Glomnes N, Rebowski G, Impens F *et al*: **NAA80 is actin's N-terminal acetyltransferase and regulates cytoskeleton assembly and cell motility**. *Proceedings of the National Academy of Sciences of the United States of America* 2018, **115**(17):4399-4404.

179. Ranatunga TD, Jervis J, Helm RF, McMillan JD, Hatzis C: **Identification of inhibitory components toxic toward zymomonas mobilis CP4(pZB5) xylose fermentation**. *Applied Biochemistry and Biotechnology* 1997, **67**(3):185.

180. Jönsson LJ, Alriksson B, Nilvebrant NO: **Bioconversion of lignocellulose: inhibitors and detoxification**. *Biotechnology for biofuels* 2013, **6**(1):16.

181. Pogorelko G, Fursova O, Lin M, Pyle E, Jass J, Zabotina OA: **Post-synthetic modification of plant cell walls by expression of microbial hydrolases in the apoplast**. *Plant Mol Biol* 2011, **77**(4-5):433-445.

182. Pogorelko G, Lionetti V, Fursova O, Sundaram RM, Qi M, Whitham SA, Bogdanove AJ, Bellincampi D, Zabotina OA: **Arabidopsis and Brachypodium distachyon transgenic plants expressing Aspergillus nidulans acetylesterases have decreased degree of polysaccharide acetylation and increased resistance to pathogens**. *Plant Physiol* 2013, **162**(1):9-23.

183. Pawar PM, Derba-Maceluch M, Chong SL, Gomez LD, Miedes E, Banasiak A, Ratke C, Gaertner C, Mouille G, McQueen-Mason SJ *et al*: **Expression of fungal acetyl xylan esterase in Arabidopsis thaliana improves saccharification of stem lignocellulose**. *Plant biotechnology journal* 2016, **14**(1):387-397.

184. Pawar PM, Derba-Maceluch M, Chong SL, Gandla ML, Bashar SS, Sparrman T, Ahvenainen P, Hedenstrom M, Ozparpucu M, Ruggeberg M *et al*: **In muro deacetylation of xylan affects lignin properties and improves saccharification of aspen wood**. *Biotechnology for biofuels* 2017, **10**:98.

185. Wang Z, Pawar PM, Derba-Maceluch M, Hedenström M, Chong SL, Tenkanen M, Jönsson LJ, Mellerowicz EJ: **Hybrid Aspen Expressing a Carbohydrate Esterase Family 5 Acetyl Xylan Esterase Under Control of a Wood-Specific Promoter Shows Improved Saccharification**. *Front Plant Sci* 2020, **11**:380.

186. Pawar PM, Ratke C, Balasubramanian VK, Chong SL, Gandla ML, Adriasola M, Sparrman T, Hedenstrom M, Szwaj K, Derba-Maceluch M *et al*: **Downregulation of RWA genes in hybrid aspen affects xylan acetylation and wood saccharification**. *The New phytologist* 2017.

187. Yang Y, Yoo CG, Winkeler KA, Collins CM, Hinchee MAW, Jawdy SS, Gunter LE, Engle NL, Pu Y, Yang X *et al*: **Overexpression of a Domain of Unknown Function 231-containing protein increases O-xylan acetylation and cellulose biosynthesis in Populus**. *Biotechnology for biofuels* 2017, **10**:311.

188. Zhong R, Cui D, Phillips DR, Richardson EA, Ye Z-H: **A Group of O-Acetyltransferases Catalyze Xyloglucan Backbone Acetylation and Can Alter Xyloglucan Xylosylation Pattern and Plant Growth When Expressed in Arabidopsis**. *Plant and Cell Physiology* 2020, **61**(6):1064-1079.

189. Bischoff V, Selbig J, Scheible WR: **Involvement of TBL/DUF231 proteins into cell wall biology**. *Plant Signal Behav* 2010, **5**(8):1057-1059.

190. Vorísek J, Rehácek Z: **Fine structural localization of alkaloid synthesis in endoplasmic reticulum of submerged Claviceps purpurea**. *Arch Microbiol* 1978, **117**(3):297-302.

191. Rawsthorne S: **Carbon flux and fatty acid synthesis in plants**. *Prog Lipid Res* 2002, **41**(2):182-196.

192. Tholl D: **Biosynthesis and biological functions of terpenoids in plants**. *Adv Biochem Eng Biotechnol* 2015, **148**:63-106.

193. Tohge T, de Souza LP, Fernie AR: **Current understanding of the pathways of flavonoid biosynthesis in model and crop plants**. *J Exp Bot* 2017, **68**(15):4013-4028.

194. Baud S, Guyon V, Kronenberger J, Wuillème S, Miquel M, Caboche M, Lepiniec L, Rochat C: **Multifunctional acetyl-CoA carboxylase 1 is essential for very long chain fatty acid elongation and embryo development in Arabidopsis**. *The Plant journal : for cell and molecular biology* 2003, **33**(1):75-86.

195. Chen C, Li C, Wang Y, Renaud J, Tian G, Kambhampati S, Saatian B, Nguyen V, Hannoufa A, Marsolais F *et al*: **Cytosolic acetyl-CoA promotes histone acetylation predominantly at H3K27 in Arabidopsis**. *Nature plants* 2017, **3**(10):814-824.

196. Wellen KE, Hatzivassiliou G, Sachdeva UM, Bui TV, Cross JR, Thompson CB: **ATP-citrate lyase links cellular metabolism to histone acetylation**. *Science* 2009, **324**(5930):1076-1080.

197. Galdieri L, Zhang T, Rogerson D, Lleshi R, Vancura A: **Protein acetylation and acetyl coenzyme a metabolism in budding yeast**. *Eukaryot Cell* 2014, **13**(12):1472-1483.

198. Xing S, Poirier Y: **The protein acetylome and the regulation of metabolism**. *Trends in plant science* 2012, **17**(7):423-430.

199. Fatland BL, Ke J, Anderson MD, Mentzen WI, Cui LW, Allred CC, Johnston JL, Nikolau BJ, Wurtele ES: **Molecular Characterization of a Heteromeric ATP-Citrate Lyase That Generates Cytosolic Acetyl-Coenzyme A in Arabidopsis**. *Plant Physiology* 2002, **130**(2):740-756.

200. Disch A, Schwender J, Müller C, Lichtenthaler HK, Rohmer M: **Distribution of the mevalonate and glyceraldehyde phosphate/pyruvate pathways for isoprenoid biosynthesis in unicellular algae and the cyanobacterium Synechocystis PCC 6714**. *Biochem J* 1998, **333 (Pt 2)**(Pt 2):381-388.

201. Fatland BL, Nikolau BJ, Wurtele ES: **Reverse genetic characterization of cytosolic acetyl-CoA generation by ATP-citrate lyase in Arabidopsis**. *The Plant cell* 2005, **17**(1):182-203.

202. Zhong R, Cui D, Richardson EA, Phillips DR, Azadi P, Lu G, Ye ZH: **Cytosolic Acetyl-CoA Generated by ATP-Citrate Lyase Is Essential for Acetylation of Cell Wall Polysaccharides**. *Plant & cell physiology* 2020, **61**(1):64-75.

203. Sarmah N, Revathi D, Sheelu G, Yamuna Rani K, Sridhar S, Mehtab V, Sumana C: **Recent advances on sources and industrial applications of lipases**. *Biotechnology Progress* 2018, **34**(1):5-28.

204. Albayati SH, Masomian M, Ishak SNH, Mohamad Ali MSb, Thean AL, Mohd Shariff Fb, Muhd Noor NDb, Raja Abd Rahman RNZ: **Main Structural Targets for Engineering Lipase Substrate Specificity**. *Catalysts* 2020, **10**(7):747.

205. Müller J, Sowa MA, Fredrich B, Brundiek H, Bornscheuer UT: **Enhancing the Acyltransferase Activity of Candida antarctica Lipase A by Rational Design**. *Chembiochem* 2015, **16**(12):1791-1796.

206. Jan AH, Subileau M, Deyrieux C, Perrier V, Dubreucq É: **Elucidation of a key position for acyltransfer activity in Candida parapsilosis lipase/acyltransferase (CpLIP2) and in Pseudozyma antarctica lipase A (CAL-A) by rational design**. *Biochimica et biophysica acta* 2016, **1864**(2):187-194.

207. Schmitt J, Brocca S, Schmid RD, Pleiss J: **Blocking the tunnel: engineering of Candida rugosa lipase mutants with short chain length specificity**. *Protein Eng* 2002, **15**(7):595-601.

208. Yu XW, Zhu SS, Xiao R, Xu Y: **Conversion of a Rhizopus chinensis lipase into an esterase by lid swapping**. *J Lipid Res* 2014, **55**(6):1044-1051.

209. Senior AW, Evans R, Jumper J, Kirkpatrick J, Sifre L, Green T, Qin C, Žídek A, Nelson AWR, Bridgland A *et al*: **Improved protein structure prediction using potentials from deep learning**. *Nature* 2020, **577**(7792):706-710.

210. Zemla A, Venclovas C, Moult J, Fidelis K: **Processing and analysis of CASP3 protein structure predictions**. *Proteins* 1999, **Suppl 3**:22-29.

211. Kryshtafovych A, Schwede T, Topf M, Fidelis K, Moult J: **Critical assessment of methods of protein structure prediction (CASP)—Round XIII**. *Proteins: Structure, Function, and Bioinformatics* 2019, **87**(12):1011-1020.

212. John Jumper RE, Alexander Pritzel, Tim Green, Michael Figurnov, Kathryn Tunyasuvunakool, Olaf Ronneberger, Russ Bates, Augustin Žídek, Alex Bridgland, Clemens Meyer, Simon A A Kohl, Anna Potapenko, Andrew J Ballard, Andrew Cowie, Bernardino Romera-Paredes, Stanislav Nikolov, Rishub Jain, Jonas Adler, Trevor Back, Stig Petersen, David Reiman, Martin Steinegger, Michalina Pacholska, David Silver, Oriol Vinyals, Andrew W Senior, Koray Kavukcuoglu, Pushmeet Kohli, Demis

Hassabis.: **High Accuracy Protein Structure Prediction Using Deep Learning**. In: *Fourteenth Critical Assessment of Techniques for Protein Structure Prediction (Abstract Book): 30 November - 4 December*. 2020: 22-24.

213. Callaway E: **'It will change everything': DeepMind's AI makes gigantic leap in solving protein structures**. *Nature* 2020, **588**(7837):203-204.

214. Kern DM, Sorum B, Hoel CM, Sridharan S, Remis JP, Toso DB, Brohawn SG: **Cryo-EM structure of the SARS-CoV-2 3a ion channel in lipid nanodiscs**. *bioRxiv* 2020:2020.2006.2017.156554.

215. Dill KA, MacCallum JL: **The protein-folding problem, 50 years on**. *Science* 2012, **338**(6110):1042-1046.